Peristaltic Motion with Nanofluid Characteristics

By

Bilal Ahmed

Department of Mathematics
Quaid-i-Azam University
Islamabad, Pakistan
2021

Peristaltic Motion with Nanofluid Characteristics

By

Bilal Ahmed

Supervised By

Prof. Dr. Tasawar Hayat

Department of Mathematics
Quaid-i-Azam University
Islamabad, Pakistan
2021

Peristaltic Motion with Nanofluid Characteristics

By

Bilal Ahmed

A THESIS SUBMITTED IN THE PARTIAL FULFILLMENT OF THE REQUIREMENT FOR THE DEGREE OF

DOCTOR OF PHILOSOPHY

IN

MATHEMATICS

Supervised By

Prof. Dr. Tasawar Hayat

Department of Mathematics
Quaid-i-Azam University
Islamabad, Pakistan
2021

Author's Declaration

I **Bilal Ahmed** hereby state that my PhD thesis titled **Peristaltic Motion with Nanofluid Characteristics** is my own work and has not been submitted previously by me for taking any degree from the Quaid-I-Azam University Islamabad, Pakistan or anywhere else in the country/world.

At any time if my statement is found to be incorrect even after my graduate the university has the right to withdraw my PhD degree.

Name of Student: **Bilal Ahmed**

Date: **13-08-2021**

Plagiarism Undertaking

I solemnly declare that research work presented in the thesis titled "**Peristaltic Motion with Nanofluid Characteristics**" is solely my research work with no significant contribution from any other person. Small contribution/help wherever taken has been duly acknowledged and that complete thesis has been written by me.

I understand the zero tolerance policy of the HEC and **Quaid-I-Azam University** towards plagiarism. Therefore, I as an Author of the above titled thesis declare that no portion of my thesis has been plagiarized and any material used as reference is properly referred/cited.

I undertake that if I am found guilty of any formal plagiarism in the above titled thesis even afterward of PhD degree, the University reserves the rights to withdraw/revoke my PhD degree and that HEC and the University has the right to publish my name on the HEC/University Website on which names of students are placed who submitted plagiarized thesis.

Student/Author Signature: 

Name: **Bilal Ahmed**

Certificate of Approval

This is to certify that the research work presented in this thesis entitled **Peristaltic Motion with Nanofluid Characteristics** was conducted by Mr. **Bilal Ahmed** under the kind supervision of **Prof. Dr. Tasawar Hayat**. No part of this thesis has been submitted anywhere else for any other degree. This thesis is submitted to the Department of Mathematics, Quaid-i-Azam University, Islamabad in partial fulfillment of the requirements for the degree of Doctor of Philosophy in field of Mathematics from Department of Mathematics, Quaid-i-Azam University Islamabad, Pakistan.

Student Name: **Bilal Ahmed** Signature:_____

External committee:

a) **External Examiner 1**: Signature:_____
Name: **Dr. Nasir Ali**
Designation: Associate Professor
Office Address: Department of Mathematics & Statistics, International Islamic University, Islamabad.

b) **External Examiner 2**: Signature:_____
Name: **Dr. Maryiam Javed**
Designation: Associate Professor
Office Address: Department of Applied Mathematics and Statistics, Institute of Space Technology (IST), Islamabad.

c) **Internal Examiner** Signature:_____
Name: **Dr. Tasawar Hayat**
Designation: Professor
Office Address: Department of Mathematics, QAU Islamabad.

Supervisor Name: Signature:_____
Prof. Dr. Tasawar Hayat

Name of Dean/HOD: Signature:_____
Prof. Dr. Sohail Nadeem

Dedicated to

My

Beloved Family

And

Respected Teachers

Acknowledgements

All praise for **"Allah Almighty"** the merciful, the beneficent, the Lord of the whole word who has given me the strength to complete this thesis. The sense of He being with me has been the sole reason of my strength throughout the time of hardships. O my Lord I can never thank you for what you have blessed me with. Countless Darood O Salam for the "**Holy Prophet Muhammad**" (peace be upon him), mercy for all the worlds, his off springs and his companions. I offer my humblest gratitude and love to the **Ahle bait** and **Sahaba e Karam**.

I express deepest gratitude to my respected and devoted supervisor **Prof. Dr. Tasawar Hayat** for their intellectual guidance, constant encouragement, suggestions and inexhaustible inspiration throughout my research work. It is a great honour for me that I am a student of **Prof. Dr. Tasawar Hayat**. His guidance and creative criticism made me what I am today.

I would like to convey my heartiest gratitude to my co-advisor **Dr. Fahad Munir Abbasi** for his kind support and guidance that helped me to complete this important work. I am also grateful to all of my respected teachers particularly **Prof. Dr. Sohail Nadeem**, **Prof. Dr. Khalid Saifullah**, **Prof. Dr. Masood Khan** and **Prof. Dr. Malik Muhammad Yousaf** and **Prof. Dr. M. Ayub** for their guidance and support in my PhD duration.

What I actually want to say about my family perhaps can't be said. Continuous struggle and untiring hard work of my father **Muhammad Aslam** is the prime reason behind every success I had. I owe my heartiest gratitude for my uncle **Muhammad Iqbal**. I always wish I can be like him, the hardest working man I never seen in my life, a man full of honour and pride. I want to convey my deepest love to my respected grandfather **Hajji Muhammad Siddiq (Late)** and my beloved mother **Sughra Bibi** (**Late**).

I would love to mention the name of my brothers and cousins **Zubair Ahmed, Akif Iqbal, Dawood Ahmed**, **M. Usman, Luqman Ahmed, Saad Ur Rehman, Mustahsan Saeed, Hassan, Umar, Fawad Haider, Jawad Haider, Abdullah, Husnain and Zain ul Abideen** for endless care and love.

I am especially indebted to all my friends whose presence around me made my life unforgettable and joyful. I am also grateful to my dear friends **Dr. Khursheed Muhammad**, **Dr. Mubashir Umar**, **Dr. Tanveer Muhammad, Dr. Arsalan Aziz** and **Dr. Khalil Ur Rehman** with whom I enjoyed different hues of life. I am thankful to my seniors specially **Dr. Jamil Ahmed**, **Dr. Rizwan Ul Haq**, **Dr. Bilal Ashraf**, **Dr. Yasir**, **Dr. Zubair**, **Dr. Usman**, **Dr. Taseer Muhammad**, **Dr. Tayyab Shah** and **Dr. Farooq** for their continuous support and love. I will never forget the time which I have spent with them.

I wish to express my special thanks to all of my colleagues specially **Dr. Shahid Farooq**, **Dr. Waqas**, **Dr. Waleed Khan**, **Dr. Ijaz Khan**, **Dr. Faisal Shah**, **Dr. Sajjad (Penroz)**, **Dr. Asif Gujjar**, **Dr. Usman**, **Dr. Zahid Nisar, Dr. Sohail, Waqar** and **Aqeela**. I am really grateful to my dear friends **Fahad Sajjad**, **Hassan Munir Khan** and **Manzar Hussain Jutt**.

At the end, I would like to pay my gratitude to all others whose names are not mentioned above and have prayed for my success.

BILAL AHMED

16-08-2020

Preface

Peristalsis is well-known activity for fluid transport in physiology. In this mechanism sinusoidal waves travel along the walls of tube like organs of human beings propelling the fluid contained within the tube in the direction of their propagation. In physiology the principle of peristalsis is seen in the transport of food through oesophagus, movement of chyme in intestines, urine transport from kidneys to bladder, bile transport in bile duct, vasomotion of blood vessels and many others. This mechanism has been adopted by the engineers in designing several industrial appliances including roller and fingers pumps and peristaltic pumps in heart lung and dialysis machines. Improvement in the heat transfer processes is core issue for the industrial and biological processes. Circulation of blood in the body causes the heat transfer amongst tissues. Therefore heat transfer mechanism amongst tissues and the effect of heat on tissues are common topics of interest. The efficiency of nuclear reactors and automobile engines depend on cooling system. Therefore thermal radiators are used to prevent engines from overheating due to friction. The ordinary fluids like water, ethylene glycol and engine oil etc. are used to cool various industrial devices by transforming heat away from the heat source. However, fluids having low thermophysical characteristics therefore minimizing the efficiency of the system. In order to overcome the limitation of the coolant processes, the nanosized particles are mixed in the ordinary fluids. Nanomaterials have unique thermophysical characteristics when compared to ordinary fluids. The homogenous mixtures of nanoparticles and base liquids are known as nanofluids. Novel concept of nanofluid greatly motivated the researchers due to its better thermal features, excellent stability, physical strength and minimal clogging. It is now established fact that the non-Newtonian materials are encountered in the physiological and engineering processes. Therefore viscous and non-Newtonian fluids are accounted in this thesis. Structure of thesis is as follows.

Chapter one has literature review of relevant previous published work and relations for conservation of mass, momentum, energy and concentration. Tensor forms for Newtonian and non-Newtonian fluids (Sisko, Carreau-Yasuda and Powell-Eyring) are presented.

Chapter two elaborates the peristaltic flow of nanofluid. Hall and Ohmic heating effects with temperature dependent viscosity are considered. Mixed convection and heat source/sink parameter are also taken. Resulting problem is solved via NDSolve technique under the lubrication approach.

Material of this chapter is submitted for publication in **Numerical methods for Partial differential equations**.

Chapter three addresses MHD peristaltic flow of nanofluid with variable viscosity. The nanofluid saturates a porous medium with variable porosity and permeability. Temperature dependent viscosity and Maxwell's thermal conductivity models are adopted. Velocity and thermal slip conditions are also taken into examination. Simplified non-dimensional equations are numerically solved. Effects of important parameters on pressure gradient, velocity, temperature and heat transfer rate are studied. Outcomes of this chapter are submitted for publication in **Numerical methods for Partial differential equations**.

Chapter four illustrates the entropy generation in peristaltic transport of nanomaterial with iron oxide. MHD and Joule heating. Energy equation further consists of heat source/sink and viscous dissipation. Velocity slip and temperature jump conditions are accounted. The data of this chapter is published in **Journal of Thermal Analysis and Calorimetry 140 (2020) 789-797.**

Chapter five examines the Hall, Ohmic heating and velocity slip effects on the peristalsis of nanofluid. Convective boundary conditions and heat generation/absorption are considered to facilitate the heat transfer characteristics. Governing equations for the peristaltic flow through a curved channel are derived in curvilinear coordinates. The equations are numerically solved. The contents of this chapter are published in **Journal of Central South University 26 (2019) 2543-2553**.

Chapter six explores the thermophysical characteristics of nanofluid for mixed convective peristaltic motion in the presence of Joule heating. Analysis has been organized for Sisko fluid. Brownian motion and thermophoresis are used to examine the nanomaterial effects. Velocity and thermal slip conditions are utilized. Zero mass flux condition is imposed. Small Reynolds number and large wavelength arguments are employed. Governing problem is nonlinear in terms of both differential equation and boundary conditions. Numerical solution to incoming nonlinear problem is computed. Findings of this chapter is published in **Journal of Thermal Analysis and Calorimetry (2020)**.

Chapter seven illustrate the peristaltic activity of Sisko nano-liquid subject to Hall and Ohmic heating effects. Fluids saturating porous space is modelled using modified Darcy's law. Thermal radiation is also accounted. In addition, the analysis is carried out subject to thermal jump, velocity slip and zero mass flux condition. Numerical solution to the resulting nonlinear problem through

lubrication approach is developed. The observations of this chapter are accepted in **Journal of Thermal Analysis and Calorimetry (2020)**.

Chapter eight communicates the numerical study for peristalsis of Carreau–Yasuda nanofluid in a symmetric channel. Constant magnetic field is applied. Modified Darcy's law and nonlinear thermal radiation effects are considered. Viscous dissipation and Ohmic heating effects are present. Long wavelength and small Reynolds number are considered. Resulting nonlinear problems are solved numerically. The contents of this chapter are published in **Journal of Thermal Analysis and Calorimetry 137 (2019) 1168-1177**.

Chapter nine addresses the flow of Carreau-Yasuda nanofluid in presence of mixed convection and Hall current. Effects of viscous dissipation, Ohmic heating and convective conditions are addressed. Zero nanoparticle mass flux condition is imposed. Wave frame analysis is employed. Coupled differential systems after long wavelength and low Reynolds number are numerically solved. The results of this chapter are published in **Result in Physics 8 (2018) 168-1177**.

Chapter ten describes the peristaltic transport of magneto nanofluid in a symmetric channel. Carreau–Yasuda model is used to explore the shear thickening and shear thinning characteristics. Joule heating and viscous dissipation effects are included in the energy equation. Effects of slip velocity, temperature jump and zero mass flux boundary conditions for channel walls are further considered. Entropy generation and Bejan number are studied. The data of this chapter is published in **Physica Scripta 95 (2020) 055804**.

Chapter eleven explores the influence of mixed convection, Hall effect and magnetic field on peristaltic motion of Powell-Eyring nanofluid in a symmetric channel. Energy equation includes the viscous dissipation, Ohmic heating and thermal radiation. Brownian motion and thermophoresis are considered to explore the nanofluid characteristics. Velocity slip, thermal jump and zero mass flux conditions are considered on the boundary wall. Further temperature dependent viscosity is taken into account. Lubrication approach is used to simplify the dimensionless form of governing equations. Final form of equations are solved numerically. Outcomes of this chapter are submitted for publication in **International Communication in Heat and Mass Transfer**.

Contents

Nomenclature			
$d_1 + d_2$	Width of channel	T	Fluid temperature
λ	Wavelength of peristaltic wave	T_m	Mean temperature
γ_2	Phase difference	l_w	Heat transfer coefficient
$(\bar{X}, \bar{Y})$	Cartesian coordinates in fixed frame	T_w	Temperature at wall
$(\bar{U}, \bar{V})$	Velocity components in fixed frame	h_1	Dimensionless shape of upper wall
b_1	Amplitude of wave at the lower wall	h_2	Dimensionless shape of lower wall
a_1	Amplitude of wave at the upper wall	p	Dimensionless pressure
c	Speed of wave	n	Dimensionless power law index
C	Concentration	Bi	Biot number
C_m	Mean concentration	d	Dimensionless amplitude of waves
t	Time	e	Electron charge
C_{nf}	Specific heat of nanofluid	n_e	Number of density of free electron
B_0	Magnetic field strength	μ_f	Viscosity of fluid
m	Hall parameter	ϕ	Nanoparticle concentration
D_T	Thermophoretic diffusion coefficients	C_f	Specific heat of fluid
D_B	Mass diffusivity	μ_{nf}	Viscosity of nanofluid
σ_{nf}	Electrical conductivity of nanofluid	σ_f	Electrical conductivity of fluid
ρ_{nf}	Density of nanofluid	ρ_f	Density of fluid
α^*	Concentration expansion coefficient	K_f	Thermal conductivity of fluid
α	Thermal expansion coefficient	ϵ	Heat source/sink parameter
$(\bar{u}, \bar{v})$	Velocity components in moving frame	Da	Darcy number
$(\bar{x}, \bar{y})$	Cartesian coordinates in moving frame	δ	Wave number
K_{nf}	Thermal conductivity of nanofluid	We	Weissenberg number
g	Gravity	θ	Dimensionless fluid temperature
$\mu(\gamma')$	Apparent viscosity	η	Dimensionless flow rate
μ_∞	Infinite shear rate viscosity	G_c	Concentration Grashof number
μ_0	Zero shear rate viscosity	G_T	Thermal Grashoff number
Γ	Non-Newtonian parameter	β	Viscosity ratio parameter

Re	Reynolds number	Pr	Prandtl number
M	Hartman number	Ec	Eckert number
P	Dimensional pressure	Br	Brinkman number
N_b	Brownian motion parameter	F	Dimensional flow rate
β_1	Velocity slip	ψ	Stream function
N_t	Thermophoresis parameter	γ	Thermal slip

Chapter 1

Literature survey

1.1 Introduction

The purpose of this chapter is to present some basic concepts and equations for understanding of subsequent chapters. A review of literature on peristaltic transport of nanofluid in the presence of different assumptions are presented. Different types of fluid models are discussed in detail.

1.2 Background

Invention of nanomaterial has brought a revolutionary impact in engineering, industrial and biological fields. Nanoscience explains the thermophysical characteristics of material at nanoscience level. Numerous types of nanomaterials are commonly used such as metals (Cu, Fe, Al and Au), oxide ceramics (CuO, TiO_2, ZnO and Al_2O_3), carbon ceramics and carbon nanotubes. Nanomaterials depict unique features like lighter weight, strength and better stability due to higher surface area and volume ratio of material. Thermal conductivity of nanomaterials is higher when compared with conventional fluids like water, kerosene oil and ethylene glycol. Lower thermal conductivity often limits their use in heat flux devices. Choi [1] proposed that thermophysical properties of conventional fluids can be remarkably enhanced by solid nanosized materials. Inclusion of nanoparticles in ordinary fluid is known as nanofluid. The presence of nanoparticles in the ordinary fluid changes the physical, chemical, electrical and mechanical properties of fluid. Due to very small size minimal clogging and stability in flow passage is

observed. Nanofluid are commonly used in nanotechnology, nuclear system, paints, biomedicine and biotechnology. In biological systems nanomaterials are used in nanoscopy, subcellular fractionation, cancer therapy, biosensors, drug delivery, artificial organ generation, tissue engineering, bioimaging, cell tracking, tissue engineering and omic data generation. Molecular imaging of tissues and cells using nanotechnology produce new techniques to diagnosis the critical diseases specially cancer. Revolutionary impact of nanofluid on the engineering and biological aspects motivate the scientists to work in various dimensions for further refinement. Maxwell [2] comprehensively studied the electricity and conducted nanofluid. Further he introduced the thermal conductivity model for viscous fluid, which gives very accurate solution. Hamilton-Crosser [3] generalized the Maxwell thermal conductivity model by introducing the shape factor. Shape factor depend on the sphericity of nanomaterial. Experimental data depicts that thermal conductivity of nanomaterial is higher as compare to ordinary fluids. The important features affecting the thermal conductivity are nanomaterial type, shape, size and temperature. Brinkman [4] proposed the empirical relation to explore the viscosity of nanofluid. Tiwari and Das [5] developed theoretical model to examine the nanofluid characteristics. Important features of this model is that we use numerical values of density, thermal conductivity, viscosity and electrical conductivity of nanomaterial and fluids predicted by experiments. Xuan et al. [6] examined the heat transfer analysis of nanofluid. The suspension of cu-nanomaterial rapidly enhances the thermal conductance of nanofluid. Hayat et al. [7] theoretically considered effect of temperature on fluid in the presence of various types of nanomaterial. By increasing the temperature viscosity of nanofluid rapidly decreases therefore velocity of nanofluid increases. Feizabadi et al. [8] examined the characteristics of nanofluid via twisted serpentine tube. The experimental results shows that inclusion of Al_2O_3 in water enhances the efficiency factor of system up to 3.73. Saadati et al. [9] practically check the impact of nanofluid on the performance of nuclear reactor. Nanofluid magnify the energy production up to 27.3% and maintain the suitable temperature. Therefore fuel cycle period and safety margin improved. Lebon et al. [10] generalized the Maxwell viscosity model of nanofluid by introducing the particle size factor and role of layers around nanoparticles. Buongiorno et al. [11] predict another mathematical model to study the nanofluid characteristics. He described the seven slip mechanism to explore the nanofluid characteristics. However thermophoresis and Brownian motion parameters are

prominent slip mechanism.

Scientists purposed numerous mathematical models to explain the diverse nature of different fluids. Shear stress and strain play vital role to explain material characteristics. Non-Newtonian fluids are commonly used in numerous industrial and biological processes such as chemical reactors, mixing of massive particles, filtration devices and membrane based separation modules. Apostolids et al. [12] examined the motion of blood nature in arterial system. Sisko [13] experimentally studied the flow of greases and other materials over a shear rate of range from 0.04 to 22000 s^{-1}. Shen et al. [14] analyzed Brownian motion and thermophoresis effects on the Sisko nanofluid. Carreau et al. [15] proposed rheological models that describe different features of fluid like stress relaxation function, shear rate, stress growth and complex viscosity of fluid simultaneously. Kefayati et al. [16] studied outcome of natural convection on Carreau-Yasuda fluid. By increasing the material parameter heat and mass transfer process is controlled. Dong et al. [17] have improved drag force model and discuss its application in simulating nanofluid flow. Nayak et al. [18] demonstrated the thermophoresis and Brownian diffusion effects on the heat transfer characteristics. Heat transfer process depicts increasing behavior in the presence of nanoparticles and higher Reynold number. Powell Eyring [19] is the non-Newtonian fluid model that comprehensively explain the shear thinning characteristics of blood flow in arteries. Powell Eyring follow the kinetic theory of liquids. Sheikholeslami et al. [20] elaborated the impact of Brownian motion and thermophoresis on temperature gradient of nanofluid in enclosure. Temperature gradient shows increasing trend for higher Rayleigh and Lewis number.

Peristalsis is a significant mechanism in which fluid moves due to contraction and expansion of channel walls. The peristaltic phenomena worked in numerous industrial, biological and physiological processes. Some naturally occurring examples of peristaltic motions are urine transport via kidney to bladder, bile motion, food digestion, blood circulation and chyme movement via intestine. Further this mechanism play vital role in mechanical instruments like hose pump, dialysis pump, power generator, cell separator and heart lung machine. Latham [21] initially explore the features of peristaltic motion of fluid. Jaffrin and Shapiro [22] studied the fundamental aspects of peristaltic transport of fluid in channel. Hayat et al. [23] explored peristaltic mechanism for the Maxwell fluid. Hayat et al. [24] examined outcome of nanomaterial on the peristaltic motion of fluid in channel. Inclusion of nanomaterial decreases the velocity as

well as temperature. Ali et al. [25] studied the heat phenomena during peristaltic motion in a curved channel. Heat transport process increases in curved channel for higher curvature parameter. Abbasi et al. [26] generalized the Brinkman viscosity model by introducing exponential temperature dependent viscosity. The temperature and velocity of nanofluid are controlled by decreasing the variable viscosity parameter. Cueva et al. [27] demonstrated the impact of silver nanomaterials in the dynamic simulator of gastrointestinal span. Composition of nanoparticle and common fluid do not disturb the bacterial configuration or metabolic procedures of human intestinal microbiota therefore nanomaterials are used for treatment. Ibrahim et al. [28] comprehensively studied the thermal radiation and variable concentration on peristaltic transport of synovial nanofluid. Synovial fluid supports the joint by high effective cartilage lubrication and it acts as a transport medium of metabolic/ nutrients. Reddy et al. [29] considered the peristaltic motion of Jeffrey nanofluid. Velocity depicts opposite behavior in lower and upper half channel for higher Jeffrey fluid parameter. Shahzad et al. [30] numerically explored the mass and heat transfer attributes in the presence of different nanomaterials. They concluded that cylindrical shaped nanoparticles are more effective as compared to spherical shape nanoparticles.

Several scientist examined effect of MHD on peristaltic motion of nanofluid due to its significance in medical science and engineering. Magnetic field plays vital role in the treatment of human diseases like cancer therapy, removal of blockage in arteries, reduction in bleeding during surgery and magnetic endoscopy. Further magneto-hydrodynamics used in industrial process such as petroleum industry, nuclear industry, power generator and polymer technology. Hayat et al. [31] discussed the magnetic field effect on peristaltic motion of hyperbolic tangent nanofluid. Velocity profile can be controlled in the presence of magnetic field therefore it is used to minimize bleeding process. Abbasi et al. [32] discussed advanced drug transportation process in the presence of copper magneto-nanomaterials. Magnetic flux are successfully used to guide the nanomaterial toward target. Therefore nanomaterial only damage the cancerous cell without effecting any other tissues. Mehrez et al. [33] explored the heat transport analysis for MHD flow of nanofluid in an open cavity. The average Nusselt number depicts increasing trend by higher nanomaterial property and Hartman number. Shahzadi et al. [34] analyzed the inclusion of nanomaterials in blood with inclined magnetic field. Due to magnetic field pressure rise per wavelength depicts the increasing trend. Reddy et al. [35] considered the

effects of complaint wall and MHD on peristaltic flow of nanofluid. The size of trapped bolus decreases due to magnetic influence. Raza et al. [36] studied the heat and mass transport activity of nanofluid in permeable asymmetric medium using magneto carbon nanotubes. The velocity profile increases near the boundary wall due to higher Darcy's number. Rashidi et al. [37] comprehensively examined the role of magnetohydrodynamic in biological phenomenon. Stream line depicts the flow pattern of fluid that can be controlled by using proper magnetic field. When the capacity of magnetic induction is higher then the strength of Hall current is not negligible. Therefore Hall effect produces that is the ratio of electron-cyclotron and electron-atom collision frequency. Abbasi et al. [38] studied the mathematical model of drug delivery process with magnetic and Hall effects. Further silver-water nanofluid are considered with thermal and velocity slip effects. Temperature profile rapidly increases due to the Joule heating effects. However Hall effect plays important role to control the temperature. Therefore Hall effect is compulsory in the magnetic resonance of angiography. Makinde et al. [39] theoretically considered Coutte-Poiseuille flow of nanofluid in rotating permeable channel with non-uniform viscosity. Further magnetic field and Hall effects are also considered. Axial velocity of fluid and temperature increase when magnetic field enhances. However in the case of Hall parameter opposite trend is noticed. Rafiq et al. [40] carried out theoretical investigation of peristaltic flow of nanofluid with Hall and ion slip effects. Heat transport performance can be enhanced by higher Hall parameter.

Mixed convection is a significant processes which occurs in many heat transfer phenomena. Density of fluid represents the decaying behavior when temperature of fluid increases. Therefore fluid velocity increases which become the cause of buoyancy force. Garoosi et al. [41] addressed impact of mixed convection on nanofluid in a square cavity. Results indicate that heat and mass transport rate enhances sharply by increasing the Grashof number. Tanveer et al. [42] examined mixed convection of nanofluid in a curved wavy medium. The results revealed that fluid velocity increases due to higher heat transfer Grashof number. However opposite trend is noticed for mass transfer Grashof number. Zeeshan et al. [43] presented the theoretical study of blood in the presence of nanomaterial with velocity slip effect. Velocity depicts increasing trend in the central portion but opposite behavior is noticed by increasing the slip parameter. Haq et al. [44] examined the impact of thermal radiation on magneto-nanofluid with slip behavior.

They observed that fluid temperature can be controlled by increasing the thermal slip parameter and decreasing thermal radiation parameter. Mustafa et al. [45] examined the wavy motion of nanofluid with complaint wall. By increasing the speed of highly viscous nanofluid the viscous dissipation increases, therefore fluid temperature enhances. Akbar et al. [46] presented the numerical solution of peristaltic motion of a Carreau nanofluid. Magnetic field enhances the pressure rise per wavelength.

Darcy [47] experimentally studied the flow resistance due to the porous medium. He introduced the Darcy law and showed how to relate with momentum equation. Porous medium commonly exists in biological peristaltic phenomenon such as capillaries, human lungs, bile duct and gall bladder. Abbasi et al. [48] theoretically studied the peristaltic motion of nanofluid in porous medium. Temperature of nanofluid can be minimized by enhancing permeability of porous space. Tan et al. [49] investigated the modified Darcy's law for an Oldroyd-B fluid. Tanveer et al. [50] highlight the significance of modified Darcy's law in peristaltic motion of Sisko fluid. By increasing the Darcy's number the temperature also increases. Kuznetsov et al. [51] modeled the zero mass flux condition to explore the characteristics of concentration of nanomaterial. In the presence of thermophoresis the normal flux of nanomaterials is zero at the boundary. Shehzad et al. [52] studied thermophoresis on peristaltic motion of nanofluid. Concentration of nanomaterial remarkably enhances for thermophoresis parameter. Numerous scientists studied various aspects of peristaltic motion of nanofluid $[53-60]$.

1.3 Basic equations

1.3.1 Continuity equation

The conservation law of mass leads to the fact that mass of a closed system remains constant, regardless of the processes acting inside the system. In absence of source or sink in the control volume, the continuity equation is given as

$$\frac{\partial \rho_f}{\partial t} + \nabla . \rho_f \bar{\mathbf{V}} = 0. \tag{1.1}$$

Here ρ_f depicts the fluid density, ∇ gradient operator and $\bar{\mathbf{V}}$ shows the velocity. For incompressible fluid (ρ_f =constant), equation (1.1) becomes:

$$\nabla.\bar{\mathbf{V}} = 0. \tag{1.2}$$

1.3.2 Equation of motion

The vectorial form of equation of motion is given as:

$$\rho_f \frac{d\bar{\mathbf{V}}}{dt} = \operatorname{div} \bar{\mathbf{T}} + \rho_f b, \tag{1.3}$$

where $\bar{\mathbf{T}}(= -\mathbf{PI} + \bar{\mathbf{S}})$ depicts the Cauchy stress tensor, $\bar{\mathbf{S}}$ the extra stress tensor, $\mathbf{I}$ identity tensor, $\rho_f b$ the body force and d/dt the material derivative given by:

$$\frac{d}{dt} = \frac{\partial}{\partial t} + u\frac{\partial}{\partial x} + v\frac{\partial}{\partial y} + w\frac{\partial}{\partial z}.$$

1.3.3 Energy equation

The conservation law of the energy describes that the increase in the internal energy of a thermodynamic system is equal to the amount of energy gained (lost) by the system. The general form of energy equation is

$$\rho c_p \frac{dT}{dt} = \bar{\mathbf{T}}.(\nabla \bar{V}) + \nabla.(k_f \nabla T), \tag{1.4}$$

where c_p depicts the specific heat and k_f stands for thermal conductivity.

1.3.4 Concentration equation

This mathematical relation follows the Fick's second law. Concentration relation for nanomaterial can be explained as:

$$\frac{dC}{dt} = D_T \frac{\nabla^2 T}{T_m} + D_B \nabla^2 C. \tag{1.5}$$

Here C depicts the concentration of nanomaterial, D_T the thermophoretic diffusion parameter, D_B Brownian motion and T_m the mean temperature of wall.

1.4 Fluid models

1.4.1 Viscous fluids

If the shear stress is directly and linearly proportional to the rate of strain then such fluids are called the viscous fluids. The Cauchy stress tensor for an incompressible viscous fluid is

$$\bar{\mathbf{T}} = -p\mathbf{I} + \bar{\mu}_f \bar{\mathbf{A}}_1, \tag{1.6}$$

in which $\bar{\mu}_f$ the dynamic viscosity and Rivlin Ericksen tensor $\bar{\mathbf{A}}_1$ is

$$\bar{\mathbf{A}}_1 = (\operatorname{grad} V) + (\operatorname{grad} V)^t, \tag{1.7}$$

$$\operatorname{grad} V = \begin{bmatrix} \frac{\partial \bar{U}}{\partial \bar{X}} & \frac{\partial \bar{U}}{\partial \bar{Y}} & \frac{\partial \bar{U}}{\partial \bar{Z}} \\ \frac{\partial \bar{V}}{\partial \bar{X}} & \frac{\partial \bar{V}}{\partial \bar{Y}} & \frac{\partial \bar{V}}{\partial \bar{Z}} \\ \frac{\partial \bar{W}}{\partial \bar{X}} & \frac{\partial \bar{W}}{\partial \bar{Y}} & \frac{\partial \bar{W}}{\partial \bar{Z}} \end{bmatrix},$$

$$(\operatorname{grad} V)^t = \begin{bmatrix} \frac{\partial \bar{U}}{\partial \bar{X}} & \frac{\partial \bar{V}}{\partial \bar{X}} & \frac{\partial \bar{W}}{\partial \bar{X}} \\ \frac{\partial \bar{U}}{\partial \bar{Y}} & \frac{\partial \bar{V}}{\partial \bar{Y}} & \frac{\partial \bar{W}}{\partial \bar{Y}} \\ \frac{\partial \bar{U}}{\partial \bar{Z}} & \frac{\partial \bar{V}}{\partial \bar{Z}} & \frac{\partial \bar{W}}{\partial \bar{Z}} \end{bmatrix}.$$

The superscript "t" represents the transpose of the matrix and $\bar{\mathbf{A}}_1$ is given by:

$$\bar{\mathbf{A}}_1 = \begin{bmatrix} 2\frac{\partial \bar{U}}{\partial \bar{X}} & \frac{\partial \bar{V}}{\partial \bar{X}} + \frac{\partial \bar{U}}{\partial \bar{Y}} & \frac{\partial \bar{U}}{\partial \bar{Z}} + \frac{\partial \bar{W}}{\partial \bar{X}} \\ \frac{\partial \bar{U}}{\partial \bar{Y}} + \frac{\partial \bar{V}}{\partial \bar{X}} & 2\frac{\partial \bar{V}}{\partial \bar{Y}} & \frac{\partial \bar{W}}{\partial \bar{Y}} + \frac{\partial \bar{V}}{\partial \bar{Z}} \\ \frac{\partial \bar{U}}{\partial \bar{Z}} + \frac{\partial \bar{W}}{\partial \bar{X}} & \frac{\partial \bar{W}}{\partial \bar{Y}} + \frac{\partial \bar{V}}{\partial \bar{Z}} & 2\,\frac{\partial \bar{W}}{\partial \bar{Z}} \end{bmatrix}. \tag{1.8}$$

Common examples of Newtonian fluids are water and gasoline.

1.4.2 Non-Newtonian fluid

The Cauchy stress tensor for non-Newtonian liquid is:

$$\bar{\mathbf{T}} = -p\mathbf{I} + \bar{\mathbf{S}}, \tag{1.9}$$

where the extra stress tensor $\bar{\mathbf{S}}$ are different for different fluid models.

Powell-Eyring fluid model

The extra stress tensor for Powell-Eyring non-Newtonian fluid is defined as follows [18]:

$$\bar{\mathbf{S}} = \left[\mu_f + \frac{1}{\beta^*\Pi}\sinh^{-1}\left(\frac{\Pi}{c^{**}}\right)\right]\mathbf{A}_1. \tag{1.10}$$

Here β^* and c^{**} depict the material characteristics of fluid. Further $\mathbf{A}_1$ (the first Rivlin-Ericksen tensor) and Π is defined by:

$$\Pi = \sqrt{\frac{1}{2}tr\left(\mathbf{A}_1^2\right)}. \tag{1.11}$$

Sisko fluid model

An extra stress tensor $\bar{\mathbf{S}}$ of Sisko fluid satisfies the following relation [15]:

$$\bar{\mathbf{S}} = \left[\alpha^* + \beta^{**}\left(\Pi\right)^{n-1}\right]\mathbf{A}_1, \tag{1.12}$$

where $\mathbf{A}_1$ depicts the first Rivilin-Ericksen tensor and Π obeys

$$\Pi = \sqrt{\frac{1}{2}tr\left(\mathbf{A}_1^2\right)}. \tag{1.13}$$

Here α^* and β^{**} depict material parameters of fluid. Power law index n provides information about shear thinning ($n \prec 1$) and shear thickening ($n \succ 1$) nature of fluid. For $\alpha^* = 0$ the Sisko model is converted into generalized power law model.

Carreau-Yasuda fluid model

The constitutive relation for the Carreau-Yasuda fluid is [31]:

$$\bar{\mathbf{S}} = \mu(\gamma')\mathbf{A}_1, \tag{1.14}$$

where apparent viscosity $\mu(\gamma')$ is defined by

$$\mu(\gamma') = \mu_\infty + (\mu_0 - \mu_\infty)\left[1 + (\Gamma\Pi)^a\right]^{\frac{n-1}{a}}, \tag{1.15}$$

with

$$\Pi = \sqrt{\frac{1}{2}tr\left(\mathbf{A}_1^2\right)}. \tag{1.16}$$

Here μ_∞ and μ_0 stand for infinite and zero shear-rate viscosities. The parameters a and Γ control the transition between the two extremes. Further "n" stands for dimensionless power law index. The results for Carreau fluid model can be obtained by considering $a = 2$ and $\mu_\infty = 0$.

1.4.3 Solution methodologies

Here we use Mathematica 9 to compute the numerical solution via NDSolve technique. NDSolve is built in shooting method. This technique guarantees the accuracy in solution of the boundary value problem using suitable step size. In this procedure we have chosen step size 0.01 for the variation in both "y" and "x". This technique attains exceptional accuracy and is stable unconditionally.

Chapter 2

Hall effects on mixed convective peristalsis of nanofluid in presence of temperature dependent viscosity

2.1 Introduction

The chapter addresses the mass and heat transfer features on peristaltic flow of nanofluid in an asymmetric channel. Ohmic heating and viscous dissipation effects are present. Viscosity of fluids depends upon temperature. A new model for the effective viscosity of nanofluid is used by combining Brinkman model of viscosity and the exponential model for the temperature dependent viscosity. The momentum and energy equations are solved for small Reynold number and long wavelength. Behaviors of temperature, velocity and pressure gradient are analyzed through graphs by using the numerical method.

2.2 Problem formulation

An incompressible peristaltic flow of nanofluid is considered in vertical asymmetric channel. Sinusoidal waves of wavelength λ propagate along the length of channel with constant speed c. $\bar{X} - axis$ is along length of channel and $\bar{Y} - axis$ normal to it. Further the width of channel

$(d_1 + d_2)$ is taken. Mathematically peristaltic wall shape is defined as:

$$\begin{aligned} \bar{H}_1(\bar{X}, \bar{t}) &= d_1 + a_1 cos(\frac{2\pi}{\lambda}(\bar{X} - c\bar{t})), \\ \bar{H}_2(\bar{X}, \bar{t}) &= -d_2 - b_1 cos(\frac{2\pi}{\lambda}(\bar{X} - c\bar{t}) + \gamma). \end{aligned} \tag{2.1}$$

Here $\bar{H}_1$ and $\bar{H}_2$ depict the upper and lower boundaries respectively and a_1 and b_1 the amplitude of the waves. Further γ represents the phase difference between these waves. We consider the temperatures T_0 and T_1 at upper and lower walls. The strength of magnetic field $\mathbf{B} = [0, 0, B_0]$ is taken. The Lorentz force is defined by:

$$\mathbf{F} = \mathbf{J} \times \mathbf{B}, \tag{2.2}$$

where $\mathbf{J}$ depicts current density. Generalized Ohmic law in the presence of Hall effect obeys:

$$\mathbf{J} = \sigma_{nf} \left[\mathbf{E} + \mathbf{V} \times \mathbf{B} - \frac{1}{en_e}[\mathbf{J} \times \mathbf{B}] \right]. \tag{2.3}$$

Note that σ_{nf} represents the electric conductivity of nanofluid, $\mathbf{V} = [\bar{U}(\bar{X}, \bar{Y}, \bar{t}), \bar{V}(\bar{X}, \bar{Y}, \bar{t}), 0]$ denotes the velocity field, e represents the electron charge and n_e stands for number of density of free electrons. Electric field $\mathbf{E}$ effects are neglected. From Eqs. (2.2) and (2.3) we obtain

$$F = \left[\frac{\sigma_{nf} B_0^2}{1 + (\sigma_{nf} B_0 / en_e)^2} (-\bar{U} + (\sigma_{nf} B_0 / en_e)\bar{V}), \frac{-\sigma_{nf} B_0^2}{1 + (\sigma_{nf} B_0 / en_e)^2} (\bar{V} + (\sigma_{nf} B_0 / en_e)\bar{U}), 0 \right]. \tag{2.4}$$

The electric conductivity of nanofluid obeys:

$$\frac{\sigma_{nf}}{\sigma_f} = 1 + \frac{3(\frac{\sigma_{np}}{\sigma_f} - 1)\phi}{(\frac{\sigma_{np}}{\sigma_f} + 2) - (\frac{\sigma_{np}}{\sigma_f} - 1)\phi}, \tag{2.5}$$

where σ_{np} represents the electrical conductivity of Fe_3O_4, σ_f denotes the electric conductivity of water and ϕ depicts the quantity of nanomaterial. The simplified form of Eq. (2.5) after substituting Eq. (2.4) yields:

$$F = \left[\frac{A_1 \sigma_f B_0^2}{1 + (A_1 m)^2} (-\bar{U} + A_1 m \bar{V}), \frac{-A_1 \sigma_f B_0^2}{1 + (A_1 m)^2} (\bar{V} + A_1 m \bar{U}), 0 \right], \tag{2.6}$$

where the Hall parameter m and A_1 are:

$$m = \frac{\sigma_f B_0}{e n_e}, A_1 = 1 + \frac{3(\frac{\sigma_{np}}{\sigma_f} - 1)\phi}{(\frac{\sigma_{np}}{\sigma_f} + 2) - (\frac{\sigma_{np}}{\sigma_f} - 1)\phi}. \tag{2.7}$$

Ohmic heating term can be described as

$$\frac{1}{\sigma_{nf}}\mathbf{J}.\mathbf{J} = \frac{A_1 \sigma_f B_0^2}{1 + (A_1 m)^2}(\bar{U}^2 + \bar{V}^2). \tag{2.8}$$

The Maxwell's model of thermal conductivity (K_{nf}) of nanofluid is:

$$\frac{K_{nf}}{K_f} = \frac{K_{np} + 2K_f - 2\phi(K_f - K_{np})}{K_{np} + 2K_f + \phi(K_f - K_{np})}. \tag{2.9}$$

The Brinkman's viscosity model is presented as:

$$\mu_{nf} = \frac{\mu_f}{(1-\phi)^{2.5}}, \tag{2.10}$$

where μ_f is the viscosity of fluid and assumed to vary with temperature as

$$\mu_w = \mu_0 e^{-\alpha(T - T_0)} = \mu_0 \left(1 - \alpha_0 (T - T_0)\right), \tag{2.11}$$

where second and higher terms are neglected as these are very small, μ_0 the viscosity of fluid at constant temperature and α an empirical constant for the viscosity. The parameter α_0 positive for liquid such as crude oil, benzene and water. Therefor μ_{nf} becomes:

$$\mu_{nf} = \frac{\mu_0 \left(1 - \alpha_0 (T - T_m)\right)}{(1-\phi)^{2.5}}. \tag{2.12}$$

The continuity, momentum and energy equations describing the current flow are explained through the expression:

$$\frac{\partial \bar{U}}{\partial \bar{X}} + \frac{\partial \bar{V}}{\partial \bar{Y}} = 0, \tag{2.13}$$

$$\begin{aligned} \rho_{nf}\left(\frac{\partial \bar{U}}{\partial \bar{t}} + \bar{U}\frac{\partial \bar{U}}{\partial \bar{X}} + \bar{V}\frac{\partial \bar{U}}{\partial \bar{Y}}\right) = -\frac{\partial \bar{P}}{\partial \bar{X}} + 2\frac{\partial}{\partial \bar{X}}\left(\mu_{nf}\frac{\partial \bar{U}}{\partial \bar{X}}\right) + \frac{\partial}{\partial \bar{Y}}\left(\mu_{nf}\left(\frac{\partial \bar{V}}{\partial \bar{X}} + \frac{\partial \bar{U}}{\partial \bar{Y}}\right)\right) \\ -\frac{A_1 \sigma_f B_0^2}{1 + (A_1 m)^2}\left(\bar{U} - A_1 m \bar{V}\right) + g(\rho\beta)_{nf}(T - T_m), \end{aligned} \tag{2.14}$$

$$\rho_{nf}\left(\frac{\partial \bar{V}}{\partial \bar{t}}+\bar{U}\frac{\partial \bar{V}}{\partial \bar{X}}+\bar{V}\frac{\partial \bar{V}}{\partial \bar{Y}}\right)=-\frac{\partial \bar{P}}{\partial \bar{Y}}+2\frac{\partial}{\partial \bar{Y}}\left(\mu_{nf}\frac{\partial \bar{V}}{\partial \bar{Y}}\right)+\frac{\partial}{\partial \bar{X}}\left(\mu_{nf}\left(\frac{\partial \bar{V}}{\partial \bar{X}}+\frac{\partial \bar{U}}{\partial \bar{Y}}\right)\right) -\frac{A_1\sigma_f B_0^2}{1+(A_1 m)^2}(\bar{V}+A_1 m\bar{U}), \tag{2.15}$$

$$(\rho C)_{nf}\left(\frac{\partial T}{\partial \bar{t}}+\bar{U}\frac{\partial T}{\partial \bar{X}}+\bar{V}\frac{\partial T}{\partial \bar{Y}}\right)=K_{nf}\left(\frac{\partial^2 T}{\partial \bar{X}^2}+\frac{\partial^2 T}{\partial \bar{Y}^2}\right)+\Phi +\mu_{nf}\left[2((\frac{\partial \bar{U}}{\partial \bar{X}})^2+(\frac{\partial \bar{V}}{\partial \bar{Y}})^2)+(\frac{\partial \bar{U}}{\partial \bar{Y}}+\frac{\partial \bar{V}}{\partial \bar{X}})^2\right]+\frac{A_1\sigma_f B_0^2}{1+(A_1 m)^2}\left(\bar{U}^2+\bar{V}^2\right). \tag{2.16}$$

In above equations g represents the acceleration due to gravity, T the temperature of fluid, $T_m\left(=\frac{T_0+T_1}{2}\right)$ the mean temperature, Φ denotes the dimensional heat generation/absorption and $\bar{P}(\bar{X},\bar{Y},\bar{t})$ the pressure. The density of nanofluid ρ_{nf} , heat capacity of nanofluid C_{nf} and thermal expansion parameter of nanofluid β_{nf} are describing through the following forms:

$$\rho_{nf}=(1-\phi)\rho_f+\phi\rho_{np},\ C_{nf}=(1-\phi)C_f+\phi C_{np}, \quad \beta_{nf}=(1-\phi)\beta_f+\phi\beta_{np}. \tag{2.17}$$

The thermophysical parameter of H_2O and Fe_3O_4 nanomaterials are presented via Table 2.1. The transformations between the fixed and moving frames are:

$$\bar{x}=\bar{X}-c\bar{t},\bar{y}=\bar{Y},\bar{u}=\bar{U}-c,\bar{v}=\bar{V},\bar{p}(\bar{x},\bar{y})=\bar{P}(\bar{X},\bar{Y},\bar{t}), \tag{2.18}$$

where $[\bar{u}(\bar{x},\bar{y}),\bar{v}(\bar{x},\bar{y}),0]$ and $\bar{p}(\bar{x},\bar{y})$ are the velocity and pressure component in the moving frame. According to above transformations, the relevant expressions become:

$$\frac{\partial \bar{u}}{\partial \bar{x}}+\frac{\partial \bar{v}}{\partial \bar{y}}=0, \tag{2.19}$$

$$\rho_{nf}\left((\bar{u}+c)\frac{\partial}{\partial \bar{x}}+\bar{v}\frac{\partial}{\partial \bar{y}}\right)(\bar{u}+c)=-\frac{\partial \bar{p}}{\partial \bar{x}}+2\frac{\partial}{\partial \bar{x}}\left(\mu_{nf}\frac{\partial \bar{u}}{\partial \bar{x}}\right)+\frac{\partial}{\partial \bar{y}}\left(\mu_{nf}\left(\frac{\partial \bar{v}}{\partial \bar{x}}+\frac{\partial \bar{u}}{\partial \bar{y}}\right)\right) -\frac{A_1\sigma_f B_0^2}{1+(A_1 m)^2}\left((\bar{u}+c)-A_1 m\bar{v}\right)+g\left(\rho\beta\right)_{nf}(T-T_m), \tag{2.20}$$

$$\rho_{nf}\left((\bar{u}+c)\frac{\partial}{\partial \bar{x}}+\bar{v}\frac{\partial}{\partial \bar{y}}\right)\bar{v}=-\frac{\partial \bar{p}}{\partial \bar{y}}+2\frac{\partial}{\partial \bar{y}}\left(\mu_{nf}\frac{\partial \bar{v}}{\partial \bar{y}}\right)+\frac{\partial}{\partial \bar{x}}\left(\mu_{nf}\left(\frac{\partial \bar{v}}{\partial \bar{x}}+\frac{\partial \bar{u}}{\partial \bar{y}}\right)\right) -\frac{A_1\sigma_f B_0^2}{1+(A_1 m)^2}\left(\bar{v}+A_1 m(\bar{u}+c)\right), \tag{2.21}$$

$$(\rho C)_{nf}\left((\bar{u}+c)\frac{\partial}{\partial \bar{x}}+\bar{v}\frac{\partial}{\partial \bar{y}}\right)T=K_{eff}\left(\frac{\partial^2 T}{\partial \bar{x}^2}+\frac{\partial^2 T}{\partial \bar{y}^2}\right)+\Phi$$
$$+\frac{\mu_{nf}}{(1-\phi)^{2.5}}\left[2\left(\left(\frac{\partial \bar{u}}{\partial \bar{x}}\right)^2+\left(\frac{\partial \bar{v}}{\partial \bar{y}}\right)^2\right)+\left(\frac{\partial \bar{u}}{\partial \bar{y}}+\frac{\partial \bar{v}}{\partial \bar{x}}\right)^2\right]+\frac{A_1\sigma_f B_0^2}{1+(A_1 m)^2}\left(\bar{u}^2+\bar{v}^2\right). \tag{2.22}$$

Peristaltic transport is studied under the assumption of small Reynolds number (inertial effects to be negligible) and large wavelength. In light of these approximations, nondimensional forms of Eqs. $(2.20)-(2.22)$ are given as:

$$\frac{\partial p}{\partial x}=\frac{1}{(1-\phi)^{2.5}}\frac{\partial}{\partial y}\left((1-\alpha\theta)\frac{\partial^2 \psi}{\partial y^2}\right)+S\theta-\frac{A_1 M^2}{1+(A_1 m)^2}\left(\frac{\partial \psi}{\partial y}+1\right), \tag{2.23}$$

$$\frac{\partial p}{\partial y}=0, \tag{2.24}$$

$$\frac{K_{nf}}{K_w}\frac{\partial^2 \theta}{\partial y^2}+\frac{Br\,(1-\alpha\theta)}{(1-\phi)^{2.5}}\left(\frac{\partial^2 \psi}{\partial y^2}\right)^2+\frac{Br A_1 M^2}{1+(A_1 m)^2}\left(\frac{\partial \psi}{\partial y}+1\right)^2+\varepsilon=0. \tag{2.25}$$

Continuity equation is uniformly satisfied by definition of stream function and Eq. (2.24) depicts that $p\neq p(y)$. In the above equations the following dimensionless parameters are used:

$$x=\frac{\bar{x}}{\lambda}, y=\frac{\bar{y}}{d_1}, u=\frac{\bar{u}}{c}, v=\frac{\bar{v}}{c\delta}, \delta=\frac{\bar{d}_1}{\lambda}, h_1=\frac{\bar{H}_1}{d_1}, h_2=\frac{\bar{H}_2}{d_1}, a=\frac{a_1}{d_1}, b=\frac{b_1}{d_1},$$
$$p=\frac{d_1^2\bar{p}}{c\lambda\mu_0}, Re=\frac{\rho_f c d_1}{\mu_0}, Ec=\frac{c^2}{C_f\,(T_1-T_0)}, Pr=\frac{\mu_0 C_f}{K_f}, M=\sqrt{\frac{\sigma_f}{\mu_0}}B_0 d_1, \alpha=\alpha_0(T_1-T_0)$$
$$Gr=\frac{\rho_f g\beta_f\,(T_1-T_0)\,d_1^2}{\mu_0 c}, \theta=\frac{T-T_m}{T_1-T_0}, Br=\Pr Ec, \varepsilon=\frac{d^2\Phi}{K_f\,(T_1-T_0)}, u=\frac{\partial \psi}{\partial y}, v=-\frac{\partial \psi}{\partial x}. \tag{2.26}$$

Here ψ represents the stream function, Re denotes Reynolds number, Br stands for Brinkman number, Ec denotes Eckert number, Pr stands for Prandtl number, M represents Hartman number, δ denotes wave number, θ stands for dimensionless temperature and ϵ represents dimensionless heat source/sink parameter. Here S appearing in above equations satisfies:

$$S=Gr\left\{1-\phi+\phi\left(\frac{(\rho\beta)_{np}}{(\rho\beta)_w}\right)\right\}. \tag{2.27}$$

Dimensionless flow rate in the fixed $\eta(=\bar{Q}/cd)$ and moving frame $F(=\bar{q}/cd)$ of reference are associated with this relation:

$$\eta=F+1+d. \tag{2.28}$$

Here $\bar{Q}$ and $\bar{q}$ are dimensional flow rates in the fixed and moving frames. Furthermore 'F' obeys:

$$F = \int_{h_1}^{h_2} \frac{\partial \psi}{\partial y} dy. \tag{2.29}$$

Velocity slip and temperature boundary conditions are given by:

$$\begin{aligned} \psi = \frac{F}{2}, \frac{\partial \psi}{\partial y} + \frac{\beta_1 (1 - \alpha\theta)}{(1-\phi)^{2.5}} \frac{\partial^2 \psi}{\partial y^2} = -1, \theta = -\frac{1}{2}, \text{ at } y = h_1, \\ \psi = -\frac{F}{2}, \frac{\partial \psi}{\partial y} - \frac{\beta_1 (1 - \alpha\theta)}{(1-\phi)^{2.5}} \frac{\partial^2 \psi}{\partial y^2} = -1, \theta = \frac{1}{2}, \text{ at } y = h_2. \end{aligned} \tag{2.30}$$

Here $h_1 = 1 + acos(2\pi x)$ and $h_2 = -d - bcos(2\pi x + \gamma)$ denote the dimensionless shape of peristaltic upper and lower walls respectively, β_1 represents the dimensionless velocity slip parameter. Here our purpose is to compute the Numerical solutions via NDSolve technique. Next section presents the analysis of the obtained results.

2.3 Discussion

Obtained numerical solutions are discussed in this section. This section provides the analysis of velocity, pressure gradient, temperature and heat transfer rate in detail subject to variations of the flow parameters.

2.3.1 Pressure gradient

Effects of nanoparticle volume fraction, Grashof number, Hartman number, Hall parameter and velocity slip parameter on pressure gradient are sketched in Figs. 2.1-2.5. Graph depicts that pressure gradient follow the oscillatory pattern due to peristaltic motion. Fig. 2.1 presents the pressure gradient corresponding to different values of the nanoparticle volume fraction. The pressure gradient decreases for the larger values of nanoparticles in the wider part of channel. Fig. 2.2 depicts the pressure gradient for various values of Grashof number. It can be seen from the fig. that pressure gradient is enhances for greater values of Grashoff number. Fig. 2.3 shows the pressure gradient for different values of Hartman number. Decaying behavior is noted in pressure gradient in the wider portion by enhancing the value of Hartman number. Fig. 2.4 presents the pressure gradient for various values of Hall parameter. Here the pressure

gradient slightly increases in the wider part and remains unperturbed in the occluded part of the channel by the variations in the hall parameter. Fig. 2.5 depicts that the pressure gradient is higher for larger values of temperature dependent viscosity parameter.

2.3.2 Velocity profile

Figs. 2.6-2.10 are plotted to examine the effects of different parameters on the velocity. These figs. depicts that for positive values of flow rate, velocity is higher near central portion of channel. Fig. 2.6 presents the axial velocity corresponding to different values of nanomaterial. Velocity profile shows decreasing behavior near the central portion by increasing the values of nanomaterial. This is due to the fact that an increment in the quantity of nanomaterial increases the effective viscosity of the nanofluid and consequently it reduces the ability of the fluid to move freely. Fig. 2.7 depicts the axial velocity for various values of Grashof number. We examined that the axial velocity is higher near the center of channel for larger values of Grashof number due to change in density. Fig. 2.8 shows the axial velocity for numerous values of Hartman number. For larger values of Hartman number fluid velocity decreases. Therefore magnetic field are used in injuries to control the bleeding process. Fig. 2.9 depicts the axial velocity for various values of Hall parameter. Here the axial velocity enhances for the higher values of Hall parameter. Physically the Hall effect balances the magnetic influence of applied magnetic field to some extent. Fig. 2.10 shows the axial velocity for different values of temperature dependent viscosity parameter. Axial velocity is enhanced near center of the channel and reverse situation is seen near the channel wall when we increase the value of "α" parameter.

2.3.3 Temperature profile

Fig. 2.11-2.15 present the effects of nanoparticle volume fraction, Grashof number, Hartman number, Hall parameter and temperature jump condition on the temperature profile. Fig. 2.11 presents that the temperature profile is lower for the larger values of the nanoparticles volume fraction. The addition of nanomaterials enhances the effective thermal conductivity of the nanofluid and as a result heat is transmitted more quickly therefore temperature decreases. This observation highlights the role of nanofluids as coolants in numerous applications. Effect

of Grashof number on temperature profile is sketched in Fig. 2.12. We observed that an enhancement in the Grashoff number increases the temperature throughout the channel. Fig. 2.13 shows the temperature profile corresponding to different values of Hartman number. Here the temperature profile increases for larger values of Hartman number. Effect of Hall number on the temperature field is explored via Fig. 2.14. Temperature field can be controlled by increasing the Hall parameter. Fig. 2.15 presents that the temperature profile is higher for the larger values of temperature dependent viscosity parameter. An increase in the temperature dependent viscosity parameter shows a decreasing behavior in temperature profile. Table 2.2 are prepared to analyze the effects of ϕ, Gr, M, m and α on the heat transfer rate. Table shows that heat transfer rate increase at the upper wall by increasing the percentage of nanomaterial in fluid, Grashof number, Hartman number and temperature dependent viscosity parameter. It also shows that heat transfer rate decrease by increasing hall parameter. However at the lower wall heat transfer rate show the opposite behavior.

2.4 Concluding remarks

Below mentioned points are the main findings.

- Viscosity of nanofluid is increased by the addition of nanomaterials in the base fluid. Therefore flow properties of nanofluid are decreased by addition of nanoparticles. Heat transfer characteristics of nanofluid are increased by the addition of nanoparticles due to their higher thermophysical properties.

- Pressure gradient depicts decaying behavior in the wider portion and increasing trend in the occluded portion of channel for nanofluid as compared to base material.

- In the presence of mixed convection, the pressure gradient, velocity profile, temperature and heat transfer rate are enhanced.

- By increasing Hartman number, the axial velocity decays but temperature increases. Hall parameter shows reverse behavior in the flow and heat transfer characteristics.

- Axial velocity is enhanced by increasing α parameter but temperature shows decreasing behavior.

Table 2.1: Numerical values of thermophysical properties [7]:

Properties	H_2O	Fe_3O_4
Density (kg/m^3)	997.1	5200
Thermal conductivity (W/mk)	0.613	80.6
Specific heat (j/kgK)	4179	670
Thermal expansion coefficient (1/k)10^{-6}	210	13
Electric conductivity (S/m)	0.05	25000

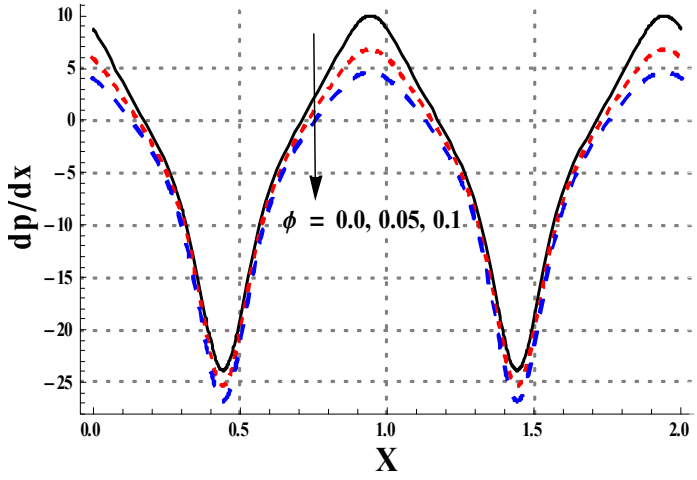

Fig. 2.1: Effects of ϕ on dp/px when $a = 0.8, b = 0.7, d = 0.7, \eta = 1.1, \gamma = \pi/4, Br = 0.2, \beta = 0.1, Gr = 3.0, M = 1.0, \alpha = 0.1, m = 0.5$ and $\varepsilon = 2.0$.

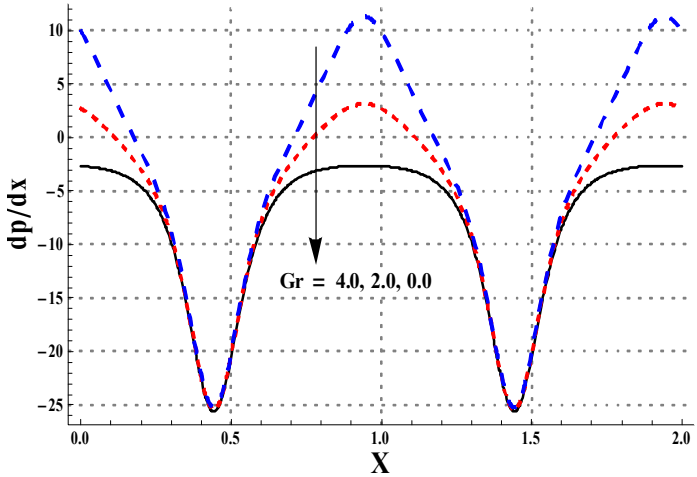

Fig. 2.2: Effects of Gr on dp/px when $a = 0.8, b = 0.7, d = 0.7, \eta = 1.1, \gamma = \pi/4, Br = 0.2, \beta = 0.1, \phi = 0.05, M = 1.0, \alpha = 0.1, m = 0.5$ and $\varepsilon = 2.0$.

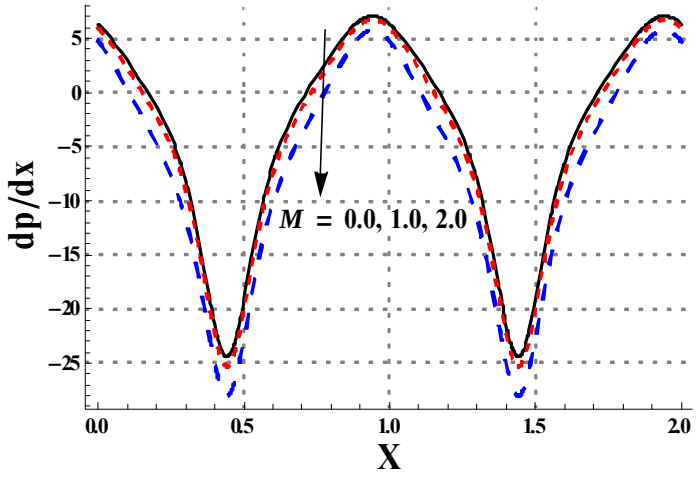

Fig. 2.3: Effects of M on dp/px when $a = 0.8, b = 0.7, d = 0.7, \eta = 1.1, \gamma = \pi/4, Br = 0.2, \beta = 0.1, Gr = 3.0, \phi = 0.05, \alpha = 0.1, m = 0.5$ and $\varepsilon = 2.0$.

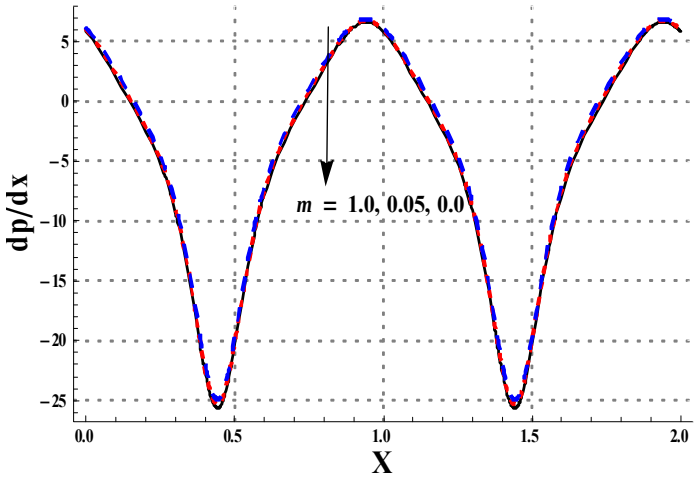

Fig. 2.4: Effects of m on dp/px when $a = 0.8, b = 0.7, d = 0.7, \eta = 1.1, \gamma = \pi/4, Br = 0.2, \beta = 0.1, Gr = 3.0, \phi = 0.05, M = 1.0, \alpha = 0.1$ and $\varepsilon = 2.0$.

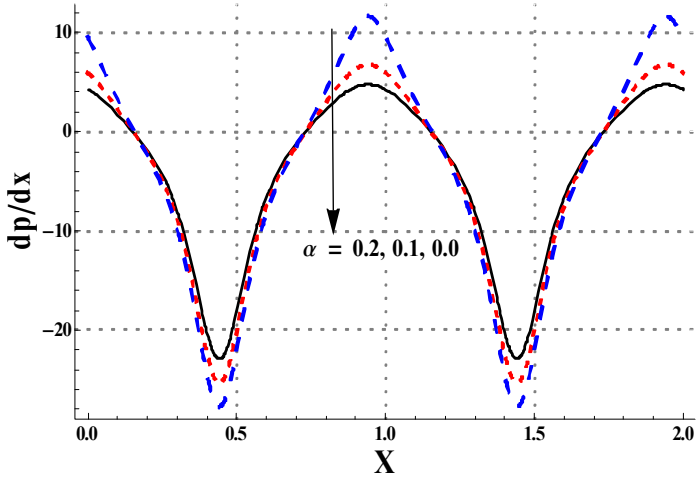

Fig. 2.5: Effects of α on dp/px when $a = 0.8, b = 0.7, d = 0.7, \eta = 1.1, \gamma = \pi/4, Br = 0.2, \beta = 0.1, Gr = 3.0, \phi = 0.05, M = 1.0, m = 0.5$ and $\varepsilon = 2.0$.

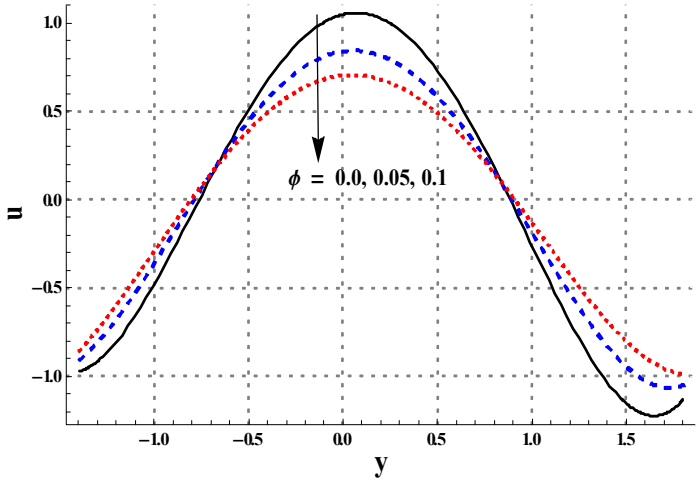

Fig. 2.6: Effects of ϕ on $\mathbf{u}$ when $a = 0.8, b = 0.7, d = 0.7, \eta = 1.1, x = 1.0, \gamma = \pi/4, Br = 0.2, \beta = 0.1, Gr = 3.0, M = 1.0, \alpha = 0.1, m = 0.5$ and $\varepsilon = 2.0$.

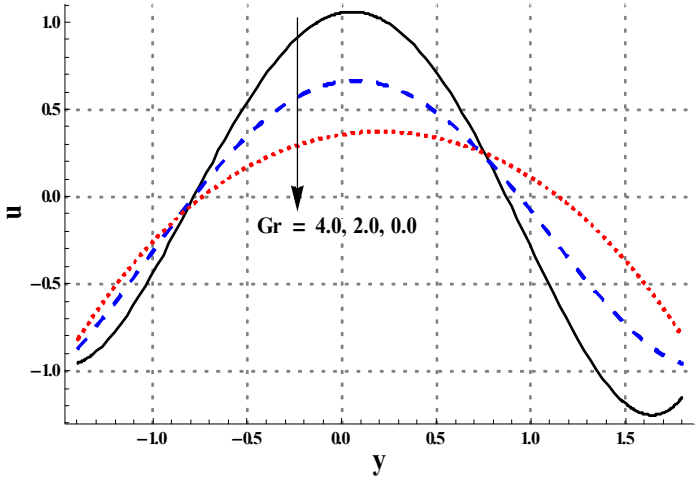

Fig. 2.7: Effects of Gr on $\mathbf{u}$ when $a = 0.8, b = 0.7, d = 0.7, \eta = 1.1, x = 1.0, \gamma = \pi/4, Br = 0.2, \beta = 0.1, \phi = 0.05, M = 1.0, \alpha = 0.1, m = 0.5$ and $\varepsilon = 2.0$.

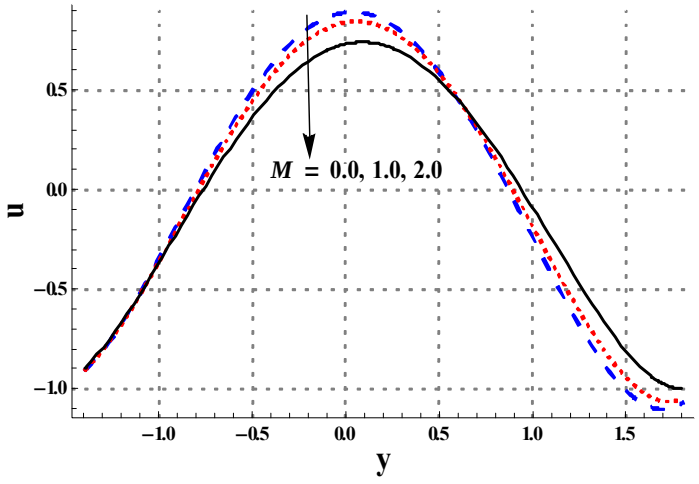

Fig. 2.8: Effects of M on $\mathbf{u}$ when $a = 0.8, b = 0.7, d = 0.7, \eta = 1.1, x = 1.0, \gamma = \pi/4, Br = 0.2, \beta = 0.1, Gr = 3.0, \phi = 0.05, \alpha = 0.1, m = 0.5$ and $\varepsilon = 2.0$.

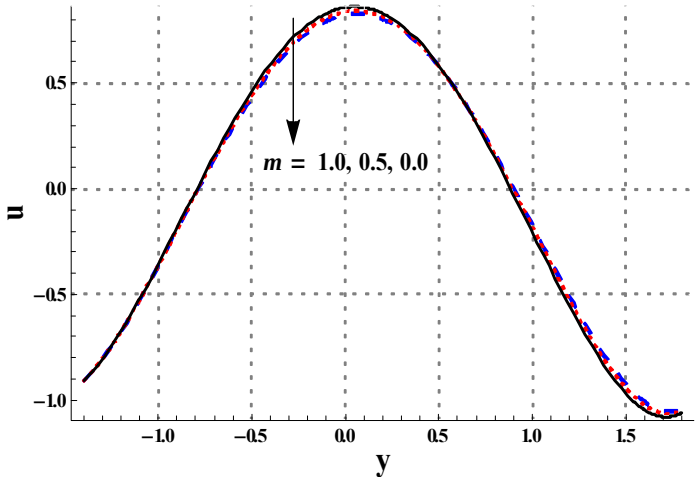

Fig. 2.9: Effects of m on $\mathbf{u}$ when $a = 0.8, b = 0.7, d = 0.7, \eta = 1.1, x = 1.0, \gamma = \pi/4, Br = 0.2, \beta = 0.1, Gr = 3.0, \phi = 0.05, M = 1.0, \alpha = 0.1$ and $\varepsilon = 2.0$.

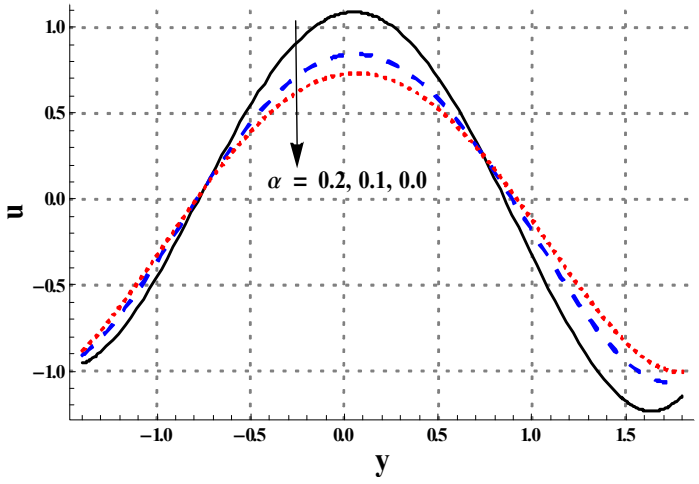

Fig. 2.10: Effects of α on $\mathbf{u}$ when $a = 0.8, b = 0.7, d = 0.7, \eta = 1.1, x = 1.0, \gamma = \pi/4, Br = 0.2, \beta = 0.1, Gr = 3.0, \phi = 0.05, M = 1.0, m = 0.5$ and $\varepsilon = 2.0$.

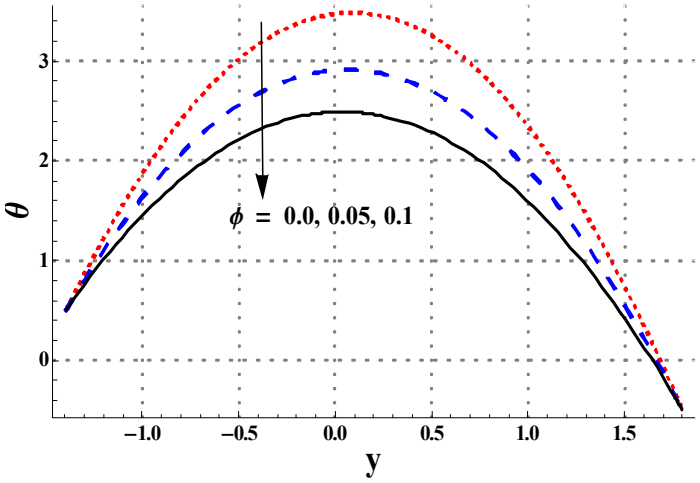

Fig. 2.11: Effects of ϕ on $\boldsymbol{\theta}$ when $a = 0.8, b = 0.7, d = 0.7, \eta = 1.1, x = 1.0, \gamma = \pi/4, Br = 0.2, \beta = 0.1, Gr = 3.0, M = 1.0, \alpha = 0.1, m = 0.5$ and $\varepsilon = 2.0$.

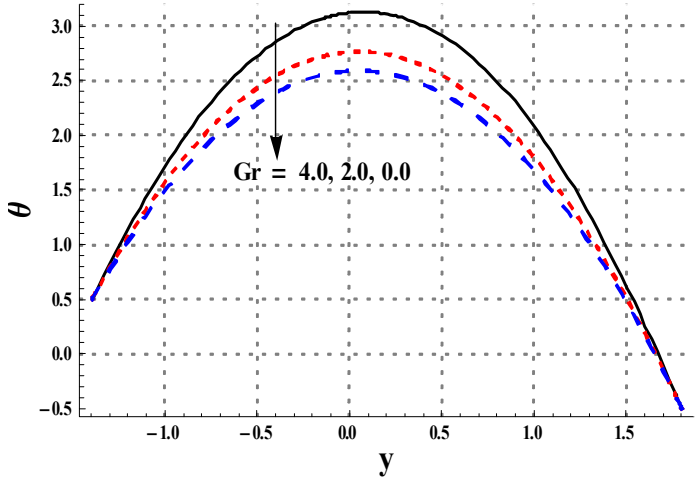

Fig. 2.12: Effects of Gr on $\boldsymbol{\theta}$ when $a = 0.8, b = 0.7, d = 0.7, \eta = 1.1, x = 1.0, \gamma = \pi/4, Br = 0.2, \beta = 0.1, \phi = 0.05, M = 1.0, \alpha = 0.1, m = 0.5$ and $\varepsilon = 2.0$.

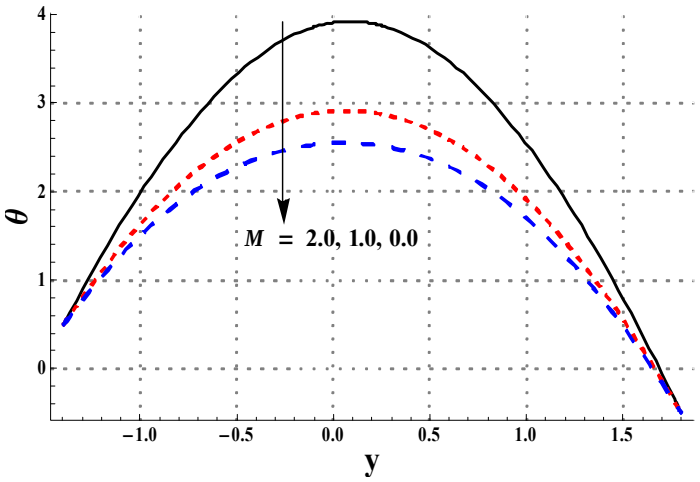

Fig. 2.13: Effects of M on $\boldsymbol{\theta}$ when $a = 0.8, b = 0.7, d = 0.7, \eta = 1.1, x = 1.0, \gamma = \pi/4, Br = 0.2, \beta = 0.1, Gr = 3.0, \phi = 0.05, \alpha = 0.1, m = 0.5$ and $\varepsilon = 2.0$.

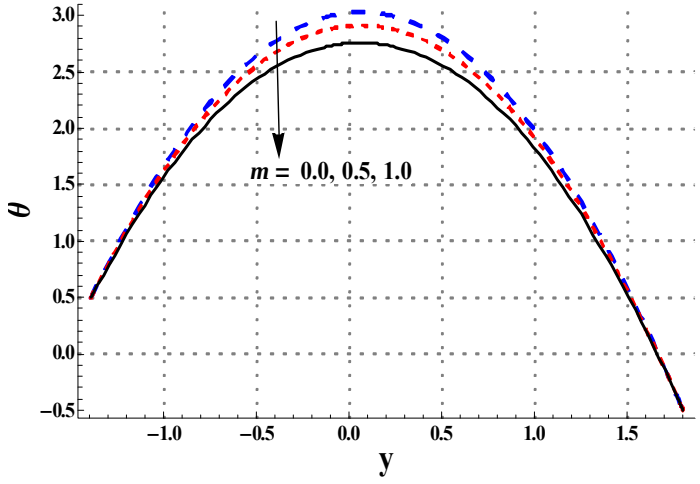

Fig. 2.14: Effects of m on $\boldsymbol{\theta}$ when $a = 0.8, b = 0.7, d = 0.7, \eta = 1.1, x = 1.0, \gamma = \pi/4, Br = 0.2, \beta = 0.1, Gr = 3.0, \phi = 0.05, M = 1.0, \alpha = 0.1$ and $\varepsilon = 2.0$.

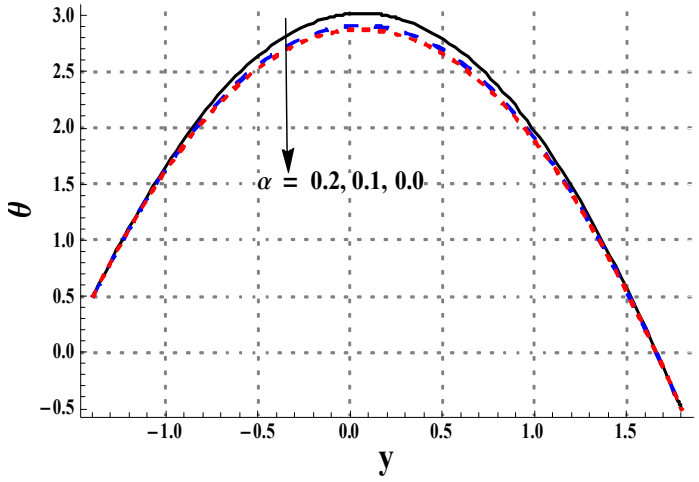

Fig. 2.15: Effects of α on $\boldsymbol{\theta}$ when $a = 0.8, b = 0.7, d = 0.7, \eta = 1.1, x = 1.0, \gamma = \pi/4, Br = 0.2, \beta = 0.1, Gr = 3.0, \phi = 0.05, M = 1.0, m = 0.5$ and $\varepsilon = 2.0$.

Table 2.2: Numerical values of heat transfer rate at the wall for variations in different embedded parameters when $a = 0.8, b = 0.7, d = 0.7, \eta = 1.1, x = 1.0, \gamma = \pi/4, Br = 0.2, \beta =$

0.1 and $\varepsilon = 2.0$.

ϕ	Gr	M	m	α	$-\frac{K_{eff}}{K_f}\theta'(h_1)$	$\frac{K_{eff}}{K_f}\theta'(h_2)$
0.00	3.0	1.0	0.5	0.1	4.44762	3.89810
0.10					4.35749	3.67321
0.20					4.47668	3.53368
0.05	0.0				4.12722	3.39170
	2.0				4.20478	3.59434
	4.0				4.63435	4.00174
	3.0	0.0			4.04987	3.38649
		1.0			4.35578	3.76011
		2.0			5.27973	4.80683
		1.0	0.0		4.45886	3.88171
			0.5		4.35578	3.76011
			1.0		4.22397	3.60181
			0.5	0.0	4.33763	3.74897
				0.1	4.35578	3.76011
				0.2	4.46124	3.83744

Chapter 3

Peristasis of nanofluid subject to variable viscosity and porosity

This chapter highlights impact of magnetic force on peristaltic transport of nanofluid via symmetric channel and porous medium. Furthermore the velocity slip and thermal slip effects are incorporated. Maxwell's model of effective thermal conductivity has been used. The resulting non-dimensional coupled equations are solved numerically. The physical characteristics of important variables are discussed through graphs and table.

3.1 Modeling

Consider the peristaltic transport of nanofluid in a symmetric inclined channel of width $2d$ and angle 'ω'. An incompressible nanofluid comprises copper nanoparticles suspended in water. Channel walls have non-variable temperature T_0. Heat source/sink parameter Φ is also considered. Cartesian coordinates are selected in such a manner that the $\bar{X} - axis$ lies across the length of the channel whereas $\bar{Y} - axis$ perpendicular to it. The flow is generated due to peristaltic waves moving along the channel boundaries. Sinusoidal waves propagate with amplitude a_1, wavelength λ and speed c. Wall shape is:

$$\pm\bar{H}(\bar{X},\bar{t}) = \pm d \pm a_1 cos(\frac{2\pi}{\lambda}(\bar{X} - c\bar{t})), \tag{3.1}$$

in which + and − signs depict the upper and lower walls, respectively. The fluid is electrically conducting in the existence of an inclined magnetic field with non-variable strength B_0. The density of nanofluid ρ_{nf}, heat capacity of nanofluid C_{nf}, thermal conductivity of nanofluid K_{nf} and electrical conductivity of nanofluid σ_{nf} are defined as:

$$\begin{gathered}
\rho_{nf} = (1-\phi)\rho_f + \phi\rho_{np}, \\
C_{nf} = (1-\phi)C_f + \phi C_{np}, \\
\frac{K_{nf}}{K_f} = \frac{K_{np} + 2K_f - 2\phi(K_f - K_{np})}{K_{np} + 2K_f + \phi(K_f - K_{np})}, \\
\frac{\sigma_{nf}}{\sigma_f} = 1 + \frac{3(\frac{\sigma_{np}}{\sigma_f} - 1)\phi}{(\frac{\sigma_{np}}{\sigma_f} + 2) - (\frac{\sigma_{np}}{\sigma_f} - 1)\phi}.
\end{gathered} \tag{3.2}$$

Mathematically Brinkman's viscosity model is defined as:

$$\mu_{nf} = \frac{\mu_f}{(1-\phi)^{2.5}}, \tag{3.3}$$

where μ_f is the viscosity of ordinary liquid and ϕ depicts the quantity of nanomaterial. It is further assumed that the viscosity of the ordinary liquid changes with temperature as:

$$\mu_f = \mu_0 e^{-\alpha_0(T-T_0)} = \mu_0(1 - \alpha_0(T - T_0)), \tag{3.4}$$

Therefore viscosity of the nanofluid becomes:

$$\mu_{nf} = \frac{\mu_0(1 - \alpha_0(T - T_0))}{(1-\phi)^{2.5}}, \tag{3.5}$$

here T, μ_0 and α_0 represent the fluid temperature, constant viscosity of water and variable viscosity coefficient. Appropriate velocity field and pressure for this problem are $\bar{V} = [U(\bar{X}, \bar{Y}, \bar{t}), V(\bar{X}, \bar{Y}, \bar{t}), 0]$ and $\bar{P}(\bar{X}, \bar{Y}, \bar{t})$ respectively. Related expressions satisfy:

$$\frac{\partial \bar{U}}{\partial \bar{X}} + \frac{\partial \bar{V}}{\partial \bar{Y}} = 0, \tag{3.6}$$

$$\begin{gathered}
\rho_{nf}\left(\frac{\partial \bar{U}}{\partial \bar{t}} + \bar{U}\frac{\partial \bar{U}}{\partial \bar{X}} + \bar{V}\frac{\partial \bar{U}}{\partial \bar{Y}}\right) = -\frac{\partial \bar{P}}{\partial \bar{X}} + 2\frac{\partial}{\partial \bar{X}}\left(\mu_{nf}\frac{\partial \bar{U}}{\partial \bar{X}}\right) + \frac{\partial}{\partial \bar{Y}}\left(\mu_{nf}\left(\frac{\partial \bar{V}}{\partial \bar{X}} + \frac{\partial \bar{U}}{\partial \bar{Y}}\right)\right) \\
-\sigma_{nf}B_0^2\cos\varphi(\bar{U}\cos\varphi - \bar{V}\sin\varphi) + g(\rho\beta)_{nf}(T - T_0)\sin\omega - \frac{\mu_{nf}\bar{U}}{k_1(\bar{y})},
\end{gathered} \tag{3.7}$$

$$\rho_{nf}\left(\frac{\partial \bar{V}}{\partial \bar{t}}+\bar{U}\frac{\partial \bar{V}}{\partial \bar{X}}+\bar{V}\frac{\partial \bar{V}}{\partial \bar{Y}}\right)=-\frac{\partial \bar{P}}{\partial \bar{Y}}+2\frac{\partial}{\partial \bar{Y}}\left(\mu_{nf}\frac{\partial \bar{V}}{\partial \bar{Y}}\right)+\frac{\partial}{\partial \bar{X}}\left(\mu_{nf}\left(\frac{\partial \bar{V}}{\partial \bar{X}}+\frac{\partial \bar{U}}{\partial \bar{Y}}\right)\right)$$
$$-\sigma_{nf}B_0^2\sin\varphi(\bar{U}\cos\varphi-\bar{V}\sin\varphi)-g(\rho\beta)_{nf}(T-T_0)\cos\omega-\frac{\mu_{nf}\bar{V}}{k_1(\bar{y})}, \tag{3.8}$$

$$(\rho C)_{nf}\left(\frac{\partial T}{\partial \bar{t}}+\bar{U}\frac{\partial T}{\partial \bar{X}}+\bar{V}\frac{\partial T}{\partial \bar{Y}}\right)=K_{nf}\left(\frac{\partial^2 T}{\partial \bar{X}^2}+\frac{\partial^2 T}{\partial \bar{Y}^2}\right)+\Phi$$
$$+\mu_{nf}\left[2((\frac{\partial \bar{U}}{\partial \bar{X}})^2+(\frac{\partial \bar{V}}{\partial \bar{Y}})^2)+(\frac{\partial \bar{U}}{\partial \bar{Y}}+\frac{\partial \bar{V}}{\partial \bar{X}})^2\right]+\sigma_{nf}B_0^2(\bar{U}\cos\varphi-\bar{V}\sin\varphi)^2+\frac{\mu_{nf}\bar{U}^2}{k_1(\bar{y})}. \tag{3.9}$$

Here g represents the acceleration due to gravity, k_1 the permeability of the porous medium and φ the inclination of the applied magnetic field. The transformations between fixed and moving frames are described as follows:

$$\bar{x}=\bar{X}-c\bar{t},\bar{y}=\bar{Y},\bar{u}=\bar{U}-c,\bar{v}=\bar{V},\bar{p}(\bar{x},\bar{y})=\bar{P}(\bar{X},\bar{Y},\bar{t}), \tag{3.10}$$

where ($\bar{u}$,$\bar{v}$) and $\bar{p}$ are the velocity field and pressure in the moving frame ($\bar{x}$, $\bar{y}$). By using these transformation the governing equations are reduced in the wave frame. Further in light of long wavelength and small Reynolds number estimations, non-dimensional forms of Eqs. (3.7)$-$(3.9) are illustrated in terms of stream function ψ :

$$\frac{\partial p}{\partial x}=\frac{1}{(1-\phi)^{2.5}}\frac{\partial}{\partial y}\left((1-\alpha\theta)\frac{\partial^2\psi}{\partial y^2}\right)+A_2Gr\theta\sin\omega-\left(A_1M^2\cos^2\varphi+\frac{(1-\alpha\theta)}{k(y)(1-\phi)^{2.5}}\right)\left(\frac{\partial\psi}{\partial y}+1\right), \tag{3.11}$$

$$\frac{\partial p}{\partial y}=0, \tag{3.12}$$

$$A_3\frac{\partial^2\theta}{\partial y^2}+\frac{Br(1-\alpha\theta)}{(1-\phi)^{2.5}}\left(\frac{\partial^2\psi}{\partial y^2}\right)^2+Br\left(A_1M^2\cos^2\varphi+\frac{(1-\alpha\theta)}{k(y)(1-\phi)^{2.5}}\right)\left(\frac{\partial\psi}{\partial y}+1\right)^2+\varepsilon=0. \tag{3.13}$$

Continuity equation is identically fulfilled and Eq. (3.12) depicts that $p\neq p(y)$. The dimensionless quantities are presented as:

$$x=\frac{\bar{x}}{\lambda},y=\frac{\bar{y}}{d},u=\frac{\bar{u}}{c},v=\frac{\bar{v}}{c\delta},\delta=\frac{\bar{d}}{\lambda},h=\frac{\bar{H}}{d},a=\frac{a_1}{d},p=\frac{d^2\bar{p}}{c\lambda\mu_f},$$
$$Re=\frac{\rho_f cd}{\mu_f},Ec=\frac{c^2}{C_fT_0},Pr=\frac{\mu_fC_f}{K_f},M=\sqrt{\frac{\sigma_f}{\mu_f}}B_0d,\alpha=\alpha_0T_0,k(y)=\frac{k_1(\bar{y})}{d^2}, \tag{3.14}$$
$$Gr=\frac{\rho_fg\beta_fT_0d^2}{\mu_fc},\theta=\frac{T-T_0}{T_0},Br=\Pr Ec,\varepsilon=\frac{d^2\Phi}{T_0K_f},u=\frac{\partial\psi}{\partial y},v=-\frac{\partial\psi}{\partial x}.$$

Here Pr denotes the Prandtl number, M the Hartman number, Re the Reynolds number, Br the Brinkman number, Ec the Eckert number, δ the wave number, θ the non-dimensional temperature and ϵ represents the non-dimensional heat sink/source parameter. Further $A_1,\ A_2$ and A_3 are the following relations:

$$A_1 = 1 + \frac{3(\frac{\sigma_{np}}{\sigma_w} - 1)\phi}{(\frac{\sigma_{np}}{\sigma_w} + 2) - (\frac{\sigma_{np}}{\sigma_w} - 1)\phi}, \tag{3.15}$$

$$A_2 = \left\{1 - \phi + \phi\left(\frac{(\rho\beta)_{np}}{(\rho\beta)_w}\right)\right\}, \tag{3.16}$$

$$A_3 = \frac{K_{np} + 2K_w - 2\phi(K_w - K_{np})}{K_{np} + 2K_w + \phi(K_w - K_{np})}. \tag{3.17}$$

The permeability of medium is expressed as:

$$k(y) = \frac{d_p^2\zeta^2}{150(1-\zeta)^2}, \tag{3.18}$$

here d_p depicts the pore diameter and variable porosity (ζ) is given as:

$$\zeta = C_0\left(1 + C_1\exp(-\frac{C_2 y}{d_p})\right).$$

The values of C_0, C_1 and C_2 are taken to be $0.37, 1.0$ and 2. The non-dimensional flow rates in the fixed $\eta(=\bar{Q}/cd)$ and moving frames $F(=\bar{q}/cd)$ of reference are associated with this relation:

$$\eta = F + 1. \tag{3.19}$$

Here $\bar{Q}$ and $\bar{q}$ are dimensional flow rates in the fixed and moving frames respectively. Moreover 'F' has the expression:

$$F = \int_0^h \frac{\partial\psi}{\partial y}dy. \tag{3.20}$$

The boundary conditions for the current flow configuration are:

$$\begin{aligned} \psi = 0, \frac{\partial^2 \psi}{\partial y^2} = 0, \frac{\partial \theta}{\partial y} = 0, \text{ at } y = 0, \\ \psi = F, \frac{\partial \psi}{\partial y} + \frac{\beta_1 (1 - \alpha\theta)}{(1-\phi)^{2.5}} \frac{\partial^2 \psi}{\partial y^2} = -1, \theta + \gamma \frac{\partial \theta}{\partial y} = 0, \text{ at } y = h. \end{aligned} \tag{3.21}$$

Here $h = 1 + acos(2\pi x)$ depicts the peristaltic walls, γ stand for thermal slip and β_1 velocity slip parameters. The system of equations subject to boundary conditions are numerically solved. Graphical inspection of the numerical data is described in the upcoming portion.

3.2 Discussion

Graphical analysis of different parameters on temperature profile, axial velocity and pressure gradient are presented. The impact of different variables on the heat transfer coefficients are also discussed via Table 3.2.

3.2.1 Flow behavior

Figs. $(3.1) - (3.5)$ represent the behavior of axial velocity for distinct values of ϕ, M, Gr, α and d_p. Nanoparticles volume fraction on velocity is shown in Fig. 3.1. It represents a considerable reduction in the velocity due to increment in ϕ. Because presence of nanoparticles create more resistance in the fluid flow. Fig. 3.2 represents the influence of Hartman number on axial velocity. Fluid velocity decays by magnetic field strength because Lorentz force act as the resistive force. The physical effect of Grashof number on the axial velocity is seen in the Fig. 3.3. Axial velocity enhances by increasing the mixed convection effect. It depicts that change in density due to the temperature variation lubricate the fluid motion. Fig. 3.4 depicts impact of variable viscosity parameter on velocity. It indicates that velocity profile is higher for larger α. When temperature dependent viscosity parameter increases then the resistance of fluid flow decreases and as a result moving speed of fluid flow increases. Increasing the value of pore diameter enhances the axial velocity (see Fig. 3.5). Effect of silver nanoparticle, Grashof number, Hartman number, temperature dependent viscosity and pore diameter on the pressure gradient are examined via Figs. $(3.6) - (3.10)$. These graphs predict the oscillatory nature of pressure gradient. Pressure gradient increases in wider portion and decreases in the occluded

portion of channel by increasing the nanomaterials quantity (see Fig. 3.6). Fig. 3.7 depicts that by increasing the Grashof number the pressure gradient increases. Pressure gradient shows increasing behavior in the extensive part of channel. Fig. 3.8 shows that presence of Hartman number slightly decreases the pressure gradient. An enhancement in "α" and "d_p" yields elevated behavior of pressure gradient in the channel (see Fig. 3.9 & 3.10).

3.2.2 Heat transfer analysis

Fig. 3.11 represents outcome of axial velocity for various values of nanomaterial volume fraction. This Fig. represents the notable reduction in the temperature field by higher amount of nanoparticles. Further temperature of base liquid is higher than nanofluid. This analysis highlights the value of nanofluid as a coolant agent in several industrial applications. Fig. 3.12 represents the rise in temperature of nanofluid by increasing the "M" factor. Fig. 3.13 indicates that temperature field of nanofluid enhances for larger Grashof number. Effect of α on temperature is studied through Fig. 3.14. When variable viscosity parameter increases then temperature profile slightly decreases. Effect of pore diameter on temperature is studied through Fig. 3.15. Temperature profile decreases for increasing value of pore diameter.

Effects of ϕ, M, Gr, α, γ, φ, d_p and ω on the heat transfer rate are studied via Table 3.2. Inclusion of nanoparticles produces higher heat transfer rate because nanoparticles have higher thermal conductivity. Therefore nanoparticles facilitate the heat transfer between the solid boundary and liquid. Grashof number has high impact on heat transport phenomena. However heat transport rate enhances for larger Grashof number and channel inclination of angle. Slight increase in the heat transport rate at wall is found when 'M' enhances. Minor decrease in heat transport process is seen for large φ, γ and α variables. The size of pore diameter show an interesting change of heat transport phenomena. When $d_p = 3$ the heat transport rate is enlarge but for $d_p > 3$ the heat transport rate slightly decreased .

3.3 Concluding remarks

Influence of silver nanoparticles on fluid is studied in the presence of inclined MHD, variable porosity and temperature dependent viscosity. Key finding of this study are described below:

- Nanofluids play an important role in comparison to base fluid in the cooling performance. Infact it enhances the heat transport process at the wall and as a result the temperature reduces.
- An increment in the nanomaterial quantity causes reduction in axial velocity for larger resistance. Further presence of nanoparticles also reduces the pressure gradient.
- Higher Hartman number slow down the flow rate. Presence of MHD enhances the temperature profile.
- In the presence of mixed convection the fluid velocity and temperature increases.
- It is observed that pressure gradient enhances when Grashoff number increases. Such enhancement is prominent in the extensive part of channel.
- Variable viscosity parameter increases the velocity of nanofluid. However it reduces the temperature of nanofluid.
- Heat transport rate depicts the decreasing trend for larger α, γ, φ and d_p.
- An enhancement in heat transport rate is noted for larger Gr, M and ω.

3.4 Graphs and tables

Table 3.1: Numerical values of the thermophysical properties [7]:

Phase	$\rho(kg/m^3)$	$K(W/mK)$	$C(J/kgK)$	$\beta(1/k) \times 10^{-6}$	$\sigma(S/m)$
Water	997.1	0.613	4179	210	0.05
Silver (Ag)	10500	429	235	18.9	6.3×10^7

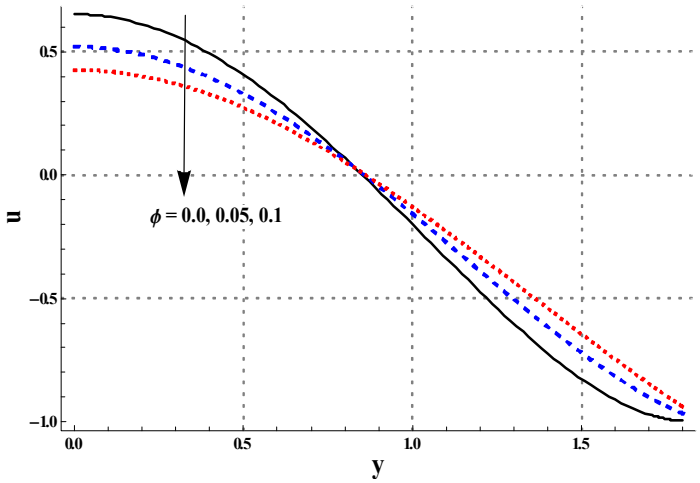

Fig. 3.1: Illustrations of the velocity for different values of nanoparticle volume fraction when $\alpha = 0.05, M = 1.0,\ Gr = 3.0, \varphi = \frac{\pi}{4}, \omega = \frac{\pi}{4}, a = 0.8,\ \eta = 0.8, x = 1.0,\ Br = 0.2,\ d_p = 5, \gamma = 0.05,\ \beta = 0.05$ and $\varepsilon = 2.0$.

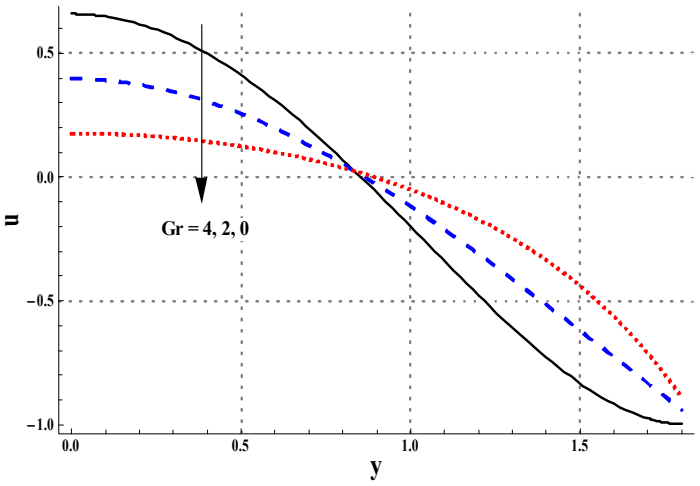

Fig. 3.2: Illustrations of the velocity for different Grashoff number when $\alpha = 0.05, M = 1.0,\ \phi = 0.05, \varphi = \frac{\pi}{4}, \omega = \frac{\pi}{4}, a = 0.8,\ \eta = 0.8, x = 1.0,\ Br = 0.2,\ d_p = 5, \gamma = 0.05,\ \beta = 0.05$ and

$\varepsilon = 2.0$.

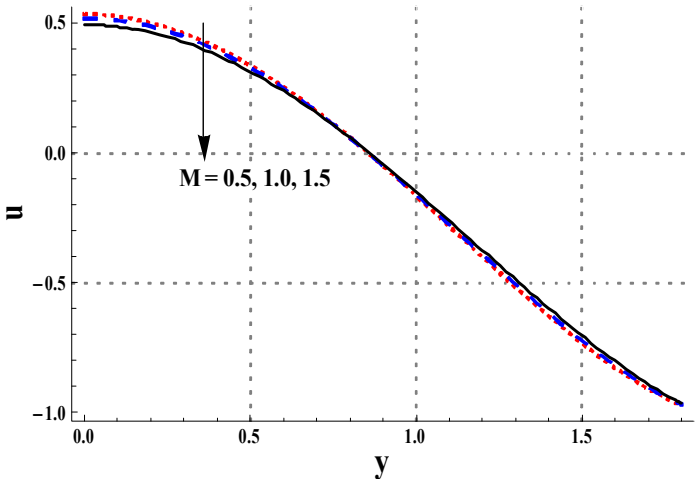

Fig. 3.3: Illustrations of the velocity for different Hartman number when $\alpha = 0.05, Gr = 3.0$, $\phi = 0.05, \varphi = \frac{\pi}{4}, \omega = \frac{\pi}{4}, a = 0.8$, $\eta = 0.8, x = 1.0$, $Br = 0.2$, $d_p = 5, \gamma = 0.05$, $\beta = 0.05$ and $\varepsilon = 2.0$.

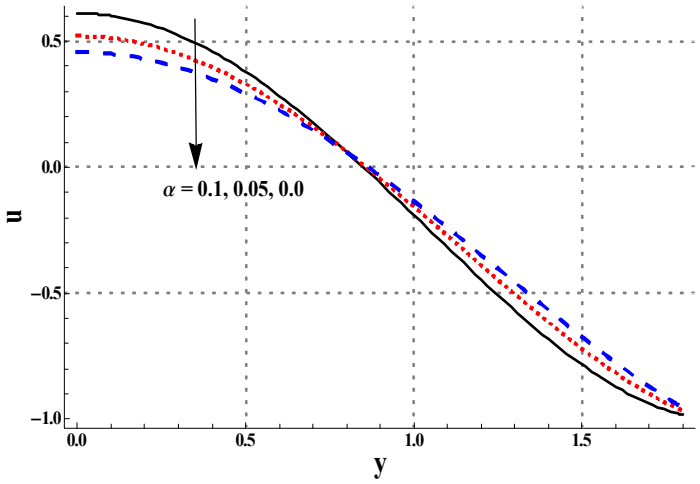

Fig. 3.4: Illustrations of velocity for different variable viscosity parameter when $M = 1.0, Gr = 3.0$, $\phi = 0.05, \varphi = \frac{\pi}{4}, \omega = \frac{\pi}{4}, a = 0.8$, $\eta = 0.8, x = 1.0$, $Br = 0.2$, $d_p = 5, \gamma = 0.05$, $\beta = 0.05$ and

$\varepsilon = 2.0$.

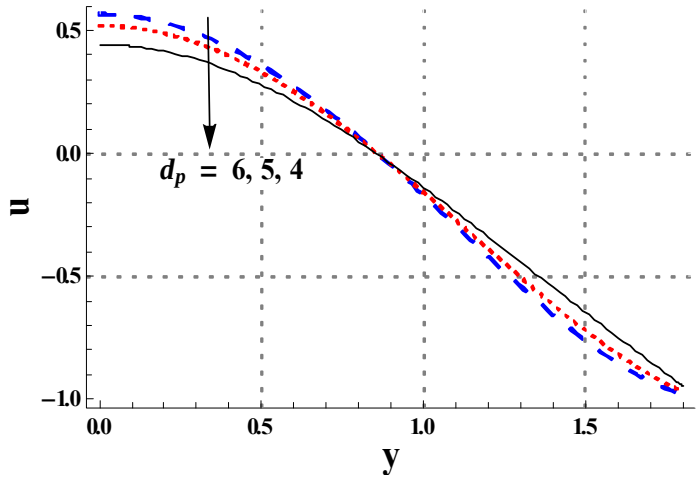

Fig. 3.5: Illustrations of the velocity for different pore diameter parameter when $M = 1.0, Gr = 3.0$, $\phi = 0.05, \varphi = \frac{\pi}{4}, \omega = \frac{\pi}{4}, a = 0.8$, $\eta = 0.8, x = 1.0$, $Br = 0.2$, $\alpha = 0.05, \gamma = 0.05$, $\beta = 0.05$ and $\varepsilon = 2.0$.

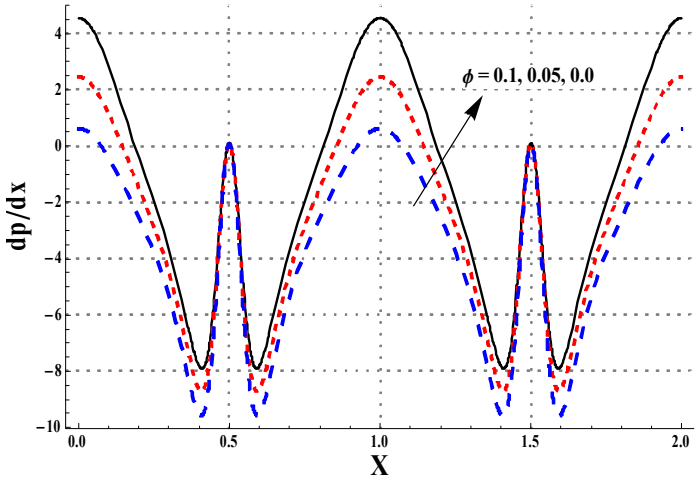

Fig. 3.6: Illustrations of the dp/dx for different nanoparticle volume fraction when $\alpha = 0.05, M = 1.0$, $Gr = 3.0, \varphi = \frac{\pi}{4}, \omega = \frac{\pi}{4}, a = 0.8$, $\eta = 0.8, x = 1.0$, $Br = 0.2$, $d_p = 5, \gamma = 0.05$,

$\beta = 0.05$ and $\varepsilon = 2.0$.

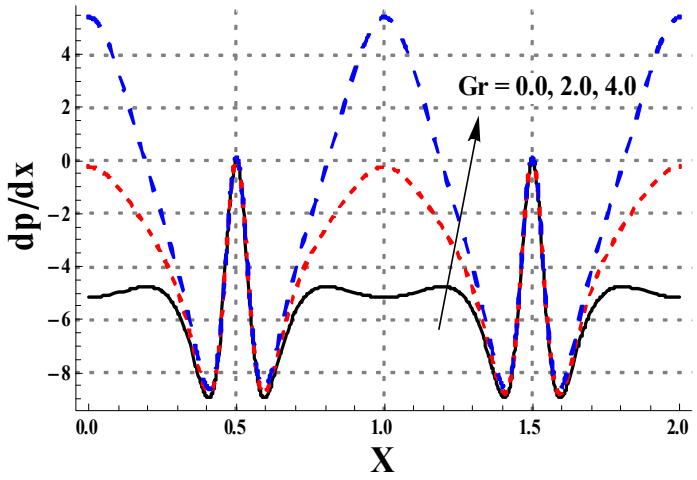

Fig. 3.7: Illustrations of dp/dx for Grashoff number when $\alpha = 0.05, M = 1.0$, $\phi = 0.05, \varphi = \frac{\pi}{4}, \omega = \frac{\pi}{4}, a = 0.8$, $\eta = 0.8, x = 1.0$, $Br = 0.2$, $d_p = 5, \gamma = 0.05$, $\beta = 0.05$ and $\varepsilon = 2.0$.

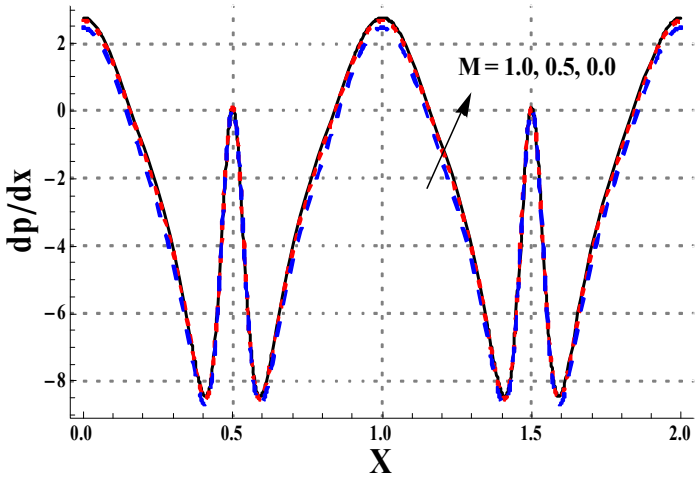

Fig. 3.8: Illustrations of dp/dx for Hartman number when $\alpha = 0.05, Gr = 3.0$, $\phi = 0.05, \varphi = \frac{\pi}{4}, \omega = \frac{\pi}{4}, a = 0.8$, $\eta = 0.8, x = 1.0$, $Br = 0.2$, $d_p = 5, \gamma = 0.05$, $\beta = 0.05$ and $\varepsilon = 2.0$.

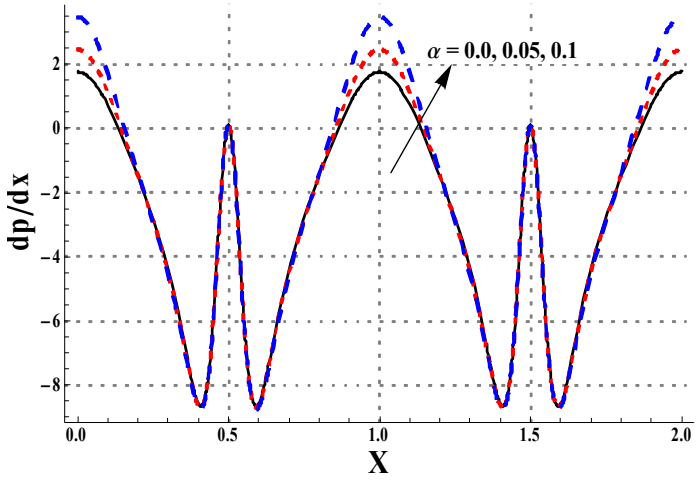

Fig. 3.9: Illustrations of dp/dx for variable viscosity parameter when $M = 1.0, Gr = 3.0$, $\phi = 0.05, \varphi = \frac{\pi}{4}, \omega = \frac{\pi}{4}, a = 0.8$, $\eta = 0.8, x = 1.0$, $Br = 0.2$, $d_p = 5, \gamma = 0.05$, $\beta = 0.05$ and $\varepsilon = 2.0$.

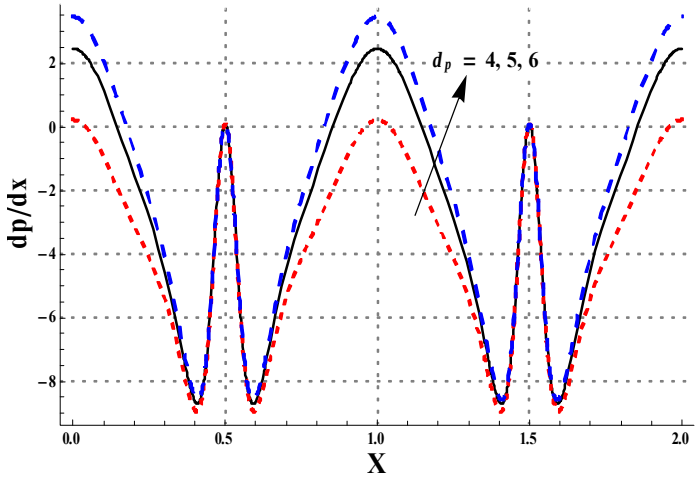

Fig. 3.10: Illustrations of dp/dx for pore diameter when $M = 1.0, Gr = 3.0$, $\phi = 0.05, \varphi = \frac{\pi}{4}, \omega = \frac{\pi}{4}, a = 0.8$, $\eta = 0.8, x = 1.0$, $Br = 0.2$, $d_p = 5, \gamma = 0.05$, $\beta = 0.05$ and $\varepsilon = 2.0$.

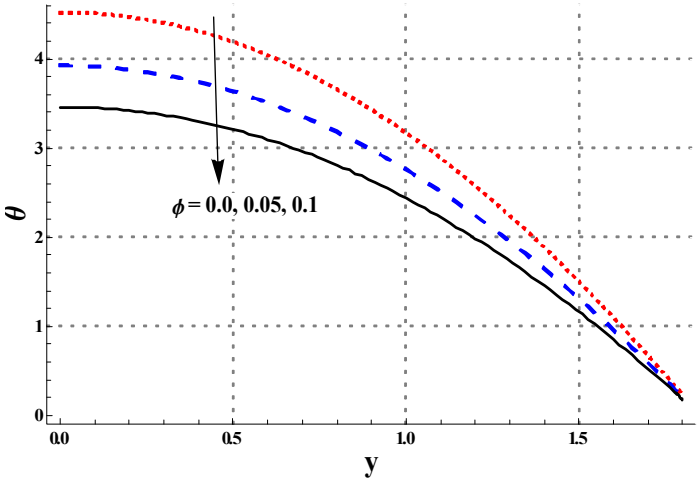

Fig. 3.11: Illustrations of temperature for nanoparticle volume fraction when $M = 1.0, Gr = 3.0$, $\alpha = 0.05, \varphi = \frac{\pi}{4}, \omega = \frac{\pi}{4}, a = 0.8$, $\eta = 0.8, x = 1.0$, $Br = 0.2$, $d_p = 5, \gamma = 0.05$, $\beta = 0.05$ and $\varepsilon = 2.0$.

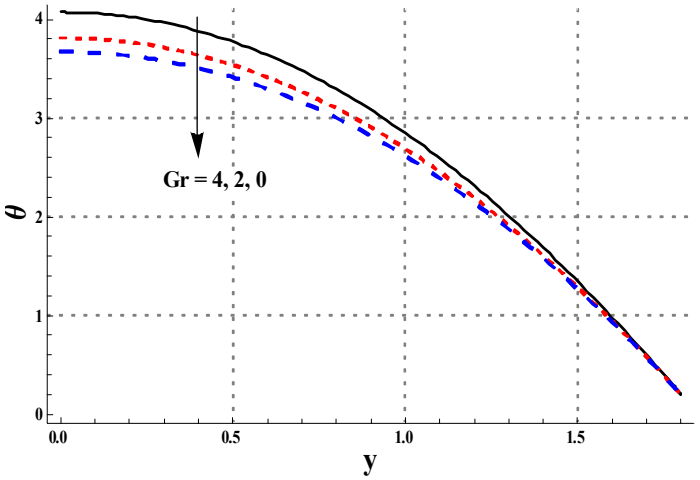

Fig. 3.12: Illustrations of temperature for Grashoff number when $M = 1.0, \phi = 0.05$, $\alpha = 0.05, \varphi = \frac{\pi}{4}, \omega = \frac{\pi}{4}, a = 0.8$, $\eta = 0.8, x = 1.0$, $Br = 0.2$, $d_p = 5, \gamma = 0.05$, $\beta = 0.05$ and $\varepsilon = 2.0$.

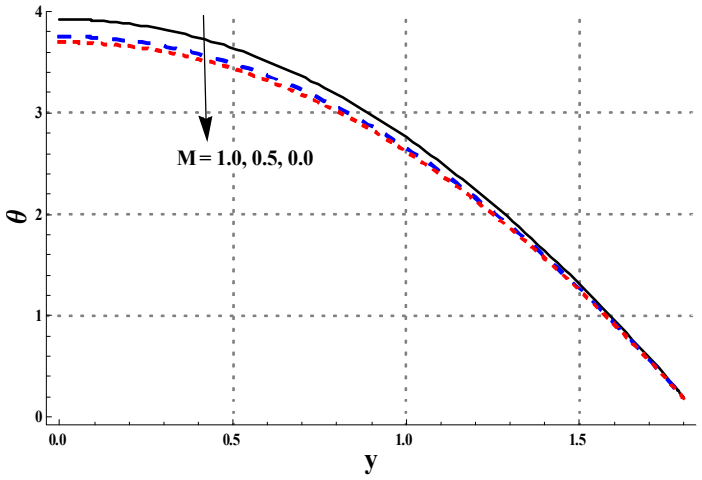

Fig. 3.13: Illustrations of temperature for Hartman number when $M = 1.0, Gr = 3.0$, $\phi = 0.05, \varphi = \frac{\pi}{4}, \omega = \frac{\pi}{4}, a = 0.8$, $\eta = 0.8, x = 1.0$, $Br = 0.2$, $d_p = 5, \gamma = 0.05$, $\beta = 0.05$ and $\varepsilon = 2.0$.

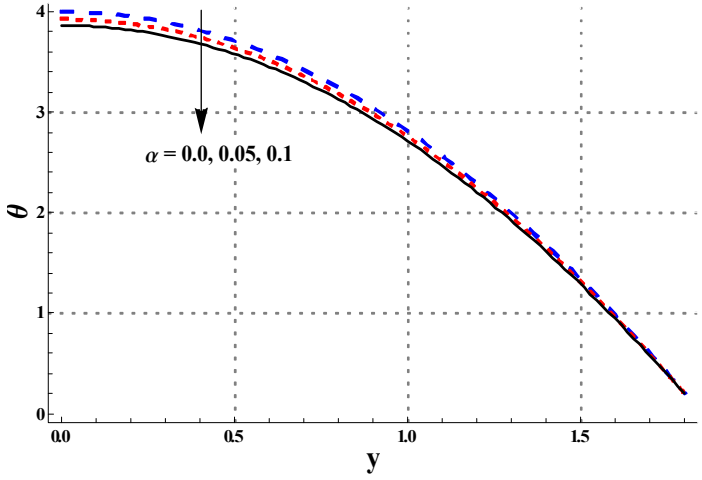

Fig. 3.14: Illustrations of temperature for variable viscosity parameter when $M = 1.0, Gr = 3.0$, $\phi = 0.05, \varphi = \frac{\pi}{4}, \omega = \frac{\pi}{4}, a = 0.8$, $\eta = 0.8, x = 1.0$, $Br = 0.2$, $d_p = 5, \gamma = 0.05$, $\beta = 0.05$ and

$\varepsilon = 2.0$.

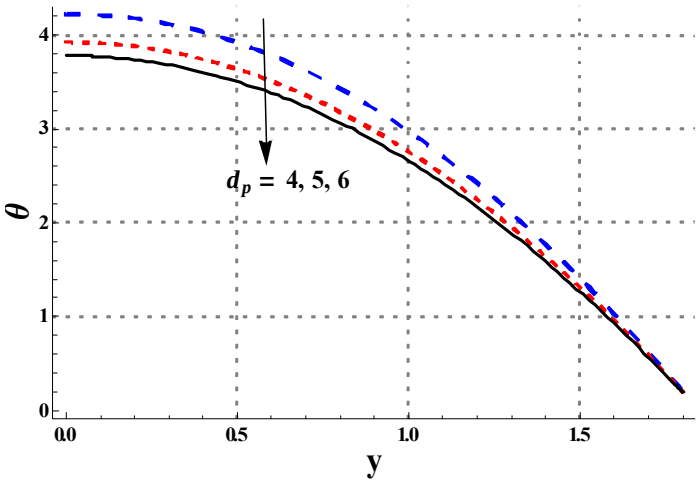

Fig. 3.15: Illustrations of temperature for pore diameter when $M = 1.0, Gr = 3.0, \phi = 0.05, \varphi = \frac{\pi}{4}, \omega = \frac{\pi}{4}, a = 0.8, \eta = 0.8, x = 1.0, Br = 0.2, \alpha = 0.05, \gamma = 0.05, \beta = 0.05$ and $\varepsilon = 2.0$.

Table 3.2. Heat transfer rate at the upper wall for different embedded parameters $\varphi =$

$\frac{\pi}{4}, \omega = \frac{\pi}{4}, a = 0.8$, $\eta = 0.8, x = 1.0$, $Br = 0.2$, $d_p = 5$, $\beta = 0.05$ and $\varepsilon = 2.0$.

ϕ	Gr	M	α	γ	d_p	φ	ω	$-\frac{K_{eff}}{K_f}\theta'[0]$
0.00	3.0	1.0	0.05	0.05	5	$\pi/4$	$\pi/4$	4.55153
0.05								4.60661
0.10								4.71184
0.15								4.85691
0.05	0.0							4.54416
	2.0							4.55092
	4.0							4.71205
	6.0							5.19033
	3.0	0.0						4.40999
		0.5						4.45940
		1.0						4.60661
		1.5						4.84897
		1.0	0.00					4.70527
			0.05					4.60661
			0.10					4.51709
			0.15					4.44558
			0.10	0.00				4.61349
				0.05				4.60661
				0.10				4.59977
				0.05	3			5.97344
				0.05	4			4.95260
					5			4.60661
					6			4.45550
					5	0		4.80078
						$\pi/4$		4.60661
						$\pi/2$		4.40999
						$\pi/4$	0	4.54416
							$\pi/4$	4.60661
							$\pi/2$	4.74737

Chapter 4

Entropy generation in peristalsis with iron oxide nanofluid

Main theme of this chapter is to examine the entropy generation in peristaltic transport of nanofluid with combined effects of MHD, Ohmic heating and viscous dissipation. Further velocity slip and thermal jump conditions are considered. Numerical simulation is used for describing the velocity, temperature, pressure gradient and entropy generation. Physical interpretation of obtained results is explored through graphs. The proposed mathematical model has relevance with modern drug delivery processes and cancer therapy.

4.1 Formulation

Peristaltic motion of nanofluid in a tube of radius a is analyzed. Waves of the speed c and wavelength λ travel along the tube walls. We select a cylindrical coordinates system $(\bar{R}, \bar{Z})$. Here $\bar{Z}$-axis lies along the centerline and R-axis in radial direction. Wall surface is defined as:

$$\bar{h} = a + b \sin \frac{2\pi}{\lambda}(\bar{Z} - c\bar{t}), \tag{4.1}$$

where b indicates wave amplitude and t time. Nanofluid is mixture of nanoparticles and ordinary fluid. Water is considered as an ordinary fluid and iron oxide nanosized particles as nanomaterials. These are considered to be in thermal equilibrium. For the present problem,

Brinkman viscosity model is considered for μ_{nf} as:

$$\mu_{nf} = \frac{\mu_f}{(1-\phi)^{2.5}}, \tag{4.2}$$

where μ_f denotes viscosity of conventional liquid and ϕ depicts nanomaterials volume fraction. In view of Maxwell model the thermal conductivity of nanofluid is:

$$\frac{K_{nf}}{K_f} = \frac{K_{np} + 2K_f - 2\phi(K_f - K_{np})}{K_{np} + 2K_f + \phi(K_f - K_{np})}. \tag{4.3}$$

The density of nanoliquids ρ_{nf}, heat capacity of nanoliquid $(\rho C)_{nf}$, thermal expansion of nanoliquid $(\rho\beta)_{nf}$ and electric conductivity (σ_{nf}) of the nanoliquid are:

$$\begin{aligned} \rho_{nf} = (1-\phi)\rho_f + \phi\rho_{np},\ (\rho C)_{nf} = (1-\phi)(\rho C)_f + \phi(\rho C)_{np}, \\ (\rho\beta)_{nf} = (1-\phi)(\rho\beta)_f + \phi(\rho\beta)_{np},\ \frac{\sigma_{nf}}{\sigma_f} = 1 + \frac{3(\frac{\sigma_{np}}{\sigma_f}-1)\phi}{(\frac{\sigma_{np}}{\sigma_f}+2)-(\frac{\sigma_{np}}{\sigma_f}-1)\phi}. \end{aligned} \tag{4.4}$$

Magnetic field of constant strength B_0 is applied. Induced magnetic field for small magnetic Reynold number is omitted. The wave $(\bar{r}, \bar{z})$ and laboratory $(\bar{R}, \bar{Z}, \bar{t})$ coordinates are related by:

$$\bar{r} = \bar{R}, \bar{z} = \bar{Z} - c\bar{t}, \bar{u} = \bar{U}, \bar{w} = \bar{W} - c, \bar{p}(\bar{z}, \bar{r}) = \bar{P}(\bar{Z}, \bar{R}, \bar{t}). \tag{4.5}$$

Here $(\bar{U}, \bar{W})$ and $\bar{P}$ denote the velocity field and pressure in the laboratory frame $(\bar{Z}, \bar{R}, \bar{t})$ and $(\bar{u}$,$\bar{w})$ and $\bar{p}$ represent the velocities and pressure in the wave frame $(\bar{z},\ \bar{r})$. Governing mathematical expressions in the wave frame are given by:

$$\frac{1}{r}\frac{\partial(\bar{r}\bar{u})}{\partial\bar{r}} + \frac{\partial\bar{w}}{\partial\bar{z}} = 0, \tag{4.6}$$

$$\begin{aligned} &\rho_{nf}\left(\bar{u}\frac{\partial}{\partial\bar{r}} + (\bar{w}+c)\frac{\partial}{\partial\bar{z}}\right)\bar{u} = -\frac{\partial\bar{p}}{\partial\bar{r}} + \mu_{nf}\left(2\frac{\partial^2\bar{u}}{\partial\bar{r}^2} + \frac{2}{r}\frac{\partial\bar{u}}{\partial\bar{r}} - 2\frac{\bar{u}}{\bar{r}^2}\right) \\ &+\mu_{nf}\frac{\partial}{\partial\bar{z}}\left[\frac{\partial\bar{u}}{\partial\bar{r}} + \frac{\partial\bar{w}}{\partial\bar{z}}\right], \end{aligned} \tag{4.7}$$

$$\rho_{nf}\left(\bar{u}\frac{\partial}{\partial\bar{r}}+(\bar{w}+c)\frac{\partial}{\partial\bar{z}}\right)(\bar{w}+c) = -\frac{\partial\bar{p}}{\partial\bar{z}}+\mu_{nf}\left[\frac{\partial}{\partial\bar{z}}\left(2\frac{\partial\bar{w}}{\partial\bar{z}}\right)+\frac{1}{r}\frac{\partial}{\partial\bar{r}}\left(r\left(\frac{\partial\bar{u}}{\partial\bar{z}}+\frac{\partial\bar{w}}{\partial\bar{r}}\right)\right)\right] - \sigma_{nf}B_0^2(\bar{w}+c), \tag{4.8}$$

$$(\rho C)_{nf}\left(\bar{u}\frac{\partial T}{\partial\bar{r}}+(\bar{w}+c)\frac{\partial T}{\partial\bar{z}}\right) = K_{nf}\left(\frac{\partial^2 T}{\partial\bar{r}^2}+\frac{1}{r}\frac{\partial T}{\partial\bar{r}}+\frac{\partial^2 T}{\partial\bar{z}^2}\right)+\sigma_{nf}B_0^2(\bar{w}+c)^2 \tag{4.9}$$
$$+\mu_{nf}\left[2\left(\left(\frac{\partial\bar{u}}{\partial\bar{r}}\right)^2+\left(\frac{\partial\bar{w}}{\partial\bar{z}}\right)^2\right)+\left(\frac{\partial\bar{u}}{\partial\bar{z}}+\frac{\partial\bar{w}}{\partial\bar{r}}\right)^2\right]+\Phi,$$

where Φ stands for dimensional heat absorption/generation. We consider following dimensionless variables:

$$\begin{gathered} z=\frac{\bar{z}}{\lambda}, r=\frac{\bar{r}}{a}, w=\frac{\bar{w}}{c}, u=\frac{\bar{u}}{c\delta}, \delta=\frac{a}{\lambda}, h=\frac{\bar{H}}{a}, p=\frac{a^2\bar{p}}{c\lambda\mu_f}, \\ Re=\frac{\rho_f ca}{\mu_f}, Ec=\frac{c^2}{C_f T_0}, Pr=\frac{\mu_f C_f}{K_f}, M=\sqrt{\frac{\sigma_f}{\mu_f}}B_0 a, \\ \theta=\frac{T-T_0}{T_0}, Br=\Pr Ec, \varepsilon=\frac{a^2\Phi}{K_f}, \end{gathered} \tag{4.10}$$

where $Re, Br, M, \delta, \theta$ and ϵ denote the Reynolds number, Brinkman parameter, Hartman number, wave number, nondimensional temperature and heat source/sink parameters respectively. In light of the long wavelength and small Reynold number supposition, we have:

$$\frac{\partial p}{\partial r}=0, \tag{4.11}$$

$$\frac{\partial p}{\partial z}=\frac{1}{(1-\phi)^{2.5}}\frac{1}{r}\frac{\partial}{\partial r}\left(r\frac{\partial w}{\partial r}\right)-\frac{\sigma_{nf}}{\sigma_f}M^2(w+1), \tag{4.12}$$

$$\frac{K_{nf}}{K_f}\frac{1}{r}\frac{\partial}{\partial r}\left(r\frac{\partial\theta}{\partial r}\right)+\frac{Br}{(1-\phi)^{2.5}}\left(\frac{\partial w}{\partial r}\right)^2+\frac{\sigma_{nf}}{\sigma_f}BrM^2(w+1)^2+\varepsilon=0. \tag{4.13}$$

Continuity equation is trivially justified and Eq. (4.11) depicts that $p\neq p(r)$. The nondimensional form of flow rate in the fixed $\eta(=\bar{Q}/ca)$ and moving $F(=\bar{q}/ca)$ frames of reference are related by:

$$\eta=F+\frac{1}{2}\left(1+\frac{\zeta^2}{2}\right). \tag{4.14}$$

Here $\bar{Q}$ and $\bar{q}$ are dimensional forms of flow rates in the fixed and moving frames. Furthermore 'F' is given as:

$$F = 2\pi \int_0^h r w dr. \tag{4.15}$$

The associated boundary conditions are:

$$\begin{gathered} \frac{\partial w}{\partial r} = 0, \frac{\partial \theta}{\partial r} = 0, \text{ at } r = 0, \\ w + \frac{\beta_1}{(1-\phi)^{2.5}} \frac{\partial w}{\partial r} = -1, \theta + \gamma \frac{\partial \theta}{\partial r} = 0, \text{ at } r = h. \end{gathered} \tag{4.16}$$

Here $h = 1 + a\sin(2\pi x)$ depicts the nondimensional configuration of peristaltic wall, β_1 represents the dimensionless velocity slip variable and γ stands for dimensionless thermal slip parameter. In this problem we use the Mathematica software to compute the numerical solutions via NDSolve technique.

4.2 Entropy generation analysis

Entropy generation expression can be defined as follows:

$$\begin{aligned} S_G = \frac{K_{nf}}{\bar{T}_0^2} \left(\left(\frac{\partial T}{\partial \bar{r}} \right)^2 + \left(\frac{\partial T}{\partial \bar{z}} \right)^2 \right) + \frac{\sigma_{nf}}{\bar{T}_0} B_0^2 (\bar{w} + c)^2 \\ + \frac{\mu_{nf}}{\bar{T}_0} \left[2 \left(\left(\frac{\partial \bar{u}}{\partial \bar{r}} \right)^2 + \left(\frac{\partial \bar{w}}{\partial \bar{z}} \right)^2 \right) + \left(\frac{\partial \bar{u}}{\partial \bar{z}} + \frac{\partial \bar{w}}{\partial \bar{r}} \right)^2 \right]. \end{aligned} \tag{4.17}$$

$$N_S = \frac{K_{nf}}{K_f} \left(\frac{\partial \theta}{\partial \bar{r}} \right)^2 + \frac{Br}{(1-\phi)^{2.5}} \left(\frac{\partial w}{\partial r} \right)^2 + \frac{\sigma_{nf}}{\sigma_f} Br M^2 (w+1)^2. \tag{4.18}$$

N_S is the dimensionless form and S_G is known as entropy generation variable. The total entropy generation can be written as

$$N_S = N_H + N_F + N_M, \tag{4.19}$$

where N_H depicts the entropy generation effects caused by the presence of characteristic heat transfer, N_F shows the entropy generation effect for the presence of fluid friction irreversibility and N_M depicts the entropy generation effect for magnetic field. Bejan number (Be) gives the comparison between the total irreversibility and irreversibility due to heat transfer. Mathemat-

ically

$$Be = \frac{N_H}{N_S}. \tag{4.20}$$

Clearly Bejan number ranging from 0 to 1 holds when the entropy generation due to combined effects of fluid friction and magnetic field dominantes. Bejan number approaching to 1 is the opposite case where heat transfer irreversibility dominants and Bejan number 0.5 corresponds to situation when contribution of both fluid friction and heat to entropy generation are equal.

4.3 Discussion

The analysis of velocity field, entropy, temperature and pressure are illustrated through Figs. (4.1)-(4.21) . For graphical analysis we have considered fixed numerical values of some parameters.

4.3.1 Velocity distribution

Figs. 4.1-4.4 illustrated the analysis of axial velocity across the tube for nanomaterials volume fraction ϕ, Hartman number M, velocity slip parameter β_1 and amplitude ratio ζ. Axial velocity reduces for larger value of nanomaterials volume fraction near center of tube (see Fig. 4.1). It is because of the fact that inclusion of nanomaterials produce more resistance to the flow and thus fluid velocity decays. Fig. 4.2 indicates effects of Hartman number on velocity distribution. It means that axial velocity reduces for larger applied magnetic field due to the retarding nature of Lorentz force. From Fig. 4.3, it is noted that axial velocity decreases near core part of tube by increasing velocity slip parameter and reverse behavior is seen near tube wall. It is noted from Fig. 4.4 that axial velocity decays by increasing the amplitude ratio.

4.3.2 Pressure distribution

Figs. 4.5-4.7 are plotted to examine the pressure gradient across the tube for various fluid parameters of interest. Fig. 4.5 depicts that pressure gradient across the tube enhances by enhancing the amount of nanomaterials. It is due to the fact that resistance of fluid motion provided by the addition of nanomaterials enhances and therefore pressure gradient elevates. Fig. 4.6 reveals that for large Hartman number, the pressure gradient increases. Physically in

the presence of strong magnetic field, more resistive force is experienced in system due to which more disturbance occurred and so pressure gradient enhances. Fig. 4.7 studies influence of velocity slip on pressure gradient. It illustrates that an increase in β_1 decays pressure gradient in the tube and prominent effects are noticed in narrow portion. Figs. 4.8-4.10 have been displayed to study effects of pertinent variables on pressure rise per wavelength (∇p_λ). These graphs depict that when the flow rate enhances then ∇p_λ decreases continuously. Graphs are generally classified in three regions known as retrograde, peristaltic and augmented pumping portions. Figs. 4.8 and 4.9 show that by enhancing the nanoparticles amount and Hartman number the pressure decays in retrograde pumping portion ($\eta < 0, \nabla p_\lambda > 0$) and peristaltic pumping portion ($\eta < 0, \nabla p_\lambda < 0$). Furthermore, opposite trend is found in augmented pumping portion ($\eta > 0, \nabla p_\lambda < 0$). Fig. 4.10 depicts that ∇p_λ increases by larger amplitude ratio parameter.

4.3.3 Temperature distribution

Figs. 4.11-4.13 displayed influences of ϕ, M and γ on temperature. Fig. 4.11 indicates temperature for different nanomaterials volume fraction. Here temperature rapidly decays for larger nanomaterials volume fraction. Nanoparticles play a role as cooling agent in fluid flow. Fig. 4.12 gives effect of Hartman number on temperature. Temperature enhances for increasing intensity of applied magnetic field due to Ohmic heating effect. Fig. 4.13 illustrates that temperature uniformly decreases by increasing thermal jump parameter. Larger values of γ parameter facilitate the heat transfer rate therefore temperature decreases.

4.3.4 Entropy distribution

Figs. 4.14-4.17 are plotted to compute variations of ϕ, M, ϵ and η on entropy generation. Effect of nanomaterials volume fraction on entropy generation is studied via Fig. 4.14. It is examined that entropy generation is decreasing function of nanoparticle volume fraction. Fig. 4.15 reveals that entropy generation enhances for Hartman number. Effect of heat source/sink on entropy generation is depicted in Fig. 4.16. Here entropy generation enhances specially near the tube wall for larger ϵ. Fig. 4.17 depicts that there is a rise in entropy generation by flow rate parameter η. Fig. 4.18 exhibits that Bejan number increases by increasing the amount of nanomaterial in system. Figs. 4.19 and 4.20 computed outcome of Hartman number and flow

rate on Bejan number. It is noticed that Bejan number is enhanced via Hartman number and flow rate. Fig. 4.21 depicts that there is a reduction in Bejan number with increasing effect of amplitude ratio ζ.

4.4 Conclusions

Key findings of this analysis are:

- Axial velocity depicts decreasing behavior by increasing nanoparticle and Hartman number.
- Presence of nanomaterials increases pressure gradient.
- Behavior of Hartman number on pressure gradient is similar to nanomaterials volume fraction.
- Temperature decays via nanomaterial volume fraction.
- Temperature for Hartman number has opposite response when compared with nanomaterial volume fraction.
- Presence of nanomaterials decreases entropy generation. Increasing the Hartman number, the total entropy generation remarkably enhances.
- Bejan number has increasing behavior for nanoparticle volume fraction, Hartman number and flow rate.

4.5 Tables

Table 4.1: Thermophysical characteristics [7]:

	$\rho\ (kg/m^3)$	$C_p\ (j/kgK)$	$K\ (W/mk)$	$\beta\ (1/k) \times 10^{-6}$	$\sigma\ (S/m)$
H_2O	997.1	4179	0.613	210	0.05
Fe_3O_4	5200	670	80.6	13	25000

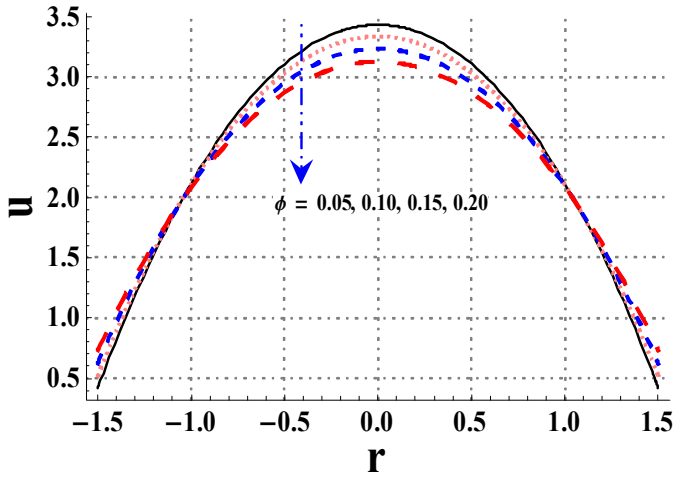

Fig. 4.1. Plot of velocity under ϕ.

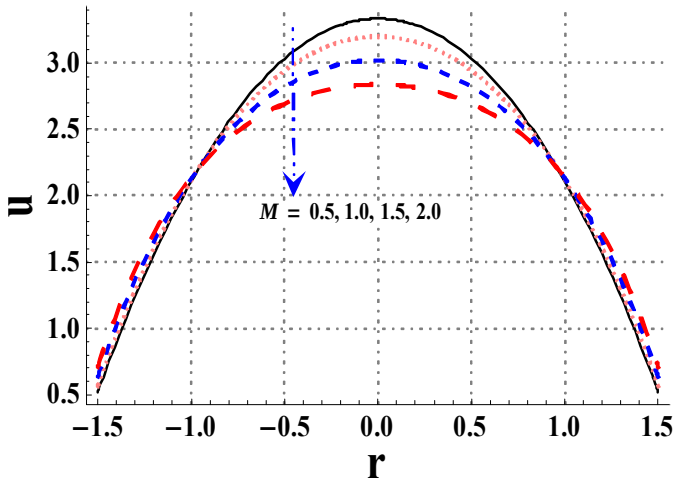

Fig. 4.2. Effect of M on velocity.

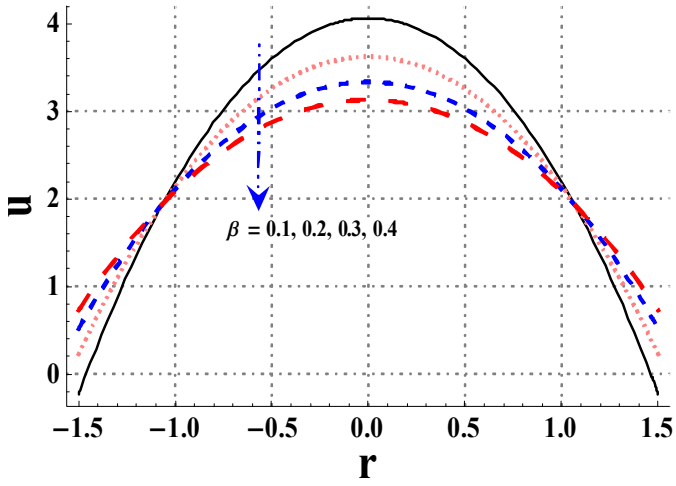

Fig. 4.3. Effect of β on velocity.

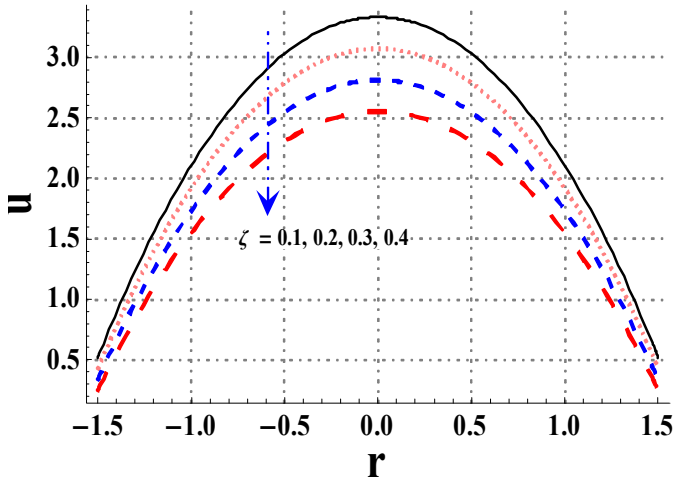

Fig. 4.4. Effect of ζ on velocity.

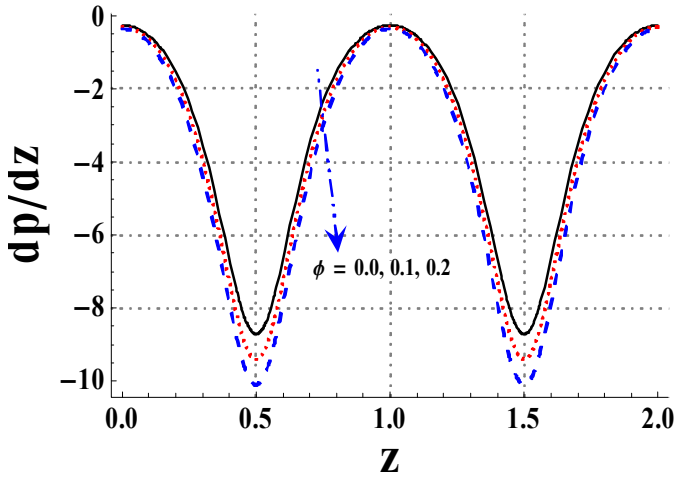

Fig. 4.5. Effect of ϕ on dp/dz.

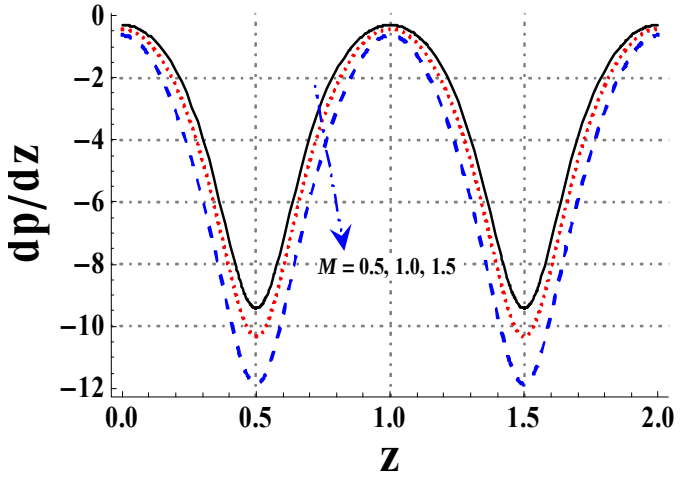

Fig. 4.6. Plot of dp/dz under M.

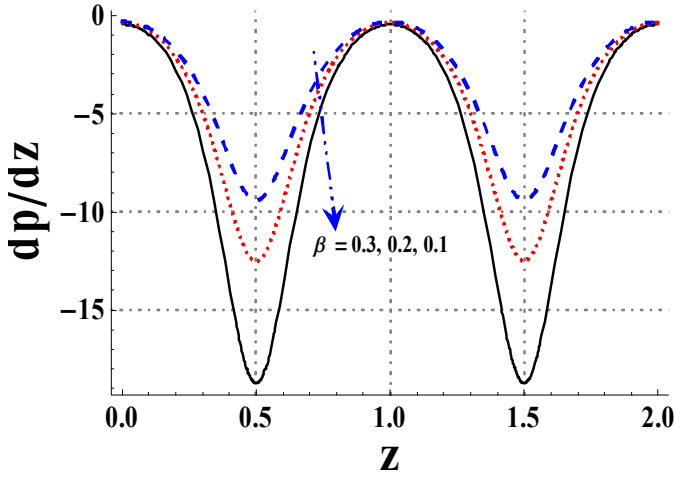

Fig. 4.7. Effect of β on dp/dz.

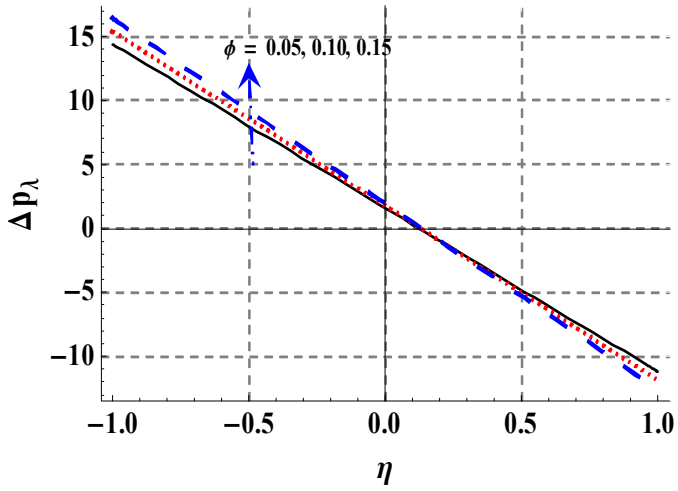

Fig. 4.8. Plot of Δp_λ for ϕ.

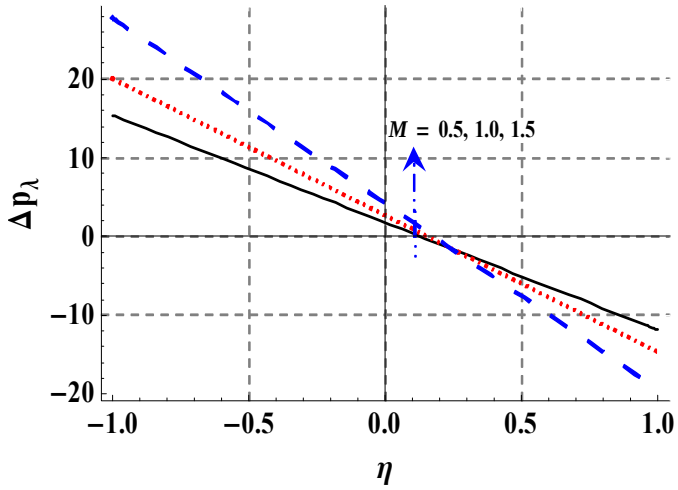

Fig. 4.9. Plot of Δp_λ for M.

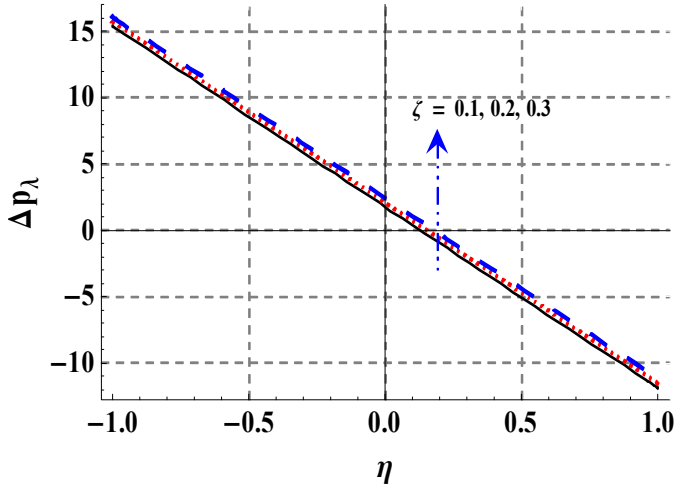

Fig. 4.10. Plot of Δp_λ for ζ.

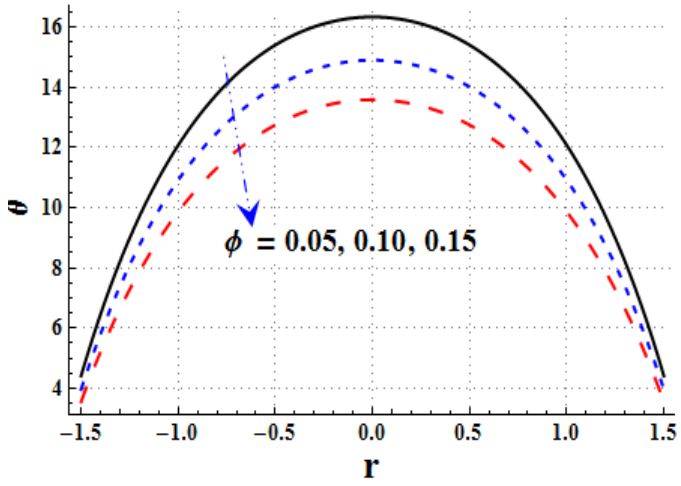

Fig. 4.11. Plot of θ for ϕ.

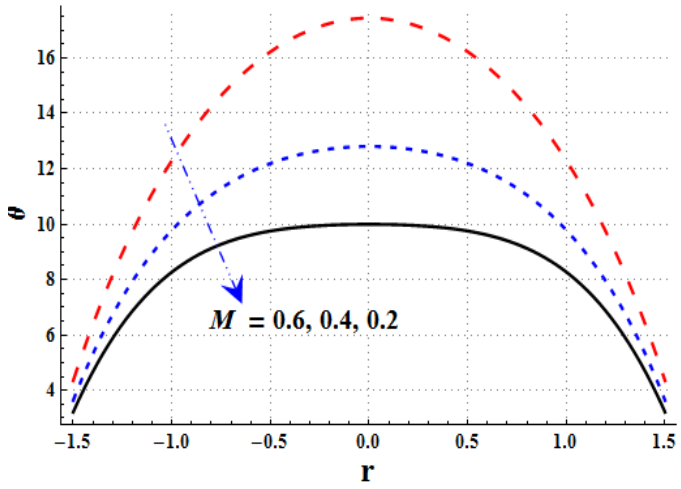

Fig. 4.12. Plot of θ for M.

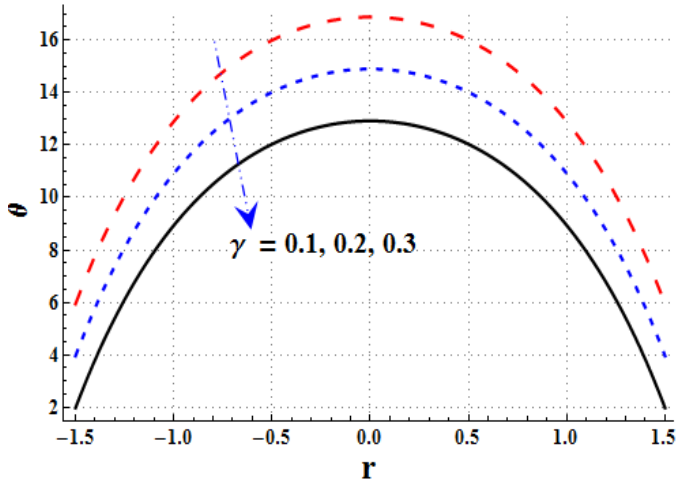

Fig. 4.13. Plot of θ for ζ.

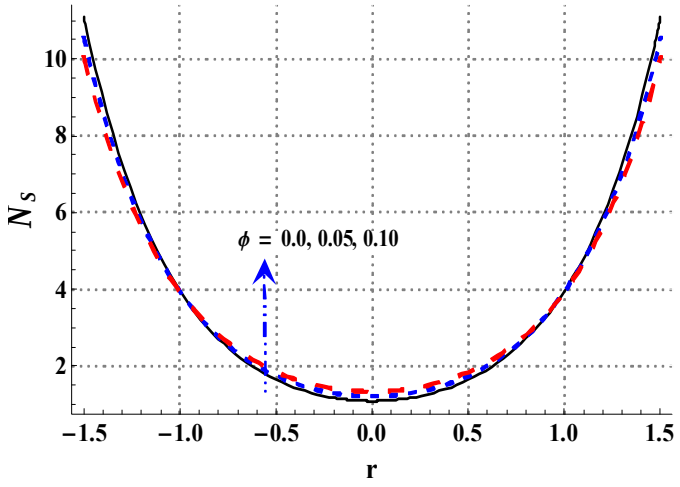

Fig. 4.14. Plot of N_S for ϕ.

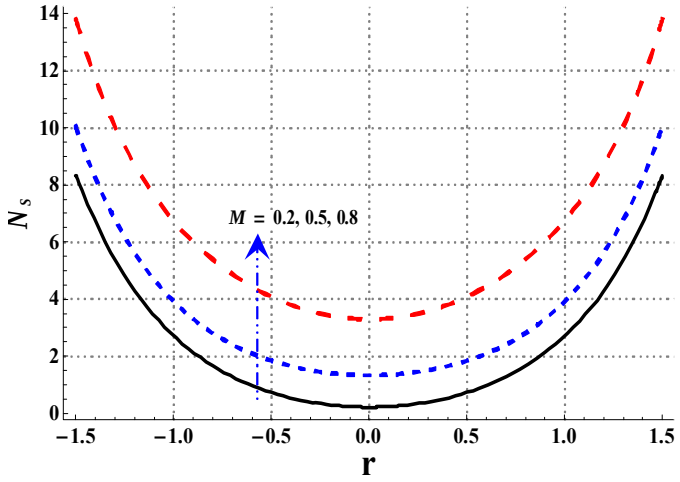

Fig. 4.15. Plot of N_S for M.

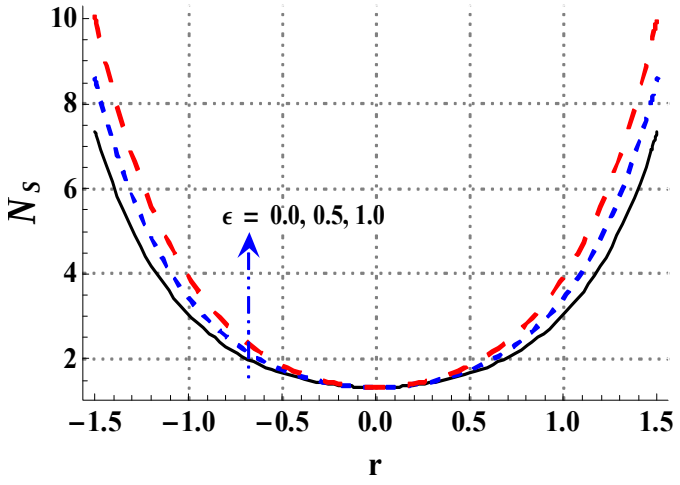

Fig. 4.16. Plot of N_S for ϵ.

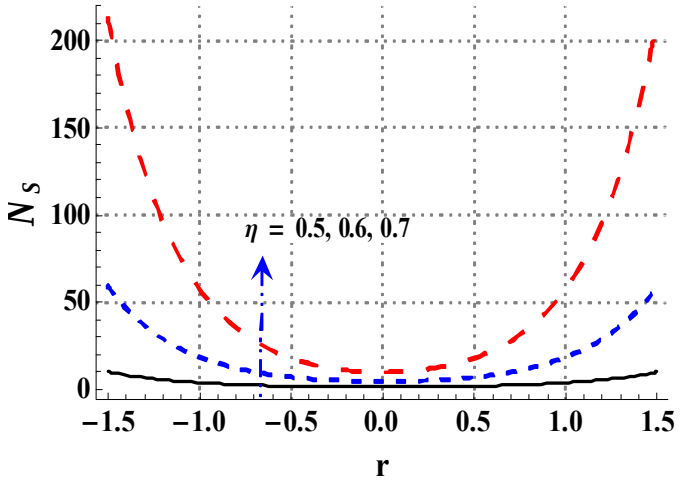

Fig. 4.17. Plot of N_S for η.

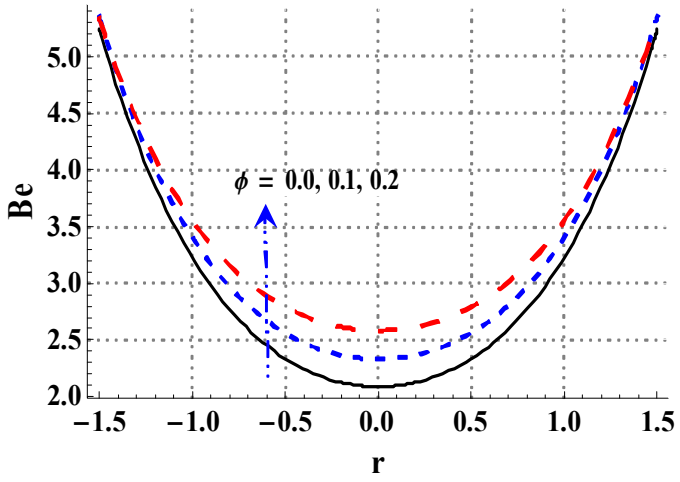

Fig. 4.18. Effect of ϕ on Bejan number.

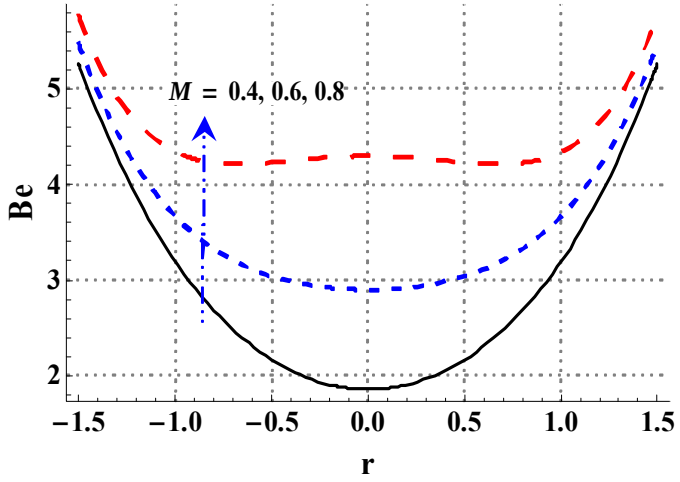

Fig. 4.19. Effect of M on Bejan number.

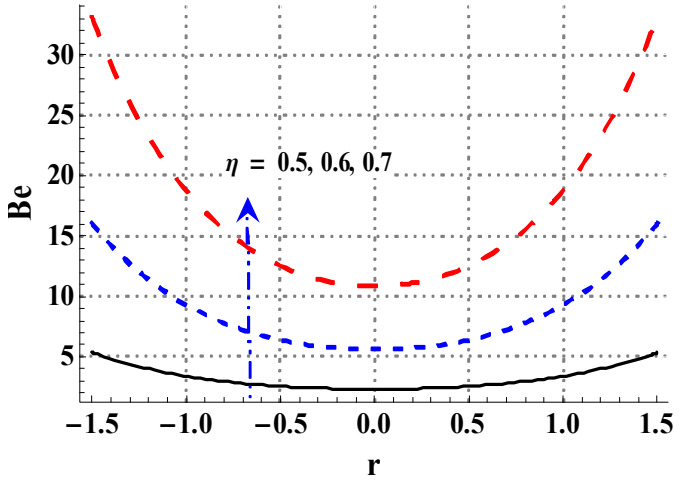

Fig. 4.20. Effect of η on Bejan number.

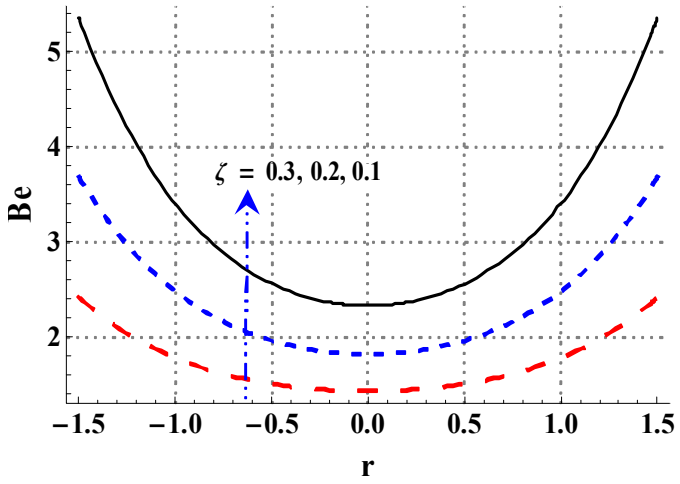

Fig. 4.21. Effect of ζ on Bejan number.

Chapter 5

Peristaltic motion of nanofluid through curved channel with Hall and Ohmic heating effects

Present chapter investigates the Ohmic heating and Hall effects on the peristaltic motion of nanofluid in a curved channel. Further convective boundary and velocity slip conditions are considered. Corresponding equations and boundary conditions are simplified by using the Lubrication approach. Dimensionless equations and boundary conditions are solved numerically. Effects of sundry variables on velocity, pressure gradient and temperature field have been depicted graphically.

5.1 Mathematical formulation

Geometry of problem includes a two-dimensional curved channel with width $2a_1$ coiled in a semi circle of radius R' and center 'O'. Coordinates of curved channel are represented in such a mode that $\bar{X}$-axis is toward the length of channel and $\bar{R}$-axis normal to it. An incompressible nanofluid is considered in channel. Fluid flow is due to the propagation of waves along the channel walls with speed c, amplitude b and wavelength λ. Geometry of problem is described as follows:

$$\bar{H}_{1,2}(\bar{X},\bar{t}) = \pm a_1 \pm bcos(\frac{2\pi}{\lambda}(\bar{X} - c\bar{t})), \tag{5.1}$$

where t is the time and $\bar{H}_1$ and $\bar{H}_2$ depict the upper and lower walls. Constant temperature T_0 and $T_1(> T_0)$ are maintained at $\bar{H}_1$ and $\bar{H}_2$ walls respectively. Axial velocity for present flow in the form $\mathbf{V} = [\bar{U}(\bar{R}, \bar{X}, \bar{t}), \bar{V}(\bar{R}, \bar{X}, \bar{t}), 0]$ where $\bar{U}$ and $\bar{V}$ represent the radial and axial components of velocity. Further radial magnetic field is applied. It is taken in the form:

$$\mathbf{B} = \left[0, 0, \frac{R' B_0}{R' + \bar{R}}\right]. \tag{5.2}$$

Lorentz force is given by:

$$\mathbf{F} = \mathbf{J} \times \mathbf{B}, \tag{5.3}$$

where current density in presence of Hall current satisfies:

$$\mathbf{J} = \left[\mathbf{V} \times \mathbf{B} - \frac{1}{en_e}[\mathbf{J} \times \mathbf{B}]\right]. \tag{5.4}$$

Finally Lorentz force becomes:

$$F = \left[\frac{\sigma_{nf}\left(\frac{R' B_0}{R'+\bar{R}}\right)^2}{1 + (\frac{R'}{R'+\bar{R}}\frac{\sigma_{nf}}{\sigma_f} m)^2}(-\bar{U} + \frac{\sigma_{nf}}{\sigma_f}\frac{R'}{R' + \bar{R}} m\bar{V}), \frac{-\sigma_{nf}\left(\frac{R' B_0}{R'+\bar{R}}\right)^2}{1 + (\frac{R'}{R'+\bar{R}}\frac{\sigma_{nf}}{\sigma_f} m)^2}(\bar{V} + \frac{\sigma_{nf}}{\sigma_f}\frac{R'}{R' + \bar{R}} m\bar{U}), 0\right]. \tag{5.5}$$

Here σ_{nf} depicts the electrical conductivity of nanofluid, $m(= \frac{\sigma_f B_0}{en_e})$ the Hall parameter, 'e' the electron charge and '$n_e\prime$ the number density of free electron. The electrical conductivity σ_w of nanofluid is defined as:

$$\frac{\sigma_{nf}}{\sigma_f} = 1 + \frac{3(\frac{\sigma_{np}}{\sigma_f} - 1)\phi}{(\frac{\sigma_{np}}{\sigma_f} + 2) - (\frac{\sigma_{np}}{\sigma_f} - 1)\phi}. \tag{5.6}$$

The Maxwell's thermal conductivity (K_{nf}) model of nanofluid is given as:

$$\frac{K_{nf}}{K_f} = \frac{K_{np} + 2K_f - 2\phi(K_f - K_{np})}{K_{np} + 2K_f + \phi(K_f - K_{np})}, \tag{5.7}$$

where subscript 'np' represent the nanoparticles and "f" represent the base fluid for water and ϕ stands for the nanoparticle volume fraction. Brinkman's viscosity model is presented as:

$$\mu_{nf} = \frac{\mu_f}{(1-\phi)^{2.5}}, \tag{5.8}$$

where μ_f is the viscosity of fluid. The equations relevant to problem under consideration are:

$$\frac{\partial}{\partial \bar{R}}\left((R'+\bar{R})\bar{U}\right) + R'\frac{\partial \bar{V}}{\partial \bar{X}} = 0, \tag{5.9}$$

$$\begin{aligned}\rho_{nf}\left(\frac{\partial \bar{U}}{\partial \bar{t}} + \bar{U}\frac{\partial \bar{U}}{\partial \bar{R}} + \frac{R'\bar{V}}{R'+\bar{R}}\frac{\partial \bar{U}}{\partial \bar{X}} - \frac{\bar{V}^2}{R'+\bar{R}}\right) &= -\frac{\partial \bar{P}}{\partial \bar{R}} + \frac{R'}{R'+\bar{R}}\frac{\partial \tau_{\bar{R}\bar{X}}}{\partial \bar{X}} \\ + \frac{1}{R'+\bar{R}}\frac{\partial}{\partial \bar{R}}\left((R'+\bar{R})\tau_{\bar{R}\bar{R}}\right) - \frac{\tau_{\bar{X}\bar{X}}}{R'+\bar{R}} - \frac{\sigma_{nf}\left(\frac{R'B_0}{R'+\bar{R}}\right)^2}{1+(\frac{R'}{R'+\bar{R}}\frac{\sigma_{nf}}{\sigma_w}m)^2}&(\bar{U} - \frac{\sigma_{nf}}{\sigma_w}\frac{R'}{R'+\bar{R}}m\bar{V}),\end{aligned} \tag{5.10}$$

$$\begin{aligned}\rho_{nf}\left(\frac{\partial \bar{V}}{\partial \bar{t}} + \bar{U}\frac{\partial \bar{V}}{\partial \bar{R}} + \frac{R'\bar{V}}{R'+\bar{R}}\frac{\partial \bar{V}}{\partial \bar{X}} + \frac{\bar{U}\bar{V}}{R'+\bar{R}}\right) &= -\frac{R'}{R'+\bar{R}}\frac{\partial \bar{P}}{\partial \bar{X}} \\ + \frac{1}{(R'+\bar{R})^2}\frac{\partial}{\partial \bar{R}}\left((R'+\bar{R})^2\tau_{\bar{X}\bar{R}}\right) + \frac{R'}{R'+\bar{R}}\frac{\partial \tau_{\bar{X}\bar{X}}}{\partial \bar{X}} - \frac{\sigma_{nf}\left(\frac{R'B_0}{R'+\bar{R}}\right)^2}{1+(\frac{R'}{R'+\bar{R}}\frac{\sigma_{nf}}{\sigma_w}m)^2}&(\bar{V} + \frac{\sigma_{nf}}{\sigma_w}\frac{R'}{R'+\bar{R}}m\bar{U}),\end{aligned} \tag{5.11}$$

$$\begin{aligned}(\rho C)_{nf}\left(\frac{\partial \bar{T}}{\partial \bar{t}} + \bar{U}\frac{\partial \bar{T}}{\partial \bar{R}} + \frac{R'\bar{V}}{R'+\bar{R}}\frac{\partial \bar{T}}{\partial \bar{X}}\right) &= K_{nf}\left(\frac{\partial^2 T}{\partial \bar{R}^2} + \frac{1}{R'+\bar{R}}\frac{\partial T}{\partial \bar{R}} + \frac{(R')^2}{(R'+\bar{R})^2}\frac{\partial^2 T}{\partial \bar{X}^2}\right) \\ + \mu_{nf}\left[\tau_{\bar{R}\bar{R}}\frac{\partial \bar{U}}{\partial \bar{R}} + \tau_{\bar{R}\bar{X}}\left(\frac{\partial \bar{V}}{\partial \bar{R}} - \frac{\bar{V}}{R'+\bar{R}}\right) + \tau_{\bar{X}\bar{R}}\left(\frac{R'}{R'+\bar{R}}\frac{\partial \bar{U}}{\partial \bar{X}}\right) + \tau_{\bar{X}\bar{X}}\left(\frac{R'}{R'+\bar{R}}\frac{\partial \bar{V}}{\partial \bar{X}} + \frac{\bar{U}}{R'+\bar{R}}\right)\right]& \\ + \frac{\sigma_{nf}\left(\frac{R'B_0}{R'+\bar{R}}\right)^2}{1+(\frac{R'}{R'+\bar{R}}\frac{\sigma_{nf}}{\sigma_w}m)^2}(\bar{U}^2+\bar{V}^2) + \Phi.&\end{aligned} \tag{5.12}$$

Here Φ stand for heat generation/absorption and $\bar{P}(\bar{R},\bar{X},\bar{t})$ the pressure. The density of nanofluid ρ_{nf} and heat capacity of nanofluid C_{nf} are evaluated by using these relations:

$$\rho_{nf} = (1-\phi)\rho_f + \phi\rho_{np},\ C_{nf} = (1-\phi)C_f + \phi C_{np}. \tag{5.13}$$

Numerical data of the thermophysical features of water and "Cu" nanomaterial are given via Table **5.1**. The relations between the fixed and moving frames are described below:

$$\bar{x} = \bar{X} - c\bar{t}, \bar{r} = \bar{R}, \bar{u} = \bar{U}, \bar{v} = \bar{V} - c, \bar{p}(\bar{r},\bar{x}) = \bar{P}(\bar{R},\bar{X},\bar{t}), \tag{5.14}$$

where $\bar{u}(\bar{r},\bar{x}), \bar{v}(\bar{r},\bar{x})$ and $\bar{p}(\bar{r},\bar{x})$ are the axial velocity and pressure in the moving frame. According to above transformations, the relative equations of momentum, mass and energy are:

$$\frac{\partial}{\partial \bar{r}}\left((R'+\bar{r})\bar{u}\right)+R'\frac{\partial \bar{v}}{\partial \bar{x}}=0, \tag{5.15}$$

$$\begin{aligned}\rho_{nf}\left(\bar{u}\frac{\partial \bar{u}}{\partial \bar{r}}+\frac{R'(\bar{v}+c)}{R'+\bar{r}}\frac{\partial \bar{u}}{\partial \bar{x}}-\frac{(\bar{v}+c)^2}{R'+\bar{r}}\right)&=-\frac{\partial \bar{p}}{\partial \bar{r}}+\frac{1}{R'+\bar{r}}\frac{\partial}{\partial \bar{r}}\left((R'+\bar{r})\tau_{\bar{r}\bar{r}}\right)\\&+\frac{R'}{R'+\bar{r}}\frac{\partial \tau_{\bar{x}\bar{r}}}{\partial \bar{x}}-\frac{\tau_{\bar{x}\bar{x}}}{R'+\bar{r}}-\frac{\sigma_{nf}\left(\frac{R'B_0}{R'+\bar{r}}\right)^2}{1+(\frac{R'}{R'+\bar{r}}\frac{\sigma_{nf}}{\sigma_w}m)^2}(\bar{u}-\frac{\sigma_{nf}}{\sigma_w}\frac{R'}{R'+\bar{r}}m(\bar{v}+c)),\end{aligned} \tag{5.16}$$

$$\begin{aligned}\rho_{nf}\left(\bar{u}\frac{\partial \bar{v}}{\partial \bar{r}}+\frac{R'(\bar{v}+c)}{R'+\bar{r}}\frac{\partial \bar{v}}{\partial \bar{x}}+\frac{\bar{u}(\bar{v}+c)}{R'+\bar{r}}\right)&=-\frac{R'}{R'+\bar{r}}\frac{\partial \bar{p}}{\partial \bar{x}}+\frac{1}{(R'+\bar{r})^2}\frac{\partial}{\partial \bar{r}}\left((R'+\bar{r})^2\tau_{\bar{x}\bar{r}}\right)\\&+\frac{R'}{R'+\bar{r}}\frac{\partial \tau_{\bar{x}\bar{x}}}{\partial \bar{x}}-\frac{\sigma_{nf}\left(\frac{R'B_0}{R'+\bar{r}}\right)^2}{1+(\frac{R'}{R'+\bar{r}}\frac{\sigma_{nf}}{\sigma_w}m)^2}((\bar{v}+c)+\frac{\sigma_{nf}}{\sigma_w}\frac{R'}{R'+\bar{r}}m\bar{u}),\end{aligned} \tag{5.17}$$

$$\begin{aligned}(\rho C)_{nf}\left(\bar{u}\frac{\partial \bar{T}}{\partial \bar{r}}+\frac{R'(\bar{v}+c)}{R'+\bar{r}}\frac{\partial \bar{T}}{\partial \bar{x}}\right)&=K_{nf}\left(\frac{\partial^2 T}{\partial \bar{r}^2}+\frac{1}{R'+\bar{r}}\frac{\partial T}{\partial \bar{r}}+\frac{(R')^2}{(R'+\bar{r})^2}\frac{\partial^2 T}{\partial \bar{x}^2}\right)\\+\mu_{nf}\left[\tau_{\bar{r}\bar{r}}\frac{\partial \bar{u}}{\partial \bar{r}}+\tau_{\bar{r}\bar{x}}\left(\frac{\partial(\bar{v}+c)}{\partial \bar{r}}-\frac{(\bar{v}+c)}{R'+\bar{r}}\right)+\tau_{\bar{x}\bar{r}}\left(\frac{R'}{R'+\bar{r}}\frac{\partial \bar{u}}{\partial \bar{x}}\right)+\tau_{\bar{x}\bar{x}}\left(\frac{R'}{R'+\bar{r}}\frac{\partial \bar{v}}{\partial \bar{x}}+\frac{\bar{u}}{R'+\bar{r}}\right)\right]&\\+\frac{\sigma_{nf}\left(\frac{R'B_0}{R'+\bar{r}}\right)^2}{1+(\frac{R'}{R'+\bar{r}}\frac{\sigma_{nf}}{\sigma_w}m)^2}(\bar{u}^2+(\bar{v}+c)^2)+\Phi.&\end{aligned} \tag{5.18}$$

Peristaltic transport are studied under small Reynolds number and long wavelength. In light of these approximations, non-dimensional forms of Eqs. (5.16) – (5.18) are described by the expressions:

$$\begin{aligned}\frac{\partial p}{\partial x}&=\frac{1}{k(k+y)}\frac{1}{(1-\phi)^{2.5}}\frac{\partial}{\partial y}\left[(k+y)^2\left(-\frac{\partial^2\psi}{\partial y^2}-\frac{1}{(k+y)}\left(1-\frac{\partial \psi}{\partial y}\right)\right)\right]\\&-\frac{kM^2A_1}{(k+y)\left(1+\left(\frac{k}{(k+y)}A_1m\right)^2\right)}\left(1-\frac{\partial \psi}{\partial y}\right)\end{aligned} \tag{5.19}$$

$$\frac{\partial p}{\partial y}=0, \tag{5.20}$$

$$\frac{K_{nf}}{K_w}\left[\frac{\partial^2\theta}{\partial y^2}+\frac{1}{(k+y)}\frac{\partial\theta}{\partial y}\right]+\frac{Br}{(1-\phi)^{2.5}}\left(\frac{\partial^2\psi}{\partial y^2}+\frac{1}{(k+y)}\left(1-\frac{\partial\psi}{\partial y}\right)\right)^2 + \frac{k^2M^2A_1Br}{(k+y)^2\left(1+\left(\frac{k}{(k+y)}A_1m\right)^2\right)}\left(1-\frac{\partial\psi}{\partial y}\right)^2+\varepsilon=0. \tag{5.21}$$

The non-dimensional parameters used in this problem are:

$$x=\frac{\bar{x}}{\lambda},y=\frac{\bar{r}}{a_1},u=\frac{\bar{u}}{c},v=\frac{\bar{v}}{c},\delta=\frac{a_1}{\lambda},h_1=\frac{\bar{H}_1}{a_1},h_2=\frac{\bar{H}_2}{a_1},d=\frac{b}{a_1},$$
$$p=\frac{a_1^2\bar{p}}{c\lambda\mu_0},Re=\frac{\rho_f c a_1}{\mu_0},Ec=\frac{c^2}{C_f\left(T_1-T_0\right)},Pr=\frac{\mu_0 C_f}{K_f},M=\sqrt{\frac{\sigma_f}{\mu_0}}B_0^2a_1^2,$$
$$\alpha=\alpha_1(T_1-T_0),\theta=\frac{T-T_m}{T_1-T_0},Br=\Pr Ec,\varepsilon=\frac{a^2\Phi}{K_f\left(T_1-T_0\right)},u=\frac{k\delta}{(k+y)}\frac{\partial\psi}{\partial x},v=-\frac{\partial\psi}{\partial y}. \tag{5.22}$$

Continuity equation is trivially verified and Eq. (5.20) depicts that $p\neq p(y)$. Here Pr, Ec, Br, Re, ψ, M, θ, δ, ϵ and $T_m\,(=(T_0+T_1)/2)$ represent the Prandtl number, Eckert number, Brinkman number, Reynolds number, stream function, Hartman number, non-dimensional temperature, wave number, non-dimensional heat source/sink parameter and mean temperature of walls respectively. Here

$$A_1=1+\frac{3(\frac{\sigma_{np}}{\sigma_f}-1)\phi}{(\frac{\sigma_{np}}{\sigma_f}+2)-(\frac{\sigma_{np}}{\sigma_f}-1)\phi}. \tag{5.23}$$

The non-dimensional flow rate in the fixed $\eta(=\bar{Q}/ca)$ and moving $F(=\bar{q}/ca)$ frames are associated with the relation:

$$\eta=F+2. \tag{5.24}$$

Furthermore 'F' is given by:

$$F=\int_{h_1}^{h_2}-\frac{\partial\psi}{\partial y}dy. \tag{5.25}$$

The convective boundary conditions are described as below:

$$-K_{nf}\frac{\partial T}{\partial y}=l_w(T-T_w). \tag{5.26}$$

Here l_w represent the coefficient of heat transfer and T_w temperature of the wall. Dimensionless velocity slip and convective boundary conditions are:

$$\psi = -\frac{F}{2}, \frac{\partial \psi}{\partial y} + \frac{\beta_1}{(1-\phi)^{2.5}}\left(\frac{\partial^2 \psi}{\partial y^2} + \frac{1}{(k+y)}\left(1 - \frac{\partial \psi}{\partial y}\right)\right) = 1, A\frac{\partial \theta}{\partial y} + Bi_1(\theta + \tfrac{1}{2}) = 0, \text{ at } y = h_1,$$
$$\psi = \frac{F}{2}, \frac{\partial \psi}{\partial y} - \frac{\beta_1}{(1-\phi)^{2.5}}\left(\frac{\partial^2 \psi}{\partial y^2} + \frac{1}{(k+y)}\left(1 - \frac{\partial \psi}{\partial y}\right)\right) = 1, A\frac{\partial \theta}{\partial y} - Bi_2(\theta - \tfrac{1}{2}) = 0, \text{ at } y = h_2. \tag{5.27}$$

$$h_1 = 1 + d\cos(2\pi x + \gamma_2), h_2 = -1 - d\cos(2\pi x + \gamma_2),$$
$$Bi_1 = (\tfrac{l_1 d_1}{K_f}), Bi_2 = (\tfrac{l_2 d_1}{K_f}),$$

where Bi_1 and Bi_2 are the Biot-numbers for the upper and lower walls and "β_1" represents the dimensionless velocity slip parameter. Here we use the Mathematica software to compute the numerical solutions via NDSolve technique. Next section presents the analysis of the obtained results.

5.2 Discussion and comparison

In this section, we analyzed effects of numerous variables on velocity field, pressure gradient and temperature are studied through graphs.

5.2.1 Velocity profile

Fig. 5.1 shows the axial velocity for various amount of nanoparticle volume fraction. As expected, insertion of nanoparticles in base fluid decreases fluid velocity. Physically when inclusion of nanomaterial enhances in the base fluid then effective viscosity of nanofluid is more and thus ability of fluid motion reduces. Effect of Hall number on nanofluid is shown in Fig. 5.2. Due to presence of Hall parameter the velocity rapidly increases rather than in absence of Hall effects. Fig. 5.3 shows magnetic field effect on velocity. As expected the velocity decreases in presence of magnetic field. Fig. 5.4 depicts effect of 'β_1' on the velocity field. By increasing parameter 'β_1', velocity increases near the channel wall and it shows reverse behavior near the center of channel. Fig. 5.5 shows the variation of velocity by varying the curvature parameter. It can be seen that increasing behavior shifted towards upper wall in view of consideration of curvature.

5.2.2 Pressure gradient

Effects of numerous parameters on the pressure gradient are depicted through Figs. (5.6)-(5.10). These graphs show sinusoidal behavior of pressure gradient and attain higher value near the extensive portion of channel. Impact of 'ϕ' on pressure gradient is depicted in Fig. 5.6. As nanoparticle volume fraction enhances, pressure gradient also increases. Fig. 5.7 shows the influence of Hall parameter on the pressure gradient. Pressure gradient reduces with the rise of Hall parameter both in wider and occluded part of channels. Impact of magnetic field on pressure gradient is shown in Fig. 5.8. Pressure gradient enhances by increasing the strength of magnetic field. Fig. 5.9 demonstrates the influence of 'β_1' parameter on pressure gradient. Pressure gradient decreases in presence of slip effects. Impact of curvature parameter on pressure gradient is shown in Fig. 5.10. Pressure gradient slightly decreases by enhancing the curvature parameter.

5.2.3 Heat transfer analysis

Effect of 'ϕ' on the temperature of nanofluid has been illustrated in Fig. 5.11. According to this Fig. temperature rapidly decreases by enhancing the nanomaterial amount in system. Fig. 5.12 exhibits the positive effect of Hall parameter on temperature. Fig. 5.13 depicts Hartman number effect on temperature. Temperature enhances for applied magnetic field. Fig. 5.14 and 5.15 indicate Biot number effect on the temperature at upper and lower channel walls. For higher Biot number, temperature profile rapidly decreases at both upper and lower walls. Temperature field for values of curvature parameter is depicted in Fig. 5.16. According to this Fig. temperature shows symmetric behavior by increasing curvature parameter.

Heat transfer rate for different values of "ϕ, m, M, Bi_1, Bi_2, Br, k, ϵ" are shown in Table 5.2. According to this table heat transport rate increases by enhancing the amount of nanomaterial, Hartman number, Biot number, Brinkman number, curvature parameter and heat source/sink parameter. However Hall parameter shows reverse behavior. Inclusion of nanoparticles in conventional fluid increases the heat transfer rate because nanoparticles have higher thermal conductivity. Larger values of Biot number facilitate the heat transport characteristics and decrease the temperature of nanofluid.

5.3 Key points

- The inclusion of nanomaterials in ordinary fluid improves the heat transport rate and decreases the temperature and axial velocity.
- Heat transport rate is improved subject to presence of magnetic field. Hartman number rapidly decreases temperature of nanofluid. Pressure gradient enhances for larger Hartman number.
- Higher Hall parameter decays pressure gradient. Further temperature and heat transfer rate also decrease.
- Convective boundary condition improves the heat transfer characteristics and it decreases the fluid temperature rapidly.
- Velocity increases near the wall by increasing velocity slip effects. However opposite trend is noticed near the center of channel. Further velocity slip parameter enhances pressure gradient.

5.4 Graphs and tables

Table 5.1: Numerical values of the thermophysical properties [7]:

Properties	H_2O	Cu
ρ (kg/m^3)	997.1	8933
K (W/mk)	0.613	401
C_p (j/kgK)	4179	385
β (1/k)10^{-6}	210	16.7
σ (S/m)	0.05	5.96×10^7

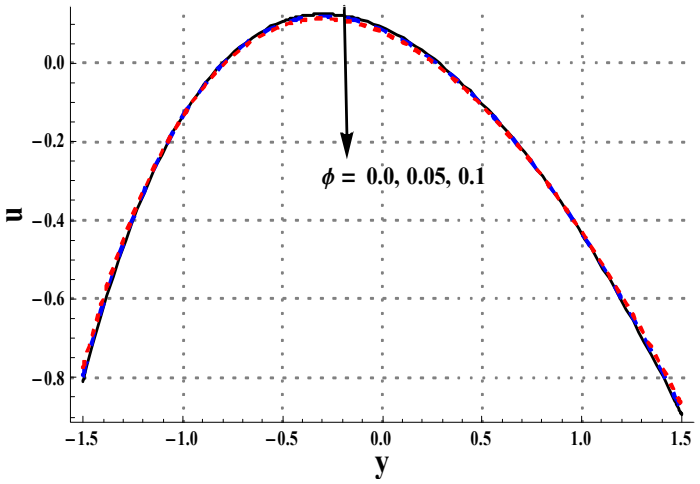

Fig.5.1. Plot of velocity for ϕ when $\eta = 1.4, x = 1.0, Br = 0.2, \epsilon = 4.0, Bi_1 = 0.9, Bi_2 = 1.2, m = 2.0, M = 1.0, \beta = 0.1$ and $k = 3.0$.

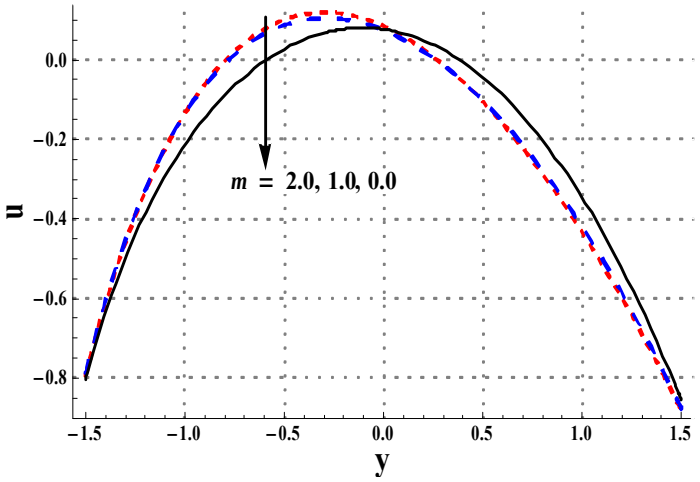

Fig.5.2. Plot of velocity for m when $\eta = 1.4, x = 1.0, Br = 0.2, \epsilon = 4.0, Bi_1 = 0.9, Bi_2 = 1.2, \phi = 0.05, M = 1.0, \beta = 0.1$ and $k = 3.0$.

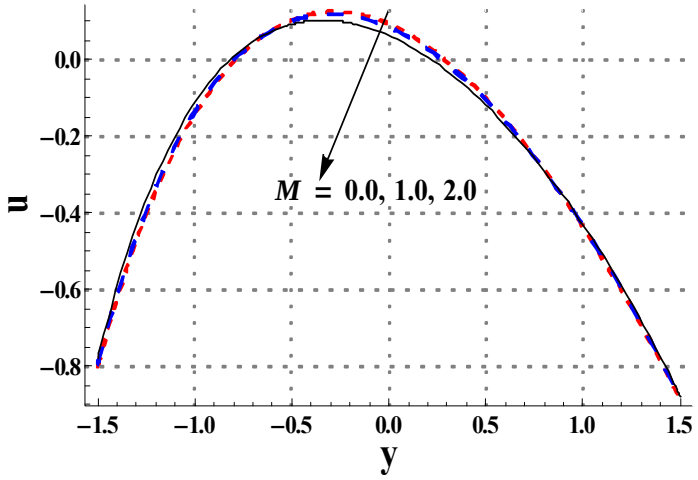

Fig.5.3. Plot of velocity for M when $\eta = 1.4, x = 1.0, Br = 0.2, \epsilon = 4.0, Bi_1 = 0.9, Bi_2 = 1.2, \phi = 0.05, m = 2.0, \beta = 0.1$ and $k = 3.0$.

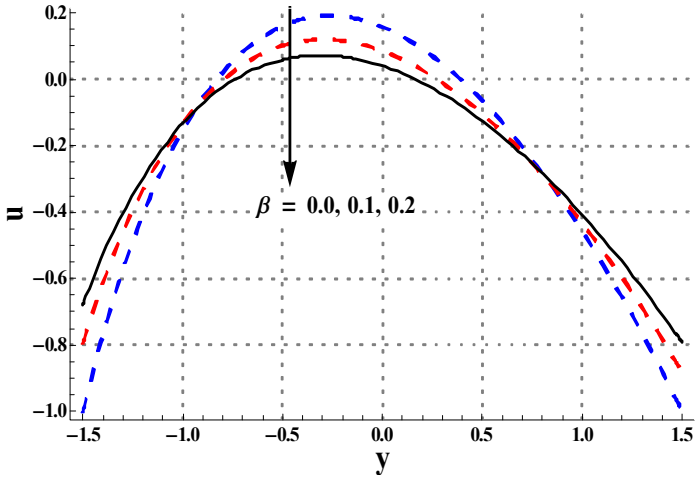

Fig.5.4. Plot of velocity for β when $\eta = 1.4, x = 1.0, Br = 0.2, \epsilon = 4.0, Bi_1 = 0.9, Bi_2 = 1.2, \phi = 0.05, M = 1.0, m = 2.0$ and $k = 3.0$.

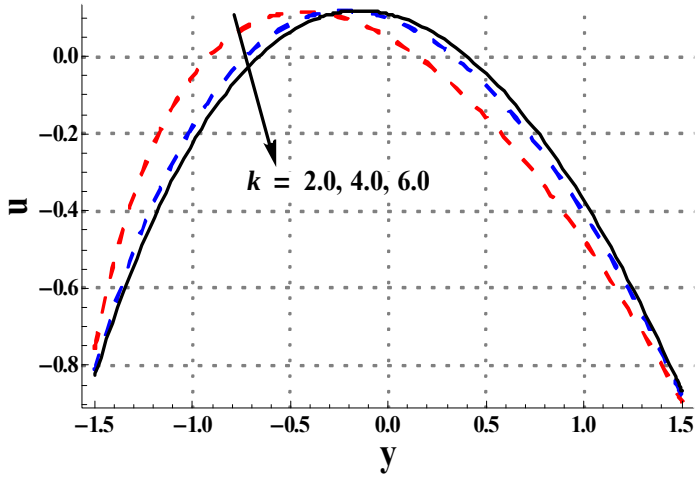

Fig.5.5. Plot of velocity for k when $\eta = 1.4, x = 1.0, Br = 0.2, \epsilon = 4.0, Bi_1 = 0.9, Bi_2 = 1.2, \phi = 0.05, M = 1.0, m = 2.0$ and $\beta = 0.1$.

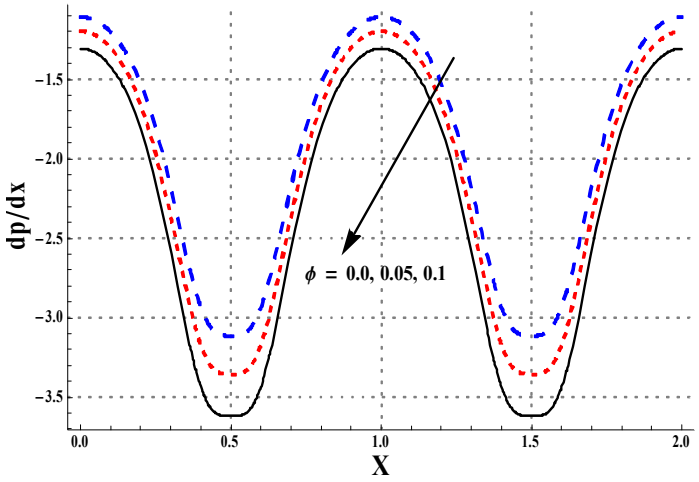

Fig.5.6. Effect of ϕ on dp/dx when $\eta = 1.4, Br = 0.2, \epsilon = 4.0, Bi_1 = 0.9, Bi_2 = 1.2, m = 2.0, M = 1.0, \beta = 0.1$ and $k = 3.0$.

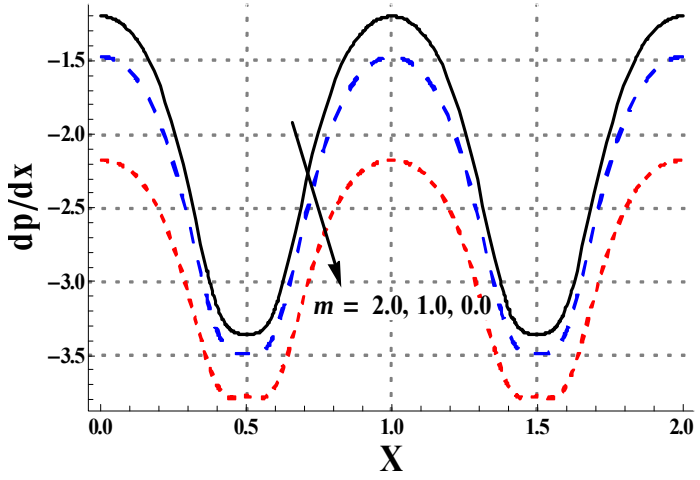

Fig.5.7. Effect of m on dp/dx when $\eta = 1.4, Br = 0.2, \epsilon = 4.0, Bi_1 = 0.9, Bi_2 = 1.2, \phi = 0.05, M = 1.0, \beta = 0.1$ and $k = 3.0$.

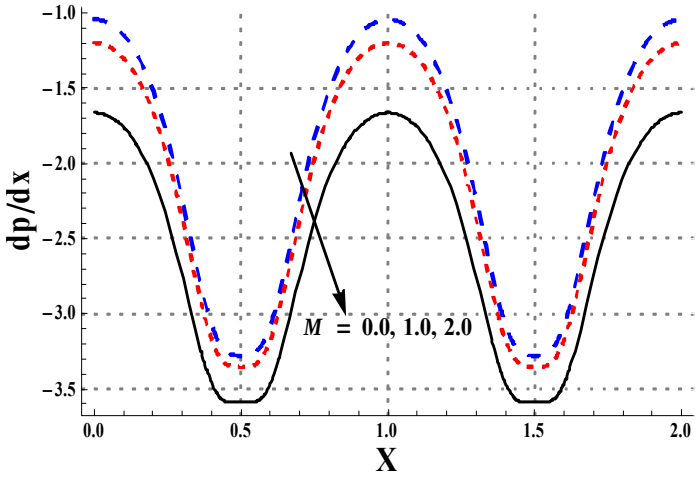

Fig.5.8. Effect of M on dp/dx when $\eta = 1.4, Br = 0.2, \epsilon = 4.0, Bi_1 = 0.9, Bi_2 = 1.2, \phi = 0.05, m = 2.0, \beta = 0.1$ and $k = 3.0$.

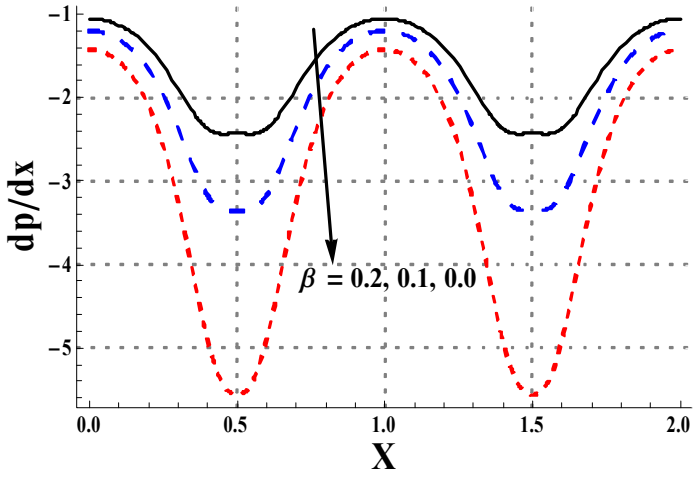

Fig.5.9. Effect of β on dp/dx when $\eta = 1.4, Br = 0.2, \epsilon = 4.0, Bi_1 = 0.9, Bi_2 = 1.2, \phi = 0.05, m = 2.0, M = 1.0$ and $k = 3.0$.

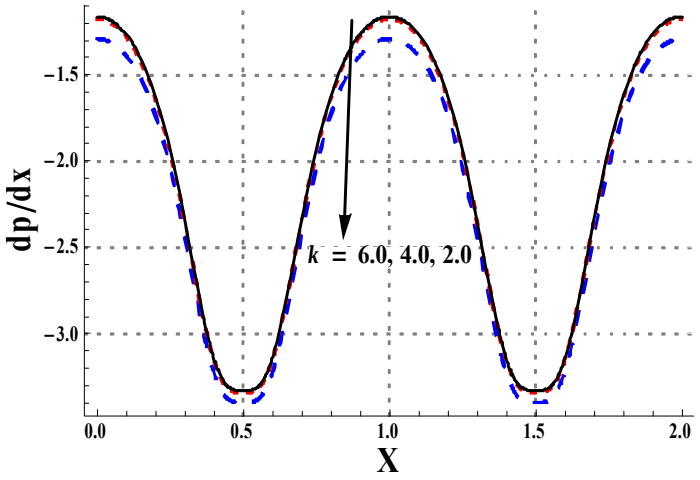

Fig.5.10. Effect of k on dp/dx when $\eta = 1.4, Br = 0.2, \epsilon = 4.0, Bi_1 = 0.9, Bi_2 = 1.2, \phi = 0.05, m = 2.0, M = 1.0$ and $\beta = 0.1$.

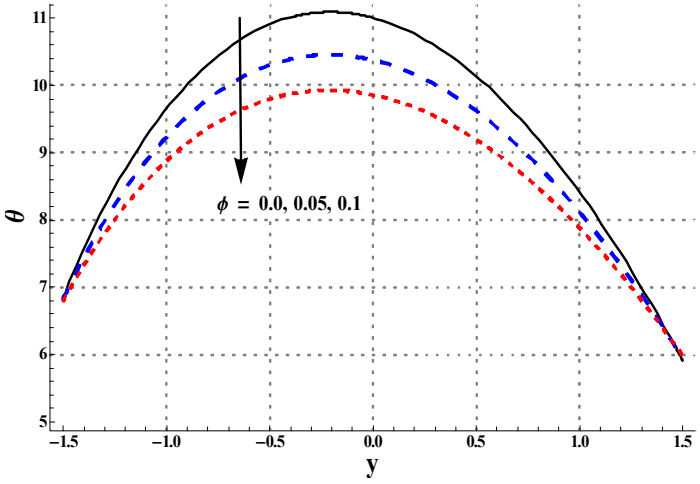

Fig.5.11. Effect of ϕ on θ when $\eta = 1.4, x = 1.0, Br = 0.2, \epsilon = 4.0, Bi_1 = 0.9, Bi_2 = 1.2, m = 2.0, M = 1.0, \beta = 0.1$ and $k = 3.0$.

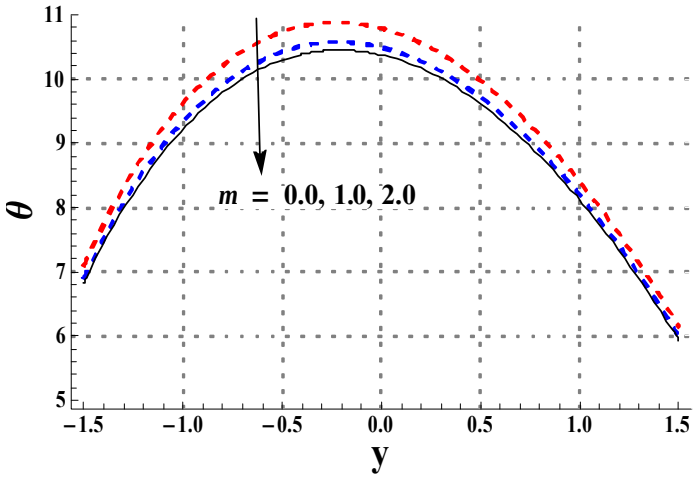

Fig.5.12. Effect of m on θ when $\eta = 1.4, x = 1.0, Br = 0.2, \epsilon = 4.0, Bi_1 = 0.9, Bi_2 = 1.2, \phi = 0.05, M = 1.0, \beta = 0.1$ and $k = 3.0$.

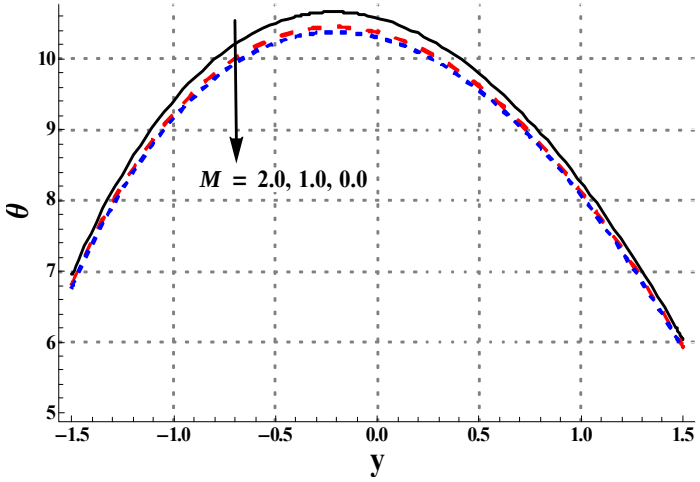

Fig.5.13. Effect of M on θ when $\eta = 1.4, x = 1.0, Br = 0.2, \epsilon = 4.0, Bi_1 = 0.9, Bi_2 = 1.2, \phi = 0.05, m = 2.0, \beta = 0.1$ and $k = 3.0$.

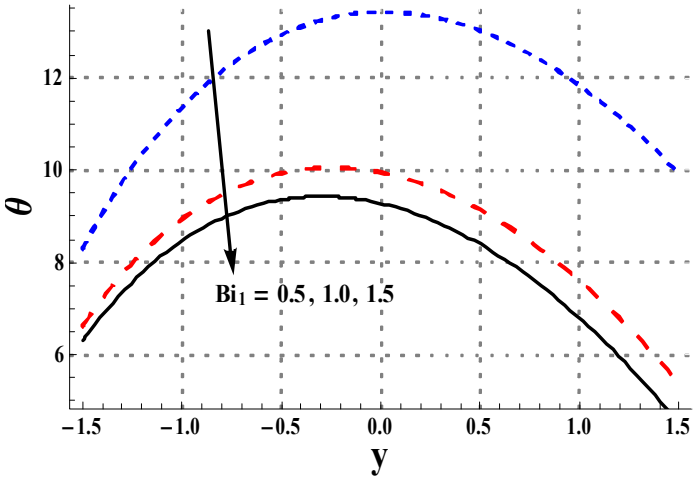

Fig.5.14. Effect of Bi_1 on θ when $\eta = 1.4, x = 1.0, Br = 0.2, \epsilon = 4.0, M = 1.0, Bi_2 = 1.2, \phi = 0.05, m = 2.0, \beta = 0.1$ and $k = 3.0$.

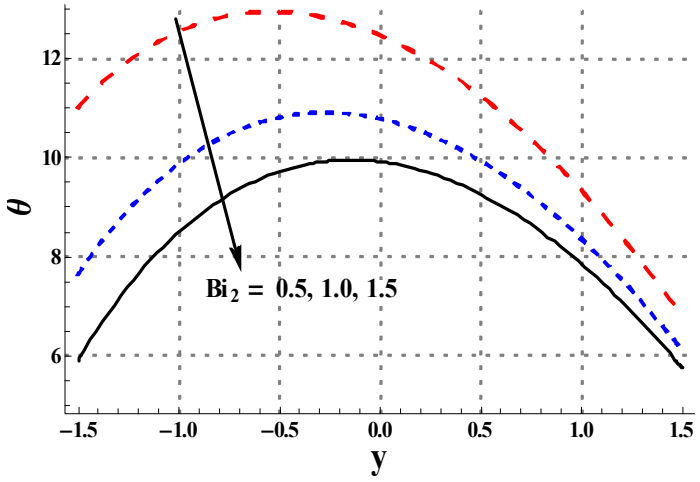

Fig.5.15. Effect of Bi_2 on θ when $\eta = 1.4, x = 1.0, Br = 0.2, \epsilon = 4.0, M = 1.0, Bi_1 = 0.9, \phi = 0.05, m = 2.0, \beta = 0.1$ and $k = 3.0$.

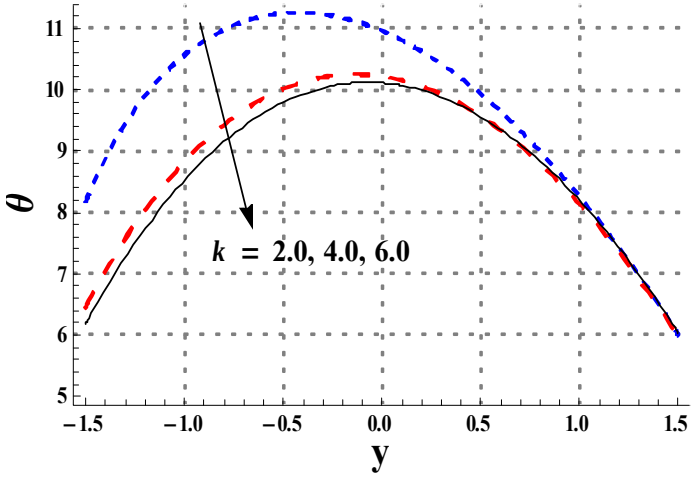

Fig.5.16. Effect of k on θ when $\eta = 1.4, x = 1.0, Br = 0.2, \epsilon = 4.0, M = 1.0, Bi_1 = 0.9, \phi = 0.05, m = 2.0, \beta = 0.1$ and $Bi_2 = 1.2$.

Table 5.2. Effects of $\phi, m, M, Bi_1, Bi_2, Br, k$ and $\in$ on heat transfer rate when $\eta = 1.4, \beta =$

0.1 and $x = 1.0$.

ϕ	m	M	Bi_1	Bi_2	Br	k	$\in$	$-\frac{K_{eff}}{K_f}\theta'[h]$
0.00	2.0	1.0	1.0	1.0	0.2	3.0	4.0	5.97795
0.05								6.02588
0.10								6.07489
0.05	0.0							6.22512
	1.0							6.08105
	2.0							6.02588
	2.0	0.0						5.99446
		1.0						6.02588
		2.0						6.11922
		1.0	0.5					5.37601
			1.0					6.02588
			1.5					6.27889
			1.0	0.5				6.63826
				1.0				6.02588
				1.5				5.70949
				1.0	0.1			5.90787
					0.2			6.02588
					0.3			6.14390
					0.2	2.0		6.01151
						4.0		6.08655
						6.0		6.17630
						3.0	2.0	3.19140
							4.0	6.02588
							6.0	8.86037

Chapter 6

Joule heating in mixed convective peristalsis of Sisko nanomaterial

Intention in this chapter is to communicate peristaltic activity of non-Newtonian nanofluid in presence of mixed convection and Joule heating. Sisko fluid constitutive equations are employed for non-Newtonian fluid. Viscous dissipation and Hall current effects are also retained. Velocity slip and thermal slip conditions are present. Analysis is arranged in presence of zero mass flux condition. The proposed mathematical model has relevance with blood circulation, hyperthermia, cancer therapy and drug delivery procedures. Related problems are modeled and computed for the results of velocity, temperature, concentration and pressure gradient. Main outcomes are summarized in conclusions.

6.1 Methodology

Peristaltic activity of Sisko nanofluid in an asymmetric channel of width $(d_1 + d_2)$ is studied. Consider the Cartesian coordinate system with $X-axis$ along the length of channel and $Y-axis$ transverse to it. Peristaltic motion is generated by sinusoidal waves travel along channel walls with wavelength λ and speed "c". The shapes of peristaltic walls in mathematical form satisfy (see Fig. 6.1):

$$\bar{H}_1(\bar{X}, \bar{t}) = d_1 + a_1 cos(\frac{2\pi}{\lambda}(\bar{X} - c\bar{t})),$$

$$\bar{H}_2(\bar{X},\bar{t}) = -d_2 - b_1 cos(\frac{2\pi}{\lambda}(\bar{X} - c\bar{t}) + \gamma^*). \tag{6.1}$$

Here $\bar{H}_1$ depicts the upper channel wall, $\bar{H}_2$ the lower walls of channel, t stands for time, γ^* depicts phase difference and a_1 and b_1 the upper and lower walls amplitudes. Nanofluid is electrically conducting subject to strong applied magnetic field and thus Hall current is accounted. Lorentz force in absence of electric field satisfies:

$$\mathbf{F} = \mathbf{J} \times \mathbf{B}, \tag{6.2}$$

where $\mathbf{B}$ is the applied magnetic field and $\mathbf{J}$ represents the current density. The Ohm's law is represented by:

$$\mathbf{J} = \sigma_{nf}\left[\mathbf{V} \times \mathbf{B} - \frac{1}{en_e}[\mathbf{J} \times \mathbf{B}]\right]. \tag{6.3}$$

Note that σ_{nf} represents the electric conductivity of nanofluid, $\mathbf{V} = [\bar{U}(\bar{X},\bar{Y},\bar{t}), \bar{V}(\bar{X},\bar{Y},\bar{t}), 0]$ denotes the velocity field, e represents the electron charge, n_e stands for number of density of free electrons and electric field being negligible. From Eqs. (6.2) and (6.3) we obtain:

$$\mathbf{F} = \left[\frac{\sigma_{nf}B_0^2}{1+m^2}(-\bar{U} + m\bar{V}), \frac{-\sigma_{nf}B_0^2}{1+m^2}(\bar{V} + m\bar{U}), 0\right], \tag{6.4}$$

where the Hall parameter m is defined as follows:

$$m = \frac{\sigma_{nf}B_0}{en_e}.$$

Joule heating expression can be described as:

$$\frac{1}{\sigma_{nf}}\mathbf{J}.\mathbf{J} = \frac{\sigma_{nf}B_0^2}{1+m^2}(\bar{U}^2 + \bar{V}^2). \tag{6.5}$$

Buongiorno model is adopted to elaborate the role of nanomaterial in system. Effects of Ohmic heating and viscous dissipation are also accounted. The governing expressions are:

$$\frac{\partial \bar{U}}{\partial \bar{X}} + \frac{\partial \bar{V}}{\partial \bar{Y}} = 0, \tag{6.6}$$

$$\rho_f\left(\frac{\partial}{\partial\bar{t}}+\bar{U}\frac{\partial}{\partial\bar{X}}+\bar{V}\frac{\partial}{\partial\bar{Y}}\right)\bar{U}=-\frac{\partial\bar{P}}{\partial\bar{X}}+\frac{\partial\bar{S}_{\bar{x}\bar{x}}}{\partial\bar{X}}+\frac{\partial\bar{S}_{\bar{x}\bar{y}}}{\partial\bar{Y}}$$
$$-\frac{\sigma_f B_0^2}{1+m^2}[\bar{U}-m\bar{V}]+g\rho_f[\zeta(T-T_m)+\zeta^*(C-C_m)], \tag{6.7}$$

$$\rho_f\left(\frac{\partial}{\partial\bar{t}}+\bar{U}\frac{\partial}{\partial\bar{X}}+\bar{V}\frac{\partial}{\partial\bar{Y}}\right)\bar{V}=-\frac{\partial\bar{P}}{\partial\bar{y}}+\frac{\partial\bar{S}_{\bar{y}\bar{x}}}{\partial\bar{X}}+\frac{\partial\bar{S}_{\bar{y}\bar{y}}}{\partial\bar{Y}}-\frac{\sigma_{nf}B_0^2}{1+m^2}[\bar{V}+m\bar{U}], \tag{6.8}$$

$$(\rho C)_f\left(\bar{U}\frac{\partial}{\partial\bar{X}}+\bar{V}\frac{\partial}{\partial\bar{Y}}\right)T=K_f\left[\frac{\partial^2T}{\partial\bar{X}^2}+\frac{\partial^2T}{\partial\bar{Y}^2}\right]+\bar{S}.\bar{L}+\frac{\sigma_f B_0^2}{1+m^2}[\bar{U}^2+\bar{V}^2]$$
$$+(\rho C)_{np}\left[D_B\left(\frac{\partial C}{\partial\bar{X}}\frac{\partial T}{\partial\bar{X}}+\frac{\partial C}{\partial\bar{Y}}\frac{\partial T}{\partial\bar{Y}}\right)+\frac{D_T}{T_m}\left(\left(\frac{\partial T}{\partial\bar{X}}\right)^2+\left(\frac{\partial T}{\partial\bar{Y}}\right)^2\right)\right], \tag{6.9}$$

$$\bar{U}\frac{\partial C}{\partial\bar{X}}+\bar{V}\frac{\partial C}{\partial\bar{Y}}=D_B\left(\frac{\partial^2C}{\partial\bar{X}^2}+\frac{\partial^2C}{\partial\bar{Y}^2}\right)+\frac{D_T}{T_m}\left(\frac{\partial^2T}{\partial\bar{X}^2}+\frac{\partial^2T}{\partial\bar{Y}^2}\right). \tag{6.10}$$

In above equations, $(\rho C)_{np}$ depicts the effective heat capacity of nanomaterials, K_f the thermal conductivity of fluid, C_f the specific heat, S_{ij} the components of extra stress tensor, σ_f the electrical conductivity of fluid, ρ_f the density of fluid, $\bar{L}$ the gradient of velocity, $\bar{S}.\bar{L}$ the viscous dissipation, C depicts concentration, $C_m(=\frac{C_0+C_1}{2})$ stands for mean concentration, T for fluid temperature, T_m for mean temperature of nanoparticles, P for pressure, D_T for thermophoretic diffusion coefficient and D_B for Brownian diffusion. An extra stress tensor $\bar{\mathbf{S}}$ in Sisko fluid satisfies the following relation:

$$\bar{\mathbf{S}}=\left[\alpha^*+\beta^{**}\left(\Pi\right)^{n-1}\right]\mathbf{A}_1, \tag{6.11}$$

where $\mathbf{A}_1$ depicts the first Rivilin-Ericksen tensor and Π obeys

$$\Pi=\sqrt{\frac{1}{2}tr\left(\mathbf{A}_1^2\right)}, \tag{6.12}$$

and

$$\mathbf{A}_1=\left[\operatorname{grad}\mathbf{V}+\left(\operatorname{grad}\mathbf{V}\right)^T\right]. \tag{6.13}$$

Here α and β^* depict material parameters of fluid. Further n describe the features of power law index. Note that for $(n = 1, \alpha = 0, \beta^* = \mu$ or $\alpha = \mu, \beta^* = 0)$ the viscous fluid model is recovered.

The zero mass flux conditions for concentration of nanofluid is:

$$D_B \frac{\partial C}{\partial \bar{Y}} + \frac{D_T}{T_m} \frac{\partial T}{\partial \bar{Y}} = 0 \text{ at } y = h_1 \text{ and } y = h_2. \tag{6.14}$$

By using the transformations:

$$\bar{x} = \bar{X} - c\bar{t}, \bar{y} = \bar{Y}, \bar{u} = \bar{U} - c, \bar{v} = \bar{V}, \bar{p}(\bar{x}, \bar{y}) = \bar{P}(\bar{X}, \bar{Y}, \bar{t}), \tag{6.15}$$

the resulting equations are:

$$\frac{\partial \bar{u}}{\partial \bar{x}} + \frac{\partial \bar{v}}{\partial \bar{y}} = 0, \tag{6.16}$$

$$\rho_f \left((\bar{u} + c) \frac{\partial}{\partial \bar{x}} + \bar{v} \frac{\partial}{\partial \bar{y}} \right) (\bar{u} + c) = -\frac{\partial \bar{p}}{\partial \bar{x}} + \frac{\partial \bar{s}_{\bar{x}\bar{x}}}{\partial \bar{x}} + \frac{\partial \bar{s}_{\bar{x}\bar{y}}}{\partial \bar{y}}$$
$$- \frac{\sigma_f B_0^2}{1 + m^2} [(\bar{u} + c) - m\bar{v}] + g\rho_f [\zeta (T - T_m) + \zeta^* (C - C_m)], \tag{6.17}$$

$$\rho_f \left((\bar{u} + c) \frac{\partial}{\partial \bar{x}} + \bar{v} \frac{\partial}{\partial \bar{y}} \right) \bar{v} = -\frac{\partial \bar{p}}{\partial \bar{y}} + \frac{\partial \bar{s}_{\bar{y}\bar{x}}}{\partial \bar{x}} + \frac{\partial \bar{s}_{\bar{y}\bar{y}}}{\partial \bar{y}} - \frac{\sigma_{nf} B_0^2}{1 + m^2} [\bar{v} + m(\bar{u} + c)], \tag{6.18}$$

$$(\rho C)_f \left((\bar{u} + c) \frac{\partial}{\partial \bar{x}} + \bar{v} \frac{\partial}{\partial \bar{y}} \right) T = K_f \left(\frac{\partial^2 T}{\partial \bar{x}^2} + \frac{\partial^2 T}{\partial \bar{y}^2} \right) + \bar{s}.\bar{L} + \frac{\sigma_f B_0^2}{1 + m^2} [(\bar{u} + c)^2 + \bar{v}^2]$$
$$+ (\rho C)_{np} \left[\frac{D_T}{T_m} \left(\left(\frac{\partial T}{\partial \bar{y}} \right)^2 + \left(\frac{\partial T}{\partial \bar{x}} \right)^2 \right) + D_B \left(\frac{\partial C}{\partial \bar{x}} \frac{\partial T}{\partial \bar{x}} + \frac{\partial C}{\partial \bar{y}} \frac{\partial T}{\partial \bar{y}} \right) \right], \tag{6.19}$$

$$(\bar{u} + c) \frac{\partial C}{\partial \bar{x}} + \bar{v} \frac{\partial C}{\partial \bar{y}} = D_B \left(\frac{\partial^2 C}{\partial \bar{x}^2} + \frac{\partial^2 C}{\partial \bar{y}^2} \right) + \frac{D_T}{T_m} \left(\frac{\partial^2 T}{\partial \bar{x}^2} + \frac{\partial^2 T}{\partial \bar{y}^2} \right), \tag{6.20}$$

$$\bar{s}_{\bar{x}\bar{x}} = 2 \left[\alpha^* + \beta^{**} \left(2 \left(\frac{\partial \bar{v}}{\partial \bar{y}} \right)^2 + \left(\frac{\partial \bar{u}}{\partial \bar{y}} + \frac{\partial \bar{v}}{\partial \bar{x}} \right)^2 + 2 \left(\frac{\partial \bar{u}}{\partial \bar{x}} \right)^2 \right)^{\frac{n-1}{2}} \right] \frac{\partial \bar{u}}{\partial \bar{x}},$$

$$\bar{s}_{\bar{x}\bar{y}} = \bar{s}_{\bar{y}\bar{x}} = \left[\alpha^* + \beta^{**} \left(2 \left(\frac{\partial \bar{v}}{\partial \bar{y}} \right)^2 + \left(\frac{\partial \bar{u}}{\partial \bar{y}} + \frac{\partial \bar{v}}{\partial \bar{x}} \right)^2 + 2 \left(\frac{\partial \bar{u}}{\partial \bar{x}} \right)^2 \right)^{\frac{n-1}{2}} \right] \left(\frac{\partial \bar{u}}{\partial \bar{y}} + \frac{\partial \bar{v}}{\partial \bar{x}} \right),$$

$$\bar{s}_{\bar{y}\bar{y}} = 2\left[\alpha^* + \beta^{**}\left(2\left(\frac{\partial \bar{v}}{\partial \bar{y}}\right)^2 + \left(\frac{\partial \bar{u}}{\partial \bar{y}} + \frac{\partial \bar{v}}{\partial \bar{x}}\right)^2 + 2\left(\frac{\partial \bar{u}}{\partial \bar{x}}\right)^2\right)^{\frac{n-1}{2}}\right]\frac{\partial \bar{v}}{\partial \bar{y}}.$$

Here following dimensionless parameters are employed:

$$x = \frac{\bar{x}}{\lambda}, y = \frac{\bar{y}}{d_1}, u = \frac{\bar{u}}{c}, v = \frac{\bar{v}}{c\delta}, \delta = \frac{\bar{d}_1}{\lambda}, h_1 = \frac{\bar{H}_1}{d_1}, h_2 = \frac{\bar{H}_2}{d_2}, d = \frac{d_2}{d_1}, a = \frac{a_1}{d_1}, b = \frac{b_1}{d_1}, p = \frac{d_1^2\bar{p}}{c\lambda\alpha},$$
$$Re = \frac{\rho_f\ cd_1}{\alpha}, Ec = \frac{c^2}{C_f(T_1 - T_0)}, Pr = \frac{\alpha C_f}{K_f}, M = \sqrt{\frac{\sigma_f}{\alpha}}B_0 d_1, N_b = \frac{\tau D_B(C_1 - C_0)}{\nu}, N_t = \frac{\tau D_T(T_1 - T_0)}{\nu T_m},$$
$$\upsilon = \frac{\alpha}{\rho_f}, G_T = \frac{\rho_f g\zeta(T_1 - T_0)d_1^2}{\alpha c}, G_c = \frac{\rho_f g\zeta^*(C_1 - C_0)d_1^2}{\alpha c}, \theta = \frac{T - T_m}{T_1 - T_0}, Br = \Pr Ec, u = \frac{\partial \psi}{\partial y}, v = -\frac{\partial \psi}{\partial x}, \tag{6.21}$$

in which $M, \Pr, Ec, G_c, G_T, \theta, \delta, Br, Re, N_t$ and N_b depict the Hartman number, Prandtl number, Eckert number, the concentration Grashoff number, the thermal Grashoff number, dimensionless temperature, wave number, Brinkman number, Reynolds number, thermophoresis parameter and Brownian motion parameter respectively. After nondimensionalizing the above equations and utilizing small Reynold number and long wavelength considerations, we have final form of equations in terms of stream function ψ:

$$p_y = 0, \tag{6.22}$$

$$p_x = \frac{\partial s_{xy}}{\partial y} + G_T\theta + G_C\phi - \frac{M^2}{1+m^2}\left(1 + \frac{\partial \psi}{\partial y}\right), \tag{6.23}$$

$$\theta_{yy} + Br\Phi + \Pr N_b\phi_y\theta_y + \Pr N_t\left(\theta_y\right)^2 + \frac{BrM^2}{1+m^2}\left(1 + \frac{\partial \psi}{\partial y}\right)^2 = 0, \tag{6.24}$$

$$N_b\phi_{yy} + N_t\theta_{yy} = 0, \tag{6.25}$$

in which continuity equation is trivially justified, Φ depicts the non-dimensional form of viscous dissipation and s_{xy} satisfies:

$$s_{xy} = s_{yx} = \left[1 + \beta(\psi_{yy})^{n-1}\right]\psi_{yy}. \tag{6.26}$$

The quantity $\mu_{app} = 1 + \beta(\psi_{yy})^{n-1}$ is called apparent viscosity. From Eqs. (6.22)-(6.26) we obtain:

$$\frac{\partial^2}{\partial y^2}\left[1 + \beta(\psi_{yy})^{n-1}\right]\psi_{yy} + G_T\theta_y + G_C\phi_y - \frac{M^2}{1+m^2}\psi_{yy} = 0, \tag{6.27}$$

$$\theta_{yy} + Br\left[1+\beta(\psi_{yy})^{n-1}\right]\psi_{yy}^2 + \Pr N_b\phi_y\theta_y + \Pr N_t\left(\theta_y\right)^2 + \frac{BrM^2}{1+m^2}\left(1+\frac{\partial\psi}{\partial y}\right)^2 = 0, \quad (6.28)$$

$$N_b\phi_{yy} + N_t\theta_{yy} = 0. \quad (6.29)$$

The dimensionless form of flow rate in the wave $F(=\bar{q}/cd_1)$ and laboratory $\eta(=\bar{Q}/cd_1)$ frames are associated through the relation:

$$\eta = F + d + 1, \quad (6.30)$$

where 'F' satisfies:

$$F = \int_{h_1}^{h_2}\frac{\partial\psi}{\partial y}dy. \quad (6.31)$$

The dimensionless slip and zero mass flux conditions are:

$$\begin{gathered}\psi = \tfrac{F}{2}, \psi_y + \beta_1\left[1+\beta(\psi_{yy})^{n-1}\right]\psi_{yy} = -1, \theta + \gamma\,\theta_y = 0 \\ \text{and } N_b\phi_y + N_t\theta_y = 0 \text{ at } y = h_1,\end{gathered} \quad (6.33)$$

$$\begin{gathered}\psi = -\tfrac{F}{2}, \psi_y - \beta_1\left[1+\beta(\psi_{yy})^{n-1}\right]\psi_{yy} = -1, \theta - \gamma\,\theta_y = 0 \\ \text{and } N_b\phi_y + N_t\theta_y = 0 \text{ at } y = h_2,\end{gathered} \quad (6.34)$$

in which β_1 and γ depicts the velocity and thermal slip variables. Final form of walls are:

$$h_1 = 1 + acos(2\pi x),$$
$$h_2 = -d - bcos(2\pi x + \gamma^{**}).$$

Here numerical approach is employed for solution of equations subject to boundary conditions. NDSolve technique is used for this purpose in Mathematica. Graphical explanation of the results is described in the next section.

6.2 Results description

Our interest here is to provide explanation for velocity, temperature, concentration and pressure gradient. Separate subsections are thus arranged for each physical quantity.

6.2.1 Axial velocity

Effect of parameters like Hartman number, non-Newtonian parameter and slip on velocity distribution are analyzed via Figs. (6.2)-(6.4). Axial velocity shows parabolic characteristics in which maximum fluid velocity is seen near the central portion of channel. Fig. 6.2 depicts the pattern of fluid velocity for different values of Hartman number. Velocity depicts decreasing trend when Hartman number enhances. The presence of magnetic force mobilized the Lorentz force that creates resistance therefore velocity decays. Impact of β parameter on the velocity is examined via Fig. 6.3. Velocity field is suppressed when non-Newtonian parameter enhances. Influence of σ on flow is exhibited in Fig. 6.4. Velocity enhances throughout the channel for higher σ.

6.2.2 Temperature

Impacts of various physical flow parameters like Hartman number, Hall parameter, temperature jump parameter, thermal Grashoff number, concentration Grashoff number and Brinkman number on temperature are exhibited in Figs (6.5)-(6.10). Influence of Hartman number on temperature distribution is presented in Fig. 6.5. It is evident that temperature enhances by enhancing the Hartman number. Further prominent effects are seen near the channel center. Temperature for Hall parameter is presented in Fig. 6.6. Temperature depicts decreasing trend for higher Hall parameter. Outcome of γ parameter on θ is computed in Fig. 6.7. It is observed that an increasing value of temperature jump variables shows decreasing trend for temperature. However temperature is more near the central portion of channel. Fig. 6.8 illustrates impact of thermal Grashoff number on temperature. Clearly the temperature slightly enhances against higher thermal Grashoff number. Fig. 6.9 depicts impact of G_C on temperature. An increase in G_c gives rise to temperature. Fig. 6.10 depicts temperature distribution for Brinkman number. Smaller Brinkman number depict higher temperature.

6.2.3 Concentration

Variation of concentration for numerous values of important parameters are illustrated in Figs. (6.11)-(6.17). Fig. 6.11 displays the influence of thermophoresis parameter on concentration. It represents that concentration of nanomaterial rapidly enhances for higher N_t. Influence

of N_b on concentration is displayed in Fig. 6.12. Clearly the concentration for higher N_b is decreased. Fig. 6.13 depicts impact of Hartman number on concentration field. It is noticed that ϕ slightly increases at central portion of channel by enhancing the strength of magnetic field. Fig. 6.14 displays the concentration for Hall number. As expected the concentration of nanomaterial decreases when Hall parameter enhances. Figs. 6.15 and 6.16 show the influences of thermal Grashoff number and concentration Grashoff number on concentration. Effect of Brinkman number on concentration is captured in Fig. 6.17. Concentration of nanomaterial against Brinkman number is increased throughout the channel.

6.2.4 Pressure gradient

Here Figs. (6.18)-(6.23) explain outcome of influential variables on the pressure gradient. A significant feature of pressure gradient trend is like sinusoidal wave. Pressure gradient remarkably increasing by increasing the magnetic field strength (see Fig. 6.18). Fig. 6.19 is organized for the Hall current impact on pressure gradient. It is apparent that pressure gradient decreases by increasing Hall number. Fig. 6.20 displays the concentration of nanomaterial for velocity slip. It is viewed that pressure gradient sharply decreases in presence of slip condition. Fig. 6.21 shows the influence of Brownian motion on pressure gradient. Higher N_b leads to a decrease in both narrow and wider portion of channel. Impact of N_t variable on dp/dx is presented in Fig. 6.22. Pressure gradient enhances with higher N_t in the wider and narrow portions of channel. Influence of non-Newtonian parameter on pressure is sketched via Fig. 6.23. Inspection of graph reveals that pressure gradient enhances in wider portion of medium by higher β.

6.3 Conclusions

Key findings here include the following points.

- Outcomes of Hartman number and non-Newtonian parameter on axial velocity are reverse to that of velocity slip variable.
- Temperature for Hartman number and Hall parameters behaves opposite.
- Temperature against Brinkman number is increased.

- An increment in thermophoresis parameter corresponds to stronger concentration. However concentration has decreasing trend for higher Brownian motion parameter.
- Concentration is enhanced for both Brinkman number and Hartman number.
- Pressure gradient has increasing behavior for higher Hartman number, thermophoresis and non-Newtonian parameters.

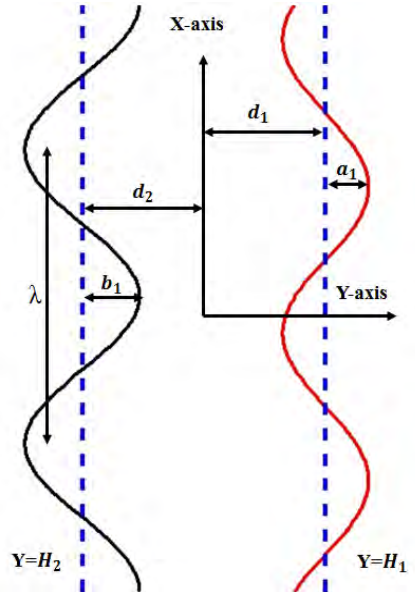

Fig. 6.1. Geometry of the problem.

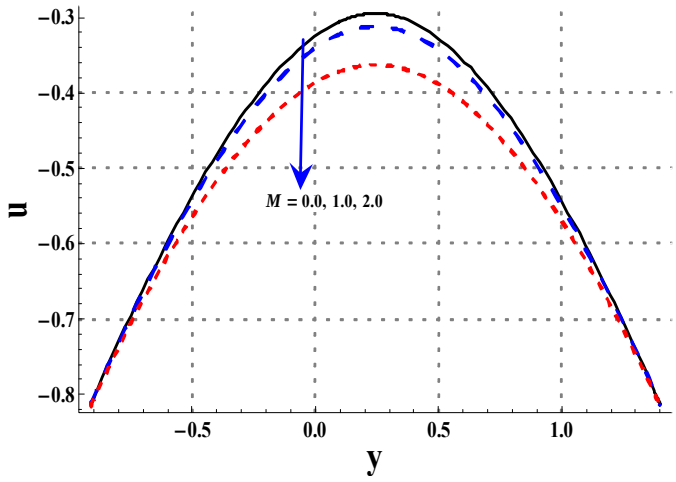

Fig. 6.2. Effect of M on velocity.

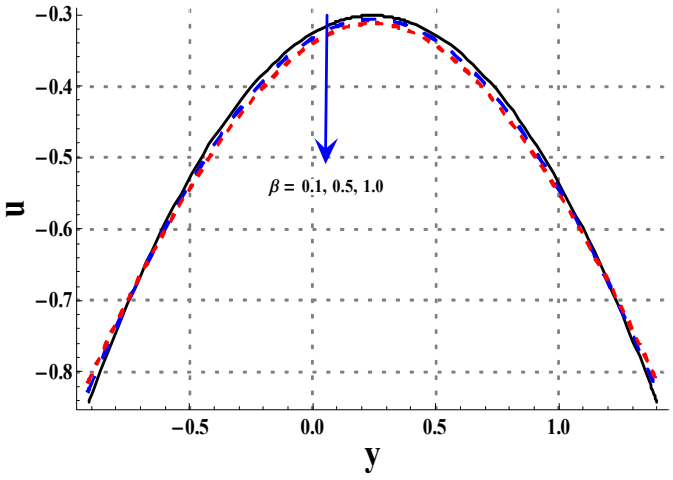

Fig. 6.3. Effect of β on velocity.

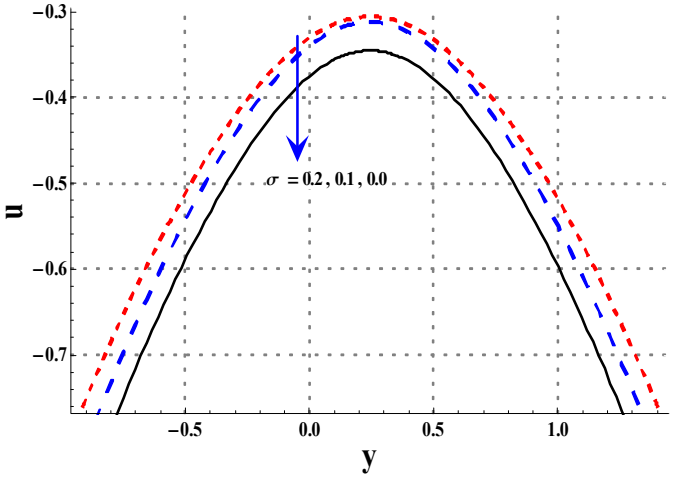

Fig. 6.4. Effect of σ on velocity.

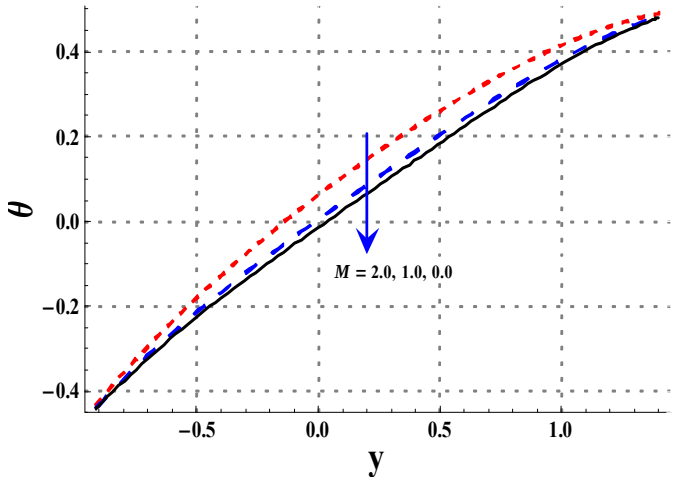

Fig. 6.5. Effect of M on θ.

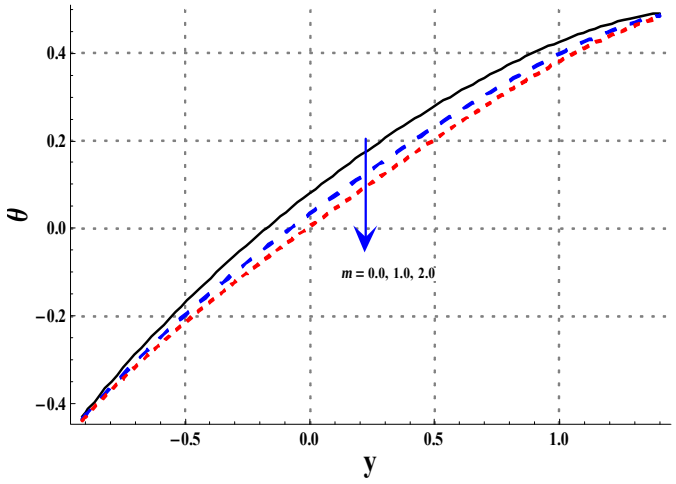

Fig. 6.6. Effect of m on θ.

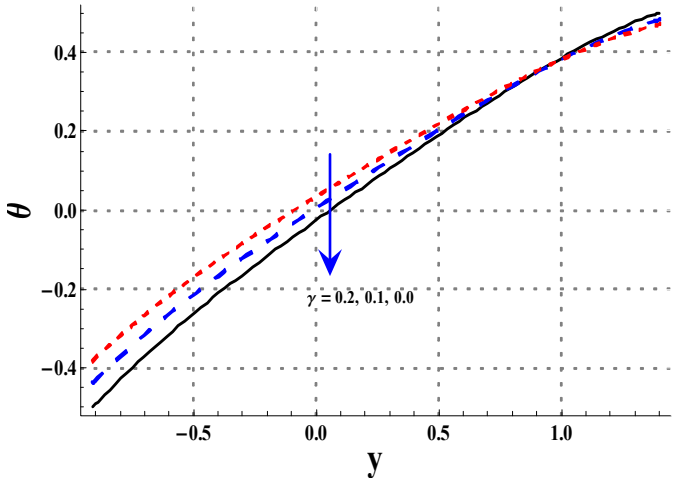

Fig. 6.7. Effect of γ on θ.

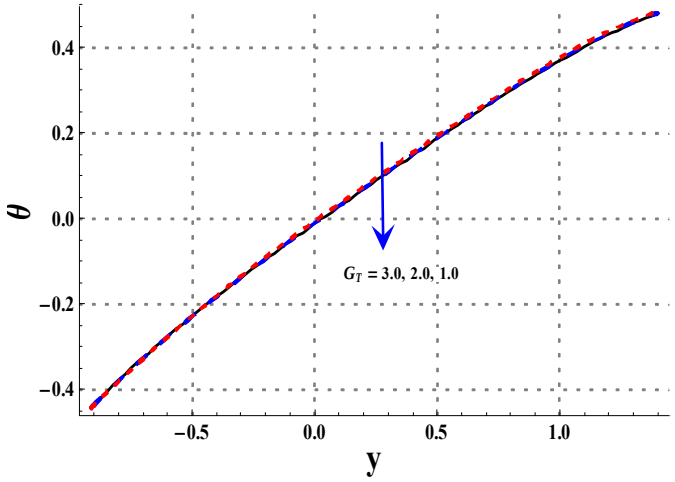

Fig. 6.8. Effect of G_T on θ.

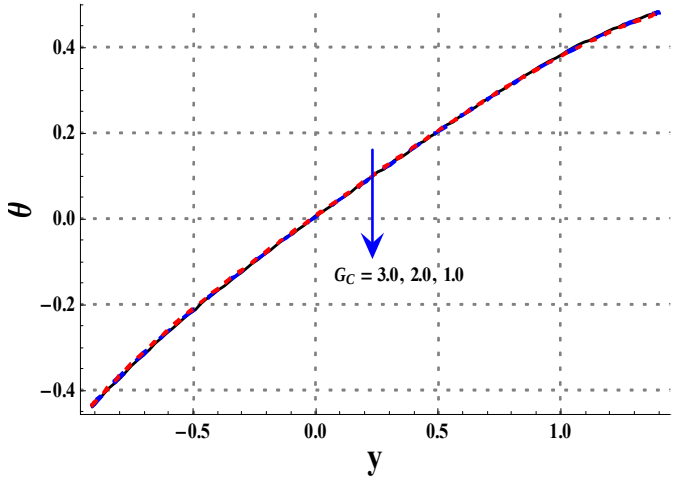

Fig. 6.9. Effect of G_C on θ.

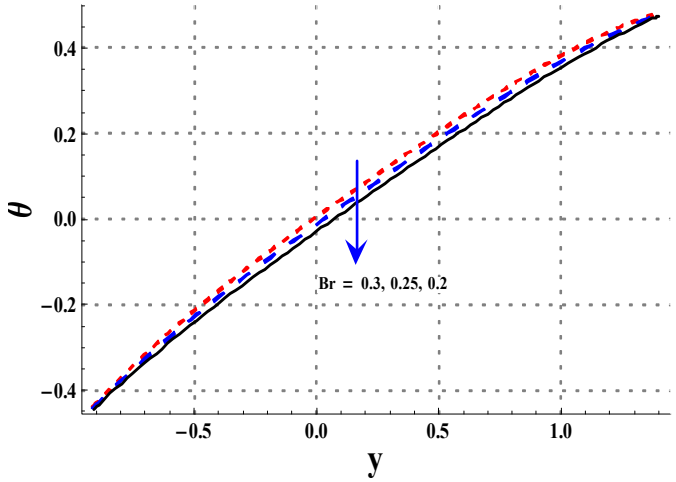

Fig. 6.10. Effect of Br on θ.

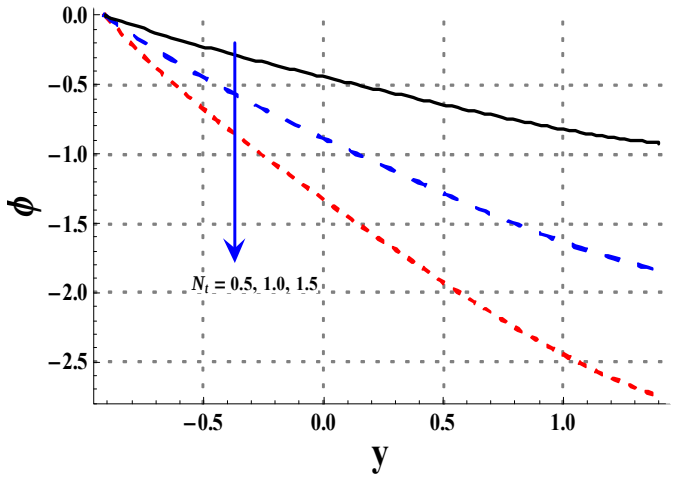

Fig. 6.11. Plot of ϕ for N_t.

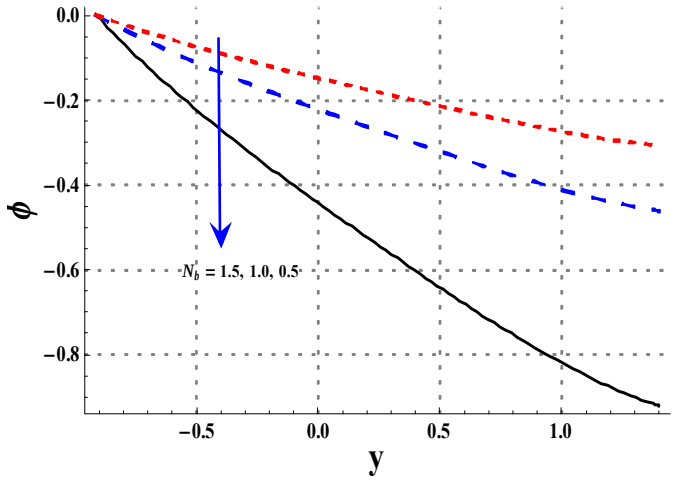

Fig. 6.12. Plot of ϕ for N_b.

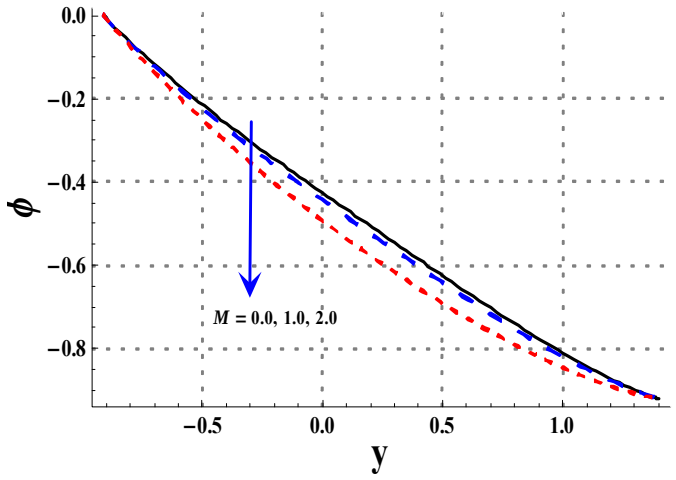

Fig. 6.13. Plot of ϕ for M.

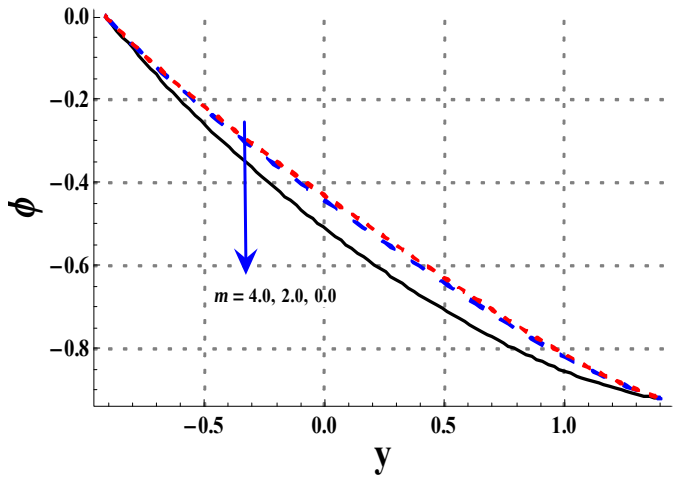

Fig. 6.14. Plot of ϕ for m.

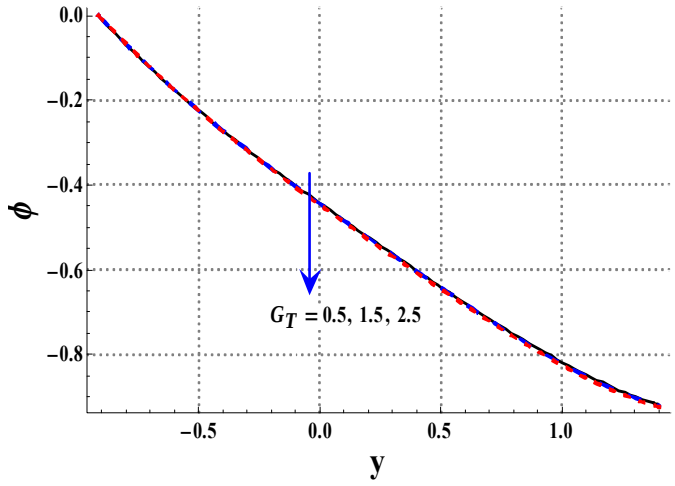

Fig. 6.15. Plot of ϕ for G_T.

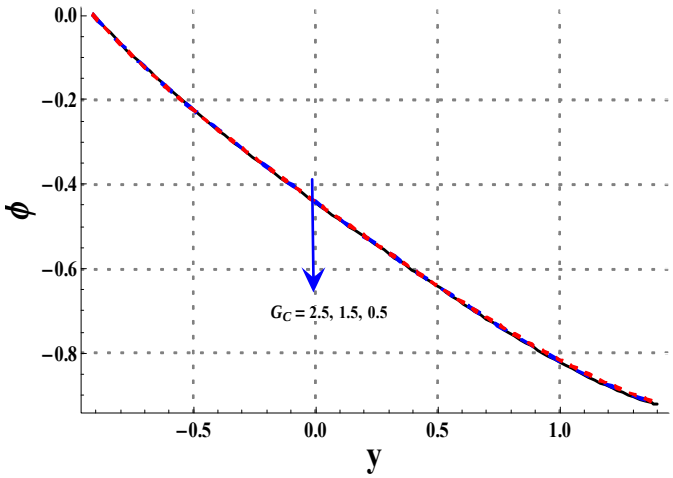

Fig. 6.16. Plot of ϕ for G_C.

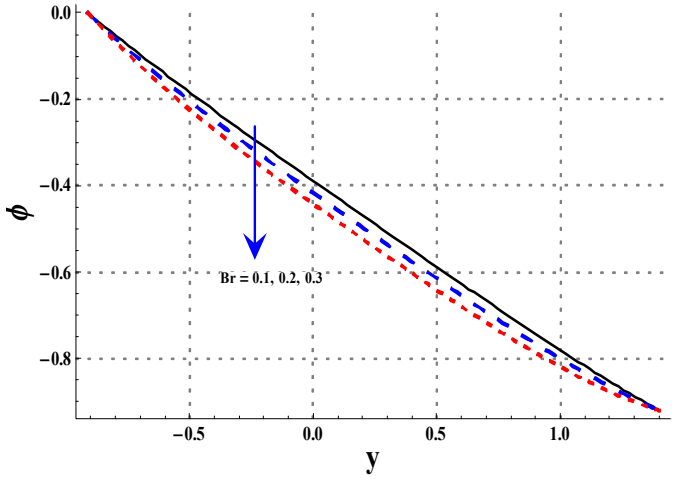

Fig. 6.17. Plot of ϕ for Br.

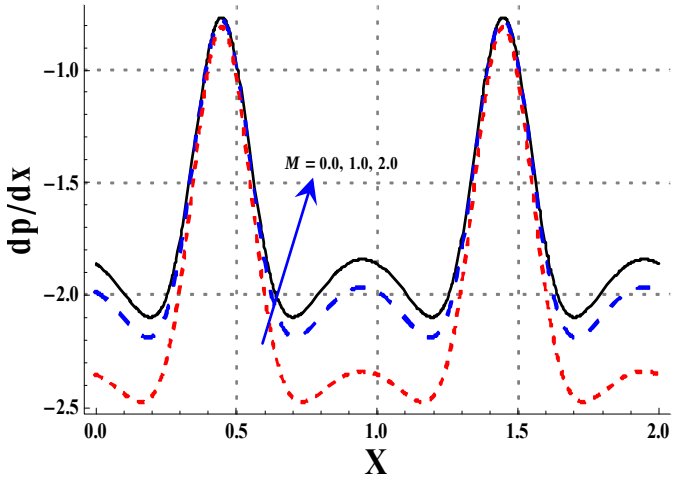

Fig. 6.18. Pressure gradient against M.

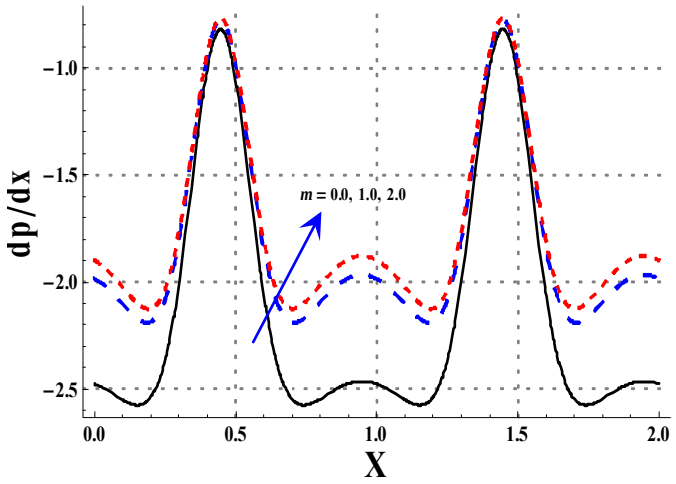

Fig. 6.19. Pressure gradient against m.

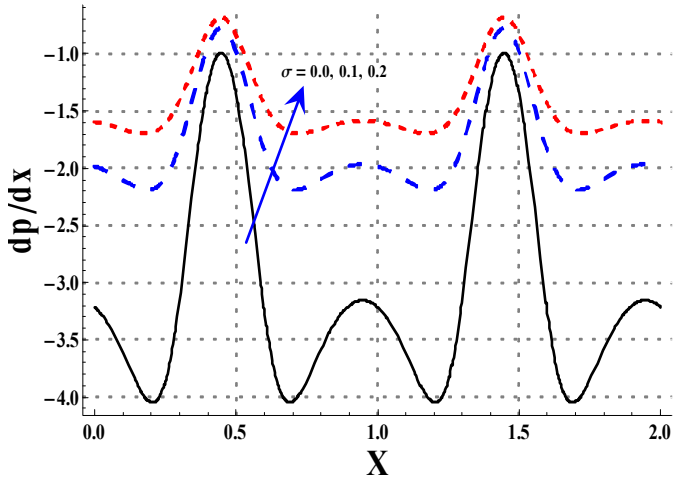

Fig. 6.20. Pressure gradient against σ.

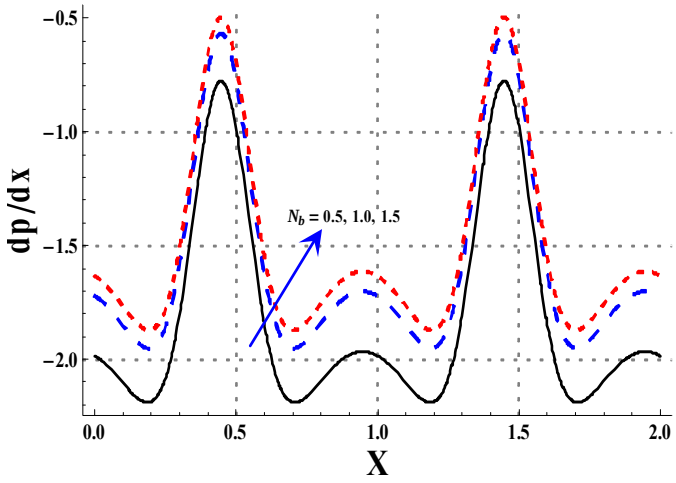

Fig. 6.21. Pressure gradient against N_b.

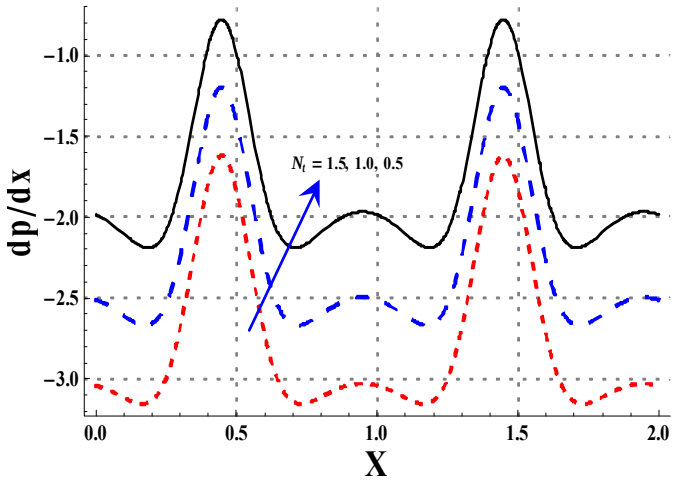

Fig. 6.22. Pressure gradient against N_t.

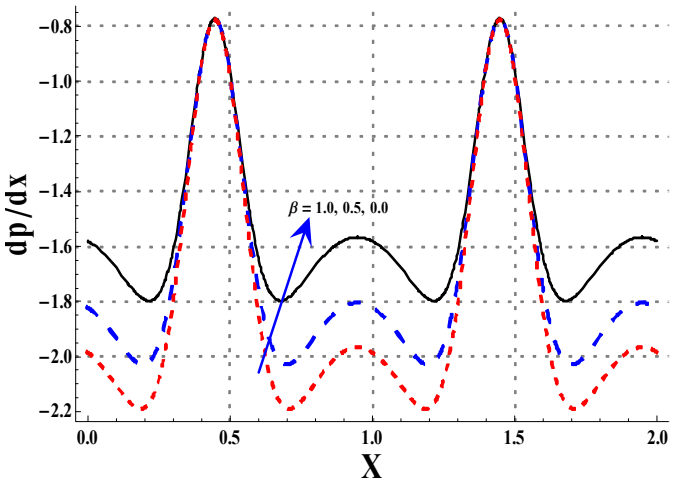

Fig. 6.23. Pressure gradient against β.

Chapter 7

Peristaltic radiative flow of Sisko nanomaterial with entropy generation and modified Darcy's law

This chapter explores peristaltic motion of Sisko fluid in presence of Hall current, Ohmic heating, dissipation and radiation are accounted. Modeling is based upon modified Darcy's law for porous medium. The relevant equations for small Reynold number and long wavelength are obtained. The computations for nonlinear system is organized employing ND Solve Mathematica. Quantities of interest like temperature, velocity, concentration and entropy generation are addressed.

7.1 Methodology

Here we consider the flow of nanofluid in a flexible walls channel having width 2a. We have taken the Cartesian coordinate system in which x-axis is along length of channel and y-axis transverse to it. The motion is produced due to the sinusoidal waves propagating along the channel wall with speed c. The mathematical formulation of the walls are:

$$\pm\bar{H}(\bar{X},\bar{t}) = \pm a \pm bcos(\frac{2\pi}{\lambda}(\bar{X}-c\bar{t})), \tag{7.1}$$

where b and λ depict the walls amplitude and wavelength respectively. The flow field is considered in the presence of applied magnetic field, porous medium and thermal radiation. Due to strong magnetic field the Hall effects also retained. Ohmic heating and viscous dissipation are also taken in energy equation. Buongiorno's nanofluid model with Brownian motion and thermophoresis elaborates characteristics of nanofluid. In this model concentration equation is also considered to study nanoparticle behavior. The velocity field for the two-dimensional flow is $\bar{\mathbf{V}} = \left[\bar{U}\left(\bar{X},\bar{Y},\bar{t}\right),\bar{V}\left(\bar{X},\bar{Y},\bar{t}\right),0\right]$. Here $\bar{U}$ and $\bar{V}$ depict the $\bar{X}$- and $\bar{Y}$-components of velocity. The governing equations for present study are:

$$\frac{\partial \bar{U}}{\partial \bar{X}} + \frac{\partial \bar{V}}{\partial \bar{Y}} = 0, \tag{7.2}$$

$$\rho_f \left[\frac{\partial \bar{U}}{\partial \bar{t}} + \bar{V}\frac{\partial \bar{U}}{\partial \bar{Y}} + \bar{U}\frac{\partial \bar{U}}{\partial \bar{X}}\right] = -\frac{\partial \bar{P}}{\partial \bar{X}} + \frac{\partial \bar{S}_{\bar{x}\bar{y}}}{\partial \bar{Y}} + \frac{\partial \bar{S}_{\bar{x}\bar{x}}}{\partial \bar{X}} - \frac{\sigma_f B_0^2}{1+m^2}\left(\bar{U} - m\bar{V}\right) + \bar{R}_{\bar{X}}, \tag{7.3}$$

$$\rho_f \left[\frac{\partial \bar{V}}{\partial \bar{t}} + \bar{V}\frac{\partial \bar{V}}{\partial \bar{Y}} + \bar{U}\frac{\partial \bar{V}}{\partial \bar{X}}\right] = -\frac{\partial \bar{P}}{\partial \bar{y}} + \frac{\partial \bar{S}_{\bar{y}\bar{y}}}{\partial \bar{Y}} + \frac{\partial \bar{S}_{\bar{y}\bar{x}}}{\partial \bar{X}} - \frac{\sigma_f B_0^2}{1+m^2}\left(\bar{V} + m\bar{U}\right) + \bar{R}_{\bar{Y}}, \tag{7.4}$$

$$\begin{aligned}(\rho C)_f \left[\frac{\partial T}{\partial \bar{t}} + \bar{V}\frac{\partial T}{\partial \bar{Y}} + \bar{U}\frac{\partial T}{\partial \bar{X}}\right] &= K_f \left[\frac{\partial^2 T}{\partial \bar{Y}^2} + \frac{\partial^2 T}{\partial \bar{X}^2}\right] + \bar{S}.\bar{L} + \frac{\sigma_f B_0^2}{1+m^2}\left(\bar{U}^2 + \bar{V}^2\right) \\ +(\rho C)_{np}\left[D_B\left(\frac{\partial C}{\partial \bar{Y}}\frac{\partial T}{\partial \bar{Y}} + \frac{\partial C}{\partial \bar{X}}\frac{\partial T}{\partial \bar{X}}\right) + \frac{D_T}{T_m}\left(\left(\frac{\partial T}{\partial \bar{Y}}\right)^2 + \left(\frac{\partial T}{\partial \bar{X}}\right)^2\right)\right] &- \frac{\partial q_r}{\partial \bar{Y}},\end{aligned} \tag{7.5}$$

$$\frac{\partial C}{\partial \bar{t}} + \bar{V}\frac{\partial C}{\partial \bar{Y}} + \bar{U}\frac{\partial C}{\partial \bar{X}} = D_B\left[\frac{\partial^2 C}{\partial \bar{Y}^2} + \frac{\partial^2 C}{\partial \bar{X}^2}\right] + \frac{D_T}{T_m}\left(\frac{\partial^2 T}{\partial \bar{Y}^2} + \frac{\partial^2 T}{\partial \bar{X}^2}\right). \tag{7.6}$$

An extra stress tensor for Sisko fluid is:

$$\bar{\mathbf{S}} = \left[\alpha^* + \beta^{**}\left(\Pi\right)^{n-1}\right]\mathbf{A}_1, \tag{7.7}$$

where $\mathbf{A}_1$ depicts the first Rivilin-Ericksen tensor and Π is described by:

$$\Pi = \sqrt{\frac{1}{2}tr\left(\mathbf{A}_1^2\right)}. \tag{7.8}$$

Further α^*, β^{**} and n depict the shear rate viscosity, consistency index of fluid and power law index. For $\alpha^* = 0$ the Sisko model is converted into generalized power law model. Modified Darcy's law obeys:

$$R = -\frac{\varepsilon}{k^*}\mu_{app}\bar{\mathbf{V}}, \tag{7.10}$$

in which k^* and ε illustrate the permeability and porosity of porous medium and μ_{app} represent the apparent viscosity. Radiative heat flux q_r in view of Rosseland's supposition is described as:

$$q_r = -\frac{16\sigma^* T_0^3}{3k}\frac{\partial T}{\partial \bar{Y}}.$$

Zero mass flux condition for concentration of nanofluid is described as:

$$D_B\frac{\partial C}{\partial \bar{Y}} + \frac{D_T}{T_m}\frac{\partial T}{\partial \bar{Y}} = 0 \text{ at } y = h. \tag{7.11}$$

By using the transformations:

$$\bar{x} = \bar{X} - c\bar{t}, \bar{y} = \bar{Y}, \bar{u} = \bar{U} - c, \bar{v} = \bar{V}, \bar{p}(\bar{x}, \bar{y}) = \bar{P}(\bar{X}, \bar{Y}, \bar{t}), \tag{7.12}$$

we have:

$$\frac{\partial \bar{u}}{\partial \bar{x}} + \frac{\partial \bar{v}}{\partial \bar{y}} = 0, \tag{7.13}$$

$$\rho_f\left(\bar{v}\frac{\partial \bar{u}}{\partial \bar{y}} + (\bar{u}+c)\frac{\partial \bar{u}}{\partial \bar{x}}\right) = -\frac{\partial \bar{p}}{\partial \bar{x}} + \frac{\partial \bar{s}_{\bar{x}\bar{y}}}{\partial \bar{y}} + \frac{\partial \bar{s}_{\bar{x}\bar{x}}}{\partial \bar{x}}$$
$$-\frac{\sigma_f B_0^2}{1+m^2}[(\bar{u}+c) - m\bar{v}] - \frac{\varepsilon}{k^*}\mu_{app}(\bar{u}+c), \tag{7.14}$$

$$\rho_f\left(\bar{v}\frac{\partial \bar{v}}{\partial \bar{y}} + (\bar{u}+c)\frac{\partial \bar{v}}{\partial \bar{x}}\right) = -\frac{\partial \bar{p}}{\partial \bar{y}} + \frac{\partial \bar{s}_{\bar{y}\bar{y}}}{\partial \bar{y}} + \frac{\partial \bar{s}_{\bar{y}\bar{x}}}{\partial \bar{x}} - \frac{\sigma_f B_0^2}{1+m^2}[\bar{v} + m(\bar{u}+c)] - \frac{\varepsilon}{k^*}\mu_{app}\bar{v}, \tag{7.15}$$

$$(\rho C)_f\left(\bar{v}\frac{\partial T}{\partial \bar{y}} + (\bar{u}+c)\frac{\partial T}{\partial \bar{x}}\right) = K_f\left(\frac{\partial^2 T}{\partial \bar{y}^2} + \frac{\partial^2 T}{\partial \bar{x}^2}\right) + \bar{s}.\bar{L} + \frac{\sigma_f B_0^2}{1+m^2}[(\bar{u}+c)^2 + \bar{v}^2]$$
$$+(\rho C)_{np}\left[\frac{D_T}{T_m}\left(\left(\frac{\partial T}{\partial \bar{x}}\right)^2 + \left(\frac{\partial T}{\partial \bar{y}}\right)^2\right) + D_B\left(\frac{\partial C}{\partial \bar{y}}\frac{\partial T}{\partial \bar{y}} + \frac{\partial C}{\partial \bar{x}}\frac{\partial T}{\partial \bar{x}}\right)\right] + \frac{16\sigma^* T_0^3}{3k}\frac{\partial^2 T}{\partial \bar{y}^2}, \tag{7.16}$$

$$(\bar{u}+c)\frac{\partial C}{\partial \bar{x}}+\bar{v}\frac{\partial C}{\partial \bar{y}}=D_B\left(\frac{\partial^2 C}{\partial \bar{y}^2}+\frac{\partial^2 C}{\partial \bar{x}^2}\right)+\frac{D_T}{T_m}\left(\frac{\partial^2 T}{\partial \bar{y}^2}+\frac{\partial^2 T}{\partial \bar{x}^2}\right), \tag{7.17}$$

$$\bar{s}_{\bar{x}\bar{x}}=2\left[\alpha^*+\beta^{**}\left(2\left(\frac{\partial \bar{v}}{\partial \bar{y}}\right)^2+\left(\frac{\partial \bar{v}}{\partial \bar{x}}+\frac{\partial \bar{u}}{\partial \bar{y}}\right)^2+2\left(\frac{\partial \bar{u}}{\partial \bar{x}}\right)^2\right)^{\frac{n-1}{2}}\right]\frac{\partial \bar{u}}{\partial \bar{x}},$$

$$\bar{s}_{\bar{x}\bar{y}}=\bar{s}_{\bar{y}\bar{x}}=\left[\alpha^*+\beta^{**}\left(2\left(\frac{\partial \bar{v}}{\partial \bar{y}}\right)^2+\left(\frac{\partial \bar{v}}{\partial \bar{x}}+\frac{\partial \bar{u}}{\partial \bar{y}}\right)^2+2\left(\frac{\partial \bar{u}}{\partial \bar{x}}\right)^2\right)^{\frac{n-1}{2}}\right]\left(\frac{\partial \bar{u}}{\partial \bar{y}}+\frac{\partial \bar{v}}{\partial \bar{x}}\right),$$

$$\bar{s}_{\bar{y}\bar{y}}=2\left[\alpha^*+\beta^{**}\left(2\left(\frac{\partial \bar{v}}{\partial \bar{y}}\right)^2+\left(\frac{\partial \bar{u}}{\partial \bar{y}}+\frac{\partial \bar{v}}{\partial \bar{x}}\right)^2+2\left(\frac{\partial \bar{u}}{\partial \bar{x}}\right)^2\right)^{\frac{n-1}{2}}\right]\frac{\partial \bar{v}}{\partial \bar{y}}.$$

The following dimensionless parameters are utilized:

$$\begin{gathered}x=\frac{\bar{x}}{\lambda},y=\frac{\bar{y}}{d},u=\frac{\bar{u}}{c},v=\frac{\bar{v}}{c\delta},\delta=\frac{\bar{d}}{\lambda},h=\frac{\bar{H}}{d},p=\frac{d^2\bar{p}}{c\lambda\alpha^*},M=\sqrt{\frac{\sigma_f}{\alpha^*}}B_0d,\\ Re=\frac{\rho_f\ cd}{\alpha^*},E=\frac{c^2}{C_fT_0},Pr=\frac{\alpha C_f}{K_f},Br=PrE,R_d=\frac{4\sigma^*T_0^3}{kK_f},Da=\frac{k^*}{\varepsilon(\alpha^*)^2},\\ N_b=\frac{\tau D_BC_0}{\nu},N_t=\frac{\tau D_TT_0}{\nu T_m},\theta=\frac{T-T_0}{T_0},\phi=\frac{C-C_0}{C_0},u=\frac{\partial\psi}{\partial y},v=-\frac{\partial\psi}{\partial x}.\end{gathered} \tag{7.18}$$

Here θ, δ, N_t, N_b, Da, R_d, m and ϕ depict the dimensionless temperature, wave number, thermophoresis parameter, Brownian motion parameter, Darcy number, radiation parameter, Hall number and dimensionless concentration respectively. After nondimensionalizing the above equations and taking the small Reynold number and long wavelength assumptions simplified form of equations are:

$$p_y=0, \tag{7.19}$$

$$p_x=\frac{\partial s_{xy}}{\partial y}-\frac{M^2}{1+m^2}\left(1+\frac{\partial\psi}{\partial y}\right)-\frac{1}{Da}\frac{\mu_{app}}{\alpha^*}\left(1+\frac{\partial\psi}{\partial y}\right), \tag{7.20}$$

$$\theta_{yy}+Br\Phi+\Pr N_b\phi_y\theta_y+\Pr N_t\left(\theta_y\right)^2+\frac{BrM^2}{1+m^2}\left(1+\frac{\partial\psi}{\partial y}\right)^2+\frac{4R_d}{3}\frac{\partial^2\theta}{\partial y^2}=0, \tag{7.21}$$

$$N_b\phi_{yy}+N_t\theta_{yy}=0. \tag{7.22}$$

Continuity equation is justified. Here Φ depicts the non-dimensional form of viscous dissipation and s_{xy} depicts the dimensionless component of extra stress tensor defined by:

$$s_{xy}=s_{yx}=\left[1+\beta(\psi_{yy})^{n-1}\right]\psi_{yy}. \tag{7.23}$$

When shear rate enhances the apparent viscosity of fluid depicts decreasing behavior. However opposite nature of fluid is called shear thickening. From Eqs. (7.18)-(7.22) we obtain:

$$\frac{\partial^2}{\partial y^2}\left[1+\beta(\psi_{yy})^{n-1}\right]\psi_{yy}-\frac{M^2}{1+m^2}\psi_{yy}-\frac{1}{Da}\frac{\partial}{\partial y}\left[\left(1+\beta(\psi_{yy})^{n-1}\right)\left(1+\frac{\partial\psi}{\partial y}\right)\right]=0, \quad (7.24)$$

$$\theta_{yy}+Br\left[1+\beta(\psi_{yy})^{n-1}\right]\psi_{yy}^2+\Pr N_b\phi_y\theta_y+\Pr N_t\left(\theta_y\right)^2+\frac{BrM^2}{1+m^2}\left(1+\frac{\partial\psi}{\partial y}\right)^2+\frac{4R_d}{3}\theta_{yy}=0, \quad (7.25)$$

$$N_b\phi_{yy}+N_t\theta_{yy}=0. \quad (7.26)$$

Dimensionless forms of flow rate in the wave $F(=\bar{q}/cd_1)$ and laboratory $\eta(=\bar{Q}/cd_1)$ frames are associated through the relation:

$$\eta=F+1. \quad (7.27)$$

Further 'F' can be defined as:

$$F=\int_0^h\frac{\partial\psi}{\partial y}dy. \quad (7.28)$$

The dimensionless boundary conditions are:

$$\psi=0,\psi_{yy}=0,\theta_y=0 \text{ and } \phi_y=0 \text{ at } y=0, \quad (7.29)$$

$$\begin{gathered}\psi=F,\psi_y+\beta_1\left[\psi_{yy}+\beta(\psi_{yy})^n\right]=-1,\theta+\gamma\theta_y=0\\ \text{and } N_b\phi_y+N_t\theta_y=0 \text{ at } y=h.\end{gathered} \quad (7.30)$$

The dimensionless form of geometric walls are

$$h_1=1+d\cos(2\pi x).$$

The numerical approach has been used for the solution of non-linear equations subject to boundary conditions.

7.2 Entropy generation

Mathematically the entropy generation is:

$$S_G = \frac{K_{nf}}{T_0^2}\left[\left(\frac{\partial T}{\partial \bar{y}}\right)^2+\left(\frac{\partial T}{\partial \bar{x}}\right)^2\right]+\frac{\sigma_{nf}B_0^2}{T_0\left(1+m^2\right)}[(\bar{u}+c)^2+\bar{v}^2]+\frac{1}{T_0^2}\frac{16\sigma^* T_0^3}{3k}\left(\frac{\partial T}{\partial \bar{y}}\right)^2 + \frac{1}{T_0}\bar{s}.\bar{L}+\frac{R^* D}{T_0}\left(\frac{\partial C}{\partial \bar{x}}\frac{\partial T}{\partial \bar{x}}+\frac{\partial C}{\partial \bar{y}}\frac{\partial T}{\partial \bar{y}}\right)+\frac{R^* D}{C_0}\left(\left(\frac{\partial C}{\partial \bar{y}}\right)^2+\left(\frac{\partial C}{\partial \bar{x}}\right)^2\right). \tag{7.31}$$

Non-dimensional form of entropy generation is given by:

$$N_s=\left[1+\frac{4R_d}{3}\right](\theta_y)^2+Br\left[1+\beta(\psi_{yy})^{n-1}\right]\psi_{yy}^2+L\phi_y\theta_y+L\left(\phi_y\right)^2+\frac{BrM^2}{1+m^2}\left(1+\frac{\partial\psi}{\partial y}\right)^2.$$

Here $L=\left(\frac{R^*DC_0}{d^2}\right)$ represents the diffusion parameter and $N_s=\left(\frac{d^2S_G}{K_{nf}}\right)$ the nondimensional form entropy generation. Further Bejan number is defined by:

$$\text{Be}=\frac{\text{Entropy generation due to mass and heat transfer}}{\text{Total entropy generation}}$$

or

$$Be=\frac{\left(1+\frac{4R_d}{3}\right)(\theta_y)^2+L\phi_y\theta_y+L\left(\phi_y\right)^2}{\left(1+\frac{4R_d}{3}\right)(\theta_y)^2+Br\left[1+\beta(\psi_{yy})^{n-1}\right]\psi_{yy}^2+L\phi_y\theta_y+L\left(\phi_y\right)^2+\frac{BrM^2}{1+m^2}\left(1+\frac{\partial\psi}{\partial y}\right)^2}.$$

Graphical explanation of the results are described in the proceeding section.

7.3 Results and discussion

Effects of physical flow variables like M, m, Da and β_1 on the velocity are studied via Figs. (7.1)-(7.4). Fig. 7.1 represents the effect of Hartman number on axial velocity. Fig. shows that when Hartman number increases then velocity of nanofluid decreases. This is physically justified due to the Lorentz force. An increment in the Hall number leads to an enhancement of velocity (see Fig. 7.2). Fig. 7.3 outlines the impact of "Da" variable on the velocity. Velocity field enhances for higher values of "Da" at central portion of channel. Effect of varying β_1 variable on the nanofluid is displayed in Fig. 7.4. We noticed that as the velocity slip parameter enhances then

velocity of nanofluid enhances near the channel wall but it depicts opposite behavior near the center of channel. Figs. (7.5)-(7.10) illustrated the temperature for numerous values of M, m, R_d, Br, γ and β parameters. Fig. 7.5 demonstrates temperature for Hartman number. Increasing "M" enhances the temperature of nanofluid rapidly. Physically this observation is correct because Joule heating plays prominent role to enhance the temperature. Fig. 7.6 shows the temperature decay against higher values of Hall parameter. Basically Hall parameter balances the effect of Hartman number on temperature and thus controls the nanofluid temperature. Fig. 7.7 depicts that temperature decreases by increasing the thermal radiation parameter. Temperature for numerous values of Brinkman number is seen in Fig. 7.8. We noticed that temperature rapidly enhances by higher "Br". Fig. 7.9 shows that temperature enhances in channel by higher thermal slip parameter. Fig. 7.10 depicts that temperature decreases when values of non-Newtonian parameter "β" increases. Figs. (7.11)-(7.16) present the impacts of M, m, N_t, N_b, β and R_d on concentration. It is observed that concentration of nanoparticles is higher near the channel wall as compared to the central portion. Fig. 7.11 depicts the effect of Hartman number on concentration. It is noticed that concentration rapidly enhances by higher "M" parameter. Fig. 7.12 illustrates the impact of Hall number on the concentration. It is demonstrated that concentration decays in the case of higher values of "m". Fig. 7.13 shows the variation in concentration profile for various values of N_t parameter. It is observed that concentration of nanoparticle enhances by enhancing the thermophoretic parameter. However N_b parameter depicts opposite trend as compared to N_t parameter on the concentration profile. Fig. 7.15 displays concentration for various values of non-Newtonian parameter. By dominating the "β" characteristics concentration profile slightly decreases. Fig. 7.16 indicates that concentration profile decreases by increasing the thermal radiation parameter. Figs. (7.17)-(7.21) exhibit the influence of entropy generation for various values of prominent factors. Fig. 7.17 is plotted to examine the effect of Hartman number on entropy generation. It predicts that entropy generation enhances due to the higher values of M. Fig. 7.18 is displayed to study behavior of entropy generation for various values of Hall parameter. Entropy generation can be minimized by increasing the Hall parameter. Fig. 7.19 depicts outcome of entropy generation for Brinkman number. It is seen that entropy generation can be minimized by decreasing the Brinkman number. Further entropy generation can also be controlled by enhancing the thermal

radiation parameter (see Fig. 7.20). Fig. 7.21 depicts the effect of "β" parameter on entropy generation. Graph shows that entropy decreases in the presence of higher thermal radiation parameter. Fig. 7.22 represents the variation of Bejan number against the Hartman number. Graph depicts that Bejan number enhances for higher values of "M". It is clear for Fig. 7.23 that Bejan number significantly tends to reduce for greater values of Hall number. Here Bejan number decays due to an increment in thermal radiation (see Fig. 7.24).

7.4 Conclusions

The important findings can summarized below:

- For higher Hartman number the velocity decays. However temperature, concentration and entropy generation of nanofluid are enhanced by higher Hartman number.
- An increment in Hall number enhances velocity and it decreases temperature of nanofluid.
- An enhancement in non-Newtonian variable "β" depicts the decaying trend of concentration and temperature.
- Decaying behavior is observed for θ and ϕ by increasing R_d.
- Concentration and temperature of nanofluid can be minimized by decreasing the value of Brinkman number.
- N_t and N_b parameters depict opposite trend for concentration of nanofluid.

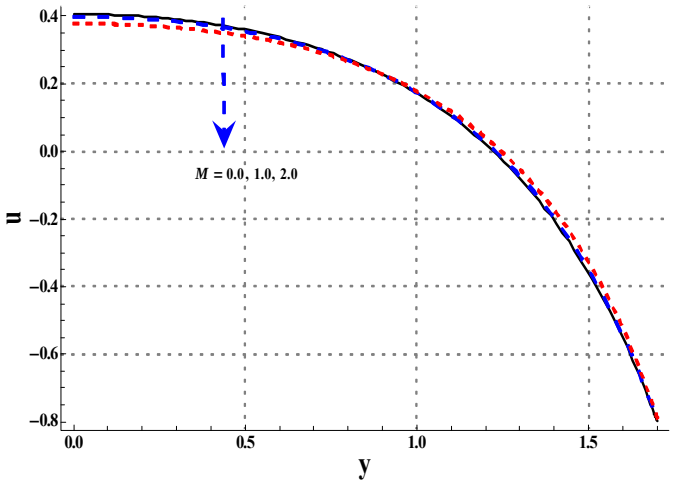

Fig. 7.1. Velocity via M.

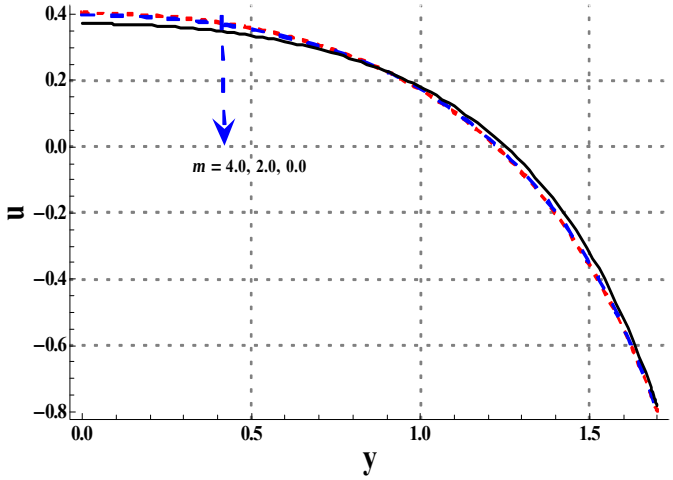

Fig. 7.2. Velocity via m.

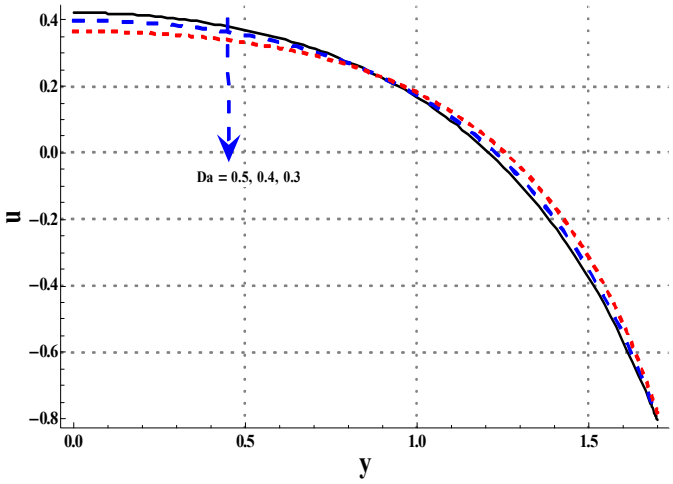

Fig. 7.3. Velocity via Da.

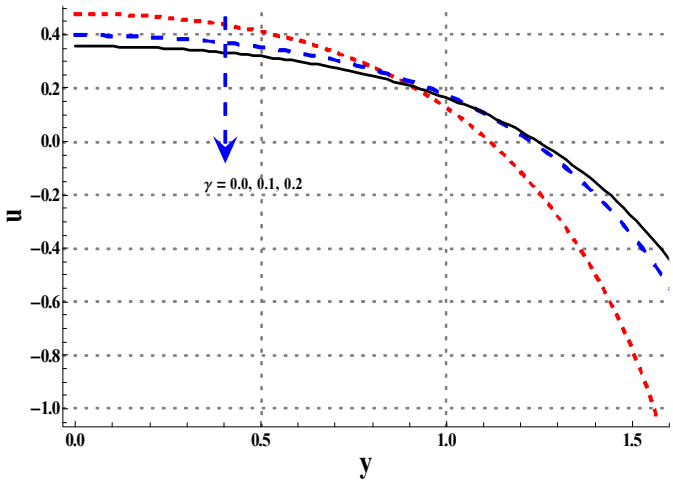

Fig. 7.4. Velocity via γ.

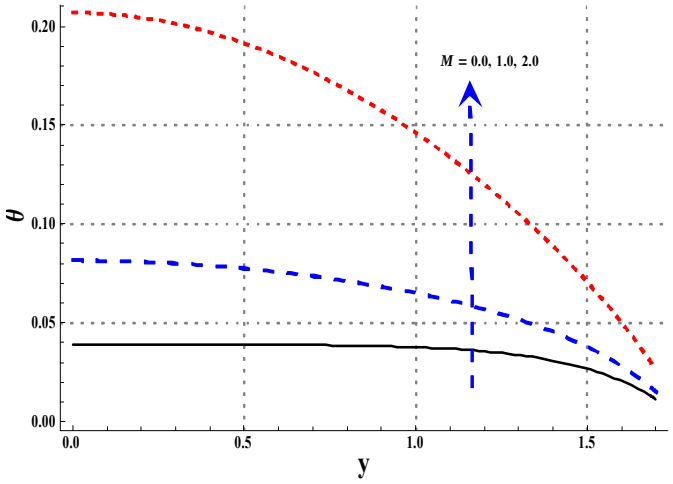

Fig. 7.5. Plot of θ for M.

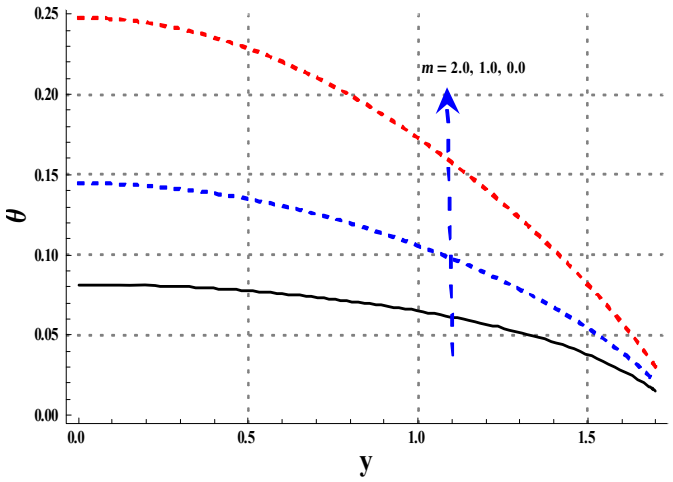

Fig. 7.6. Plot of θ for m.

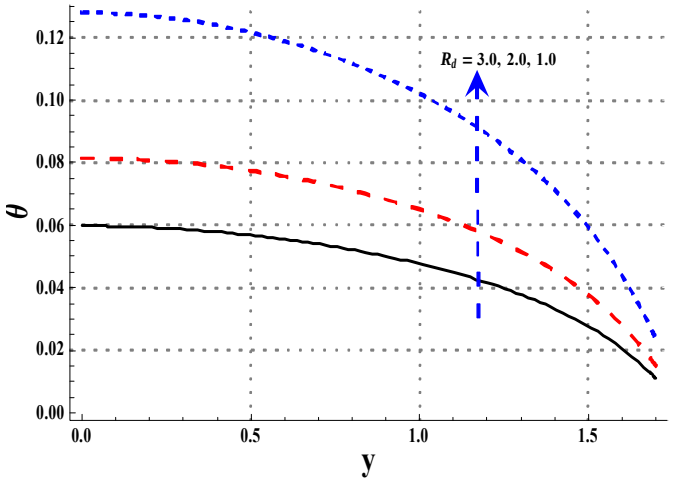

Fig. 7.7. Plot of θ for R_d.

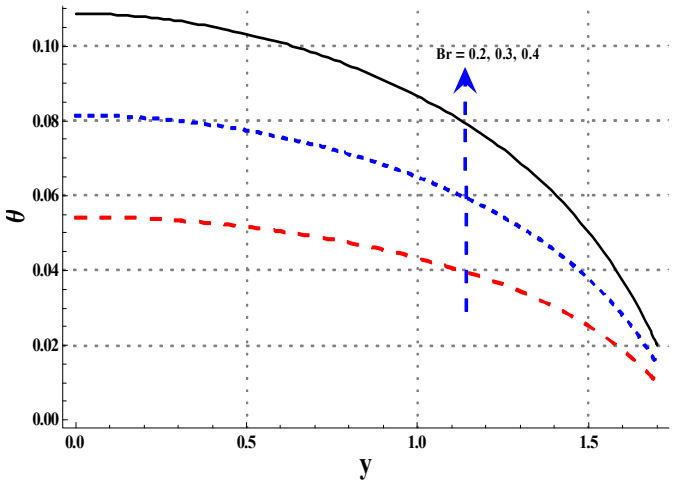

Fig. 7.8. Plot of θ for Br.

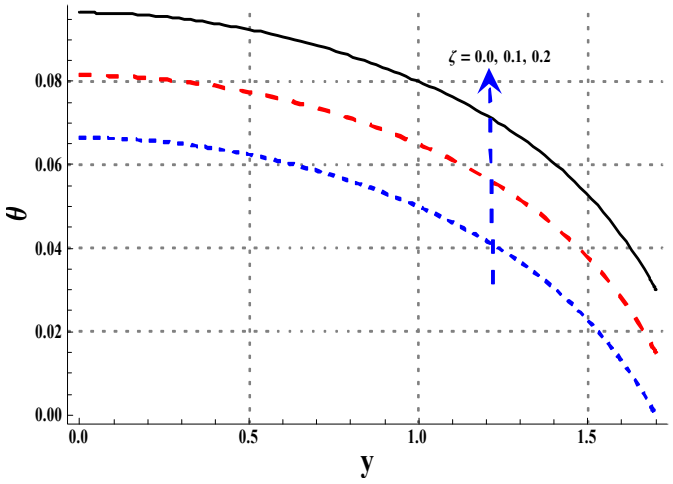

Fig. 7.9. Plot of θ for ζ.

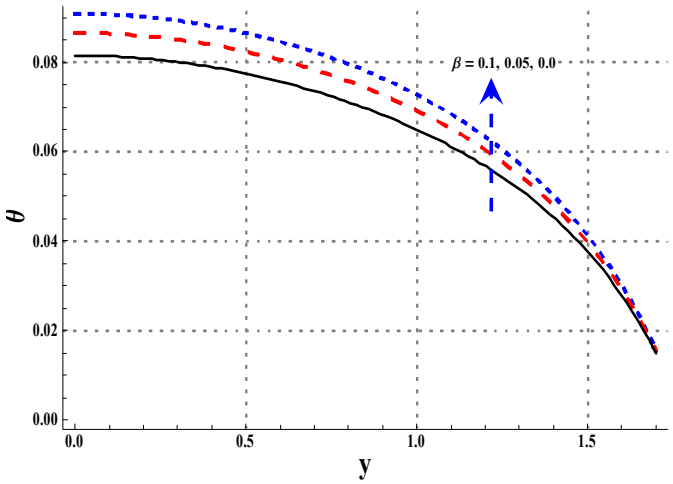

Fig. 7.10. Plot of θ for β.

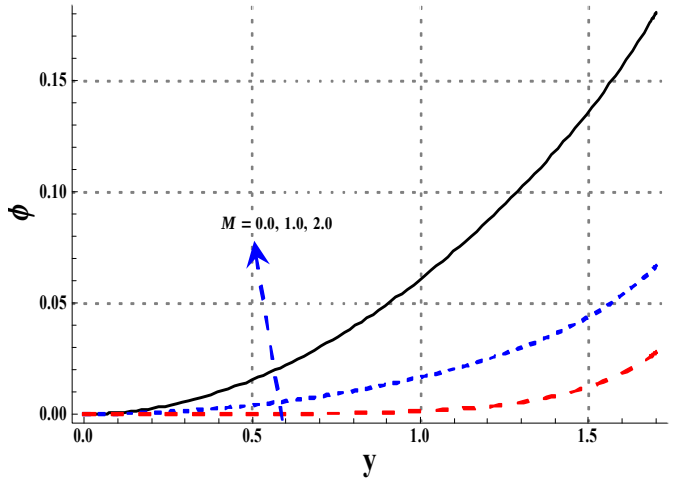

Fig. 7.11. Effect of M on ϕ.

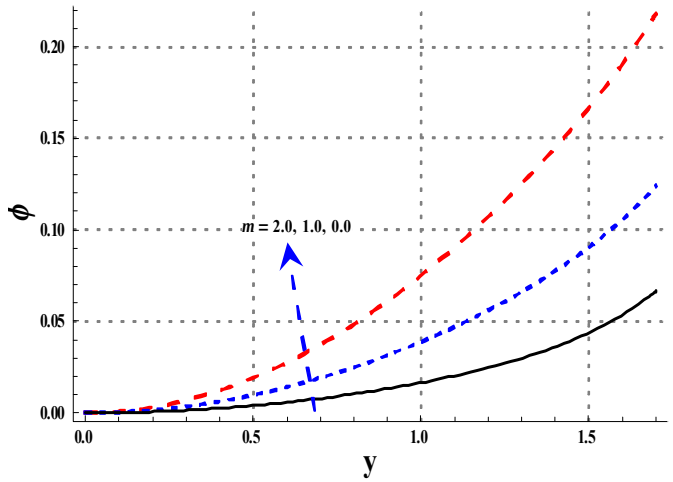

Fig. 7.12. Effect of m on ϕ.

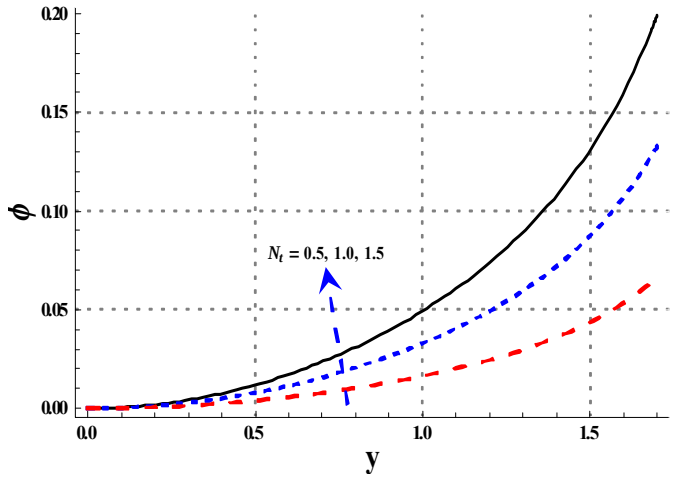

Fig. 7.13. Effect of N_t on ϕ.

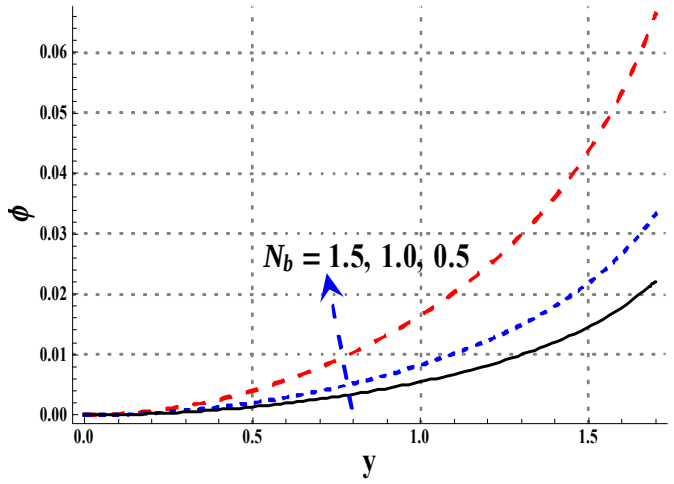

Fig. 7.14. Effect of N_b on ϕ.

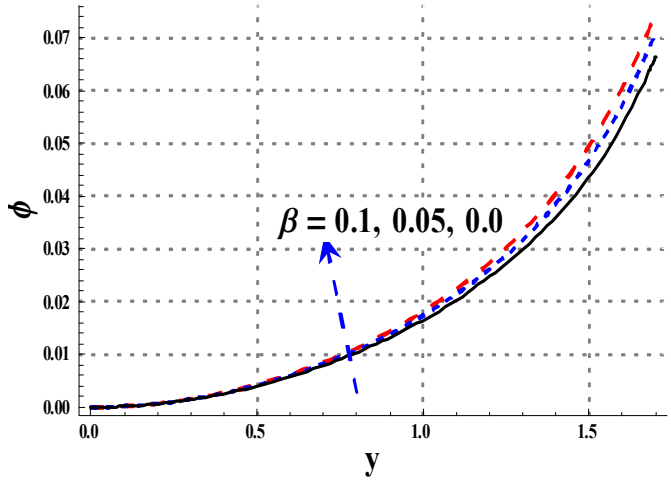

Fig. 7.15. Effect of β on ϕ.

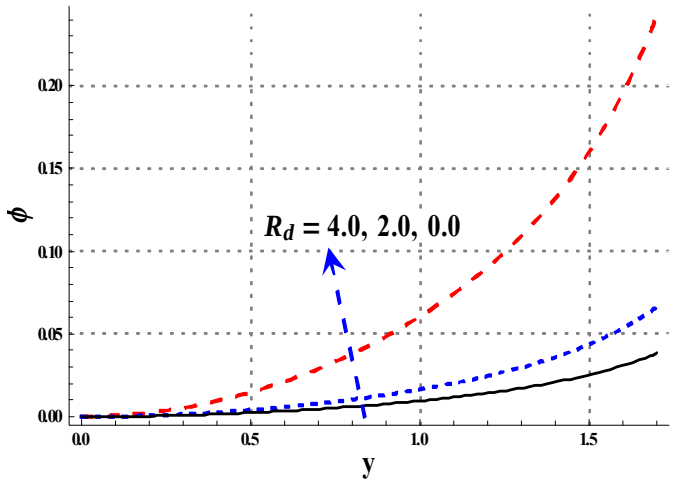

Fig. 7.16. Effect of R_d on ϕ.

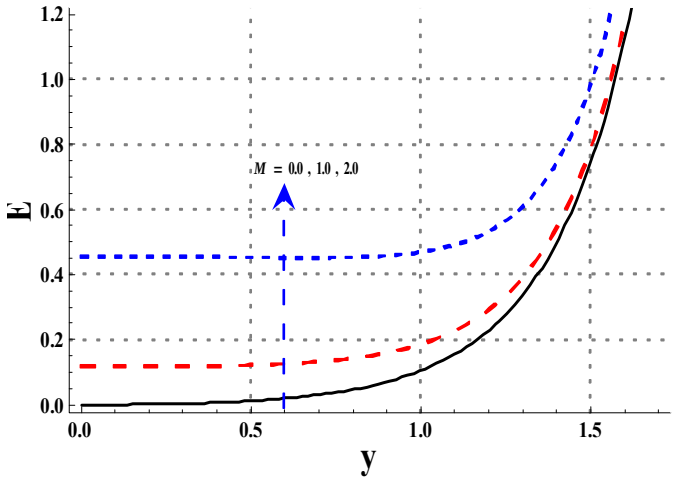

Fig. 7.17. Effect of M on entropy.

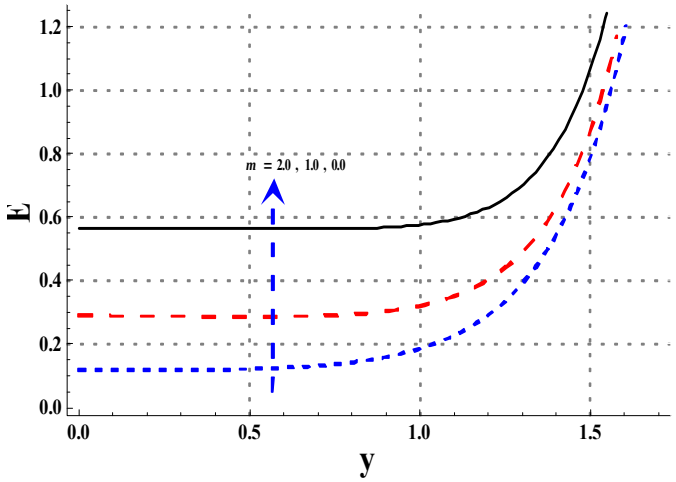

Fig. 7.18. Effect of m on entropy.

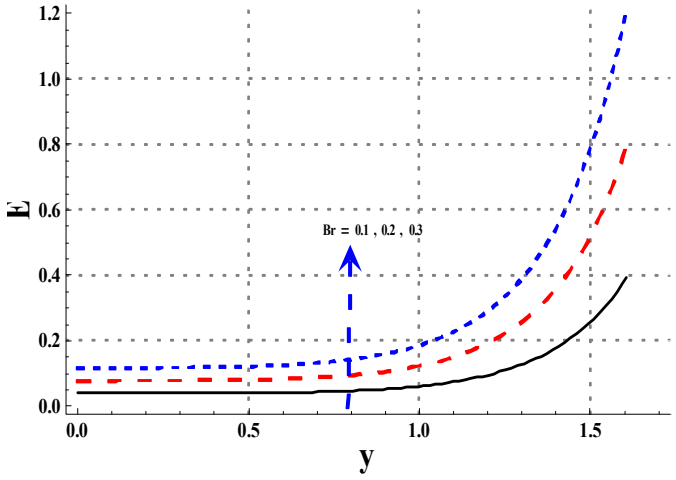

Fig. 7.19. Effect of Br on entropy.

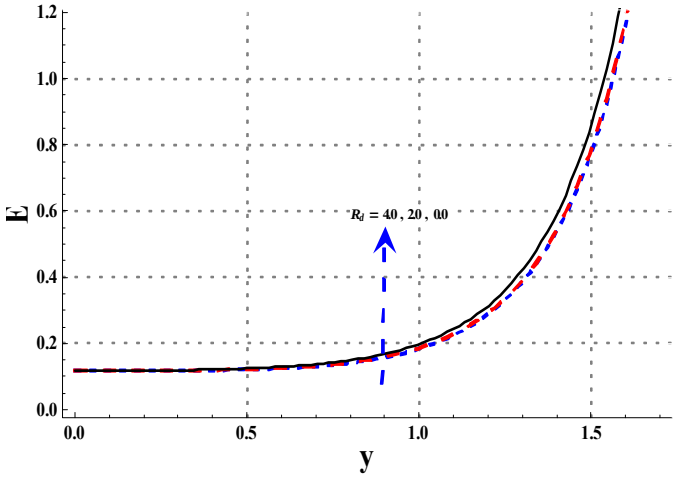

Fig. 7.20. Effect of R_d on entropy.

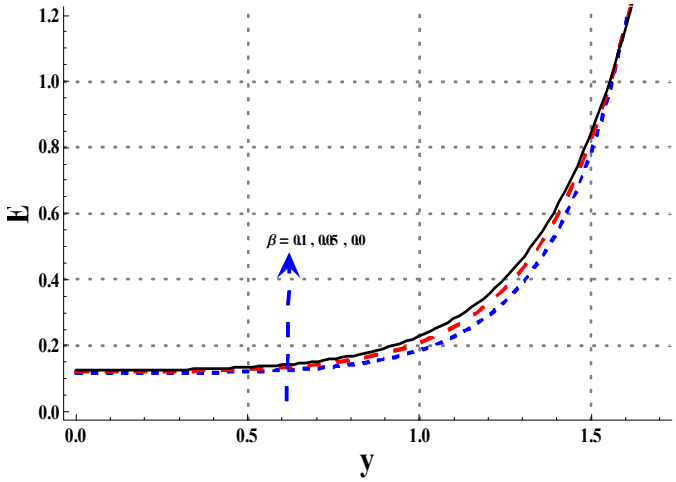

Fig. 7.21. Effect of β on entropy.

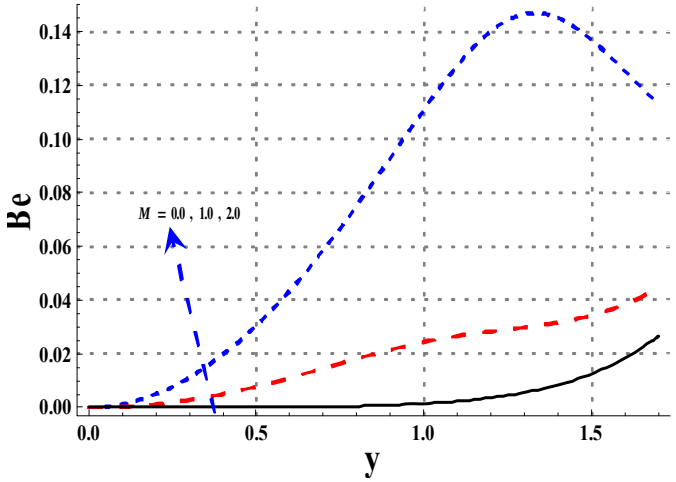

Fig. 7.22. Effect of M on Bejan number.

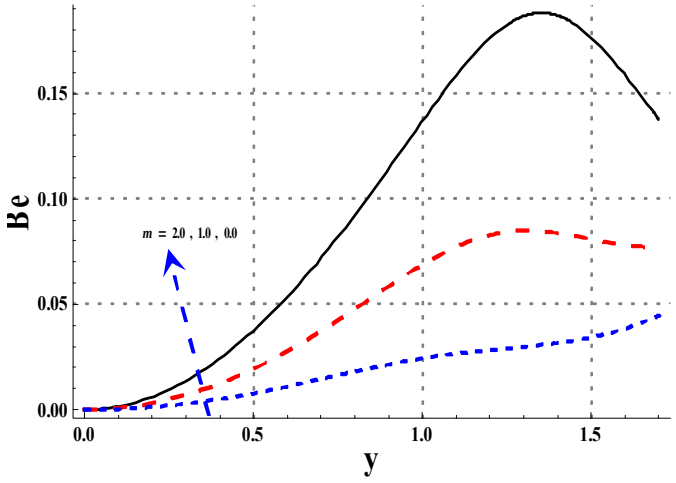

Fig. 7.23. Effect of m on Bejan number.

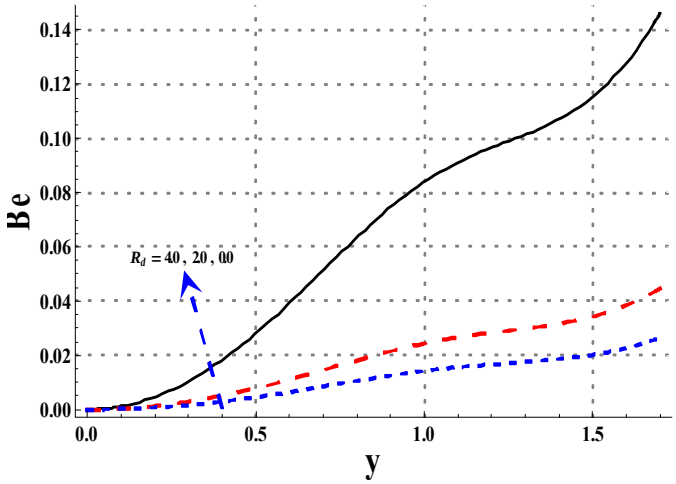

Fig. 7.24. Effect of R_d on Bejan number.

Chapter 8

Peristalsis of Carreau-Yasuda magneto nanofluid with modified Darcy law and radiation

Here our focus is to discuss flow of Carreau-Yasuda nanofluid subject to thermophoresis and non-linear thermal radiation. Further modified Darcys law and magnetic field are also considered. Lubrication approach is used. Graphs are displayed in order to explore the outcomes of pertinent variables. Tabulated values analyzed the mass and heat transfer rates.

8.1 Mathematical formulation

Here two-dimensional flow of Carreau-Yasuda incompressible nanofluid in a symmetric channel has been considered. The width of channel is $2a$ and the waves propagate in the axial direction with wavelength λ and wave speed "c" (see Fig. 8.1). Consider the rectangular coordinates $(\bar{X}, \bar{Y})$ such that X-axis along the center line and Y-axis perpendicular to it. The peristaltic waves along upper and lower boundaries are represented as:

$$\pm\bar{H}(\bar{X}, \bar{t}) = \pm a \pm bcos(\frac{2\pi}{\lambda}(\bar{X} - c\bar{t})), \tag{8.1}$$

in which "b" denotes the waves amplitude and $\bar{X}$ direction of wave propagation. The nanomaterial and base fluid are considered in equilibrium. A magnetic field of constant magnitude B_0 is applied. Further the temperature T_0 and mass concentration C_0 are assumed on both walls of channel. The velocity field for this flow behavior is $\bar{\mathbf{V}} = [\bar{U}(\bar{X}, \bar{Y}, \bar{t}), \bar{V}(\bar{X}, \bar{Y}, \bar{t}), 0]$. The governing expressions in the presence of non-linear thermal radiation, viscous dissipation and porous medium given below:

$$\frac{\partial \bar{U}}{\partial \bar{X}} + \frac{\partial \bar{V}}{\partial \bar{Y}} = 0, \tag{8.2}$$

$$\rho_{nf}\left(\frac{\partial}{\partial \bar{t}} + \bar{U}\frac{\partial}{\partial \bar{X}} + \bar{V}\frac{\partial}{\partial \bar{Y}}\right)\bar{U} = -\frac{\partial \bar{P}}{\partial \bar{X}} + \frac{\partial \bar{S}_{\bar{x}\bar{x}}}{\partial \bar{X}} + \frac{\partial \bar{S}_{\bar{x}\bar{y}}}{\partial \bar{Y}} - \sigma_{nf}B_0^2\bar{U} + \bar{R}_{\bar{X}}, \tag{8.3}$$

$$\rho_{nf}\left(\frac{\partial}{\partial \bar{t}} + \bar{U}\frac{\partial}{\partial \bar{X}} + \bar{V}\frac{\partial}{\partial \bar{Y}}\right)\bar{V} = -\frac{\partial \bar{P}}{\partial \bar{y}} + \frac{\partial \bar{S}_{\bar{y}\bar{x}}}{\partial \bar{X}} + \frac{\partial \bar{S}_{\bar{y}\bar{y}}}{\partial \bar{Y}} - \sigma_{nf}B_0^2\bar{V} + \bar{R}_{\bar{Y}}, \tag{8.4}$$

$$\begin{aligned}(\rho C)_{nf}\left(\frac{\partial}{\partial \bar{t}} + \bar{U}\frac{\partial}{\partial \bar{X}} + \bar{V}\frac{\partial}{\partial \bar{Y}}\right)T = K_{nf}\left[\frac{\partial^2 T}{\partial \bar{X}^2} + \frac{\partial^2 T}{\partial \bar{Y}^2}\right] + \bar{S}.\bar{L} + \sigma_{nf}B_0^2\bar{U}^2 + \frac{\partial q_r}{\partial \bar{Y}} \\ +(\rho C)_{np}\left[D_B\left(\frac{\partial C}{\partial \bar{X}}\frac{\partial T}{\partial \bar{X}} + \frac{\partial C}{\partial \bar{Y}}\frac{\partial T}{\partial \bar{Y}}\right) + \frac{D_T}{T_m}\left(\left(\frac{\partial T}{\partial \bar{X}}\right)^2 + \left(\frac{\partial T}{\partial \bar{Y}}\right)^2\right)\right],\end{aligned} \tag{8.5}$$

$$\frac{\partial C}{\partial \bar{t}} + \bar{U}\frac{\partial C}{\partial \bar{X}} + \bar{V}\frac{\partial C}{\partial \bar{Y}} = D_B\left(\frac{\partial^2 C}{\partial \bar{X}^2} + \frac{\partial^2 C}{\partial \bar{Y}^2}\right) + \frac{D_T}{T_m}\left(\frac{\partial^2 T}{\partial \bar{X}^2} + \frac{\partial^2 T}{\partial \bar{Y}^2}\right). \tag{8.6}$$

In these equations, $\bar{P}$ denotes the pressure, σ_{nf} the electric conductivity of nanofluid, ρ_{nf} the density of nanofluid, $\bar{S}_{ij}$ the components of extra stress tensor, T the fluid temperature, C the concentration, $\bar{S}.\bar{L}$ the viscous dissipation, $\bar{L}$ the gradient of velocity, K_{nf} the thermal conductivity of nanofluid, C_{nf} specific heat of nanofluid, D_B the mass diffusivity, D_T thermophoretic diffusion coefficient and $(\rho C)_{np}$ the effective heat capacity of nanoparticles. Here the modified Darcy's resistance law [32] has been used for porous medium and thus $\bar{R} = (\bar{R}_{\bar{X}}, \bar{R}_{\bar{Y}}, 0)$ satisfies:

$$\bar{R} = -\frac{\varepsilon}{k}\mu(\gamma')\bar{V}, \tag{8.7}$$

in which k depicts the permeability and ε porosity of porous medium. Further we recover the Darcy law from generalized model by putting $n = 1$ or $\beta = 0$. Radiative heat flux q_r in view of

Rosseland's approximation is defined as:

$$q_r = -\frac{4\sigma^*}{3k}\frac{\partial T^4}{\partial y}. \tag{8.8}$$

The constitutive relation for the Carreau-Yasuda fluid is:

$$\bar{\mathbf{S}} = \mu(\gamma')\mathbf{A}_1, \tag{8.9}$$

where $\mu(\gamma')$ is the apparent viscosity and A_1 is the first Rivilin-Ericksen tensor defined by

$$\mu(\gamma') = \mu_\infty + (\mu_0 - \mu_\infty)\left[1 + (\Gamma\Pi)^a\right]^{\frac{n-1}{a}}, \tag{8.10}$$

with

$$\Pi = \sqrt{\frac{1}{2}tr\left(\mathbf{A}_1^2\right)}.$$

Here μ_∞ and μ_0 stand for infinite and zero shear-rate viscosities respectively. The parameters a and Γ control the transition between the two extremes. Further "n" stands for dimensionless power law index. The C-Y fluid model shows the shear thickening and shear thinning nature for $n > 1$ and $n < 1$ respectively and viscous fluid model when $n = 1$. The results for Carreau fluid model can be obtained by considering $a = 2$. Here μ_∞ is considered to be zero. If $(\bar{U}, \bar{V})$ and $(\bar{u}, \bar{v})$ denote velocity components in the moving and stationary frames then the relations between these frames are:

$$\bar{x} = \bar{X} - c\bar{t}, \bar{y} = \bar{Y}, \bar{u} = \bar{U} - c, \bar{v} = \bar{V}, \bar{p}(\bar{x}, \bar{y}) = \bar{P}(\bar{X}, \bar{Y}, \bar{t}). \tag{8.11}$$

We have following equations:

$$\frac{\partial \bar{u}}{\partial \bar{x}} + \frac{\partial \bar{v}}{\partial \bar{y}} = 0, \tag{8.12}$$

$$\begin{aligned}\rho_{nf}\left((\bar{u}+c)\frac{\partial}{\partial \bar{x}} + \bar{v}\frac{\partial}{\partial \bar{y}}\right)(\bar{u}+c) = -\frac{\partial \bar{p}}{\partial \bar{x}} + \frac{\partial \bar{s}_{\bar{x}\bar{x}}}{\partial \bar{x}} + \frac{\partial \bar{s}_{\bar{x}\bar{y}}}{\partial \bar{y}} \\ -\sigma_{nf}B_0^2(\bar{u}+c) - \frac{\varepsilon}{k}\mu(\gamma')(\bar{u}+c),\end{aligned} \tag{8.13}$$

$$\rho_{nf}\left((\bar{u}+c)\frac{\partial}{\partial\bar{x}}+\bar{v}\frac{\partial}{\partial\bar{y}}\right)\bar{v}=-\frac{\partial\bar{p}}{\partial\bar{y}}+\frac{\partial\bar{s}_{\bar{y}\bar{x}}}{\partial\bar{x}}+\frac{\partial\bar{s}_{\bar{y}\bar{y}}}{\partial\bar{y}}-\sigma_{nf}B_0^2\bar{v}-\frac{\varepsilon}{k}\mu(\gamma')\bar{v}, \tag{8.14}$$

$$\begin{aligned}(\rho C)_{nf}\left((\bar{u}+c)\frac{\partial}{\partial\bar{x}}+\bar{v}\frac{\partial}{\partial\bar{y}}\right)T=K_{nf}\left[\frac{\partial^2T}{\partial\bar{x}^2}+\frac{\partial^2T}{\partial\bar{y}^2}\right]+\bar{s}.\bar{L}+\sigma_{nf}B_0^2(\bar{u}+c)^2\\ +(\rho C)_{np}\left[D_B\left(\frac{\partial C}{\partial\bar{x}}\frac{\partial T}{\partial\bar{x}}+\frac{\partial C}{\partial\bar{y}}\frac{\partial T}{\partial\bar{y}}\right)+\frac{D_T}{T_m}\left(\left(\frac{\partial T}{\partial\bar{x}}\right)^2+\left(\frac{\partial T}{\partial\bar{y}}\right)^2\right)\right]-\frac{4\sigma}{3k}\frac{\partial^2T^4}{\partial\bar{y}^2},\end{aligned} \tag{8.15}$$

$$(\bar{u}+c)\frac{\partial C}{\partial\bar{x}}+\bar{v}\frac{\partial C}{\partial\bar{y}}=D_B\left(\frac{\partial^2C}{\partial\bar{x}^2}+\frac{\partial^2C}{\partial\bar{y}^2}\right)+\frac{D_T}{T_m}\left(\frac{\partial^2T}{\partial\bar{x}^2}+\frac{\partial^2T}{\partial\bar{y}^2}\right). \tag{8.16}$$

The dimensionless parameters are defined as:

$$\begin{aligned}x=\frac{\bar{x}}{\lambda},y=\frac{\bar{y}}{a},u=\frac{\bar{u}}{c},v=\frac{\bar{v}}{c\delta},\delta=\frac{\bar{d}_1}{\lambda},h=\frac{\bar{H}}{a},d=\frac{b}{a},p=\frac{a^2\bar{p}}{c\lambda\mu_f},Da=\frac{k}{\varepsilon a^2},\\ Re=\frac{\rho_f\ ca}{\mu_f},E=\frac{c^2}{C_fT_0},Pr=\frac{\mu_fC_f}{K_{nf}},M=\sqrt{\frac{\sigma_f}{\mu_f}}B_0a,N_b=\frac{\tau D_BC_0}{\nu},N_t=\frac{\tau D_TT_0}{\nu T_m},\\ R_d=\frac{4\sigma^*T_0^3}{kK_{nf}},\upsilon=\frac{\mu_f}{\rho_f},\theta=\frac{T-T_0}{T_0},\phi=\frac{C-C_0}{C_0},Br=PrE,u=\frac{\partial\psi}{\partial y},v=-\frac{\partial\psi}{\partial x}.\end{aligned} \tag{8.17}$$

Here $Br, Re, Ec, \Pr, M, \delta, \theta, N_b$ and N_t denote the Brinkman number, Reynolds number, Eckert number, Prandtl number, Hartman number, wave number, dimensionless temperature, the Brownian motion parameter and the thermophoresis parameter. Applying long wavelength and small Reynolds number assumptions, the non-dimensional governing equations yield:

$$p_y=0, \tag{8.18}$$

$$p_x=\frac{\partial s_{xy}}{\partial y}-M^2\left(1+\frac{\partial\psi}{\partial y}\right)-\frac{1}{Da}\frac{\mu(\gamma')}{\mu_0}\left(1+\frac{\partial\psi}{\partial y}\right), \tag{8.19}$$

$$\theta_{yy}+Br\Phi+\Pr N_b\phi_y\theta_y+\Pr N_t\left(\theta_y\right)^2+BrM^2\left(1+\frac{\partial\psi}{\partial y}\right)^2-\frac{R_d}{3}\frac{\partial^2(\theta+1)^4}{\partial y^2}=0, \tag{8.20}$$

$$N_b\phi_{yy}+N_t\theta_{yy}=0, \tag{8.21}$$

and the continuity equation is justified trivially. Here Φ is the dimensionless viscous dissipation term and s_{xy} the dimensionless component of extra stress tensor after lubrication approach given by:

$$s_{xy}=s_{yx}=\left[1+\frac{(n-1)We^a}{a}(\psi_{yy})^a\right]\psi_{yy}. \tag{8.22}$$

Here $We = \frac{\Gamma c}{d_1}$ denotes the Weissenberg number. Substitution the values of s_{xy} from Eq. (8.22) into Eqs. (8.18)-(8.21) gives:

$$\frac{\partial^2}{\partial y^2}\left[1+\frac{(n-1)We^a}{a}(\psi_{yy})^a\right]\psi_{yy} - M^2\psi_{yy} - \frac{1}{Da}\frac{\partial}{\partial y}\left[1+\frac{(n-1)We^a}{a}(\psi_{yy})^a\right]\left(1+\frac{\partial\psi}{\partial y}\right) = 0, \tag{8.23}$$

$$\begin{aligned}\theta_{yy} + Br\left[1+\tfrac{(n-1)We^a}{a}(\psi_{yy})^a\right]\psi_{yy}^2 + \Pr N_b\phi_y\theta_y + \Pr N_t\left(\theta_y\right)^2 \\ +BrM^2\left(1+\tfrac{\partial\psi}{\partial y}\right)^2 - \tfrac{R_d}{3}\tfrac{\partial^2(\theta+1)^4}{\partial y^2} = 0,\end{aligned} \tag{8.24}$$

$$N_b\phi_{yy} + N_t\theta_{yy} = 0. \tag{8.25}$$

Non-dimensional flow rates in the wave $F(=\bar{q}/ca)$ and laboratory $\eta(=\bar{Q}/ca)$ frames are associated through the relation

$$\eta = F + 1, \tag{8.26}$$

where $\bar{Q}$ and $\bar{q}$ are dimensional flow rates in the laboratory and wave frames. Further 'F' is expressed by:

$$F = \int_0^h \frac{\partial\psi}{\partial y}dy. \tag{8.27}$$

Dimensionless boundary conditions are:

$$\begin{aligned}\psi = 0, \psi_{yy} = 0, \theta_y = 0, \phi_y = 0 \text{ at } y = 0, \\ \psi = F, \psi_y = -1, \theta = 0, N_b\phi_y + N_t\theta_y = 0 \text{ at } y = h,\end{aligned} \tag{8.28}$$

where $h = 1 + d\cos(2\pi x)$. The system of equations subject to boundary conditions is solved numerically by Mathematica. Analysis of results is given below.

8.2 Analysis

Here axial velocity, temperature and concentration via graphs are analyzed. Numerical results of heat and mass transport process at the upper wall are studied via tables.

8.2.1 Velocity

Figs. (8.2)-(8.4) are organized to analyze the effects of M, We and Da parameters on the axial velocity. These Figs. depict that axial velocity is higher near the center of channel. Fig. 8.2

depicts that for higher values of Hartman number the axial velocity decreases. Physically it is convenient due to retarding nature of the Lorentz force when the magnetic force is perpendicularly applied to the direction of fluid motion. Increasing value of Weissenberg number enhances velocity profile (see Fig. 8.3). Viscous forces are decayed by enhancing "We" therefore axial velocity increases. "Da" number has an enhancing effect of velocity near the center of channel and reverse behavior near the channel wall (see Fig. 8.4).

8.2.2 Temperature

Figs. (8.5)-(8.11) are prepared to examine the temperature via M, We, a, Da, N_t and N_b. Substantial increase in temperature is seen by enhancing Weissenberg number (see Fig. 8.5). Hartman number has an increasing affect on temperature (see Fig. 8.6). It is convenient for Joule heating. Temperature rapidly increases when Hartman number enhances due to the viscous dissipation. Significant rise in temperature is seen when non-linear thermal radiation parameter is increased (see Fig. 8.7). Fig. 8.8 shows that temperature enhances by increasing "Da" number specially near boundaries. Temperature of fluid slightly decreases by enhancing the non-Newtonian parameter "a" (see Fig. 8.9). Effects of Brownian motion and thermophoresis on temperature are studied via Figs. (8.10)-(8.11). Increase in N_t and N_b enhances the temperature. Ratio between surface and reference temperatures enhances due to an increment in thermophoresis parameter and so temperature increases.

8.2.3 Concentration

Effects of embedded parameters for concentration are examined via Figs. (8.12)-(8.18). Fig. 8.12 shows a decrease in concentration when Weissenberg number is enhanced. Fig. 8.13 represents that concentration of nanomaterial rapidly enhances with Hartman number. This is generally due to presence of Joule heating and thermophoresis. Concentration of nanomaterial decreases for non-Newtonian parameter "a" (see Fig. 8.14). Fig. 8.15 shows an increase in concentration of nanomaterials when thermophoresis parameter is enhanced. However opposite behavior is seen in case of Brownian motion (see Fig. 8.16). It is due to the fact that Brownian forces push the particles in opposite direction of concentration gradient and make the nanofluid more homogeneous. Fig. 8.17 shows that decrease in concentration appears when "Da" number

increases. Increasing value of R_d parameter decrease the concentration of nanomaterials (see Fig. 8.18).

8.2.4 Heat and mass transfer rate

Heat and mass transport process corresponding to different values of embedded parameters are numerically given in table 8.1. It is concluded that increasing Weissenberg number and Hartman number decrease the heat and mass transport process. Further the non-Newtonian parameter "a" shows an increase in heat and mass transport process. This table indicates that higher "Da" number and "R_d" decay the heat and mass transport process. Larger thermophoresis variable rapidly increases mass transfer rate. However "N_b" decreases mass transfer rate.

8.3 Conclusions

Numerical solution for flow of an incompressible Carreau-Yasuda nanofluid model is studied. Key findings are summarized below.

- Large Weissenberg number depicts an increasing behavior for axial velocity and temperature near channel center. Further concentration decreases against Weissenberg number.
- Both temperature and concentration show decaying behavior when non-Newtonian parameter increases.
- By enhancing "Da" number both velocity and temperature depict increasing behavior near the center of channel while opposite effect is guaranteed for concentration.
- Larger Hartman number depicts higher temperature and concentration.
- For larger thermophoresis parameter the heat and mass transport process increase.
- Non-linear thermal radiation enhances temperature while heat transfer rate decays.
- Brownian motion has opposite effects for temperature and concentration.

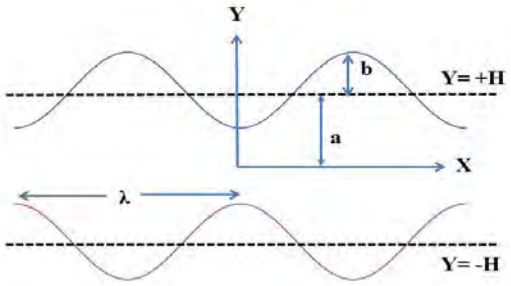

Fig. 8.1. Geometry of the problem.

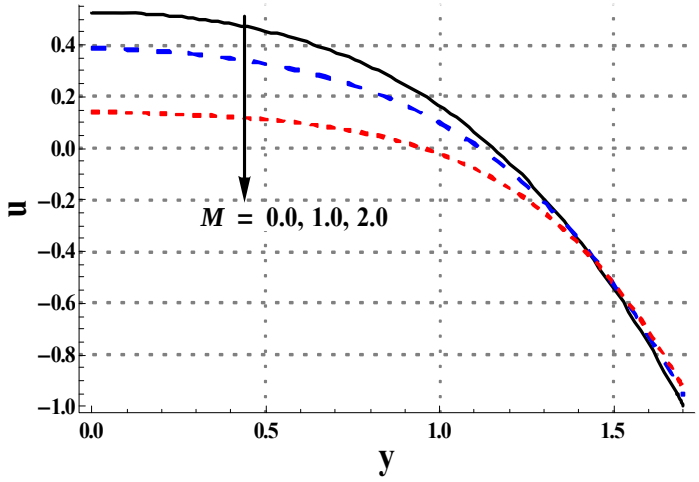

Fig. 8.2. Effects of M on velocity.

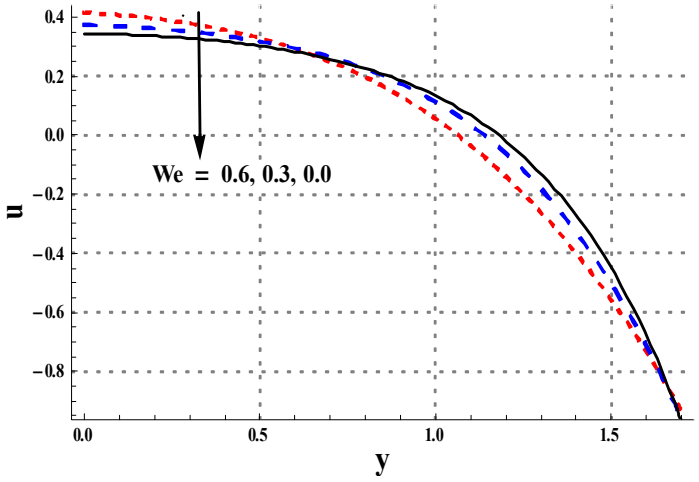

Fig. 8.3. Effects of We on velocity.

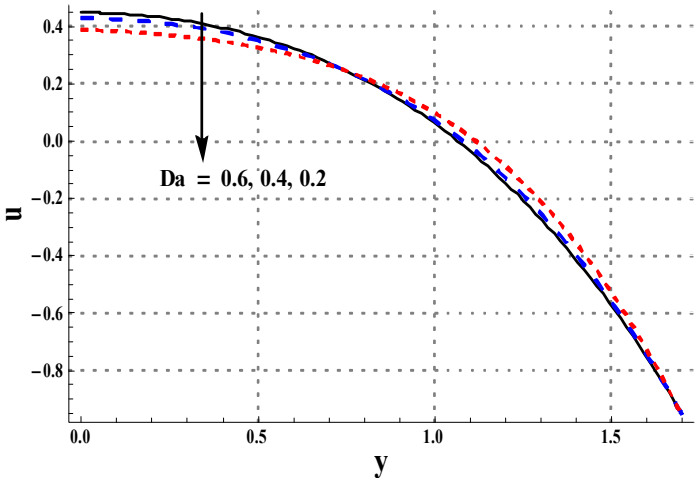

Fig. 8.4. Effects of Da on velocity.

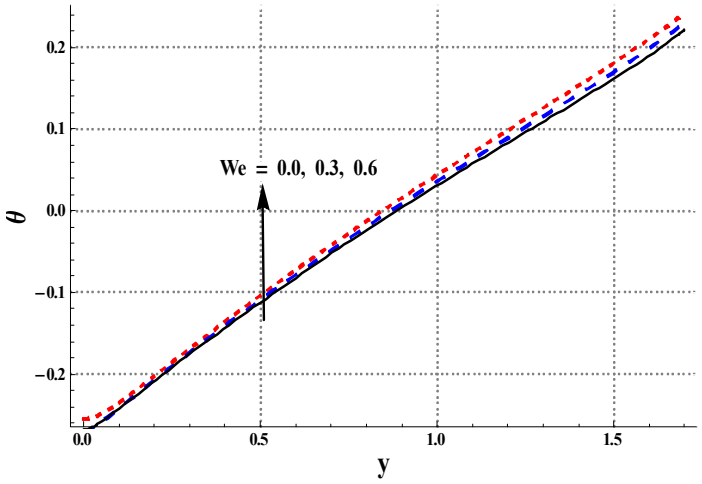

Fig. 8.5. Effects of We on θ.

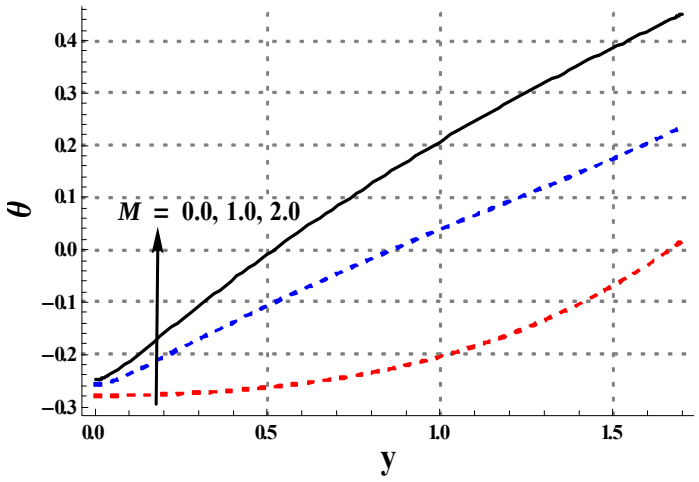

Fig. 8.6. Effects of M on θ.

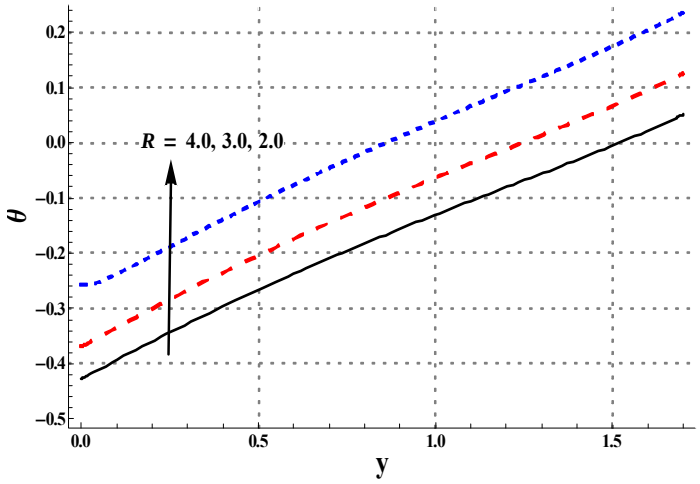

Fig. 8.7. Effects of R_d on θ.

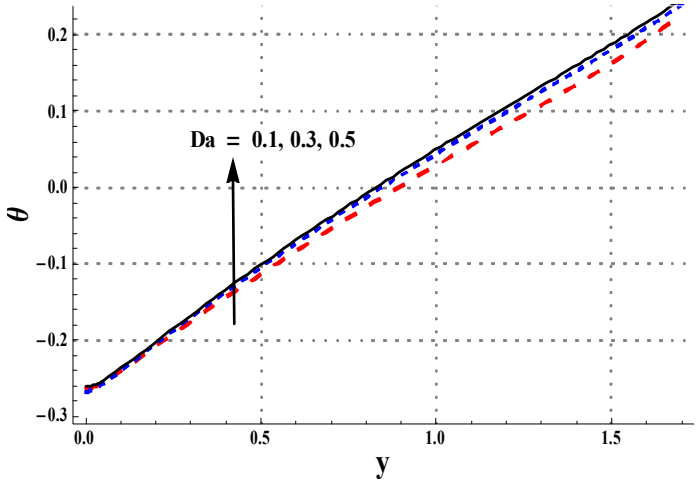

Fig. 8.8. Effects of Da on θ.

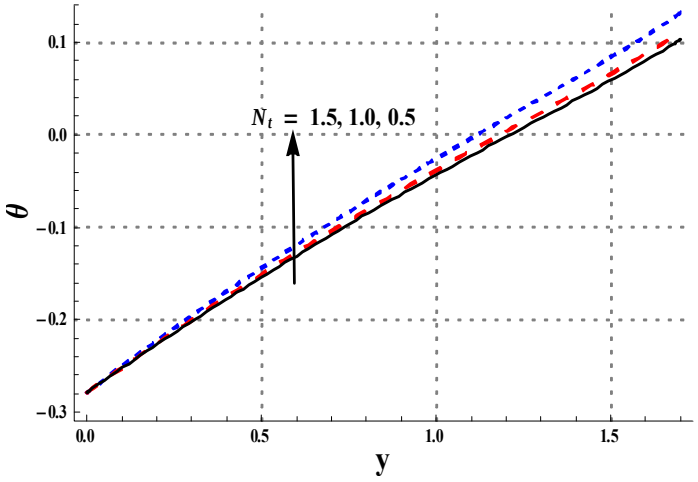

Fig. 8.9. Effects of N_t on θ.

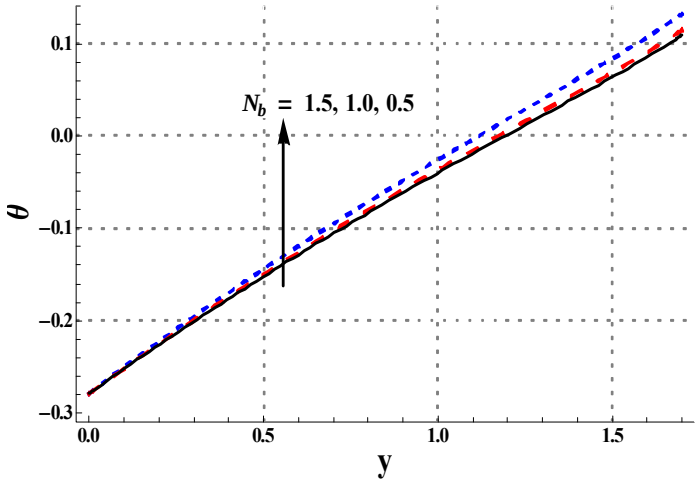

Fig. 8.10. Effects of N_b on θ.

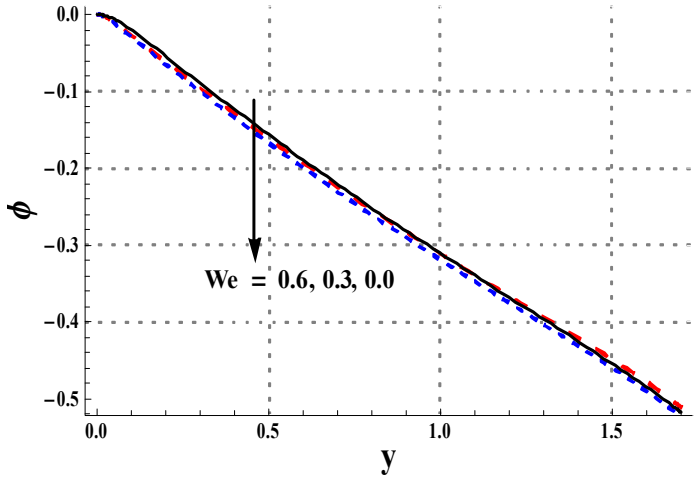

Fig. 8.11. Effects of We on concentration.

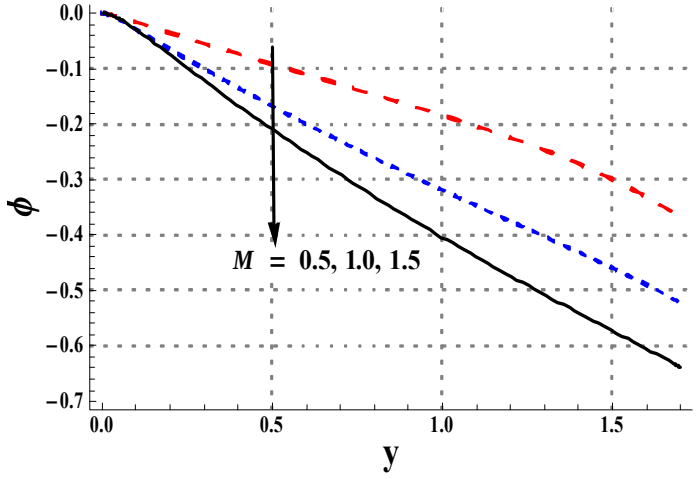

Fig. 8.12. Effects of M on concentration.

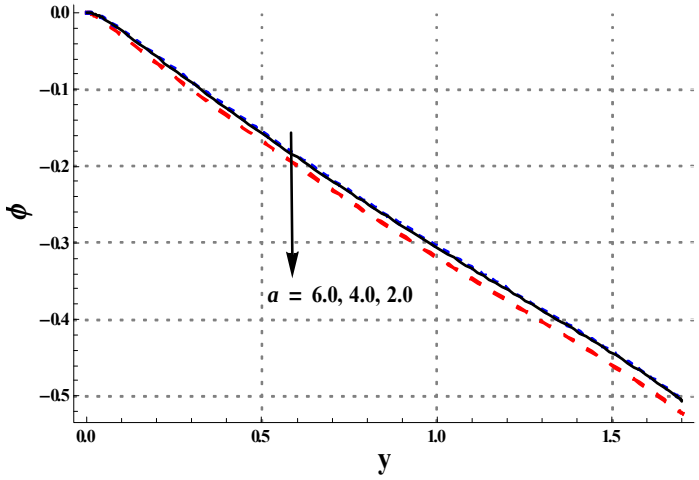

Fig. 8.13. Effects of a on concentration.

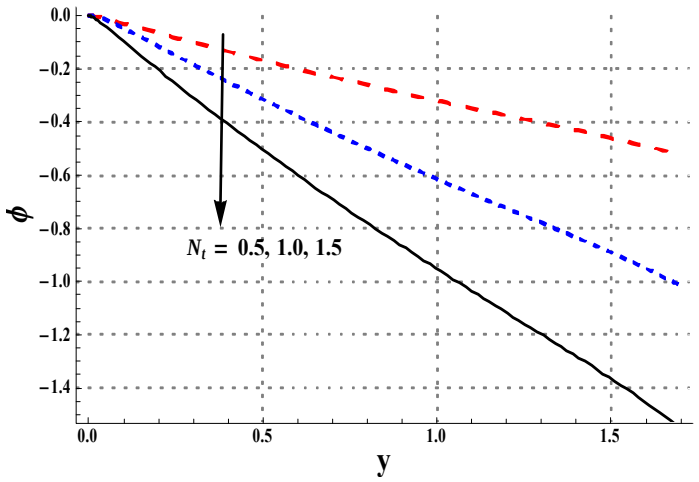

Fig. 8.14. Effects of N_t on concentration.

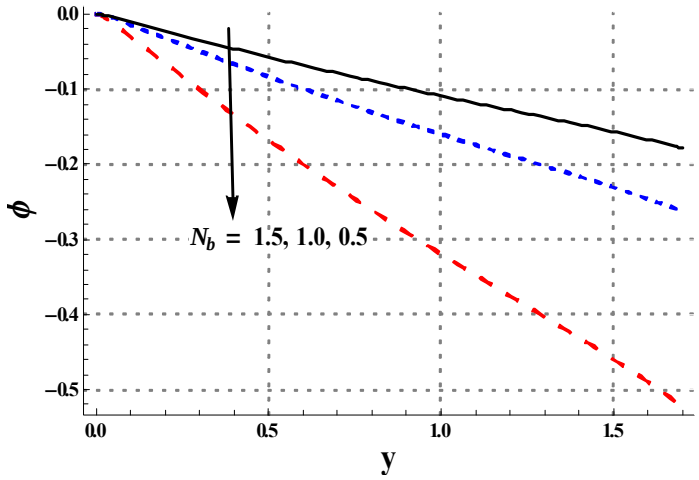

Fig. 8.15. Effects of N_b on concentration.

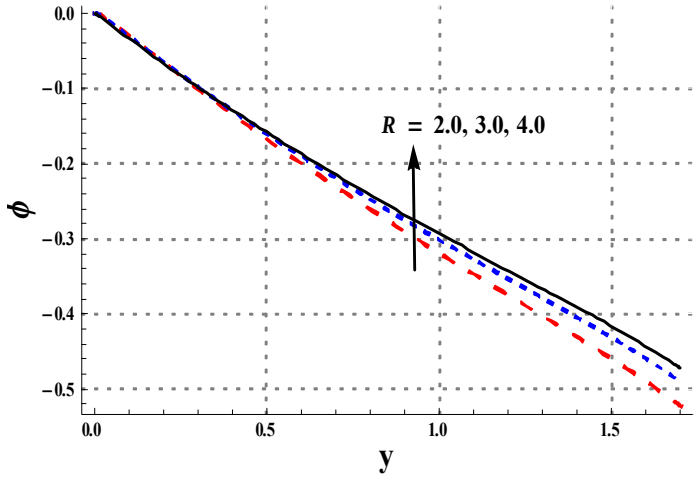

Fig. 8.16. Effects of R_d on concentration.

Table 8.1: Effect of embedded parameters on heat and mass rate.

We	M	a	Da	R	N_t	N_b	$-\theta'(h)$	$\phi'(h)$
0.0	1.0	2.0	0.2	0.2	0.5	0.5	0.798858	0.944304
0.3							0.774853	0.918494
0.6							0.736244	0.877082
0.3	0.5						0.978356	1.006850
	1.0						0.774853	0.918494
	1.5						0.673886	0.871912
	1.0	2.0					0.774853	0.918494
		4.0					0.791814	0.935982
		6.0					0.795791	0.940520
		2.0	0.2				0.774853	0.918494
			0.3				0.732663	0.878502
			0.4				0.711439	0.859291
			0.2	0.2			0.774853	0.918494
				0.3			0.649985	0.851924
				0.4			0.580960	0.816411
				0.2	0.5		0.774853	0.918494
					1.0		0.776464	1.721720
					1.5		0.776913	2.502060
					1.0	0.5	0.774853	0.918494
						1.0	0.774601	0.452167
						1.5	0.775668	0.296788

Chapter 9

Peristaltic activity of Carreau-Yasuda nanomaterial with convective and zero mass flux conditions

This chapter explores Hall and Ohmic heating effects in peristaltic transport of non-Newtonian nanomaterial. Non-Newtonian fluids are no doubt used in physiological and industrial phenomena. Fluid subject to nanomaterial are used in tumor analysis, oil recovery, cancer therapy and many others. Here we consider the peristaltic transport of Carreau-Yasuda nanofluid subject to mixed convection. The thermal convective and zero nanoparticles mass flux conditions are used in view of very little information on this topic. Modelling is constructed for long wavelength and low Reynolds number. Resulting nonlinear equations are numerically solved. Graphical analysis of velocity, temperature and concentration is analyzed.

9.1 Problem formulation

Flow of Carreau-Yasuda (CY) fluid in an asymmetric channel is assumed. Flow is driven by the movement of peristaltic waves with wavelength λ and speed "c" along the channel boundaries.

Consider $X-axis$ along length of channel and $Y-axis$ normal to it. Geometry of peristaltic walls (see Fig. 9.1) is described in the forms:

$$\bar{H}_1(\bar{X},\bar{t}) = d_1 + a_1 cos(\frac{2\pi}{\lambda}(\bar{X}-c\bar{t})),$$

$$\bar{H}_2(\bar{X},\bar{t}) = -d_2 - b_1 cos(\frac{2\pi}{\lambda}(\bar{X}-c\bar{t})+\gamma_2). \tag{9.1}$$

Here $\bar{H}_1$ and $\bar{H}_2$ are the upper and lower walls of channel, γ_2 stands for phase difference, t for time, a_1 and b_1 denote the amplitudes of upper and lower waves respectively. Fluid is electrically conducting in presence of strong applied magnetic field. Hall effect is retained. Velocity field for this flow is $\bar{\mathbf{V}} = [\bar{U}(\bar{X},\bar{Y},\bar{t}),\bar{V}(\bar{X},\bar{Y},\bar{t}),0]$. Viscous dissipation and Ohmic heating are present. Effects of Brownian motion and thermophoresis are also considered to explore nanomaterial characteristics. Associated equations for the current problem under consideration are:

$$\frac{\partial \bar{U}}{\partial \bar{X}} + \frac{\partial \bar{V}}{\partial \bar{Y}} = 0, \tag{9.2}$$

$$\rho_f\left(\frac{\partial}{\partial \bar{t}} + \bar{U}\frac{\partial}{\partial \bar{X}} + \bar{V}\frac{\partial}{\partial \bar{Y}}\right)\bar{U} = -\frac{\partial \bar{P}}{\partial \bar{X}} + \frac{\partial \bar{S}_{\bar{x}\bar{x}}}{\partial \bar{X}} + \frac{\partial \bar{S}_{\bar{x}\bar{y}}}{\partial \bar{Y}}$$
$$-\frac{\sigma_f B_0^2}{1+m^2}[\bar{U}-m\bar{V}] + g\rho_f[\alpha(T-T_m)+\alpha^*(C-C_m)], \tag{9.3}$$

$$\rho_f\left(\frac{\partial}{\partial \bar{t}} + \bar{U}\frac{\partial}{\partial \bar{X}} + \bar{V}\frac{\partial}{\partial \bar{Y}}\right)\bar{V} = -\frac{\partial \bar{P}}{\partial \bar{y}} + \frac{\partial \bar{S}_{\bar{y}\bar{x}}}{\partial \bar{X}} + \frac{\partial \bar{S}_{\bar{y}\bar{y}}}{\partial \bar{Y}} - \frac{\sigma_f B_0^2}{1+m^2}[\bar{V}+m\bar{U}], \tag{9.4}$$

$$(\rho C)_f\left(\bar{U}\frac{\partial}{\partial \bar{X}} + \bar{V}\frac{\partial}{\partial \bar{Y}}\right)T = K_f\left[\frac{\partial^2 T}{\partial \bar{X}^2} + \frac{\partial^2 T}{\partial \bar{Y}^2}\right] + \bar{S}.\bar{L} + \frac{\sigma_f B_0^2}{1+m^2}[\bar{U}^2+\bar{V}^2]$$
$$+(\rho C)_{np}\left[D_B\left(\frac{\partial C}{\partial \bar{X}}\frac{\partial T}{\partial \bar{X}} + \frac{\partial C}{\partial \bar{Y}}\frac{\partial T}{\partial \bar{Y}}\right) + \frac{D_T}{T_m}\left(\left(\frac{\partial T}{\partial \bar{X}}\right)^2 + \left(\frac{\partial T}{\partial \bar{Y}}\right)^2\right)\right], \tag{9.5}$$

$$\bar{U}\frac{\partial C}{\partial \bar{X}} + \bar{V}\frac{\partial C}{\partial \bar{Y}} = D_B\left(\frac{\partial^2 C}{\partial \bar{X}^2} + \frac{\partial^2 C}{\partial \bar{Y}^2}\right) + \frac{D_T}{T_m}\left(\frac{\partial^2 T}{\partial \bar{X}^2} + \frac{\partial^2 T}{\partial \bar{Y}^2}\right). \tag{9.6}$$

In these equations, P stands for pressure, σ_f for electrical conductivity of fluid, B_0 for applied magnetic field strength, $m(=\frac{\sigma_f B_0}{en_e})$ for Hall parameter, $C_m(=\frac{C_0+C_1}{2})$ denotes the mean concentration of nanoparticles, $T_m(=\frac{T_0+T_1}{2})$ the mean temperature of nanoparticles, ρ_f the density of fluid, S_{ij} the components of extra stress tensor, T the fluid temperature, C the concentration, $\bar{S}.\bar{L}$ the viscous dissipation term, $\bar{L}$ the gradient of velocity, C_f the specific heat of fluid, K_f the thermal conductivity of fluid, D_B the mass diffusivity, D_T the thermophoretic diffusion coefficients and $(\rho C)_{np}$ the effective heat capacity of the nanoparticles. An extra stress tensor for the Carreau-Yasuda fluid is:

$$\bar{\mathbf{S}} = \mu(\gamma')\mathbf{A}_1,$$

where $\mathbf{A}_1$ is the first Rivilin-Ericksen tensor and the apparent viscosity $\mu(\gamma')$ is:

$$\mu(\gamma') = \mu_\infty + (\mu_0 - \mu_\infty)\left[1 + (\Gamma\Pi)^a\right]^{\frac{n-1}{a}}, \tag{9.7}$$

with

$$\Pi = \sqrt{\frac{1}{2}tr(\mathbf{A}_1^2)},$$

and

$$\mathbf{A}_1 = \left[\operatorname{grad}\mathbf{V} + (\operatorname{grad}\mathbf{V})^T\right].$$

Here μ_∞ denotes the infinite shear rate viscosity and μ_0 stands for zero shear-rate viscosity. The non-Newtonian parameters a and Γ control the transition between the two extremes. Further "n" depicts the characteristics of power law index that explore the nature of thickening and thinning of material. The thermal convective and zero nanoparticles mass flux conditions are defined as follows:

$$-K_f\frac{\partial T}{\partial y} = l_w(T - T_w), \tag{9.8}$$

$$D_B\frac{\partial C}{\partial \bar{Y}} + \frac{D_T}{T_m}\frac{\partial T}{\partial \bar{Y}} = 0 \text{ at } y = h_1 \text{ and } y = h_2, \tag{9.9}$$

in which l_w and T_w stand for heat transfer coefficient and temperature at the walls. By using the transformations:

$$\bar{x} = \bar{X} - c\bar{t}, \bar{y} = \bar{Y}, \bar{u} = \bar{U} - c, \bar{v} = \bar{V}, \bar{p}(\bar{x}, \bar{y}) = \bar{P}(\bar{X}, \bar{Y}, \bar{t}), \tag{9.10}$$

the resulting equations:

$$\frac{\partial \bar{u}}{\partial \bar{x}}+\frac{\partial \bar{v}}{\partial \bar{y}}=0, \tag{9.11}$$

$$\rho_f\left((\bar{u}+c)\frac{\partial}{\partial \bar{x}}+\bar{v}\frac{\partial}{\partial \bar{y}}\right)(\bar{u}+c)=-\frac{\partial \bar{p}}{\partial \bar{x}}+\frac{\partial \bar{s}_{\bar{x}\bar{x}}}{\partial \bar{x}}+\frac{\partial \bar{s}_{\bar{x}\bar{y}}}{\partial \bar{y}}$$
$$-\frac{\sigma_f B_0^2}{1+m^2}[(\bar{u}+c)-m\bar{v}]+g\rho_f[\alpha(T-T_m)+\alpha^*(C-C_m)], \tag{9.12}$$

$$\rho_f\left((\bar{u}+c)\frac{\partial}{\partial \bar{x}}+\bar{v}\frac{\partial}{\partial \bar{y}}\right)\bar{v}=-\frac{\partial \bar{p}}{\partial \bar{y}}+\frac{\partial \bar{s}_{\bar{y}\bar{x}}}{\partial \bar{x}}+\frac{\partial \bar{s}_{\bar{y}\bar{y}}}{\partial \bar{y}}-\frac{\sigma_f B_0^2}{1+m^2}[\bar{v}+m(\bar{u}+c)], \tag{9.13}$$

$$(\rho C)_f\left((\bar{u}+c)\frac{\partial}{\partial \bar{x}}+\bar{v}\frac{\partial}{\partial \bar{y}}\right)T=K_f\left[\frac{\partial^2 T}{\partial \bar{x}^2}+\frac{\partial^2 T}{\partial \bar{y}^2}\right]+\bar{s}.\bar{L}+\frac{\sigma_f B_0^2}{1+m^2}[(\bar{u}+c)^2+\bar{v}^2]$$
$$+(\rho C)_{np}\left[D_B\left(\frac{\partial C}{\partial \bar{x}}\frac{\partial T}{\partial \bar{x}}+\frac{\partial C}{\partial \bar{y}}\frac{\partial T}{\partial \bar{y}}\right)+\frac{D_T}{T_m}\left(\left(\frac{\partial T}{\partial \bar{x}}\right)^2+\left(\frac{\partial T}{\partial \bar{y}}\right)^2\right)\right], \tag{9.14}$$

$$(\bar{u}+c)\frac{\partial C}{\partial \bar{x}}+\bar{v}\frac{\partial C}{\partial \bar{y}}=D_B\left(\frac{\partial^2 C}{\partial \bar{x}^2}+\frac{\partial^2 C}{\partial \bar{y}^2}\right)+\frac{D_T}{T_m}\left(\frac{\partial^2 T}{\partial \bar{x}^2}+\frac{\partial^2 T}{\partial \bar{y}^2}\right), \tag{9.15}$$

where

$$x=\frac{\bar{x}}{\lambda}, y=\frac{\bar{y}}{d_1}, u=\frac{\bar{u}}{c}, v=\frac{\bar{v}}{c\delta}, \delta=\frac{\bar{d_1}}{\lambda}, h_1=\frac{\bar{H}_1}{d_1}, h_2=\frac{\bar{H}_2}{d_2}, d=\frac{d_2}{d_1}, a_2=\frac{a_1}{d_1}, b=\frac{b_1}{d_1}, p=\frac{d_1^2\bar{p}}{c\lambda\mu_f},$$
$$Re=\frac{\rho_f\ cd_1}{\mu_f}, E=\frac{c^2}{C_f(T_1-T_0)}, Pr=\frac{\mu_f C_f}{K_f}, M=\sqrt{\frac{\sigma_f}{\mu_f}}B_0 d_1, N_b=\frac{\tau D_B(C_1-C_0)}{\nu}, N_t=\frac{\tau D_T(T_1-T_0)}{\nu T_m},$$
$$\upsilon=\frac{\mu_f}{\rho_f}, G_T=\frac{\rho_f g\alpha(T_1-T_0)d_1^2}{\mu_f c}, G_c=\frac{\rho_f g\alpha^*(C_1-C_0)d_1^2}{\mu_f c}, \theta=\frac{T-T_m}{T_1-T_0}, Br=PrE, u=\frac{\partial\psi}{\partial y}, v=-\frac{\partial\psi}{\partial x}. \tag{9.16}$$

Here $Re, Br, Ec, \mathrm{Pr}, M, \delta, \theta, G_T, G_c, N_b$ and N_t denote the Reynolds number, Brinkman number, Eckert number, Prandtl number, Hartman number, wave number, dimensionless temperature, the thermal Grashoff number, the concentration Grashoff number, the Brownian motion parameter and the thermophoresis variable. Applying the long wavelength and low Reynold number suppositions the simplified form of equations we obtain:

$$p_y=0, \tag{9.17}$$

$$p_x = \frac{\partial s_{xy}}{\partial y} + G_T\theta + G_C\phi - \frac{M^2}{1+m^2}\left(1+\frac{\partial \psi}{\partial y}\right), \tag{9.18}$$

$$\theta_{yy} + Br\Phi + \Pr N_b\phi_y\theta_y + \Pr N_t\left(\theta_y\right)^2 + \frac{BrM^2}{1+m^2}\left(1+\frac{\partial \psi}{\partial y}\right)^2 = 0, \tag{9.19}$$

$$N_b\phi_{yy} + N_t\theta_{yy} = 0 \tag{9.20}$$

Incompressibility condition is trivially satisfied. Here Φ is the dimensionless viscous dissipation term and nondimensional form of s_{xy} can be described as:

$$s_{xy} = s_{yx} = \left[1 + \frac{(1-\beta)(n-1)We^a}{a}(\psi_{yy})^a\right]\psi_{yy}, \tag{9.21}$$

in which $\beta = \frac{\mu_\infty}{\mu_0}$ stands for viscosity ratio parameter, ψ the stream function and We=$\frac{\Gamma c}{d_1}$ the Weissenberg number. From Eqs. (9.17)-(9.21) we obtain:

$$\frac{\partial^2}{\partial y^2}\left[1 + \frac{(1-\beta)(n-1)We^a}{a}(\psi_{yy})^a\right]\psi_{yy} + G_T\theta_y + G_C\phi_y - \frac{M^2}{1+m^2}\psi_{yy} = 0, \tag{9.22}$$

$$\theta_{yy}+Br\left[1 + \frac{(1-\beta)(n-1)We^a}{a}(\psi_{yy})^a\right]\psi_{yy}^2+\Pr N_b\phi_y\theta_y+\Pr N_t\left(\theta_y\right)^2+\frac{BrM^2}{1+m^2}\left(1+\frac{\partial \psi}{\partial y}\right)^2 = 0, \tag{9.23}$$

$$N_b\phi_{yy} + N_t\theta_{yy} = 0. \tag{9.24}$$

Dimensionless flow rate in the laboratory $\eta(=\bar{Q}/cd_1)$ and wave $F(=\bar{q}/cd_1)$ frames are related via the relation:

$$\eta = F + d + 1, \tag{9.25}$$

in which $\bar{Q}$ and $\bar{q}$ are dimensional flow rates in the laboratory and wave frames. Further 'F' is given by:

$$F = \int_{h_2}^{h_1}\frac{\partial \psi}{\partial y}dy. \tag{9.26}$$

The dimensionless boundary conditions are given by:

$$\begin{aligned}\psi = \tfrac{F}{2}, \frac{\partial \psi}{\partial y} = -1, \frac{\partial \theta}{\partial y} + Bi_1(\theta + \tfrac{1}{2}) = 0 \text{ and } N_b\phi_y + N_t\theta_y = 0 \text{ at } y = h_1,\\ \psi = -\tfrac{F}{2}, \frac{\partial \psi}{\partial y} = -1, \frac{\partial \theta}{\partial y} - Bi_2(\theta - \tfrac{1}{2}) = 0 \text{ and } N_b\phi_y + N_t\theta_y = 0 \text{ at } y = h_2,\end{aligned} \tag{9.27}$$

$$h_1 = 1 + a_2 cos(2\pi x), h_2 = -d - bcos(2\pi x + \gamma_2),$$
$$Bi_1 = (\frac{l_1 d_1}{K_f}), Bi_2 = (\frac{l_2 d_1}{K_f}),$$

in which Bi_1 and Bi_2 depicts Biot-numbers for upper and lower walls. Numerical approach are used to solve the system of equations in presence of boundary constraints. Analysis of the results are explored in next section.

9.2 Discussion

Here graphs are plotted for the velocity, temperature and concentration against embedded variables. Numerical data of heat and mass transport rates at the upper wall is presented in Table 9.1.

9.2.1 Axial velocity

Effects of M, m and We on axial velocity are depicted in Figs. (9.2)-(9.4). Velocity profile follows parabolic path. Maximum velocity is attained near the central portion of medium. Impact of Hartman number on velocity in Fig. 9.2. Fluid velocity is maximum for smaller values of "M". Fig. 9.3 gives the description of velocity for various values of Hall parameter. Hall parameter enahnces the fluid velocity near central portion of medium. Both Hartman and Hall parameters depict similar behavior for shear thickening ($n > 1$) and shear thinning ($n < 1$) materials. Fig. 9.4 gives velocity behavior for Weissenberg number. An increment in Weissenberg number shows increasing behavior for shear thickening case while reverse behavior is noticed for shear thinning fluids.

9.2.2 Temperature

Impacts of M, m, G_T, We, a, β and N_t on temperature are plotted (see Figs. (9.5)-(9.10). Temperature for Hartman number is studied in Fig. 9.5. It is noticed that temperature rapidly increases in the presence of magnetic field. Hall variable shows opposite affect on temperature when compared with Hartman number (see Fig. 9.6). Hall parameter decreases temperature of fluid. Effect of mixed convection variable G_T on temperature is depicted in Fig. 9.7. Temperature enhances near lower wall and it decays near upper wall for larger G_T. Fig. 9.8 shows

temperature behavior via Weissenberg number. An increase in temperature for shear thickening fluid is observed. Temperature decreases for shear thinning fluids. Fig. 9.9 indicates contribution of non-Newtonian parameter "a" on temperature. An enhancement in "a" depicts decaying behavior for shear thickening case ($n > 1$) while reverse situation is observed for ($n < 1$) case. Effect of viscosity ratio parameter "β" on temperature is depicted in Fig. 9.10. Higher values of "β" increase the temperature for shear thinning fluid. However situation for shear thickening behavior is reverse.

9.2.3 Concentration

Figs. (9.11)-(9.16) show concentration against M, m, G_C, We, N_t and N_b. For higher Hartman number, the concentration decreases for both shear thickening and shear thinning fluids (see Fig. 9.11). Fig. 9.12 indicates that concentration profile enhances for Hall parameter. Note that concentration decreases for higher G_C parameter (see Fig. 9.13). Clearly presence of Weissenberg number increases concentration for shear thinning fluid (see Fig. 9.14). Concentration decreases for shear thickening fluids. Effects of Brownian motion and thermophoresis on concentration are discussed in Figs. (9.15)-(9.16). Concentration decays by increasing Brownian motion and it enhances by increasing thermophoresis.

9.2.4 Concentration and temperature rates

Heat and mass transfer rates behavior in an asymmetric channel for M, m, We, a, N_t, N_b, G_T, Bi_1 and n are depicted in Table 9.1. Clearly presence of magnetic field increases the heat and mass transport characteristics. It is evident that Hall parameter has opposite trend for heat and mass transport rates when compared with Hartman number. Further for larger values of Weissenberg number, both heat and mass transport rates decay. Heat and mass transport rates also increase when non-Newtonian parameters "a" and "n" are enhanced. Thermophoresis parameter enhances the heat and mass transfer rates but Brownian motion decreases these. Presence of "G_T" variable decays heat and mass transport rates. However higher values of Biot number facilitate the heat transport rate.

9.3 Conclusions

Key findings of present analysis include the following points.

- Velocity and concentration distributions decay for shear thickening and shear thinning cases when Hartman number increases.
- Presence of Hall parameter increases the concentration and it decreases temperature.
- Weissenberg number shows opposite behaviour for shear thinning and shear thickening fluids.
- Increasing value of non-Newtonian parameters "a" and "β" enhance the temperature for shear thinning fluids. The results are reverse for shear thickening fluids.
- Larger Brownian motion parameter decrease concentration for both shear thickening and thinning fluids. However increasing values of thermophoresis parameter give concentration enhancement.

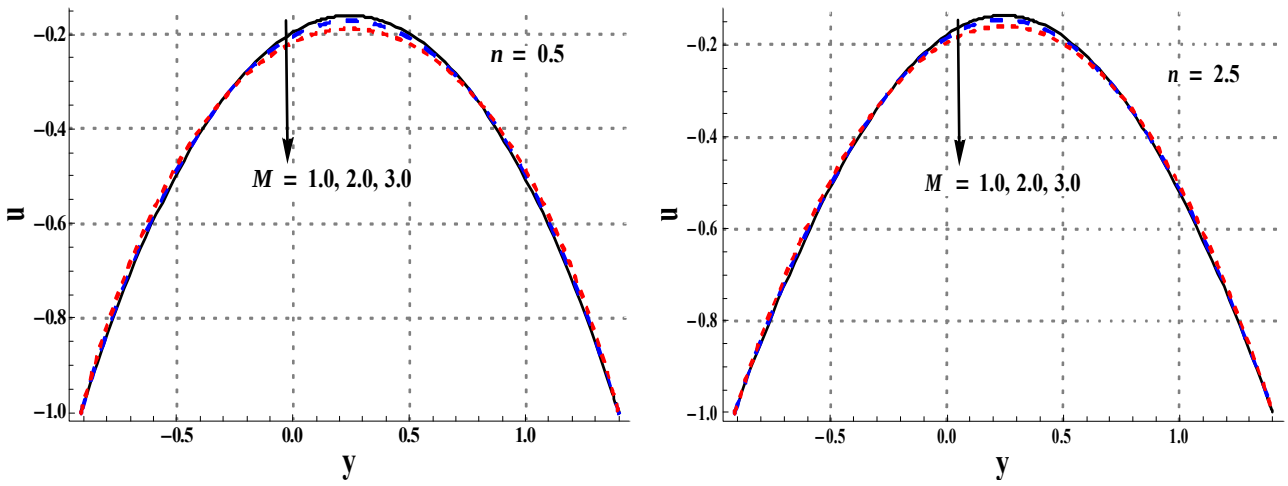

Fig. 9.2. Effect of M on velocity when d=0.7, η=0.7, x=0.0, γ=$\pi/4$, a_1=0.4, b=0.3, Br=0.3, Pr=0.5, We=0.4, G_T=1.0, G_C=1.0, Bi_1=0.9, Bi_2=1.2, m=2.0, β=0.1, a=2.0, N_t=0.5 and

N_b=0.5.

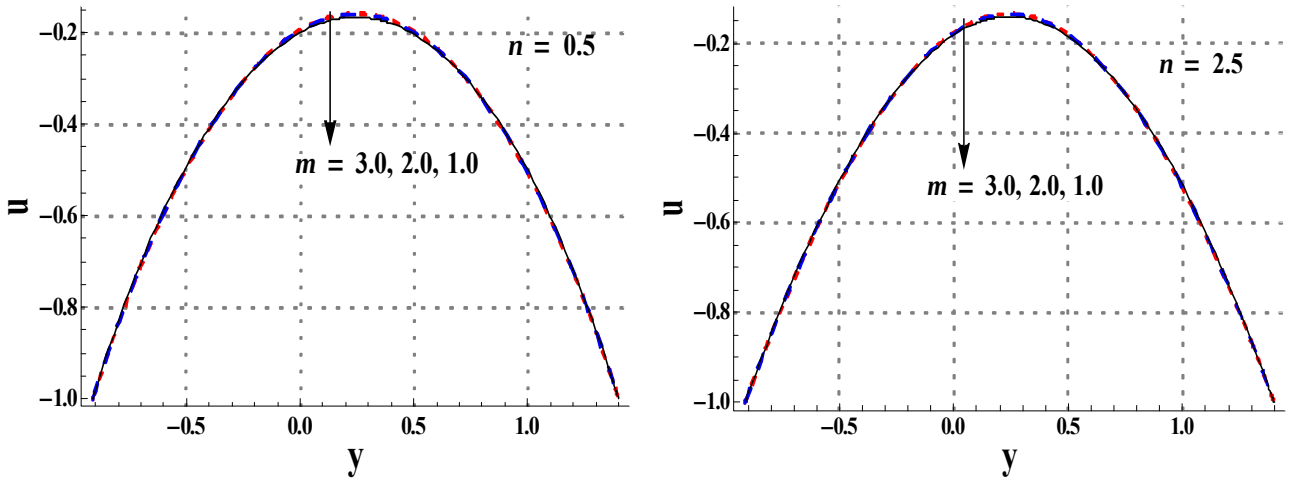

Fig. 9.3. Effect of m on velocity when d=0.7, η=0.7, x=0.0, γ=$\pi/4$, a_1=0.4, b=0.3, Br=0.3, Pr=0.5, We=0.4, G_T=1.0, G_C=1.0, Bi_1=0.9, Bi_2=1.2, M=1.0, β=0.1, a=2.0, N_t=0.5 and N_b=0.5.

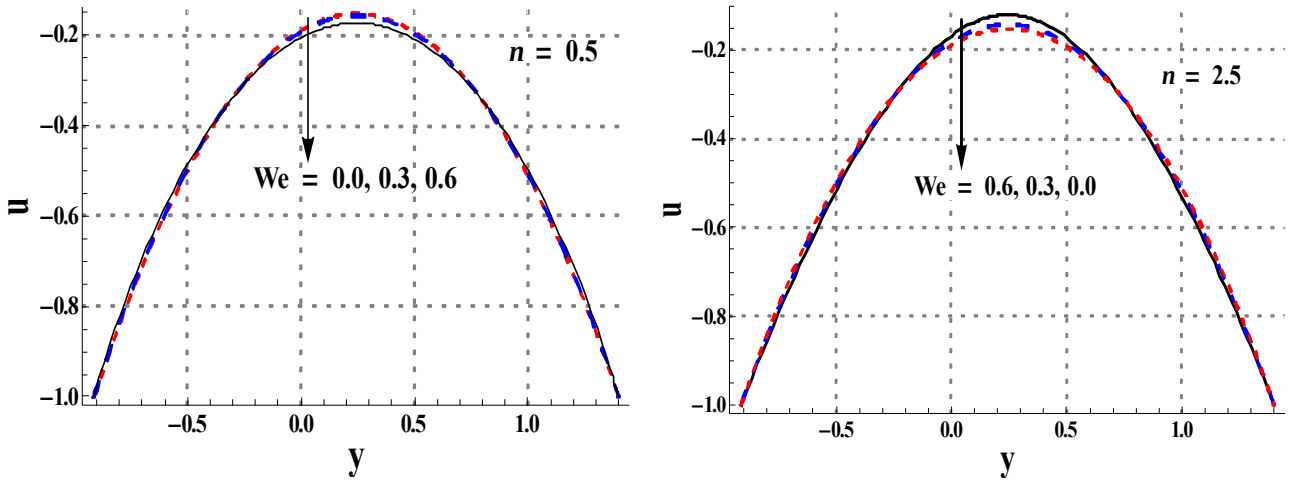

Fig. 9.4. Effect of We on velocity when d=0.7, η=0.7, x=0.0, γ=$\pi/4$, a_1=0.4, b=0.3, Br=0.3, Pr=0.5, G_T=1.0, G_C=1.0, Bi_1=0.9, Bi_2=1.2, M=1.0, m=2.0, β=0.1, a=2.0, N_t=0.5 and

N_b=0.5.

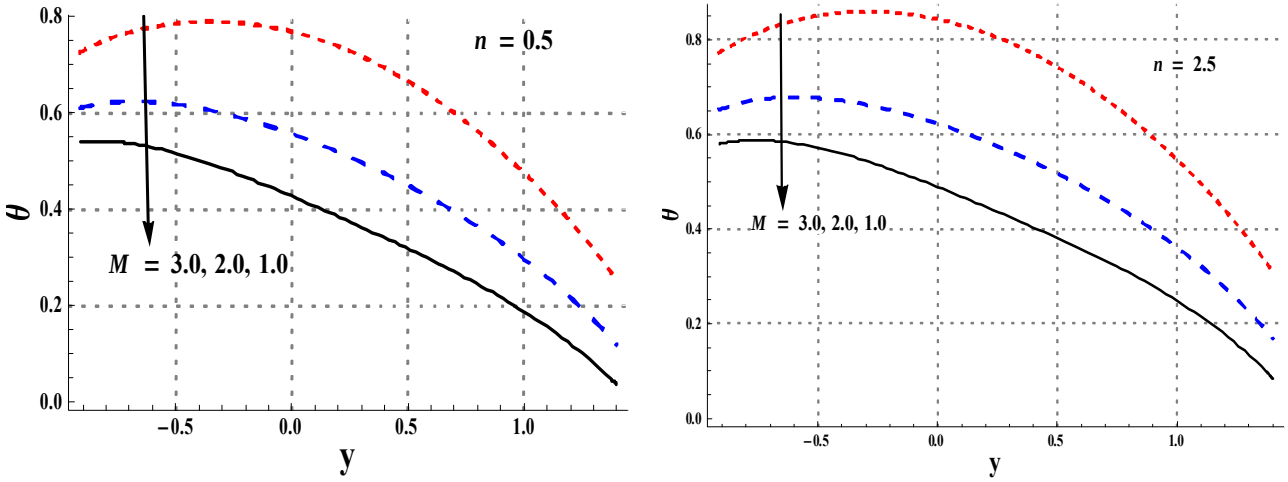

Fig. 9.5. Effect of M on temperature when d=0.7, η=0.7, x=0.0, γ=$\pi/4$, a_1=0.4, b=0.3, Br=0.3, Pr=0.5, We=0.4, G_T=1.0, G_C=1.0, Bi_1=0.9, Bi_2=1.2, m=2.0, β=0.1, a=2.0, N_t=0.5 and N_b=0.5.

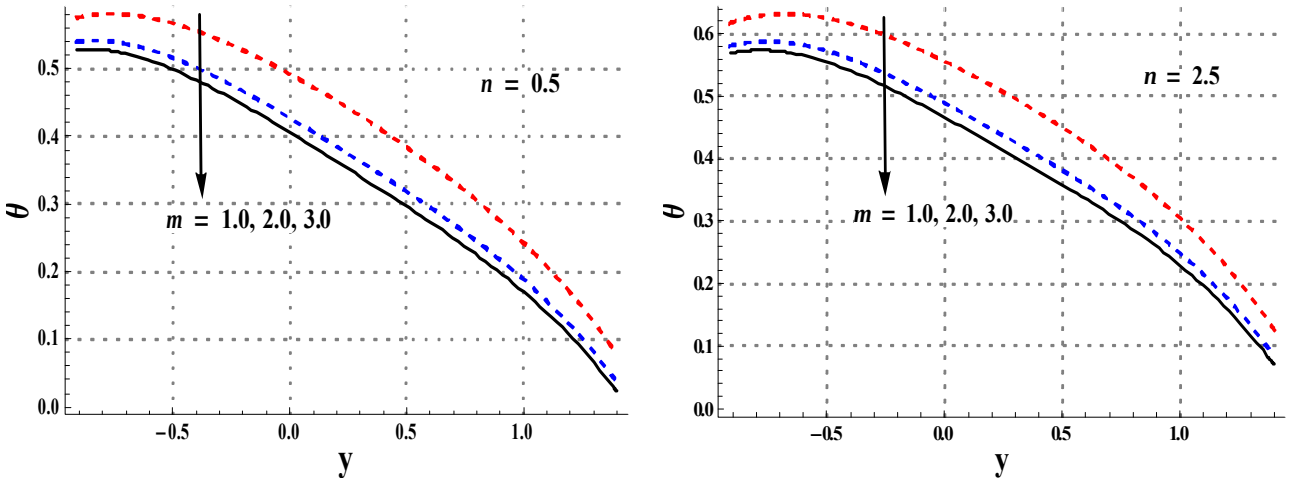

Fig. 9.6. Effect of m on temperature when d=0.7, η=0.7, x=0.0, γ=$\pi/4$, a_1=0.4, b=0.3, Br=0.3, Pr=0.5, We=0.4, G_T=1.0, G_C=1.0, Bi_1=0.9, Bi_2=1.2, M=1.0, β=0.1, a=2.0, N_t=0.5

and N_b=0.5.

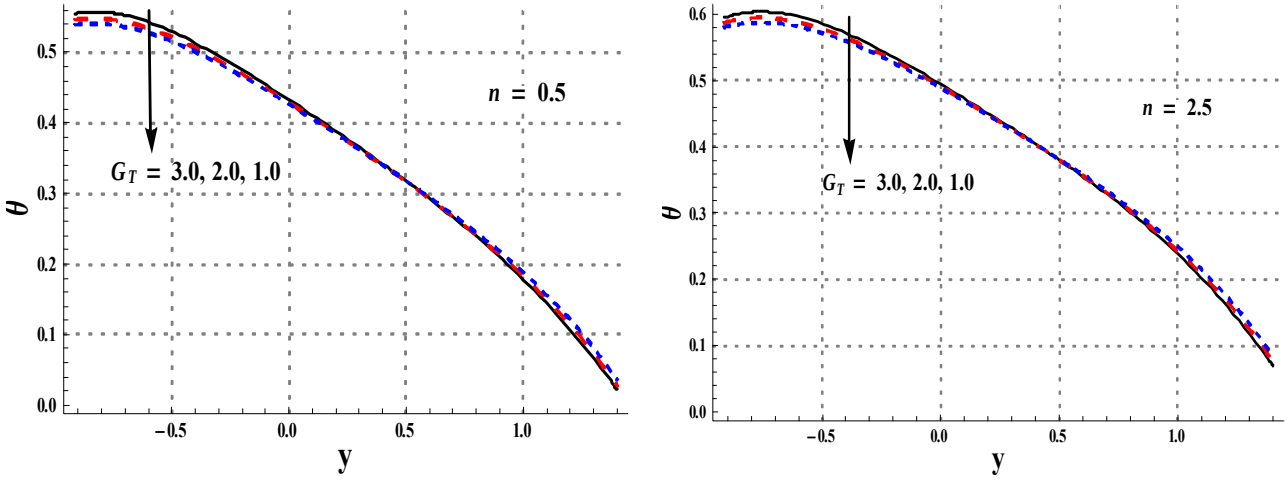

Fig. 9.7. Effect of G_T on temperature when d=0.7, η=0.7, x=0.0, γ=$\pi/4$, a_1=0.4, b=0.3, Br=0.3, Pr=0.5, We=0.4, G_C=1.0, Bi_1=0.9, Bi_2=1.2, M=1.0, m=2.0, β=0.1, a=2.0, N_t=0.5 and N_b=0.5.

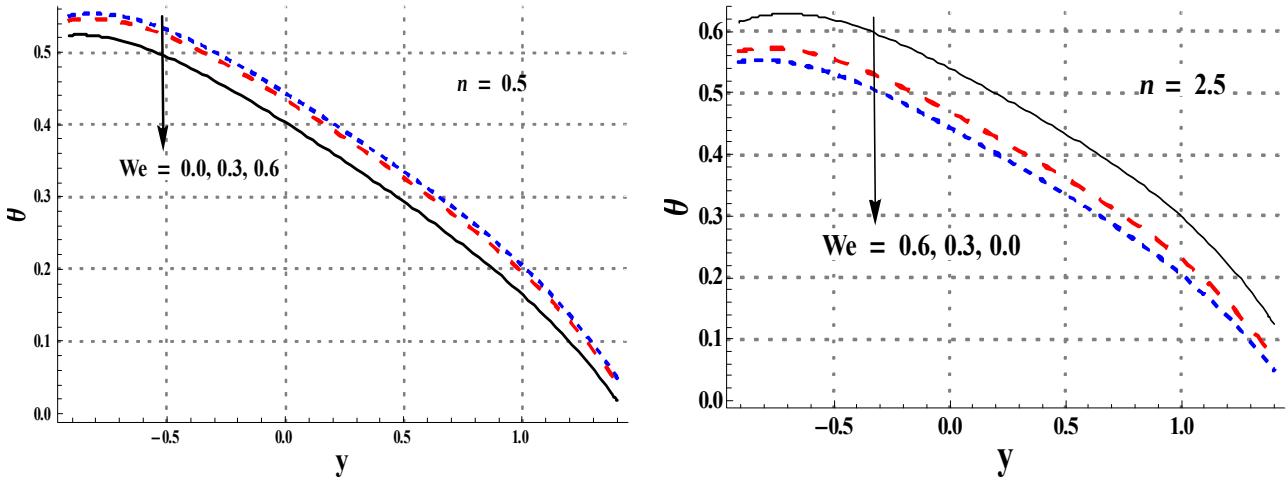

Fig. 9.8. Effect of We on velocity when d=0.7, η=0.7, x=0.0, γ=$\pi/4$, a_1=0.4, b=0.3, Br=0.3, Pr=0.5, G_T=1.0, G_C=1.0, Bi_1=0.9, Bi_2=1.2, M=1.0, m=2.0, β=0.1, a=2.0, N_t=0.5 and

N_b=0.5.

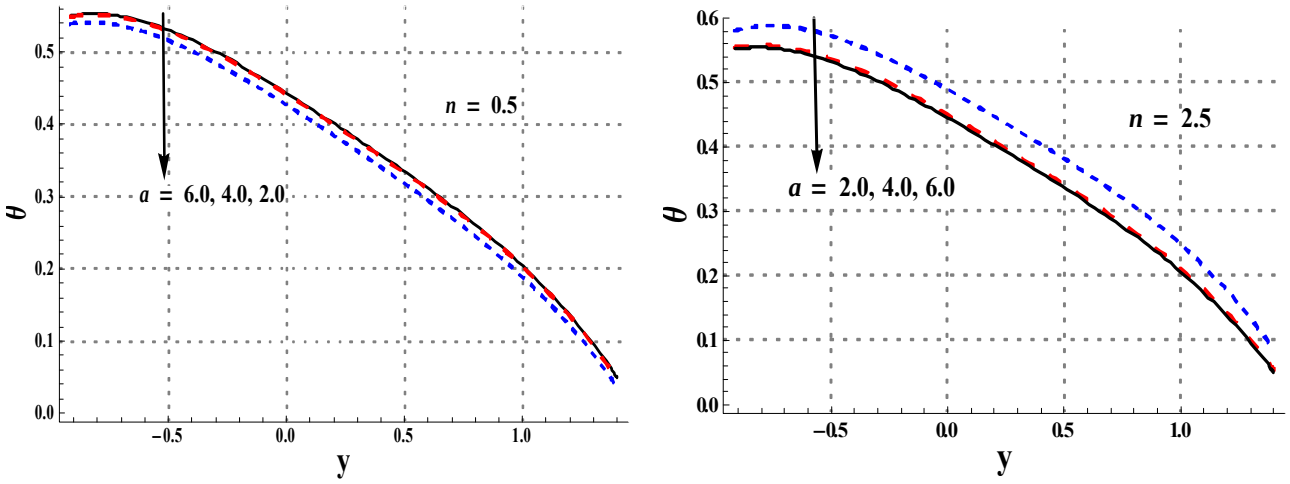

Fig. 9.9. Effect of a on temperature when d=0.7, η=0.7, x=0.0, γ=$\pi/4$, a_1=0.4, b=0.3, Br=0.3, Pr=0.5, We=0.4, G_T=1.0, G_C=1.0, Bi_1=0.9, Bi_2=1.2, M=1.0, m=2.0, β=0.1, N_t=0.5 and N_b=0.5.

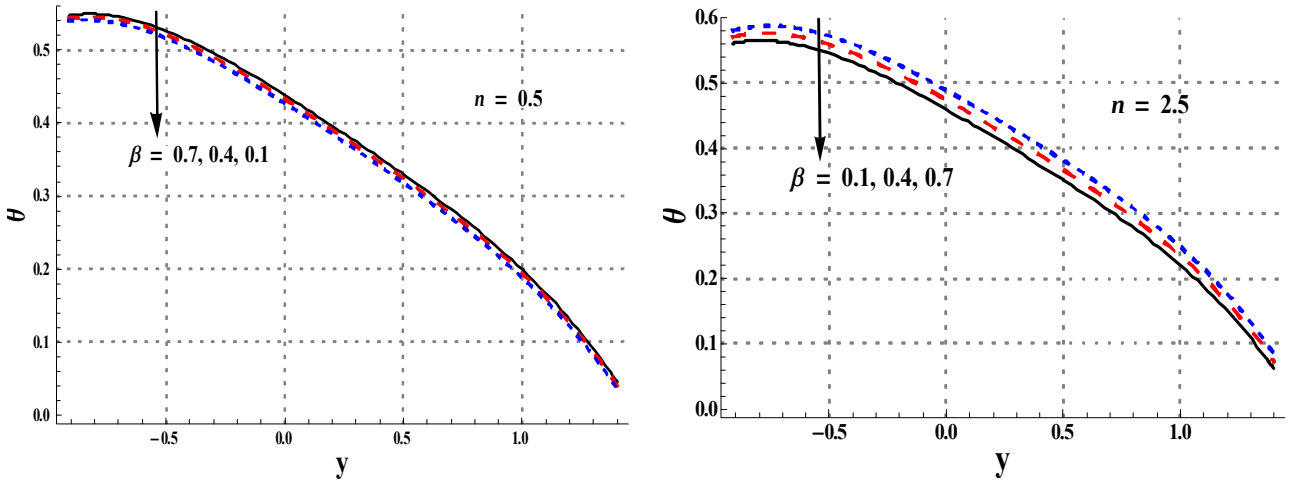

Fig. 9.10. Effect of β on temperature when d=0.7, η=0.7, x=0.0, γ=$\pi/4$, a_1=0.4, b=0.3, Br=0.3, Pr=0.5, We=0.4, G_T=1.0, G_C=1.0, Bi_1=0.9, Bi_2=1.2, M=1.0, m=2.0, a=2.0,

N_t=0.5 and N_b=0.5.

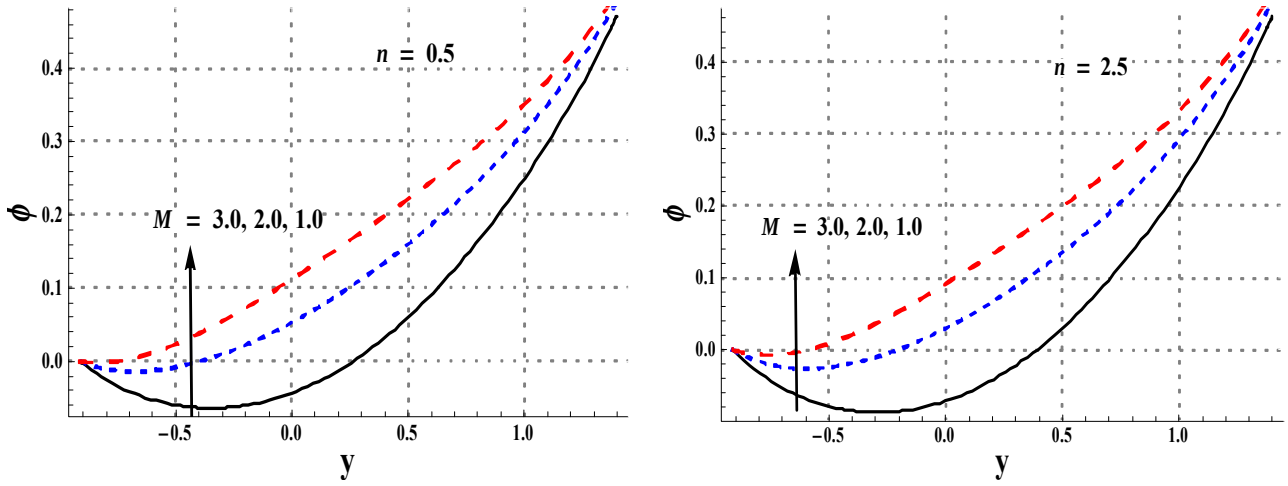

Fig. 9.11. Effect of M on concentration when d=0.7, η=0.7, x=0.0, γ=$\pi/4$, a_1=0.4, b=0.3, Br=0.3, Pr=0.5, We=0.4, G_T=1.0, G_C=1.0, Bi_1=0.9, Bi_2=1.2, m=2.0, β=0.1, a=2.0, N_t=0.5 and N_b=0.5.

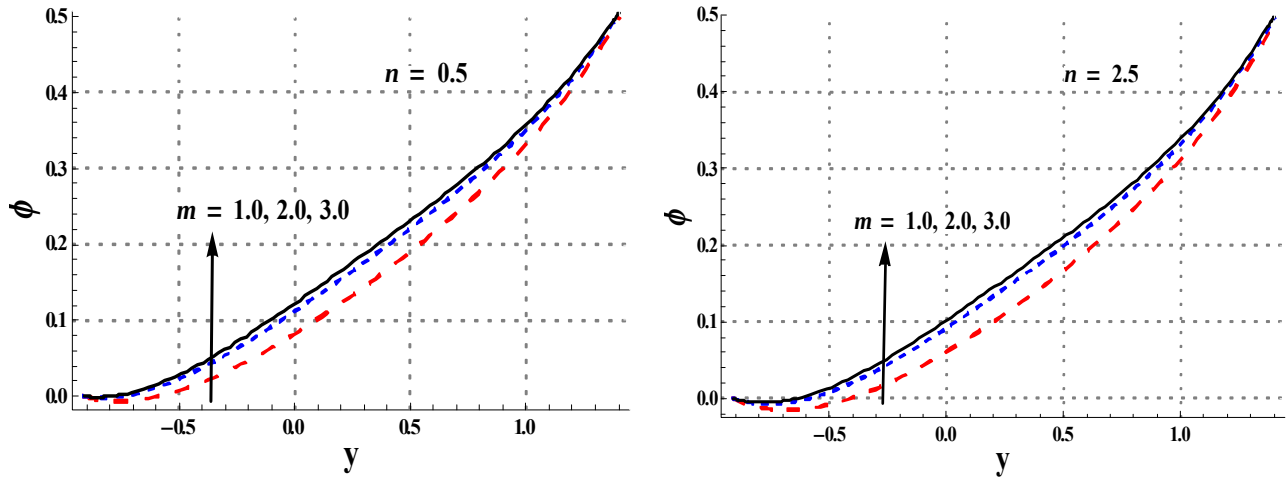

Fig. 9.12. Effect of m on concentration when d=0.7, η=0.7, x=0.0, γ=$\pi/4$, a_1=0.4, b=0.3, Br=0.3, Pr=0.5, We=0.4, G_T=1.0, G_C=1.0, Bi_1=0.9, Bi_2=1.2, M=1.0, β=0.1, a=2.0, N_t=0.5

and N_b=0.5.

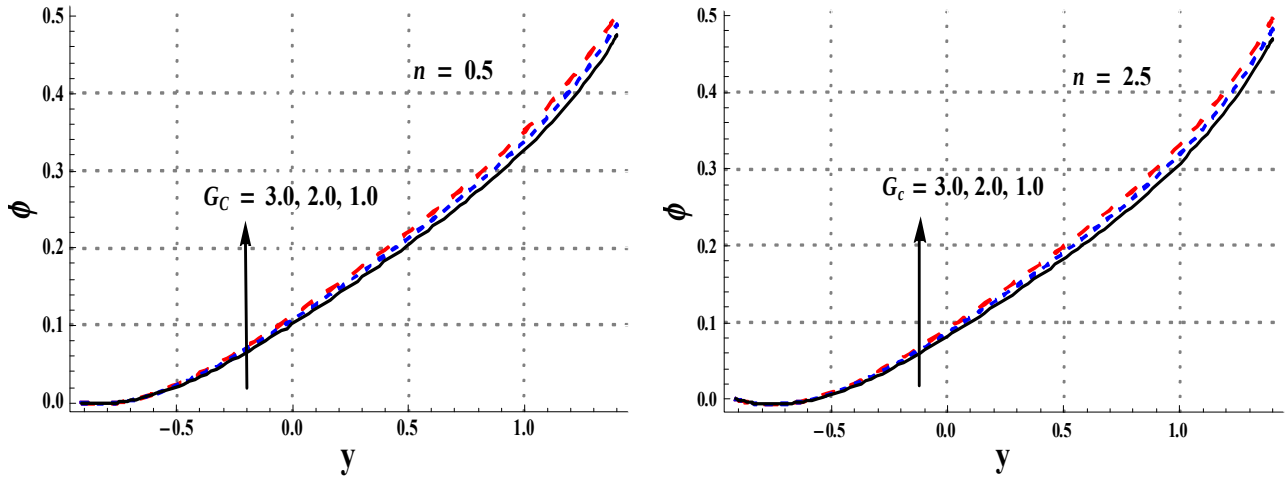

Fig. 9.13. Effect of G_C on concentration when d=0.7, η=0.7, x=0.0, γ=$\pi/4$, a_1=0.4, b=0.3, Br=0.3, Pr=0.5, We=0.4, G_T=1.0, G_C=1.0, Bi_1=0.9, Bi_2=1.2, M=1.0 ,m=2.0, β=0.1, a=2.0, N_t=0.5 and N_b=0.5.

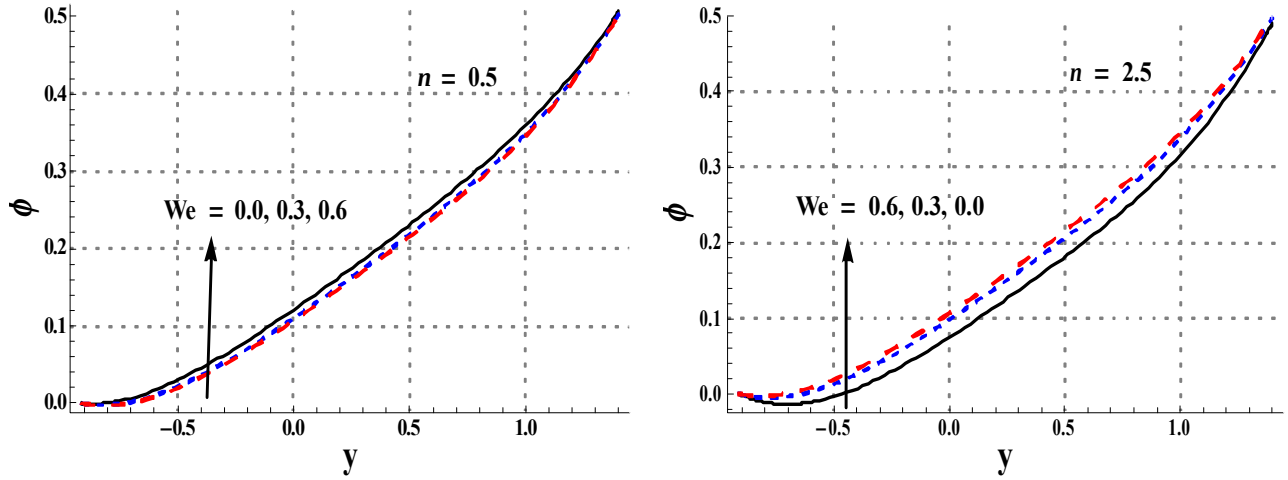

Fig. 9.14. Effect of We on concentration when d=0.7, η=0.7 ,x=0.0, γ=$\pi/4$, a_1=0.4, b=0.3, Br=0.3, Pr=0.5, We=0.4, G_T=1.0, G_C=1.0, Bi_1=0.9, Bi_2=1.2, M=1.0, m=2.0, β=0.1,

a=2.0, N_t=0.5 and N_b=0.5.

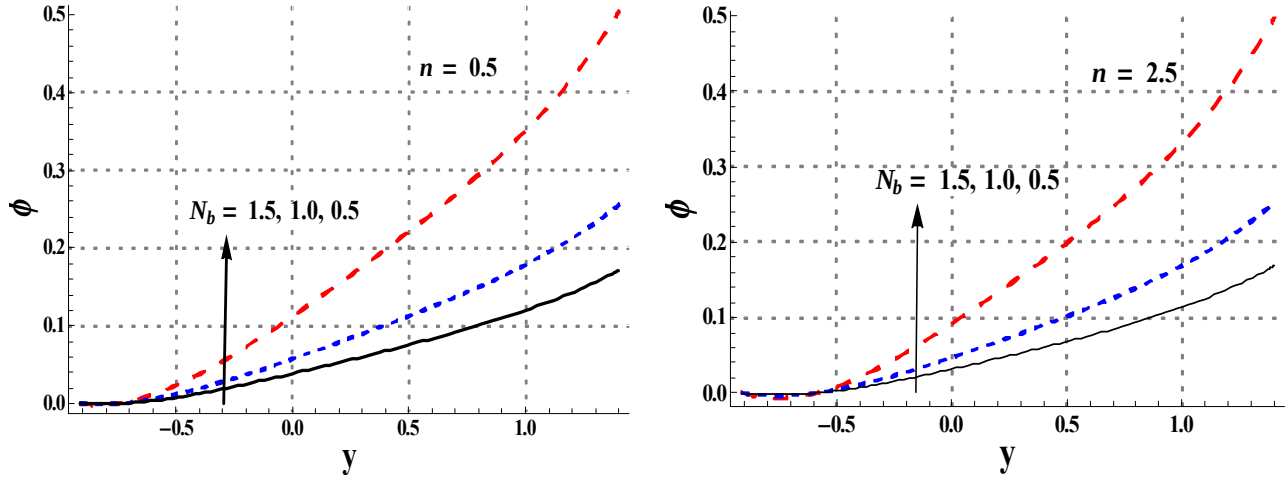

Fig. 9.15. Effect of N_b on concentration when d=0.7, η=0.7, x=0.0, γ=$\pi/4$, a_1=0.4, b=0.3, Br=0.3, Pr=0.5, We=0.4, G_T=1.0, G_C=1.0, Bi_1=0.9, Bi_2=1.2, M=1.0, m=2.0, β=0.1, a=2.0 and N_t=0.5.

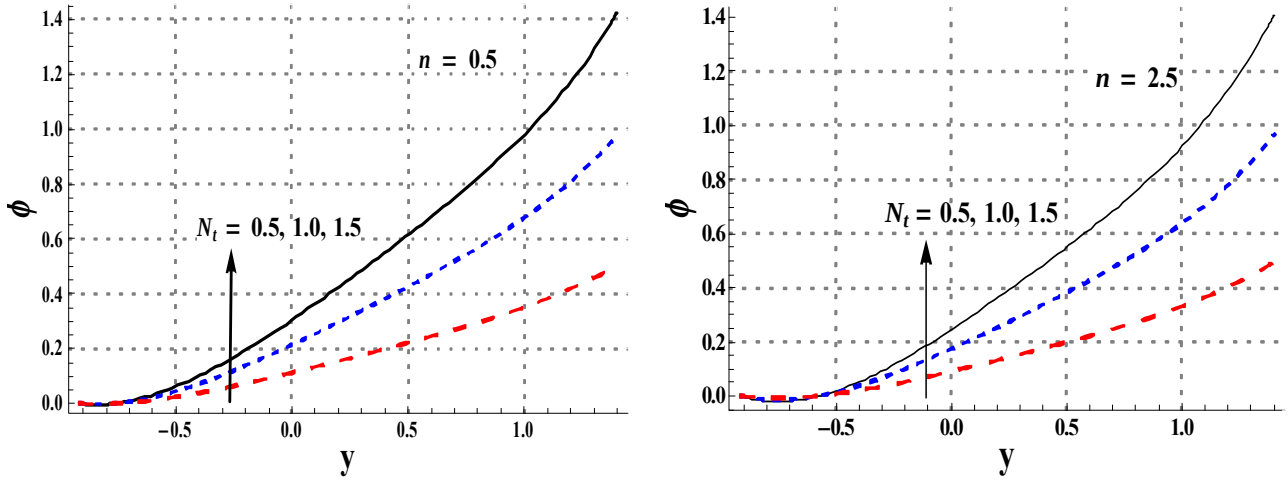

Fig. 9.16. Effect of N_t on concentration when d=0.7, η=0.7, x=0.0, γ=$\pi/4$, a_1=0.4, b=0.3, Br=0.3, Pr=0.5, We=0.4, G_T=1.0, G_C=1.0, Bi_1=0.9, Bi_2=1.2, M=1.0, m=2.0, β=0.1, a=2.0 and N_b=0.5.

Table 9.1. Effect of embedded variables on heat and mass transfer rates when d=0.7, η=0.7, x=0.0, $\gamma=\pi/4$,a_1=0.4 ,b=0.3, Br=0.3, Pr=0.5, G_C=1.0 and Bi_2=1.2.

M	m	We	a	N_t	N_b	G_T	Bi_1	n	$-\theta'[h_1]$	$-\phi'[h_1]$
0.0	2.0	0.4	2.0	0.5	0.5	1.0	1.0	0.5	0.471893	-0.471893
1.0									0.498409	-0.498409
2.0									0.577498	-0.577498
1.0	0.0								0.603717	-0.603717
	1.0								0.538037	-0.538037
	2.0								0.498409	-0.498409
	2.0	0.0							0.509397	-0.509397
		0.3							0.503306	-0.503306
		0.6							0.483118	-0.483118
		0.4	1.0						0.502130	-0.50213
			2.0						0.498409	-0.498409
			3.0						0.540164	-0.509065
			2.0	0.1					0.492520	-0.098503
				0.5					0.498409	-0.498409
				0.9					0.504913	-0.908844
				0.5	0.1				0.535037	-2.675180
					0.5				0.498409	-0.498409
					0.9				0.495053	-0.275029
					0.5	0.5			0.502410	-0.502410
						1.0			0.498409	-0.498409
						1.5			0.494648	-0.494648
						1.0	0.5		0.404584	-0.404584
							1.0		0.498409	-0.498409
							1.5		0.540164	-0.540164
							1.0	0.5	0.498409	-0.498409
								1.0	0.509397	-0.509397
								1.5	0.519809	-0.519809

Chapter 10

Entropy generation analysis for peristaltic motion of Carreau-Yasuda nanomaterial

This chapter concentrates on the peristalsis of nanofluid in presence of Hall current. Therefore our main aim of this analysis is to elaborate peristaltic motion of magneto-nanofluid. Hall current, Joule heating, viscous dissipation and mixed convection effects are presented. Velocity slip, temperature jump and zero mass flux condition are employed. Further entropy generation analysis is discussed in detail. Long wavelength and small Reynolds number are employed. Nonlinear coupled equations are numerically solved and analyzed.

10.1 Modeling

Consider peristaltic flow of Carreau-Yasuda (CY) fluid in a symmetric channel. Cartesian coordinate system $(\bar{X}, \bar{Y}, \bar{t})$ are used. The propagating waves describing the wall geometry (see Fig. 10.1) is in the following forms:

$$\bar{H}(\bar{X}, \bar{t}) = b + \sum_{i=1}^{q} \bar{\phi}_i \cos(\frac{2i\pi}{\lambda}(\bar{X} - c\bar{t})). \tag{10.1}$$

Here $b, \bar{\phi}_i, \lambda$ and c represent the half width of channel, amplitude of the several (q) waves, wavelength and speed of waves. Mixed convection and slip conditions for velocity and temperature are discussed. Zero mass flux condition is imposed. Viscous dissipation in energy equation is presented. Uniform magnetic field with constant strength B_0 is taken in presence of Hall effects. Thermophoresis and Brownian motion are also taken for nanofluid. The equations for problem under examination are:

$$\frac{\partial \bar{U}}{\partial \bar{X}} + \frac{\partial \bar{V}}{\partial \bar{Y}} = 0, \tag{10.2}$$

$$\rho_f \left(\frac{\partial}{\partial \bar{t}} + \bar{U}\frac{\partial}{\partial \bar{X}} + \bar{V}\frac{\partial}{\partial \bar{Y}} \right) \bar{U} = -\frac{\partial \bar{P}}{\partial \bar{X}} + \frac{\partial \bar{S}_{\bar{x}\bar{x}}}{\partial \bar{X}} + \frac{\partial \bar{S}_{\bar{x}\bar{y}}}{\partial \bar{Y}}$$
$$-\frac{\sigma_f B_0^2}{1+m^2}[\bar{U} - m\bar{V}] + g\rho_f[\zeta(T - T_0) + \zeta^*(C - C_0)], \tag{10.3}$$

$$\rho_f \left(\frac{\partial}{\partial \bar{t}} + \bar{U}\frac{\partial}{\partial \bar{X}} + \bar{V}\frac{\partial}{\partial \bar{Y}} \right) \bar{V} = -\frac{\partial \bar{P}}{\partial \bar{y}} + \frac{\partial \bar{S}_{\bar{y}\bar{x}}}{\partial \bar{X}} + \frac{\partial \bar{S}_{\bar{y}\bar{y}}}{\partial \bar{Y}} - \frac{\sigma_f B_0^2}{1+m^2}[\bar{V} + m\bar{U}], \tag{10.4}$$

$$(\rho C)_f \left(\bar{U}\frac{\partial}{\partial \bar{X}} + \bar{V}\frac{\partial}{\partial \bar{Y}} \right) T = K_f \left[\frac{\partial^2 T}{\partial \bar{X}^2} + \frac{\partial^2 T}{\partial \bar{Y}^2} \right] + \bar{S}.\bar{L} + \frac{\sigma_f B_0^2}{1+m^2}[\bar{U}^2 + \bar{V}^2]$$
$$+(\rho C)_{np} \left[D_B \left(\frac{\partial C}{\partial \bar{X}}\frac{\partial T}{\partial \bar{X}} + \frac{\partial C}{\partial \bar{Y}}\frac{\partial T}{\partial \bar{Y}} \right) + \frac{D_T}{T_m} \left(\left(\frac{\partial T}{\partial \bar{X}} \right)^2 + \left(\frac{\partial T}{\partial \bar{Y}} \right)^2 \right) \right], \tag{10.5}$$

$$\bar{U}\frac{\partial C}{\partial \bar{X}} + \bar{V}\frac{\partial C}{\partial \bar{Y}} = D_B \left(\frac{\partial^2 C}{\partial \bar{X}^2} + \frac{\partial^2 C}{\partial \bar{Y}^2} \right) + \frac{D_T}{T_m} \left(\frac{\partial^2 T}{\partial \bar{X}^2} + \frac{\partial^2 T}{\partial \bar{Y}^2} \right). \tag{10.6}$$

Here P depicts the pressure, ρ_f represents the density of nanofluid, $m(= \frac{\sigma_f B_0}{en_e})$ stands for Hall number, σ_f denotes electrical conductivity of nanofluid, S_{ij} depicts extra stress tensor components, $\bar{S}.\bar{L}$ the viscous dissipation term, C the concentration of nanomaterial, T the fluid temperature, D_T the thermophoretic diffusion coefficients, D_B the mass diffusivity, K_f the thermal conductivity and C_f the specific heat of nanofluid. The stress tensor for the Carreau-Yasuda fluid is:

$$\bar{\mathbf{S}} = \mu(\gamma')\mathbf{A}_1. \tag{10.7}$$

$\mathbf{A}_1$ described the first Rivlin-Ericksen tensor and $\mu(\gamma')$ the apparent viscosity is:

$$\mu(\gamma') = \mu_\infty + (\mu_0 - \mu_\infty)\left[1 + (\Gamma\Pi)^a\right]^{\frac{n-1}{a}}, \tag{10.8}$$

$$\Pi = \sqrt{\frac{1}{2}tr(\mathbf{A}_1^2)},$$

$$\mathbf{A}_1 = \left[\text{grad}\,\mathbf{V} + (\text{grad}\,\mathbf{V})^T\right],$$

where μ_0 and μ_∞ denote the zero and infinite shear rate viscosities. Here a and Γ described non-Newtonian characteristics of CY fluid. Further "n" represents the power law index. The Carreau-Yasuda model behaves as a shear thinning fluid for $(n < 1)$, shear thickening material for $(n > 1)$ and show viscous behavior for $n = 1$. Involvement of five parameters in this fluid is preferred over the power law model confining two parameters to describe the fluid rheology. For $a = 2$ C-Y fluid model shows the characteristics of Carreau fluid. At intermediate shear rates, a Carreau fluid behaves like a power-law material. Carreau-Yasuda model has been employed to simulate various chemicals, molten plastic, slurries, paints, blood at low shear rate etc. By using the transformations:

$$\bar{x} = \bar{X} - c\bar{t}, \bar{y} = \bar{Y}, \bar{u} = \bar{U} - c, \bar{v} = \bar{V}, \bar{p}(\bar{x}, \bar{y}) = \bar{P}(\bar{X}, \bar{Y}, \bar{t}), \tag{10.9}$$

the resulting equations are:

$$\frac{\partial \bar{u}}{\partial \bar{x}} + \frac{\partial \bar{v}}{\partial \bar{y}} = 0, \tag{10.10}$$

$$\rho_f\left((\bar{u}+c)\frac{\partial}{\partial \bar{x}} + \bar{v}\frac{\partial}{\partial \bar{y}}\right)(\bar{u}+c) = -\frac{\partial \bar{p}}{\partial \bar{x}} + \frac{\partial \bar{s}_{\bar{x}\bar{x}}}{\partial \bar{x}} + \frac{\partial \bar{s}_{\bar{x}\bar{y}}}{\partial \bar{y}}$$
$$-\frac{\sigma_f B_0^2}{1+m^2}[(\bar{u}+c) - m\bar{v}] + g\rho_f[\zeta(T - T_0) + \zeta^*(C - C_0)], \tag{10.11}$$

$$\rho_f\left((\bar{u}+c)\frac{\partial}{\partial \bar{x}} + \bar{v}\frac{\partial}{\partial \bar{y}}\right)\bar{v} = -\frac{\partial \bar{p}}{\partial \bar{y}} + \frac{\partial \bar{s}_{\bar{y}\bar{x}}}{\partial \bar{x}} + \frac{\partial \bar{s}_{\bar{y}\bar{y}}}{\partial \bar{y}} - \frac{\sigma_f B_0^2}{1+m^2}[\bar{v} + m(\bar{u}+c)], \tag{10.12}$$

$$(\rho C)_f\left((\bar{u}+c)\frac{\partial}{\partial\bar{x}}+\bar{v}\frac{\partial}{\partial\bar{y}}\right)T=K_{nf}\left[\frac{\partial^2 T}{\partial\bar{x}^2}+\frac{\partial^2 T}{\partial\bar{y}^2}\right]+\bar{s}.\bar{L}+\frac{\sigma_f B_0^2}{1+m^2}[(\bar{u}+c)^2+\bar{v}^2]$$
$$+(\rho C)_{np}\left[D_B\left(\frac{\partial C}{\partial\bar{x}}\frac{\partial T}{\partial\bar{x}}+\frac{\partial C}{\partial\bar{y}}\frac{\partial T}{\partial\bar{y}}\right)+\frac{D_T}{T_m}\left(\left(\frac{\partial T}{\partial\bar{x}}\right)^2+\left(\frac{\partial T}{\partial\bar{y}}\right)^2\right)\right], \tag{10.13}$$

$$(\bar{u}+c)\frac{\partial C}{\partial\bar{x}}+\bar{v}\frac{\partial C}{\partial\bar{y}}=D_B\left(\frac{\partial^2 C}{\partial\bar{y}^2}+\frac{\partial^2 C}{\partial\bar{x}^2}\right)+\frac{D_T}{T_m}\left(\frac{\partial^2 T}{\partial\bar{y}^2}+\frac{\partial^2 T}{\partial\bar{x}^2}\right). \tag{10.14}$$

Following dimensionless parameters are used:

$$x=\frac{\bar{x}}{\lambda},y=\frac{\bar{y}}{b},u=\frac{\bar{u}}{c},v=\frac{\bar{v}}{c\delta},\delta=\frac{b}{\lambda},h=\frac{\bar{H}}{b},p=\frac{b^2\bar{p}}{c\lambda\mu_f},\phi_i=\frac{\bar{\phi}_i}{b},$$
$$Re=\frac{\rho_f\ cb}{\mu_f},E=\frac{c^2}{C_fT_0},Pr=\frac{\mu_fC_f}{K_f},M=\sqrt{\frac{\sigma_f}{\mu_f}}B_0b,N_b=\frac{\tau D_BC_0}{\nu},N_t=\frac{\tau D_TT_0}{\nu T_m},$$
$$\upsilon=\frac{\mu_f}{\rho_f},G_T=\frac{\rho_f g\zeta T_0b^2}{\mu_fc},G_c=\frac{\rho_f g\zeta^*C_0b^2}{\mu_fc},\theta=\frac{T-T_0}{T_0},Br=PrE,u=\frac{\partial\psi}{\partial y},v=-\frac{\partial\psi}{\partial x}. \tag{10.15}$$

Here $N_t, N_b, G_c, G_T, \theta, \delta, M, \mathrm{Pr}, Ec, Br$ and Re denote the thermophoresis parameter, the Brownian motion parameter, the concentration Grashoff number, the thermal Grashoff number, dimensionless temperature, wave number, Hartman number, Prandtl number, Eckert number, Brinkman number and the Reynolds number. Large wavelength and small Reynold number assumptions are utilized for the simplification of dimensionless equations then we have:

$$p_y=0, \tag{10.16}$$

$$p_x=\frac{\partial}{\partial y}\left[1+\frac{(1-\beta)(n-1)We^a}{a}(\psi_{yy})^a\right]\psi_{yy}+G_T\theta+G_C\phi-\frac{M^2}{1+m^2}\left(1+\frac{\partial\psi}{\partial y}\right), \tag{10.17}$$

$$\theta_{yy}+Br\Phi+\mathrm{Pr}\,N_b\phi_y\theta_y+\mathrm{Pr}\,N_t\,(\theta_y)^2+\frac{BrM^2}{1+m^2}\left(1+\frac{\partial\psi}{\partial y}\right)^2=0, \tag{10.18}$$

$$N_b\phi_{yy}+N_t\theta_{yy}=0. \tag{10.19}$$

Continuity equation is trivially justified and Φ depicts the dimensionless viscous dissipation term. Here $\beta=\frac{\mu_\infty}{\mu_0}$ represents the ratio of viscosity parameter, We=$\frac{\Gamma c}{b}$ stands for Weissenberg number and ψ shows the stream function. From Eqs. (9.16)-(9.19) we obtain:

$$\frac{\partial^2}{\partial y^2}\left[1+\frac{(1-\beta)(n-1)We^a}{a}(\psi_{yy})^a\right]\psi_{yy}+G_T\theta_y+G_C\phi_y-\frac{M^2}{1+m^2}\psi_{yy}=0, \tag{10.20}$$

$$\theta_{yy}+Br\left[1+\frac{(1-\beta)(n-1)We^{a}}{a}(\psi_{yy})^{a}\right]\psi_{yy}^{2}+\Pr N_b\phi_y\theta_y+\Pr N_t\left(\theta_y\right)^2+\frac{BrM^2}{1+m^2}\left(1+\frac{\partial\psi}{\partial y}\right)^2=0, \tag{10.21}$$

$$N_b\phi_{yy}+N_t\theta_{yy}=0. \tag{10.22}$$

The nondimensional form of flow rates in the laboratory $\eta(=\bar{Q}/cd_1)$ and wave $F(=\bar{q}/cd_1)$ frames are related by:

$$\eta=F+1. \tag{10.23}$$

Furthermore 'F' is defined as:

$$F=\int_0^h\frac{\partial\psi}{\partial y}dy. \tag{10.24}$$

The dimensionless boundary conditions are:

$$\begin{gathered}\psi=0,\frac{\partial^2\psi}{\partial y^2}=0,\frac{\partial\theta}{\partial y}=0\text{ and }\phi_y=0\text{ at }y=0,\\ \psi=F,\frac{\partial\psi}{\partial y}+\xi s_{xy}=-1,\theta+\gamma\frac{\partial\theta}{\partial y}=0\text{ and }N_b\phi_y+N_t\theta_y=0\text{ at }y=h,\end{gathered} \tag{10.25}$$

$$h=1+\sum_{i=1}^{q}\phi_i cos(2i\pi x).$$

In this study, we take $q=10$ and the values of amplitude is taken as: $\phi_1=0.01,\phi_2=0.02,\phi_3=0.03,\phi_4=0.04,\phi_5=0.05,\phi_6=0.06,\phi_7=0.07,\phi_8=0.1,\phi_9=0.2$ and $\phi_{10}=0.3$ that fulfill the basic criteria $1\succeq\sum_{i=1}^{q}\phi_i$ to forbid the interference of upper and lower walls.

10.1.1 Solution methodology

The dimensionless forms of equations with appropriate boundary constraints are solved via numerical approach. Graphical interpretation of the results is described in proceeding section.

10.2 Entropy generation rate

By using the second law of thermodynamics, the entropy generation at each point of the fluid can be calculated as follows:

$$(S_{gen})=(S_{gen})_{heat}+(S_{gen})_{fric}+(S_{gen})_{mag},$$

where $(S_{gen})_{heat}$ depicts the entropy generation due to heat transport, $(S_{gen})_{fric}$ represents entropy generation due to fluid friction and $(S_{gen})_{mag}$ shows the entropy generation effects due to applied magnetic field. We write:

$$(S_{gen})_{heat} = \frac{K_{nf}}{(\bar{T}_0)^2}\left[\left(\frac{\partial T}{\partial \bar{x}}\right)^2 + \left(\frac{\partial T}{\partial \bar{y}}\right)^2\right],$$

$$(S_{gen})_{fric} = \frac{\mu_0}{\bar{T}_0}\left[1 + \frac{(1-\beta)(n-1)We^a}{a}(\Gamma\gamma')^a\right]\left[2\left(\left(\frac{\partial \bar{u}}{\partial \bar{x}}\right)^2 + \left(\frac{\partial \bar{v}}{\partial \bar{y}}\right)^2\right) + \left(\frac{\partial \bar{u}}{\partial \bar{y}} + \frac{\partial \bar{v}}{\partial \bar{x}}\right)^2\right],$$

$$(S_{gen})_{mag} = \frac{1}{\bar{T}_0}\frac{\sigma_{nf}B_0^2}{1+m^2}[(\bar{u}+c)^2 + \bar{v}^2].$$

Dimensionless form of entropy generation can be described as:

$$E = \theta_{yy} + Br\left[1 + \frac{(1-\beta)(n-1)We^a}{a}(\psi_{yy})^a\right]\psi_{yy}^2 + \frac{BrM^2}{1+m^2}\left(1 + \frac{\partial \psi}{\partial y}\right)^2.$$

Bejan number in nondimensional form is:

$$\text{Be} = \frac{\text{Entropy generation due to heat transfer}}{\text{Total entropy generation}}.$$

10.3 Discussion

Graphical analysis of velocity in symmetric channel is presented in Figs. (10.2)-(10.5). Graph depicts that fluid velocity is maximum near central portion of channel. Fig. 10.2 depicts the velocity for various values of Hartman variable. An increase in "M" variable yields decay of axial velocity near channel center. Velocity decays due to the resisting nature of Lorentz force when magnetic field is applied in the transverse direction. Fig. 10.3 indicates velocity for Hall parameter. Hall parameter shows reverse behavior on velocity when compared with Hartman number. Physically this is justified because the Hall number commonly balances the magnetic force of applied magnetics by some extent. In Fig. 10.4 velocity for Weissenberg number is shown. Velocity decreases by increasing viscosity ratio parameter. Fig. 10.5 shows that velocity enhances for velocity slip parameter. Prominent effect is seen near the channel wall. Figs. (10.6)-(10.11) depict outcomes of embedded variables on temperature. Fig. 10.6

indicates variation of temperature for different Hartman number. It is seen that an increment in Hartman number leads to higher temperature. Temperature depicts increasing behavior due to Ohmic heating. Fig. 10.7 depicts the effect of Hall variable on temperature. It is found that temperature shows decreasing trend for larger Hall number. Temperature shows decreasing trend for higher Hall parameter. In fact Hall parameter has reverse effect when compared with Ohmic heating. Fig. 10.8 illustrates temperature characteristics for thermal Grashof number. Temperature is an increasing for G_t. Temperature for non-Newtonian parameter "a" is shown in Fig. 10.9. It is concluded that temperature is increased by larger "a". It is obvious from Fig. 10.10 that temperature rapidly increases throughout the channel by higher temperature jump parameter. Variation in temperature for different thermophoresis parameter is shown in Fig. 10.11. It is observed that larger N_t lead to temperature decay. Figs. (10.12)-(10.15) are plotted for impacts of M, G_C, N_b and N_t on concentration. Fig. 10.12 depicts effect of Hartman number on concentration of nanomaterial. Concentration rapidly decreases by increasing Hartman number. Fig. 10.13 shows behavior of concentration for various values of concentration Grashof number G_C. Concentration decreases by increasing G_C. Fig. 10.14 exhibits concentration of nanomaterial for Brownian motion parameter. Concentration of nanomaterial shows decreasing trend for larger N_b. Basically the Brownian force pushes the particles in the reverse direction of concentration gradient and make the nanofluid more homogenous. Fig. 10.15 shows effect of thermophoresis parameter on concentration. Clearly concentration rapidly enhances near channel wall by increasing N_t. Physically an increment in thermophoresis variable means that nanomaterials are shifted towards cold region from hot region. Therefore the maximum nanoparticles are dragged away from the warm region due to which nanomaterial concentration enhances near wall. Figs. (10.16)-(10.20) show the variations of entropy generation for M, m, Br, a and n. In Fig. 10.16 we present effect of Hartman number on entropy generation. Here entropy generation increases by larger Hartman number. Physically for strong magnetic field more resistive force is experienced in system due to which more disturbance occurred and so entropy rate enhances. In Fig. 10.17, variation of entropy generation for Hall parameter is exhibited. Entropy generation shows decreasing trend for larger Hall parameter. Fig. 10.18 represents Brinkman number impact on entropy generation. Entropy generation enhances rapidly by increasing Brinkman number. It depicts that entropy generation increases due to loss of

kinetic energy when fluid particles collide with each other. Fig. 10.19 shows that entropy generation enhances by larger non-Newtonian parameter "a". Fig. 10.20 depicts that entropy generation is larger for shear thinning fluid when compared with shear thickening material. Effects of M, m, N_t and "a" on Bejan number are shown in Figs. (10.21)-(10.24). Hartman number impact on Bejan number is shown in Fig. 10.21. Bejan number increases for rise of M. Influence of Hall parameter on Bejan number is displayed in Fig. 10.22. When Hall parameter increases then Bejan number decreases rapidly. Fig. 10.23 shows that Bejan number is inversely proportional to thermophoresis parameter N_t. Fig. 10.24 indicates increasing behavior of Bejan number for non-Newtonian parameter "a". Table 10.1 shows the numerical values of heat transport rate for different values of M and We. It also provides the comparison between the shear thinning and shear thickening fluids. The data indicates that heat transport rate for shear thickening fluid are higher when compared with shear thinning fluid. Table 10.2 depicts the concentration characteristics for various values of N_t and N_b. Concentration transport rate at wall for shear thickening fluid is higher when compared with shear thinning material.

10.4 Conclusions

Here following points are worth mentioning.

- Hartman and Hall parameter have reverse effects for fluid velocity. Velocity slip parameter has an increasing effect on velocity.
- Temperature is controlled by increasing Hall parameter. Situation for Hartman number on temperature is reverse.
- Temperature enhances with increasing thermal Grashof number and non-Newtonian parameter "a".
- For higher thermophoresis parameter, the temperature decreases but concentration enhances.
- Concentration decreases via Hartman number and Grashof number.
- Entropy generation is decreasing function of Hall parameter.

- Bejan number decreases by increasing Hall and thermophoresis parameters.

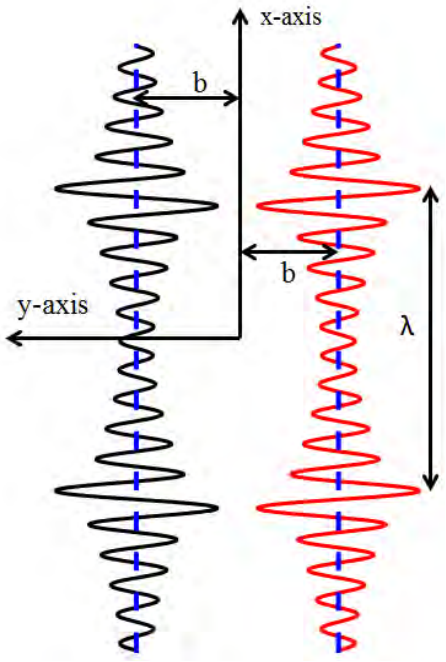

Fig. 10.1. Geometry of the problem.

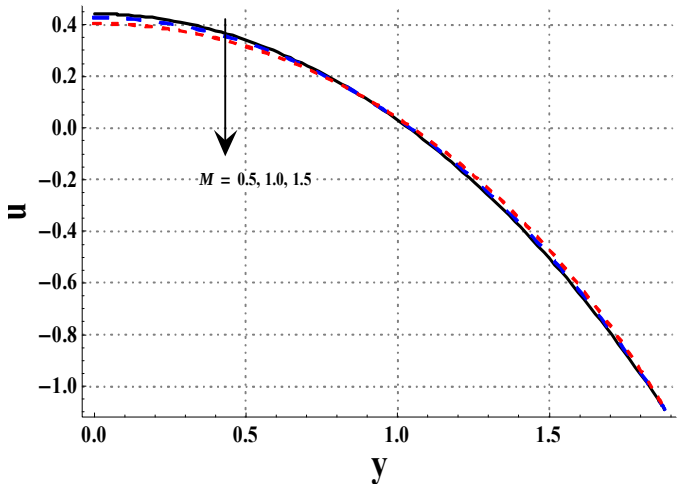

Fig. 10.2. Velocity via M when $\eta = 0.9,\ Br = 0.3,\ \mathrm{Pr} = 0.4,\ We = 0.4,\ G_T = 1.0,\ G_C = 1.0,\ m = 2.0,\ \beta = 0.1,\ a = 2.0,\ n = 0.5, \zeta = 0.1,\ \gamma = 0.1, N_t = 0.5$ and $N_b = 0.5$.

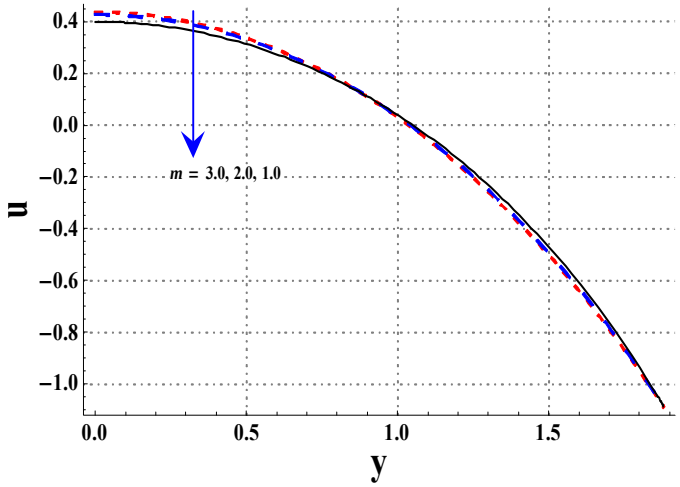

Fig. 10.3. Velocity via m when $\eta = 0.9,\ Br = 0.3,\ \mathrm{Pr} = 0.4,\ We = 0.4,\ G_T = 1.0,\ G_C = 1.0,\ M = 1.0,\ \beta = 0.1,\ a = 2.0,\ n = 0.5, \zeta = 0.1,\ \gamma = 0.1, N_t = 0.5$ and $N_b = 0.5$.

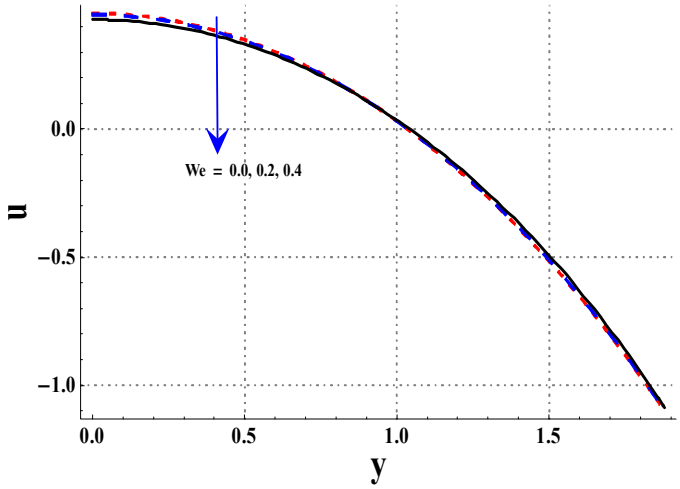

Fig. 10.4. Velocity via We when $\eta = 0.9$, $Br = 0.3$, Pr $= 0.4$, $G_T = 1.0$, $G_C = 1.0$, $M = 1.0$, $m = 2.0$, $\beta = 0.1$, $a = 2.0$, $n = 0.5, \zeta = 0.1$, $\gamma = 0.1, N_t = 0.5$ and $N_b = 0.5$.

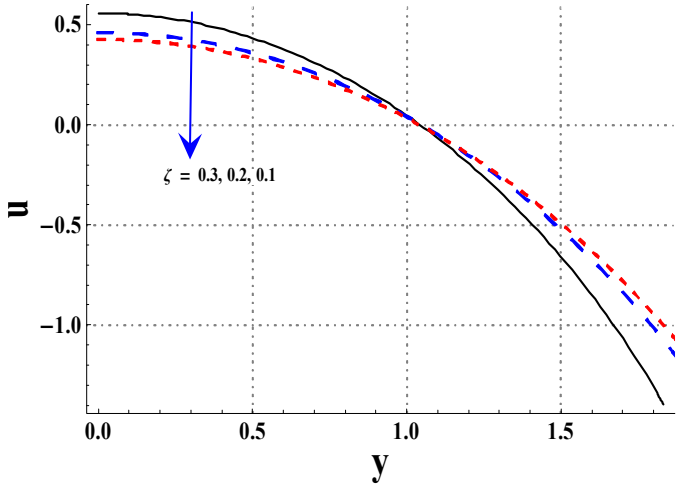

Fig. 10.5. Velocity via ζ when $\eta = 0.9$, $Br = 0.3$, Pr $= 0.4$, $We = 0.4$, $G_T = 1.0$, $G_C = 1.0$, $M = 1.0$, $m = 2.0$, $\beta = 0.1$, $a = 2.0$, $n = 0.5, \gamma = 0.1, N_t = 0.5$ and $N_b = 0.5$.

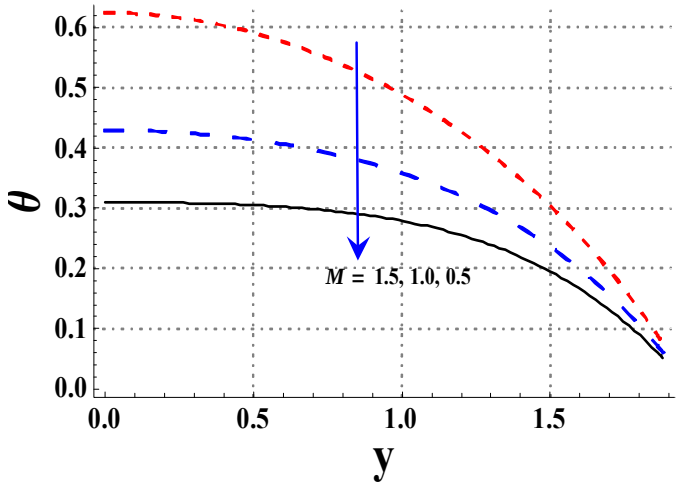

Fig. 10.6. Temperature field via M when $\eta = 0.9,\ Br = 0.3,\ \mathrm{Pr} = 0.4,\ We = 0.4,\ G_T = 1.0,\ G_C = 1.0,\ m = 2.0,\ \beta = 0.1,\ a = 2.0,\ n = 0.5, \zeta = 0.1,\ \gamma = 0.1, N_t = 0.5$ and $N_b = 0.5$.

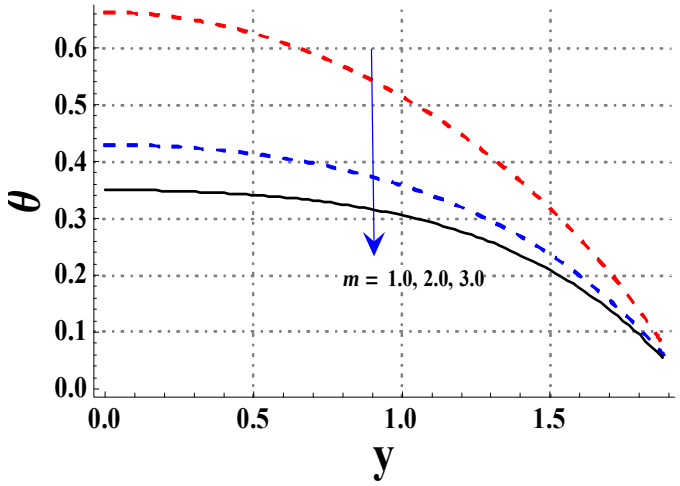

Fig. 10.7. Temperature field via m when $\eta = 0.9,\ Br = 0.3,\ \mathrm{Pr} = 0.4,\ We = 0.4,\ G_T = 1.0,\ G_C = 1.0,\ M = 1.0,\ \beta = 0.1,\ a = 2.0,\ n = 0.5, \zeta = 0.1,\ \gamma = 0.1, N_t = 0.5$ and $N_b = 0.5$.

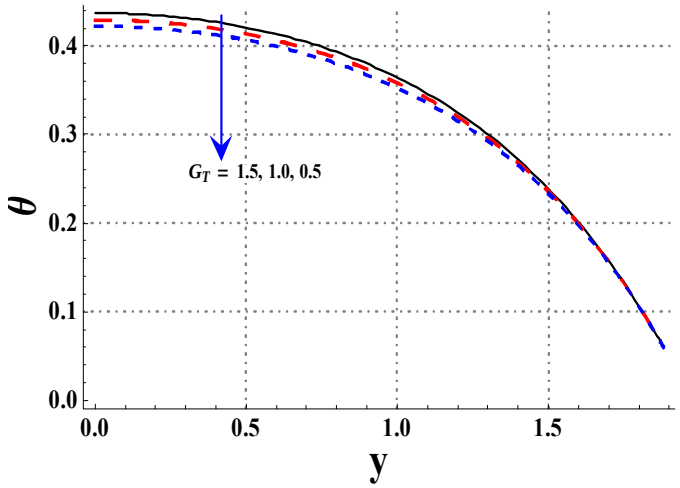

Fig. 10.8. Temperature field via G_T when $\eta = 0.9,\ Br = 0.3,\ \mathrm{Pr} = 0.4,\ We = 0.4,\ G_C = 1.0,\ M = 1.0,\ m = 2.0,\ \beta = 0.1,\ a = 2.0,\ n = 0.5, \zeta = 0.1,\ \gamma = 0.1, N_t = 0.5$ and $N_b = 0.5$.

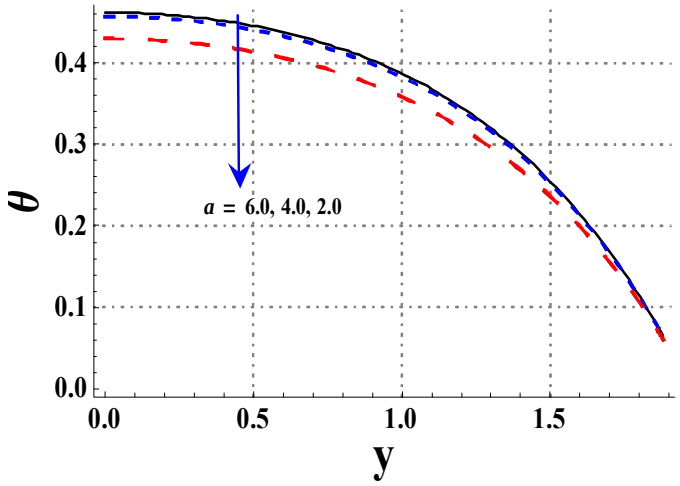

Fig. 10.9. Temperature field via a when $\eta = 0.9,\ Br = 0.3,\ \mathrm{Pr} = 0.4,\ We = 0.4,\ G_T = 1.0,\ G_C = 1.0,\ M = 1.0,\ m = 2.0,\ \beta = 0.1,\ n = 0.5, \zeta = 0.1,\ \gamma = 0.1, N_t = 0.5$ and $N_b = 0.5$.

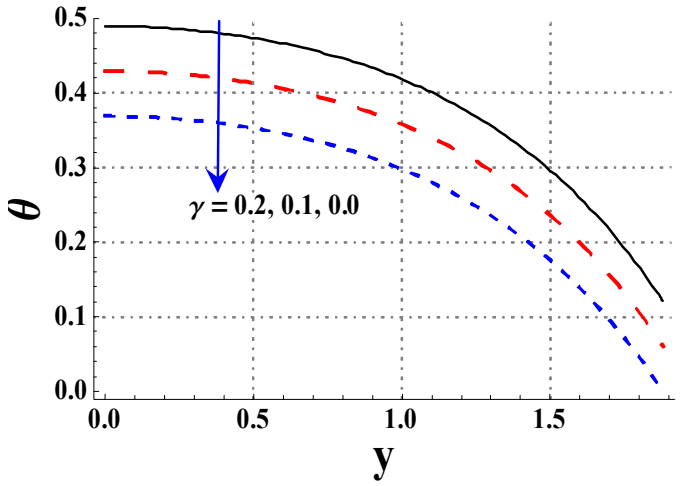

Fig. 10.10. Temperature field via γ when $\eta = 0.9,\ Br = 0.3,\ \mathrm{Pr} = 0.4,\ We = 0.4,\ G_T = 1.0,\ G_C = 1.0,\ M = 1.0,\ m = 2.0,\ \beta = 0.1,\ a = 2.0,\ n = 0.5, \zeta = 0.1,\ N_t = 0.5$ and $N_b = 0.5$.

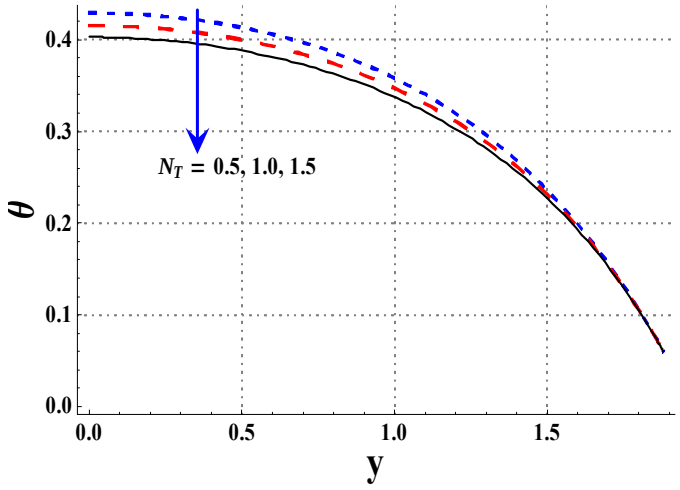

Fig. 10.11. Temperature field via N_T when $\eta = 0.9,\ Br = 0.3,\ \mathrm{Pr} = 0.4,\ We = 0.4,\ G_T = 1.0,\ G_C = 1.0,\ M = 1.0,\ m = 2.0,\ \beta = 0.1,\ a = 2.0,\ n = 0.5, \zeta = 0.1,\ \gamma = 0.1$ and $N_b = 0.5$.

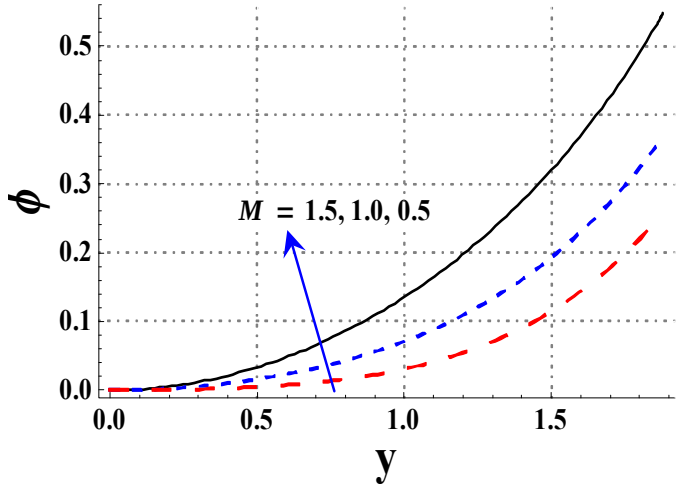

Fig. 10.12. Effect of M on mass transfer when $\eta = 0.9,\ Br = 0.3,\ \mathrm{Pr} = 0.4,\ We = 0.4,\ G_T = 1.0,\ G_C = 1.0,\ m = 2.0,\ \beta = 0.1,\ a = 2.0,\ n = 0.5, \zeta = 0.1,\ \gamma = 0.1, N_t = 0.5$ and $N_b = 0.5$.

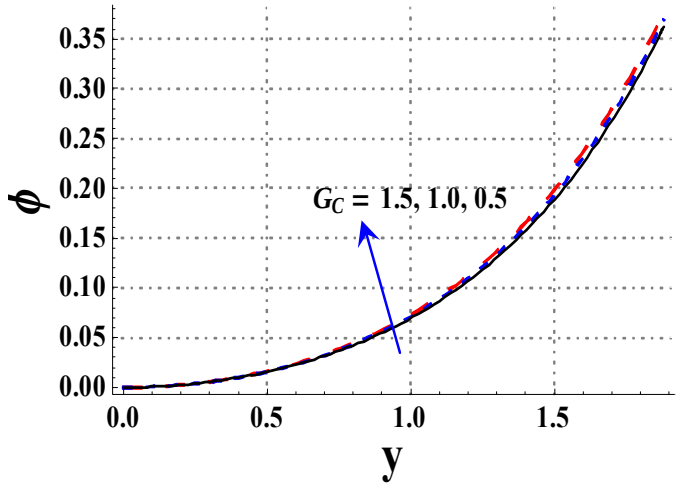

Fig. 10.13. Effect of G_C on mass transfer when $\eta = 0.9,\ Br = 0.3,\ \mathrm{Pr} = 0.4,\ We = 0.4,\ G_T = 1.0,\ M = 1.0,\ m = 2.0,\ \beta = 0.1,\ a = 2.0,\ n = 0.5, \zeta = 0.1,\ \gamma = 0.1, N_t = 0.5$ and $N_b = 0.5$.

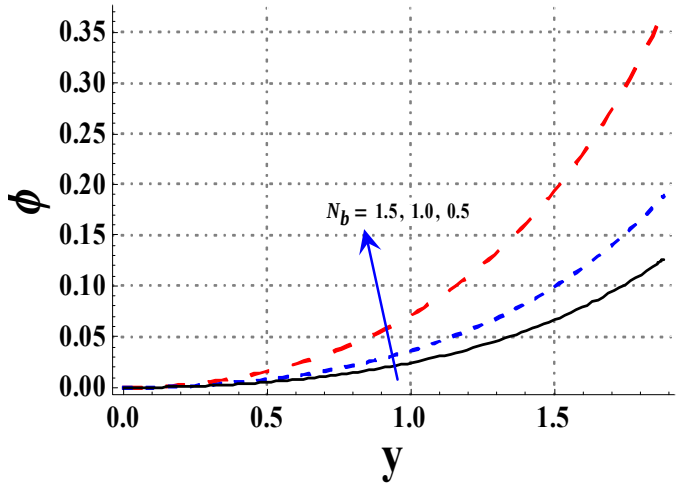

Fig. 10.14. Effect of N_b on mass transfer when $\eta = 0.9,\ Br = 0.3,\ \mathrm{Pr} = 0.4,\ We = 0.4,\ G_T = 1.0,\ G_C = 1.0,\ M = 1.0,\ m = 2.0,\ \beta = 0.1,\ a = 2.0,\ n = 0.5, \zeta = 0.1,\ \gamma = 0.1$ and $N_t = 0.5$.

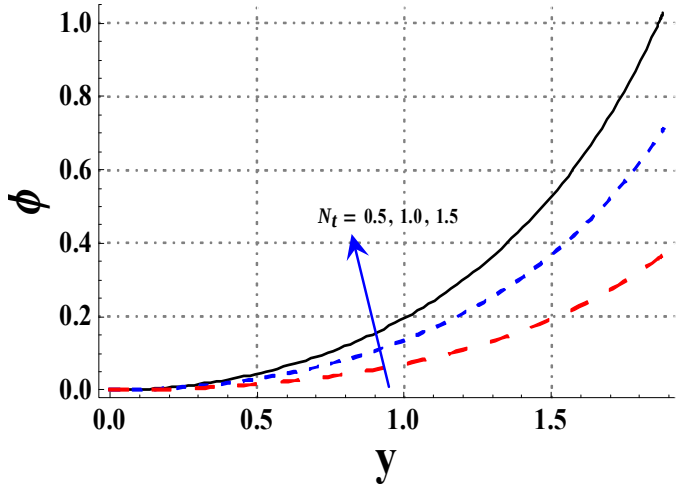

Fig. 10.15. Effect of N_t on mass transfer when $\eta = 0.9,\ Br = 0.3,\ \mathrm{Pr} = 0.4,\ We = 0.4,\ G_T = 1.0,\ G_C = 1.0,\ M = 1.0,\ m = 2.0,\ \beta = 0.1,\ a = 2.0,\ n = 0.5, \zeta = 0.1,\ \gamma = 0.1$ and $N_b = 0.5$.

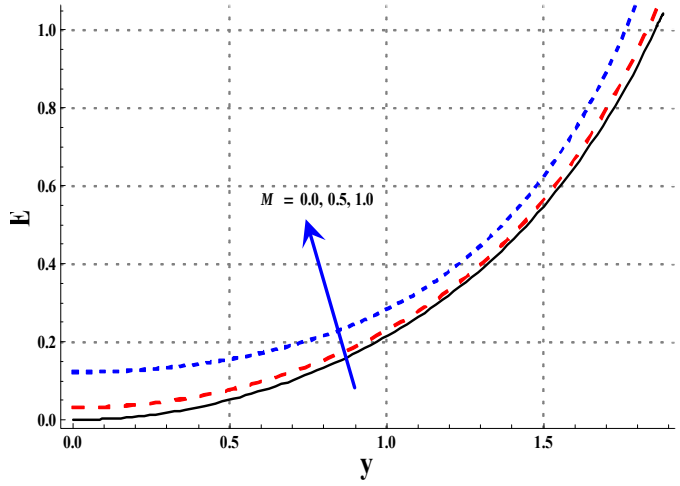

Fig. 10.16. Effect of M on Entropy generation when $\eta = 0.9,\ Br = 0.3,\ \mathrm{Pr} = 0.4,\ We = 0.4,\ G_T = 1.0,\ G_C = 1.0,\ m = 2.0,\ \beta = 0.1,\ a = 2.0,\ n = 0.5, \zeta = 0.1,\ \gamma = 0.1, N_t = 0.5$ and

$N_b = 0.5$.

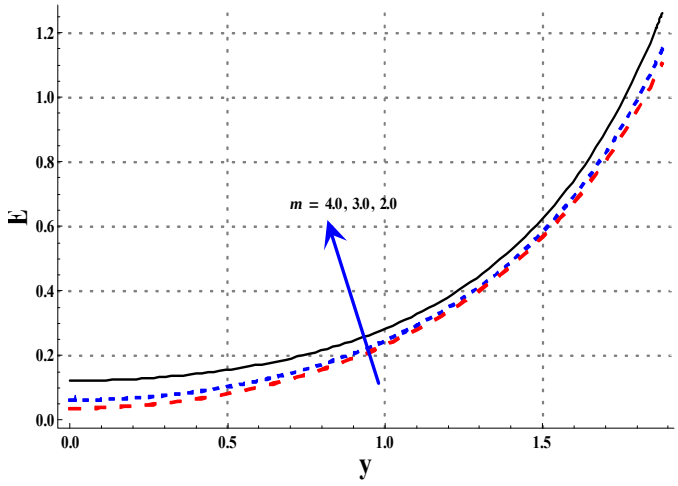

Fig. 10.17. Effect of m on Entropy generation when $\eta = 0.9$, $Br = 0.3$, $\Pr = 0.4$, $We = 0.4$, $G_T = 1.0$, $G_C = 1.0$, $M = 1.0$, $\beta = 0.1$, $a = 2.0$, $n = 0.5, \zeta = 0.1$, $\gamma = 0.1, N_t = 0.5$ and $N_b = 0.5$.

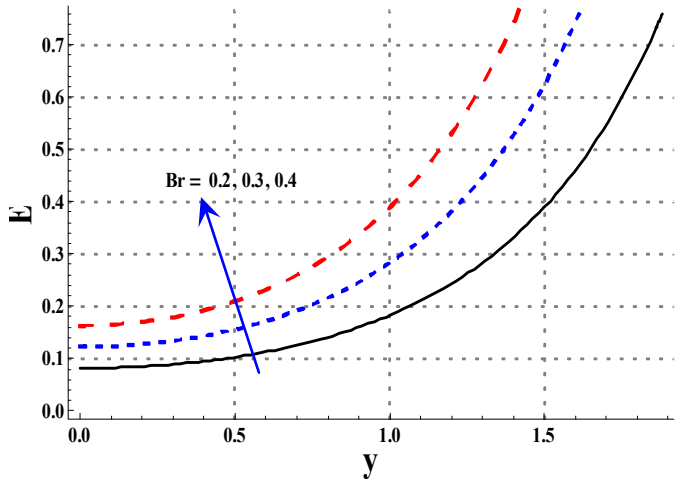

Fig. 10.18. Effect of Br on Entropy generation when $\eta = 0.9$, $\Pr = 0.4$, $We = 0.4$, $G_T = 1.0$, $G_C = 1.0$, $M = 1.0$, $m = 2.0$, $\beta = 0.1$, $a = 2.0$, $n = 0.5, \zeta = 0.1$, $\gamma = 0.1, N_t = 0.5$ and

$N_b = 0.5$.

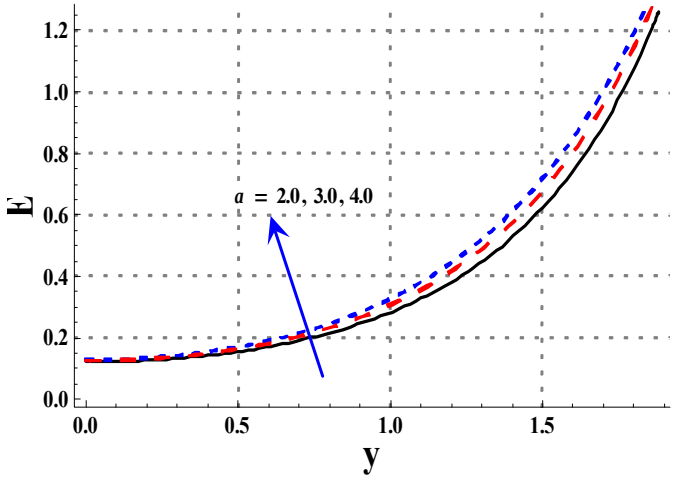

Fig. 10.19. Effect of a on Entropy generation when $\eta = 0.9$, $Br = 0.3$, Pr $= 0.4$, $We = 0.4$, $G_T = 1.0$, $G_C = 1.0$, $M = 1.0$, $m = 2.0$, $\beta = 0.1$, $n = 0.5, \zeta = 0.1$, $\gamma = 0.1, N_t = 0.5$ and $N_b = 0.5$.

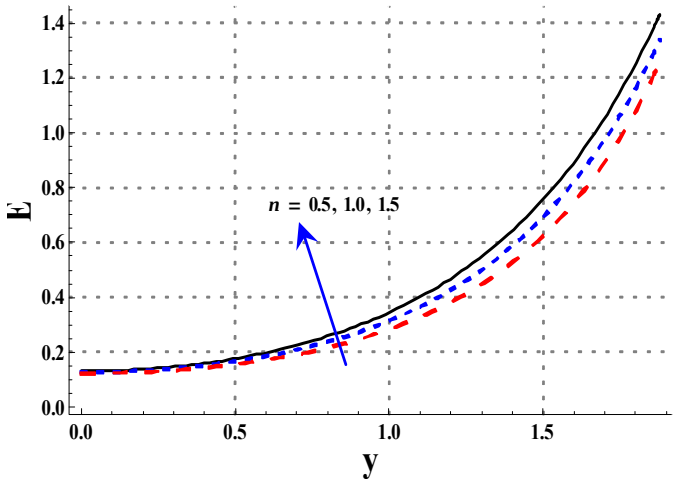

Fig. 10.20. Effect of n on Entropy generation when $\eta = 0.9$, $Br = 0.3$, Pr $= 0.4$, $We = 0.4$, $G_T = 1.0$, $G_C = 1.0$, $M = 1.0$, $m = 2.0$, $\beta = 0.1$, $a = 2.0, \zeta = 0.1$, $\gamma = 0.1, N_t = 0.5$ and

$N_b = 0.5$.

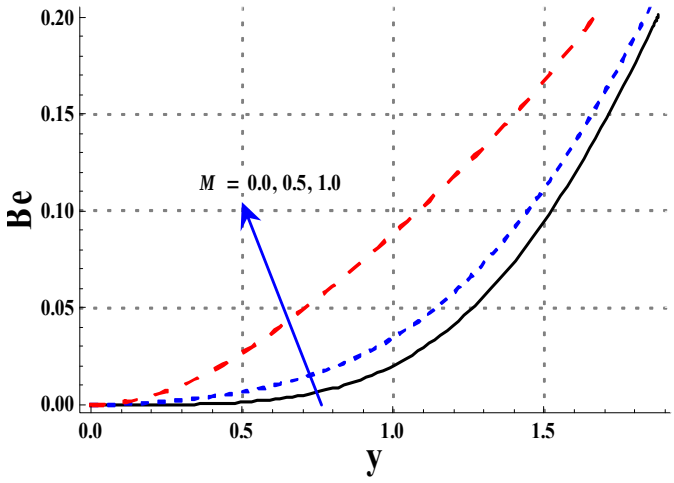

Fig. 10.21. Effect of M on Bejan number when $\eta = 0.9,\ Br = 0.3,\ \mathrm{Pr} = 0.4,\ We = 0.4,\ G_T = 1.0,\ G_C = 1.0,\ m = 2.0,\ \beta = 0.1,\ a = 2.0,\ n = 0.5, \zeta = 0.1,\ \gamma = 0.1, N_t = 0.5$ and $N_b = 0.5$.

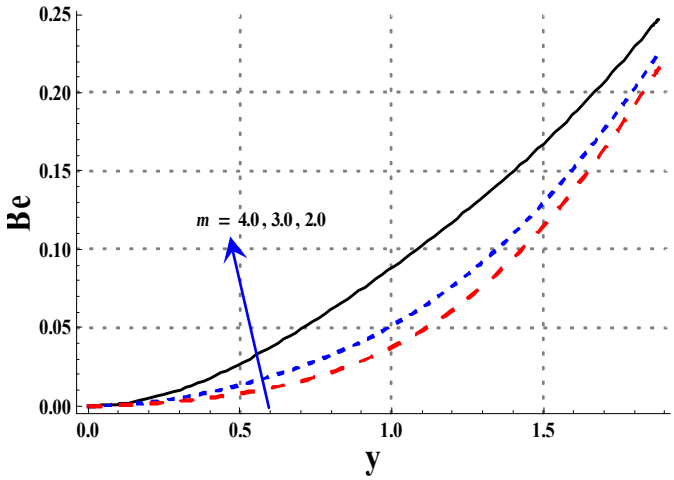

Fig. 10.22. Effect of m on velocity when $\eta = 0.9,\ Br = 0.3,\ \mathrm{Pr} = 0.4,\ We = 0.4,\ G_T = 1.0,\ G_C = 1.0,\ M = 1.0,\ \beta = 0.1,\ a = 2.0,\ n = 0.5, \zeta = 0.1,\ \gamma = 0.1, N_t = 0.5$ and $N_b = 0.5$.

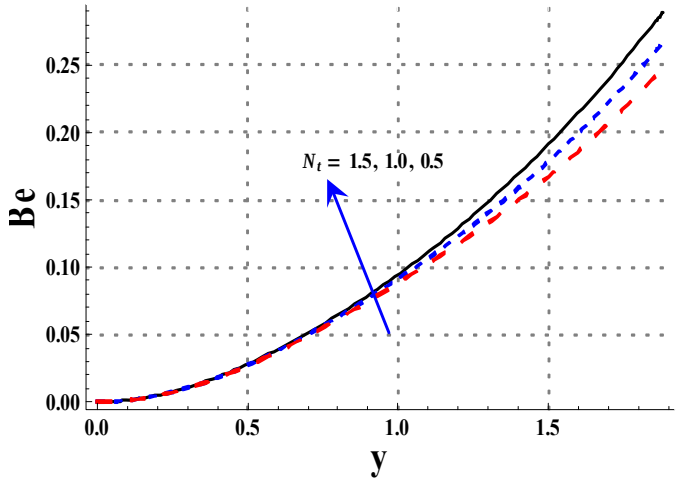

Fig. 10.23. Effect of N_t on Bejan number when $\eta = 0.9,\ Br = 0.3,\ \mathrm{Pr} = 0.4,\ We = 0.4,\ G_T = 1.0,\ G_C = 1.0,\ M = 1.0,\ m = 2.0,\ \beta = 0.1,\ a = 2.0,\ n = 0.5, \zeta = 0.1,\ \gamma = 0.1$ and $N_b = 0.5$.

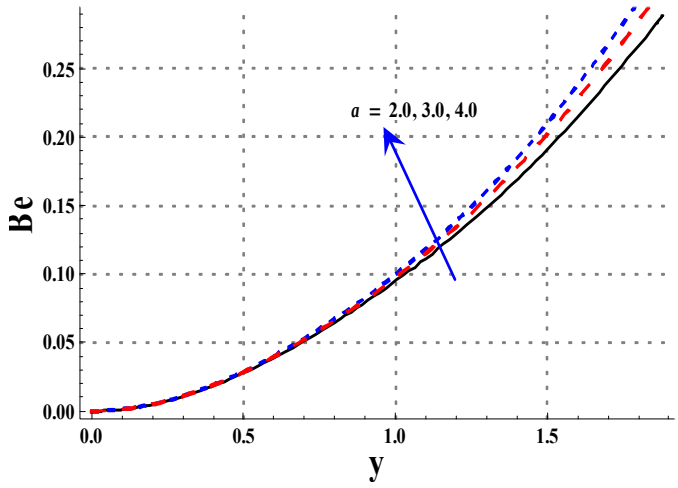

Fig. 10.24. Effect of a on Bejan number when $\eta = 0.9,\ Br = 0.3,\ \mathrm{Pr} = 0.4,\ We = 0.4,\ G_T = 1.0,\ G_C = 1.0,\ M = 1.0,\ m = 2.0,\ \beta = 0.1,\ n = 0.5, \zeta = 0.1,\ \gamma = 0.1, N_t = 0.5$ and $N_b = 0.5$.

M	We	$n = 0.5$ $\theta'(h)$	$n = 1.5$ $\theta'(h)$
0.0	0.4	0.482084	0.566054
1.0		0.603485	0.694317
2.0		0.959875	1.075010
1.0	0.2	0.638645	0.661132
	0.3	0.624287	0.675006
	0.4	0.603485	0.694317

Table 10.1. Effect of various parameters on heat transfer rate for shear thinning and shear thickening fluids when $Br = 0.3,\ \mathrm{Pr} = 0.4,\ G_T = 1.0,\ G_C = 1.0,\ a = 2.0,\ m = 2.0,\ \beta = 0.1, \zeta = 0.1,\ \gamma = 0.1, N_t = 0.5$ and $N_b = 0.5$.

N_t	N_b	$n = 0.5$ $\phi'(h)$	$n = 1.5$ $\phi'(h)$
0.5	0.5	0.624287	0.675006
1.0		1.246740	1.353350
1.5		1.869820	2.037600
0.5	0.5	0.624287	0.675006
	1.0	0.312564	0.337283
	1.5	0.208491	0.224829

Table 10.2. Effect of various parameters on mass transfer rate for shear thinning and shear thickening fluids when $Br = 0.3,\ \mathrm{Pr} = 0.4,\ G_T = 1.0,\ G_C = 1.0,\ a = 2.0,\ m = 2.0,\ \beta = 0.1, \zeta = 0.1,\ \gamma = 0.1, N_t = 0.5$ and $N_b = 0.5$.

Chapter 11

Mixed convection and thermal radiation effects on MHD peristalsis of Powell-Eyring nanomaterial

Here mathematical developments are made for peristaltic transport of Powell-Eyring nanofluid through symmetric channel. Heat and mass transport analyses are presented in the presence of mixed convection. Joule heating, viscous dissipation and thermal radiation are considered in energy equation. Further slip effects at boundaries are not ignored. Lubrication approach is utilized for nonlinear equations. Systems of equations are numerically solved via NDsolve. The velocity field, temperature, concentration and entropy generation behavior are analyzed via graphs.

11.1 Methodology

Peristaltic flow of nanofluid is examined in a flexible channel having width 2a. Peristalsis occurred due to the sinusoidal waves that propagate along the channel walls with constant speed c. Mathematical representation of wave propagation along channel walls are:

$$\pm\bar{H}(\bar{X},\bar{t}) = \pm a \pm bcos(\frac{2\pi}{\lambda}(\bar{X}-c\bar{t})), \tag{11.1}$$

where b, λ and t depict the wall amplitude, wavelength and time. The velocity configuration for the two-dimensional flow is $\bar{\mathbf{V}} = \left[\bar{U}\left(\bar{X},\bar{Y},\bar{t}\right),\bar{V}\left(\bar{X},\bar{Y},\bar{t}\right),0\right]$. The extra stress tensor for Powell-Eyring non-Newtonian fluid is defined as follows:

$$\bar{\mathbf{S}} = \left[\mu + \frac{1}{\beta^*\Pi}\sinh^{-1}\left(\frac{\Pi}{c^*}\right)\right]\mathbf{A}_1. \tag{11.2}$$

in which β^* and c^* depict the material characteristics of fluid. Further $\mathbf{A}_1$ (the first Rivlin-Ericksen tensor) and Π are defined by:

$$\Pi = \sqrt{\frac{1}{2}tr\left(\mathbf{A}_1^2\right)}. \tag{11.3}$$

The temperature dependent viscosity coefficient (μ) can be expressed as:

$$\mu = \mu_0\left(1-\alpha_0\left(T-T_0\right)\right),$$

where μ_0 denotes the constant viscosity of material, α_0 temperature dependent viscosity parameter, T temperature of fluid and T_0 depicts temperature of wall. By considering the

$$\sinh^{-1}\left(\frac{\Pi}{c^*}\right) \approx \frac{\Pi}{c^*} - \frac{1}{6}\left(\frac{\Pi}{c^*}\right)^3$$

$\bar{\mathbf{S}}$ finally becomes:

$$\bar{\mathbf{S}} = \left[\mu_0\left(1-\alpha_0\left(T-T_0\right)\right) + \frac{1}{\beta^* c^*} - \frac{\Pi^2}{6\beta^*\left(c^*\right)^3}\right]\mathbf{A}_1. \tag{11.4}$$

The fluid motion is assumed in the presence of strong magnetic field. Therefore Hall effect is also retained. Because of magnetic field the Ohmic heating is considered in the energy equation. Brownian motion and thermophoresis are also introduced due to the Buongiorno's nanofluid model. Concentration equation is also considered. Related expressions include:

$$\frac{\partial\bar{u}}{\partial\bar{x}} + \frac{\partial\bar{v}}{\partial\bar{y}} = 0, \tag{11.5}$$

$$\rho_f\left(\bar{v}\frac{\partial\bar{u}}{\partial\bar{y}}+(\bar{u}+c)\frac{\partial\bar{u}}{\partial\bar{x}}\right)=-\frac{\partial\bar{p}}{\partial\bar{x}}+\frac{\partial\bar{s}_{\bar{x}\bar{y}}}{\partial\bar{y}}+\frac{\partial\bar{s}_{\bar{x}\bar{x}}}{\partial\bar{x}}$$
$$-\frac{\sigma_f B_0^2}{1+m^2}[(\bar{u}+c)-m\bar{v}]-g\rho_f\left[\varsigma\left(T-T_0\right)+\varsigma^*\left(C-C_0\right)\right], \tag{11.6}$$

$$\rho_f\left(\bar{v}\frac{\partial\bar{v}}{\partial\bar{y}}+(\bar{u}+c)\frac{\partial\bar{v}}{\partial\bar{x}}\right)=-\frac{\partial\bar{p}}{\partial\bar{y}}+\frac{\partial\bar{s}_{\bar{y}\bar{y}}}{\partial\bar{y}}+\frac{\partial\bar{s}_{\bar{y}\bar{x}}}{\partial\bar{x}}-\frac{\sigma_f B_0^2}{1+m^2}[\bar{v}+m(\bar{u}+c)], \tag{11.7}$$

$$(\rho C)_f\left(\bar{v}\frac{\partial T}{\partial\bar{y}}+(\bar{u}+c)\frac{\partial T}{\partial\bar{x}}\right)=K_f\left(\frac{\partial^2 T}{\partial\bar{y}^2}+\frac{\partial^2 T}{\partial\bar{x}^2}\right)+\bar{s}.\bar{L}+\frac{\sigma_f B_0^2}{1+m^2}[(\bar{u}+c)^2+\bar{v}^2]$$
$$+(\rho C)_{np}\left[\frac{D_T}{T_m}\left(\left(\frac{\partial T}{\partial\bar{x}}\right)^2+\left(\frac{\partial T}{\partial\bar{y}}\right)^2\right)+D_B\left(\frac{\partial C}{\partial\bar{y}}\frac{\partial T}{\partial\bar{y}}+\frac{\partial C}{\partial\bar{x}}\frac{\partial T}{\partial\bar{x}}\right)\right]-\frac{\partial q_r}{\partial\bar{y}}, \tag{11.8}$$

$$(\bar{u}+c)\frac{\partial C}{\partial\bar{x}}+\bar{v}\frac{\partial C}{\partial\bar{y}}=D_B\left(\frac{\partial^2 C}{\partial\bar{y}^2}+\frac{\partial^2 C}{\partial\bar{x}^2}\right)+\frac{D_T}{T_m}\left(\frac{\partial^2 T}{\partial\bar{y}^2}+\frac{\partial^2 T}{\partial\bar{x}^2}\right). \tag{11.9}$$

Here ρ_f depicts the density, σ_f electrical conductivity, g gravity, B_0 applied magnetic field strength, $m=\frac{\sigma_f B_0}{en_e}$ Hall parameter, ς thermal expansion coefficient, ς^* Concentration expansion coefficient, C Concentration of nanomaterial, $(\rho C)_{np}$ effective heat capacity of nanomaterial, K_f thermal conductivity of fluid, $\bar{s}.\bar{L}$ viscous dissipation, D_T thermophoretic diffusion coefficient, D_B Brownian diffusion and $\bar{s}_{ij}$ component of extra stress tensor. Radiative heat flux q_r in view of Rosseland's approximation is described as:

$$q_r=-\frac{16\sigma^* T_0^3}{3k}\frac{\partial T}{\partial\bar{Y}}. \tag{11.10}$$

The following dimensionless parameters are employed:

$$x=\frac{\bar{x}}{\lambda},y=\frac{\bar{y}}{d},u=\frac{\bar{u}}{c},v=\frac{\bar{v}}{c\delta},\delta=\frac{\bar{d}}{\lambda},h=\frac{\bar{H}}{d},p=\frac{d^2\bar{p}}{c\lambda\mu_0},M=\sqrt{\frac{\sigma_f}{\mu_0}}B_0 d,$$
$$Re=\frac{\rho_f\ cd}{\mu_0},E=\frac{c^2}{C_f T_0},Pr=\frac{\mu_0 C_f}{K_f},Br=PrE,G_T=\frac{\rho_f g\varsigma T_0 d^2}{\mu_0 c},G_C=\frac{\rho_f g\varsigma^* C_0 d^2}{\mu_0 c}$$
$$R_d=\frac{4\sigma^* T_0^3}{kK_f},N_b=\frac{\tau D_B C_0}{\nu},N_t=\frac{\tau D_T T_0}{\nu T_m},\theta=\frac{T-T_0}{T_0},\phi=\frac{C-C_0}{C_0},u=\frac{\partial\psi}{\partial y},v=-\frac{\partial\psi}{\partial x}. \tag{11.11}$$

Here M, Pr, E, θ, δ, Br, Re, N_t, N_b, R_d, G_T, G_C and ϕ depict the Hartman number, Prandtl number, Eckert number, dimensionless temperature, wave number, Brinkman number, Reynolds number, thermophoresis parameter, Brownian motion parameter, radiation parame-

ter, thermal Grashof number, concentration Grashof number and dimensionless concentration respectively. The dimensionless forms of above Eqs. (11.5)-(11.9) are:

$$\frac{c}{\lambda}\frac{\partial u}{\partial x}+\frac{c}{\lambda}\frac{\partial v}{\partial y}=0, \tag{11.12}$$

$$\begin{aligned}\mathrm{Re}\,\delta\left(v\frac{\partial u}{\partial y}+(u+1)\frac{\partial u}{\partial x}\right)&=-\frac{\partial p}{\partial x}+\frac{\partial s_{xy}}{\partial y}+\delta\frac{\partial s_{xx}}{\partial x}\\&-\frac{M^2}{1+m^2}[(u+1)-m\delta v]+G_T\theta+G_C\phi,\end{aligned} \tag{11.13}$$

$$\mathrm{Re}\,\delta^3\left(v\frac{\partial v}{\partial y}+(u+1)\frac{\partial v}{\partial x}\right)=-\frac{\partial p}{\partial y}+\delta\frac{\partial s_{yy}}{\partial y}+\delta^2\frac{\partial s_{yx}}{\partial x}-\delta\frac{M^2}{1+m^2}[\delta v+m(u+1)], \tag{11.14}$$

$$\begin{aligned}\mathrm{Re}\,\mathrm{Pr}\,\delta\left(v\frac{\partial\theta}{\partial y}+(u+1)\frac{\partial\theta}{\partial x}\right)&=\left(\frac{\partial^2\theta}{\partial y^2}+\delta^2\frac{\partial^2\theta}{\partial x^2}\right)+Br.\Phi+\frac{M^2}{1+m^2}[(u+1)^2+\delta^2v^2]\\&+\mathrm{Pr}\,N_t\left(\delta^2\left(\frac{\partial\theta}{\partial x}\right)^2+\left(\frac{\partial\theta}{\partial y}\right)^2\right)+\mathrm{Pr}\,N_b\left(\frac{\partial\phi}{\partial y}\frac{\partial\theta}{\partial y}+\frac{\partial\phi}{\partial x}\frac{\partial\theta}{\partial x}\right)+\frac{4}{3}R_d\frac{\partial^2\theta}{\partial y^2},\end{aligned} \tag{11.15}$$

$$\mathrm{Re}\,.\delta\left((u+1)\frac{\partial\phi}{\partial x}+v\frac{\partial\phi}{\partial y}\right)=N_b\left(\frac{\partial^2\phi}{\partial y^2}+\delta^2\frac{\partial^2\phi}{\partial x^2}\right)+N_t\left(\delta^2\left(\frac{\partial\theta}{\partial x}\right)^2+\left(\frac{\partial\theta}{\partial y}\right)^2\right). \tag{11.16}$$

The simplified forms of above equations (11.13)-(11.16) by taking the small Reynold number and long wavelength assumptions are:

$$p_y=0, \tag{11.17}$$

$$p_x=\frac{\partial s_{xy}}{\partial y}-\frac{M^2}{1+m^2}\left(1+\frac{\partial\psi}{\partial y}\right)+G_T\theta+G_C\phi, \tag{11.18}$$

$$\theta_{yy}+Br\Phi+\mathrm{Pr}\,N_b\phi_y\theta_y+\mathrm{Pr}\,N_t\,(\theta_y)^2+\frac{BrM^2}{1+m^2}\left(1+\frac{\partial\psi}{\partial y}\right)^2+\frac{4R_d}{3}\frac{\partial^2\theta}{\partial y^2}=0, \tag{11.19}$$

$$N_b\phi_{yy}+N_t\theta_{yy}=0. \tag{11.20}$$

Continuity equation is satisfied. Here Φ depicts the non-dimensional form of viscous dissipation and s_{xy} depicts the dimensionless component of extra stress tensor defined by:

$$s_{xy}=s_{yx}=(1-\alpha\theta)\,\psi_{yy}+A\psi_{yy}-B\left(\psi_{yy}\right)^3. \tag{11.21}$$

When shear rate enhances then the apparent viscosity of fluid has decreasing behavior. However opposite nature of fluid is called shear thickening. From Eqs. (11.17)-(11.21) we obtain:

$$\frac{\partial^2}{\partial y^2}\left[(1-\alpha\theta)\,\psi_{yy}+A\psi_{yy}-B\left(\psi_{yy}\right)^3\right]-\frac{M^2}{1+m^2}\psi_{yy}+G_T\theta+G_C\phi=0, \tag{11.22}$$

$$\begin{aligned}&\theta_{yy}+\tfrac{4R_d}{3}\theta_{yy}+\tfrac{BrM^2}{1+m^2}\left(1+\tfrac{\partial\psi}{\partial y}\right)^2+\Pr N_b\phi_y\theta_y+\Pr N_t\\&+Br\left[(1-\alpha\theta+A)\,(\psi_{yy})^2-B\left(\psi_{yy}\right)^4\right]=0,\end{aligned} \tag{11.23}$$

$$N_b\phi_{yy}+N_t\theta_{yy}=0. \tag{11.24}$$

Dimensionless forms of flow rate in the wave $F(=\bar{q}/cd_1)$ and laboratory $\eta(=\bar{Q}/cd_1)$ frames are associated through the relation:

$$\eta=F+1. \tag{11.25}$$

Further 'F' can be defined as:

$$F=\int_0^h\frac{\partial\psi}{\partial y}dy.$$

The dimensionless boundary conditions are:

$$\psi=0,\psi_{yy}=0,\theta_y=0 \text{ and } \phi_y=0 \text{ at } y=0, \tag{11.26}$$

$$\begin{aligned}\psi=F,\psi_y+\xi\left[(1-\alpha\theta)\,\psi_{yy}+A\psi_{yy}-B\left(\psi_{yy}\right)^3\right]=-1,\\ \theta+\gamma\theta_y=0 \text{ and } N_b\phi_y+N_t\theta_y=0 \text{ at } y=h.\end{aligned} \tag{11.27}$$

The dimensionless form of geometric walls are:

$$h=1+d\cos(2\pi x).$$

Numerical approach has been used for the solution of non-linear system.

11.2 Entropy generation

Mathematically the entropy generation is:

$$S_G = \frac{K_f}{T_0^2}\left[\left(\frac{\partial T}{\partial \bar{y}}\right)^2+\left(\frac{\partial T}{\partial \bar{x}}\right)^2\right]+\frac{\sigma_f B_0^2}{T_0\left(1+m^2\right)}[(\bar{u}+c)^2+\bar{v}^2]+\frac{1}{T_0^2}\frac{16\sigma^* T_0^3}{3k}\left(\frac{\partial T}{\partial \bar{y}}\right)^2 + \frac{1}{T_0}\bar{s}.\bar{L}+\frac{R^* D}{T_0}\left(\frac{\partial C}{\partial \bar{x}}\frac{\partial T}{\partial \bar{x}}+\frac{\partial C}{\partial \bar{y}}\frac{\partial T}{\partial \bar{y}}\right)+\frac{R^* D}{C_0}\left(\left(\frac{\partial C}{\partial \bar{y}}\right)^2+\left(\frac{\partial C}{\partial \bar{x}}\right)^2\right). \quad (11.28)$$

Non-dimensional form of entropy generation is:

$$N_s = \left[1+\frac{4R_d}{3}\right](\theta_y)^2+Br\left[1-\alpha\theta+A-B\left(\psi_{yy}\right)^2\right]\psi_{yy}^2+L\phi_y\theta_y+L\left(\phi_y\right)^2+\frac{BrM^2}{1+m^2}\left(1+\frac{\partial\psi}{\partial y}\right)^2.$$

Here $L=\left(\frac{R^* DC_0}{d^2}\right)$ depicts the diffusion parameter and $N_s=\left(\frac{d^2 S_G}{K_{nf}}\right)$ the dimensionless entropy generation. Graphical explanation of the results are described in the next section.

11.3 Discussion

Here the graphical representation of velocity, temperature, concentration and entropy generation are analyzed. Figures (11.1)-(11.4) describe the influences of some physical parameters on the axial velocity. Fig. 11.1 highlights the decreasing trend of velocity due to magnetic field. The presence of magnetic field enhances Lorentz force that creates the resistance therefore axial velocity decreases. Fig. 11.2 depicts the axial velocity of fluid against Hall number. Hall number depicts opposite behavior when compared to Hartman number. Fig. 11.3 explains the effect of material parameter "A" on the velocity. By increasing "A" parameter the velocity decays near central part of channel. However opposite trend is noticed near channel wall. Fig. 11.4 describes the velocity profile against different values of velocity slip parameter. Velocity shows increasing trend near boundary wall of channel for higher "β".

Figs. (11.5)-(11.11) are sketched to observe the temperature for various values of M, m, G_T, A, Br, γ and R_d. Fig. 11.5 is sketched to observe the temperature for increasing values of Hartman number. This graph depicts increasing trend of temperature for higher values of M. Decreasing trend of temperature is noticed for higher values of Hall number in Fig. 11.6. Therefore Hall parameter is used in biological phenomena to balance the effect of increasing

trend of magnetic field on temperature. Fig. 11.7 ensure that rising values of thermal Grashof number enhances the temperature. Impact of "A" on temperature is demonstrated in Fig. 11.8. Temperature continuously enhances by increasing the fluid parameter "A". Impact of Brinkman number on temperature is captured in Fig. 11.9. Brinkman number is inversely proportional to the thermal conductivity of nanofluid therefore rise in Brinkman number leads to fluid temperature enhancement. Fig. 11.10 is sketched to explain the temperature behavior for thermal slip parameter. It is noteworthy that in the presence of "γ" temperature decreases. Fig. 11.11 presents the temperature for different R_d. Temperature rapidly decreases by increasing the thermal radiation parameter. Heat transfer rate increases by higher γ and R_d parameters therefore temperature of the system decreases.

Figs. (11.12)-(11.14) indicate the behavior of concentration for various values of M, N_t and N_b. Fig. 11.12 displays the increasing trend of concentration for higher values of Hartman number. It is because of the fact that magnetic field decreases the flow of nanofluid therefore concentration of nanomaterial increases. Fig. 11.13 presents that higher values of thermophoresis parameter enhances the concentration of Powell Eyring nanofluid. Fig. 11.14 demonstrates the decaying behavior of concentration for higher Brownian parameter. Figs. (11.15)-(11.19) depict the entropy generation for some significant variables. Fig. 11.15 presents the generation analysis against different values of Hartman number. Entropy generation significantly increases through magnetic field. Joule heating effect increases temperature of nanofluid therefore entropy also enhances. Fig. 11.16 indicates the decreasing trend of entropy generation for higher Hall number. Hall effects are used with magnetic field to balance the energy losses. Analysis of Fig. 11.17 reveals that entropy generation can be controlled by increasing the radiation parameter. Fig. 11.18 illustrates the entropy generation behavior against various values of Brinkman number. By increasing Brinkman number the temperature of nanofluid increases so an enhancement occurs in entropy generation. Fig. 11.19 depicts that entropy generation can be controlled by decreasing the material parameter.

11.4 Conclusions

The influences of Hartman number, Hall parameter, slip parameter, mixed convection and non-Newtonian material parameter on peristalsis have been studied. Following points are the main findings.

1.
   - Axial velocity depicts decreasing trend for higher values of Hartman number and material parameter "A".
   - By increasing the Hartman number, the thermal Grashof number and Brinkman number the temperature enhances.
   - Decreasing behavior of temperature is noticed by higher Hall number and thermal radiation parameter.
   - Concentration of nanoparticles increases by rising values of Hartman number and thermophoresis parameters. However Brownian motion parameter depicts opposite trend.
   - Increasing behavior of entropy generation is noticed due to presence of magnetic field while entropy generation can be controlled by increasing Hall parameter.
   - Entropy generation can be minimized by decreasing the Brinkman number and material parameter.

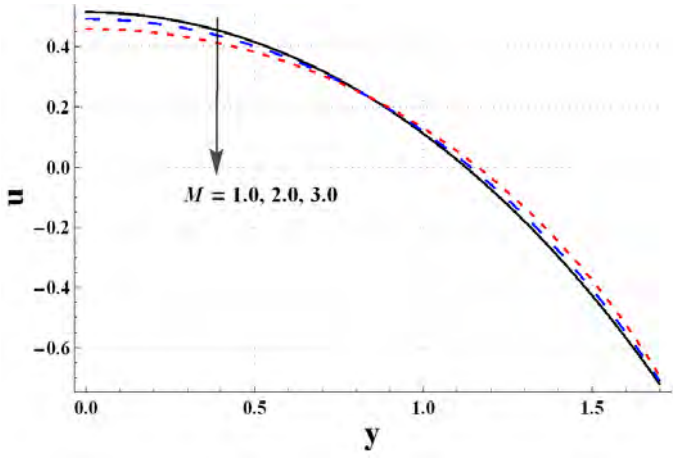

Fig. 11.1. Plot of u for M.

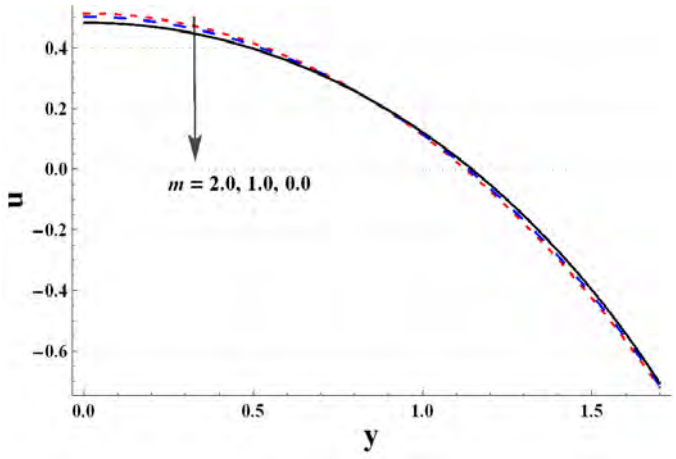

Fig. 11.2. Plot of u for m.

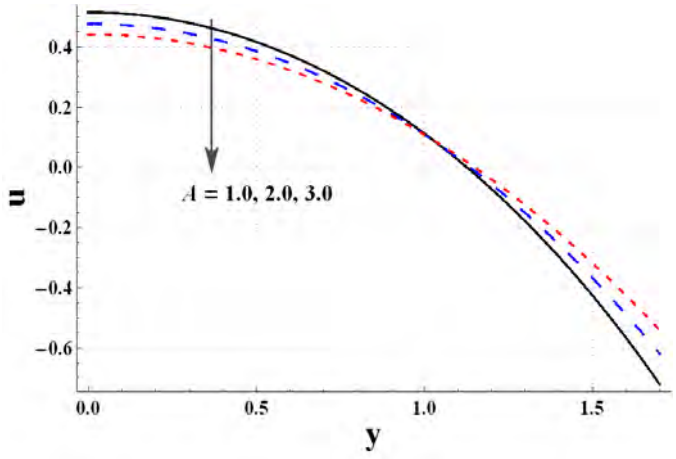

Fig. 11.3. Plot of u for A.

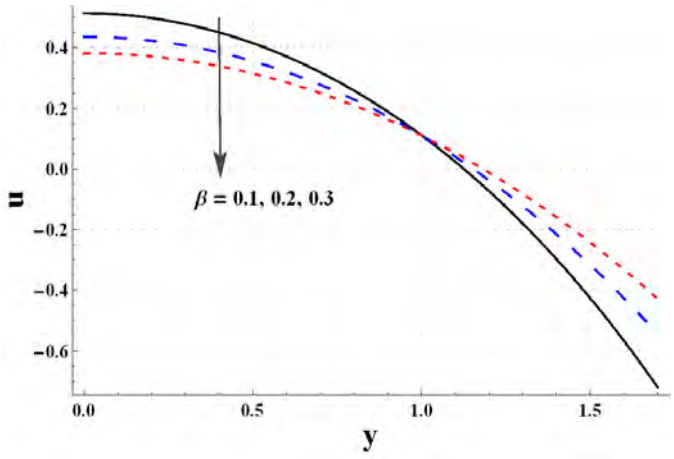

Fig. 11.4. Plot of u for β.

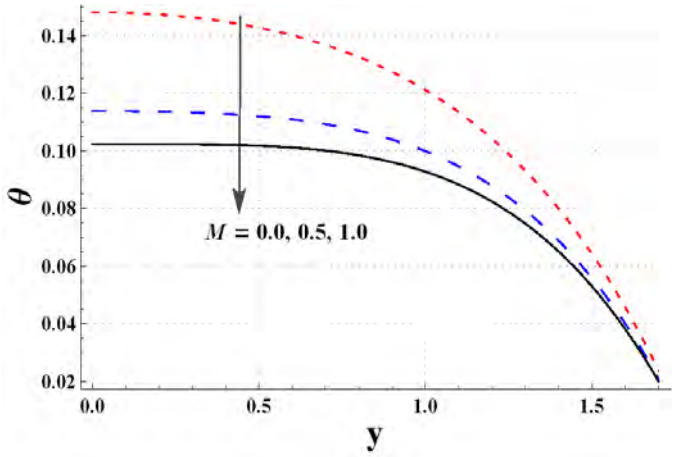

Fig. 11.5. Plot of θ for M.

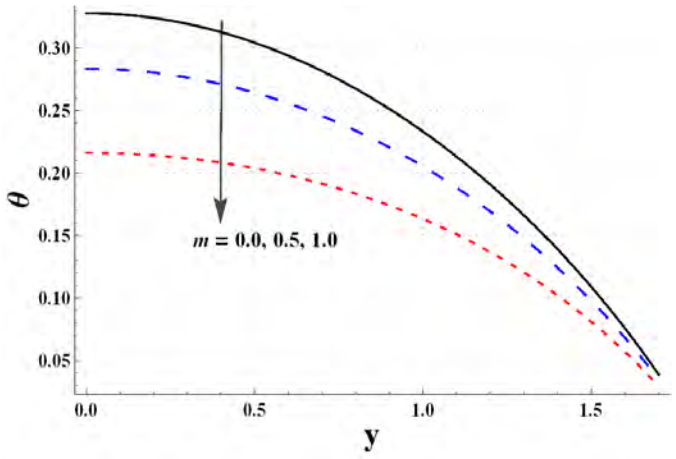

Fig. 11.6. Plot of θ for m.

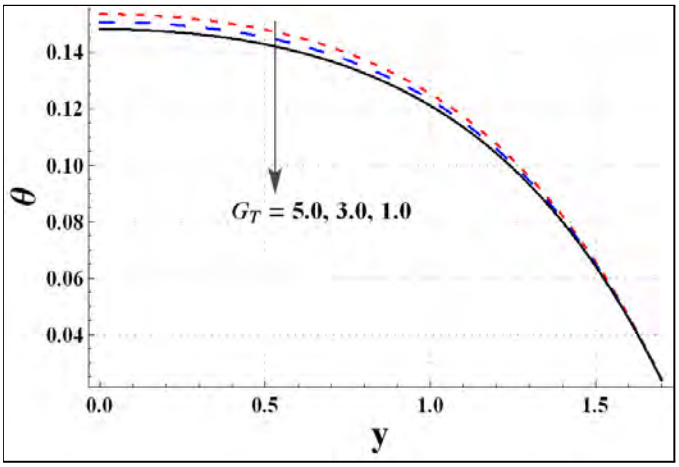

Fig. 11.7. Plot of θ for G_T.

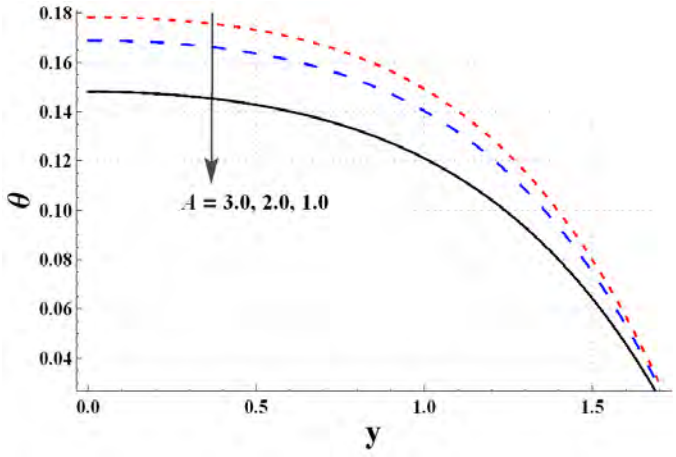

Fig. 11.8. Plot of θ for A.

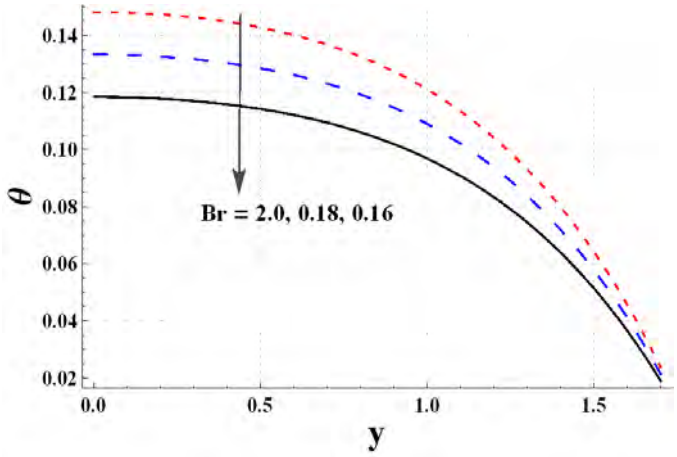

Fig. 11.9. Plot of θ for Br.

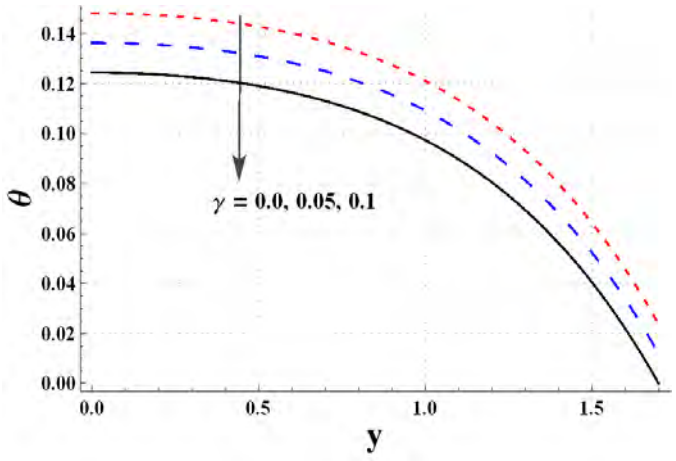

Fig. 11.10. Plot of θ for γ.

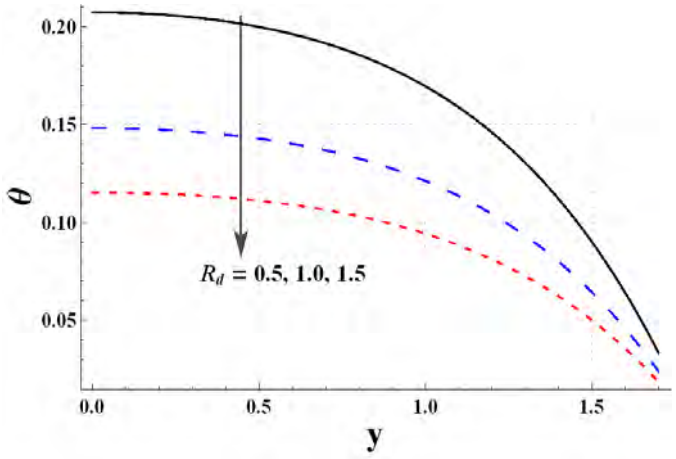

Fig. 11.11. Plot of θ for R_d.

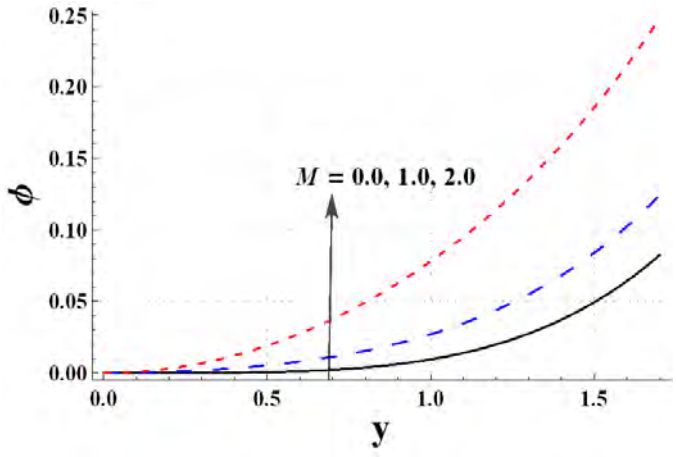

Fig. 11.12. Plot of ϕ for M.

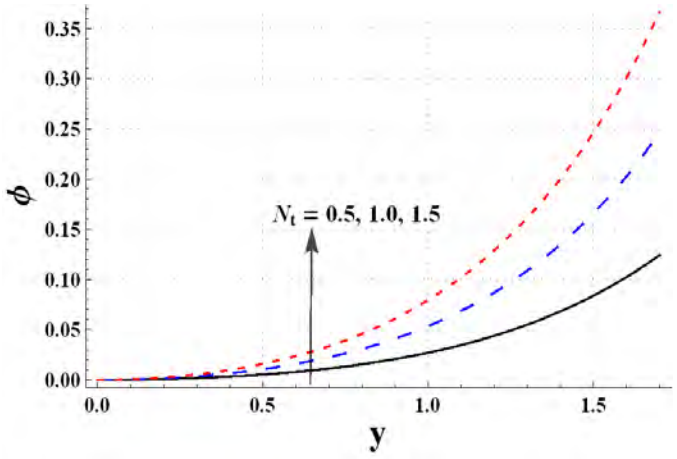

Fig. 11.13. Plot of ϕ for N_t.

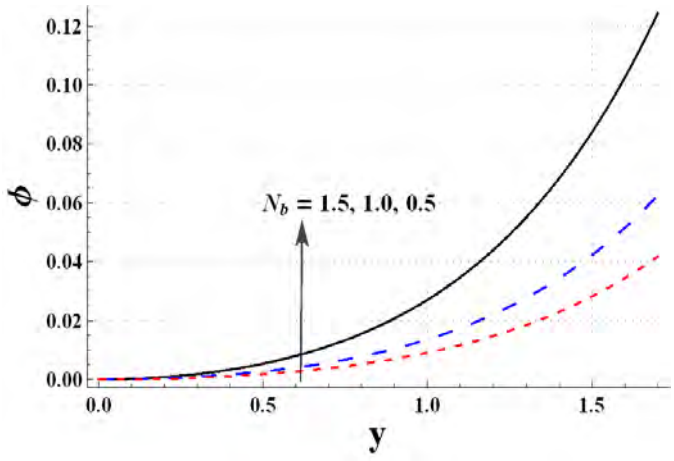

Fig. 11.14. Plot of ϕ for N_b.

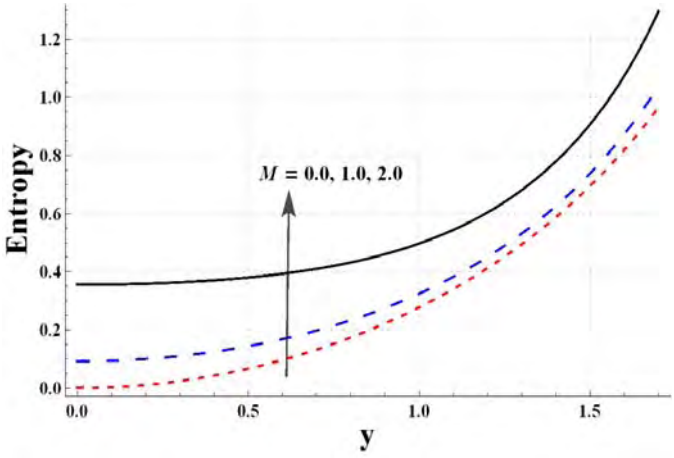

Fig. 11.15. Plot of N_S for M.

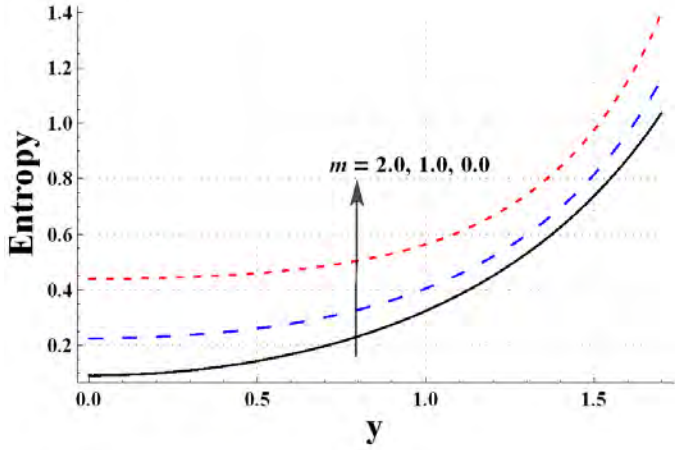

Fig. 11.16. Plot of N_S for m.

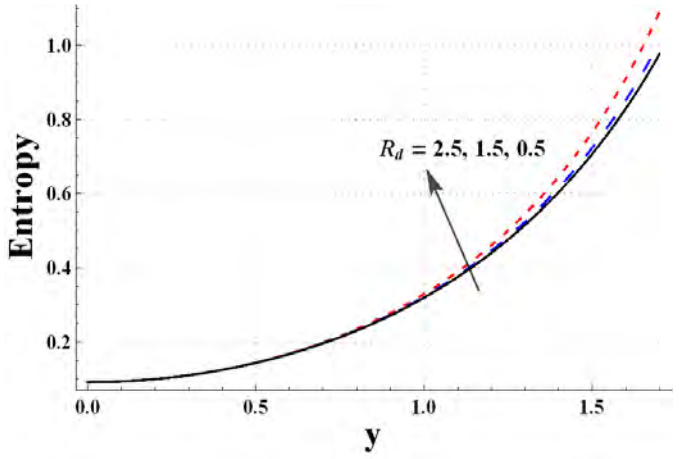

Fig. 11.17. Plot of N_S for R_d.

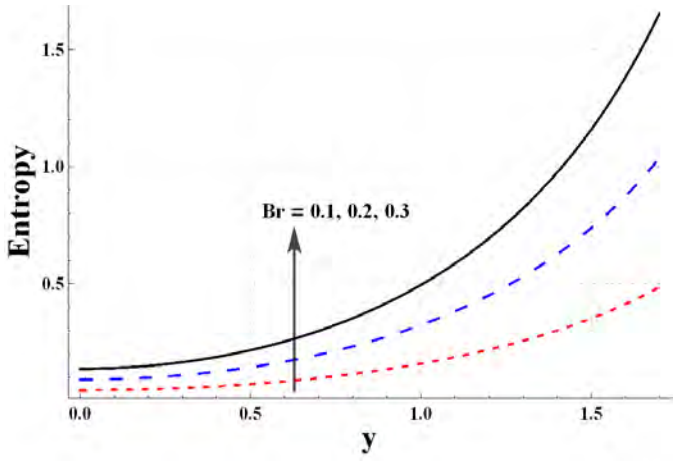

Fig. 11.18. Plot of N_S for Br.

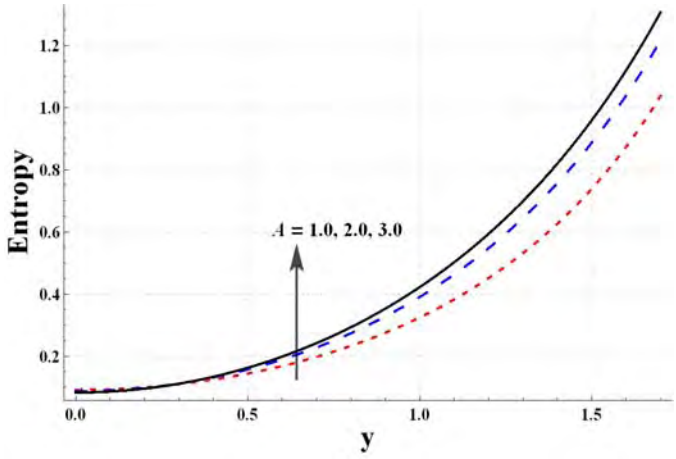

Fig. 11.19. Plot of N_S for A.

Bibliography

[1] S.U.S. Choi, Enhancing thermal conductivity of fluids with nanoparticles. ASME Fluids Eng. Div. 231 (1995) 99-105.

[2] J. C. Maxwell, A treatise on electricity and magnetism. 2nd Edition Oxford University press, Cambridge, 1904, 435-441.

[3] R. L. Hamilton and O. K. Crosser, Thermal conductivity of heterogeneous two component systems. EC Fundam. 1 (1962) 187-191.

[4] H. C. Brinkman, The viscosity of concentrated suspensions and solutions. J. Chem. Phys. 20 (1952) 571-581.

[5] R. K. Tiwari and M. K. Das, Heat transfer augmentation in a two-sided lid-driven differentially heated square cavity utilization nanofluids. International Journal of Heat and Mass transfer, 50 (2007) 2002-2018.

[6] Y. Xuan and Li Qiang, Heat transfer enhancement of nanofluids. International J of Heat and fluid flow. 21 (2000) 58-64.

[7] T. Hayat, B. Ahmed, F. M. Abbasi and A. Alsaedi, Hydromagnetic peristalsis of water based nanofluids with temperature dependent viscosity: A comparative study. J. Molecular Liquid, 234(2017) 324-329.

[8] A. Feizabadi, M. K. Aliabadi and A. B. Rahimi, Numerical investigation on Al2O3/water nanofluid flow through twisted-serpentine tube with empirical validation. J Applied Thermal Engineering, 137 (2018) 296-309.

[9] H. Saadati, K. Hadad and A. Rabiee, Safety margin and fuel cycle period enhancements of VVER-1000 nuclear reactor using water/silver nanofluid. Nuclear Engineering and Technology 50 (2018) 639-647.

[10] G. Lebon and H. Machrafi, A thermodynamic model of nanofluid viscosity based on a generalized Maxwell-type constitutive equation. J. Non-Newtonian Fluid Mechanics, 253 (2018) 1-6.

[11] J. Buongiorno, Convective transport in Nanofluids. ASME Journal of Heat transfer, 128 (2006) 240-250.

[12] A. J. Apostolidis, A. P. Moyer and A. N. Beris, Non-Newtonian effects in simulations of coronary arterial blood flow. J. Non-Newtonian Fluid Mechanics, 233 (2016) 155-165.

[13] A. W. Sisko, The flow of lubricating greases. Industrial and Engineering Chemistry, 50 (1958) 1789-1792.

[14] M. Shen, L. Chen, M. Zhang and F. Liu, A renovated Buongiorno's model for unsteady Sisko nanofluid with fractional Cattaneo heat flux. International Journal of Heat and Mass transfer, 126 (2018) 277-286.

[15] P. J. Carreau, Rheological equations from moleculae network theories. J Rheol, 16 (1972) 99-127.

[16] G. R. Kefayati and H. Tang, Three dimensional Lattice Boltzmann simulation on thermosolutal convection and entropy generation of Carreau-Yasuda fluids. International Journal of Heat and Mass Transfer, 131 (2019) 346-364.

[17] S. Dong, L. Zheng, X Zhang and P Lin, Improved drag force model and its application in simulating nanofluid flow. J. Microfluid Nanofluid, 17 (2014) 253-261.

[18] R. K. Nayak, S Bhattacharyya and I. Pop, Effect of nanoparticles dispersion on the mixed convection of nanofluid in a skewed enclosure. Int. Journal of Heat and Mass transfer, 125 (2018) 908-919.

[19] M. Sheikholeslami, A. J. Chamkha, P. Rana and R. Moradi, Combined thermophoresis and Brownian motion effects on nanofluid free convection heat transfer in an L-shaped enclosure. Chinese Journal of Physics, 55 (2017) 2356-2370.

[20] R. E. Powell and H. Eyring, Mechanism for the relaxation theory of viscosity, Nature 154 (1944) 427-428.

[21] T. W. Latham, Fluid motion in a peristaltic pump, MS Thesies, MIT Cambridge, MA, 1996.

[22] M. Y. Jaffrin and A. H. Shapiro, Peristaltic pumping, Ann. Rev. Fluid Mech. 3 (1971) 13-16.

[23] T. Hayat and N. Ali, Peristaltic mechanism of a Maxwell fluid in an asymmetric channel, Nonlinear Anal: Real Word Appl. 9 (2008) 1474-1490.

[24] T. Hayat, B. Ahmed, F. M. Abbasi and B. Ahmad, Mixed convective peristaltic flow of carbon nanotubes submerged in water using different thermal conductivity models, Computer Methods and Programs in Biomedicine 135 (2016) 141-150.

[25] N. Ali, M. Sajid, T. Javed and Z. Abbas, Heat transfer analysis of peristaltic flow in a curved channel. International Journal of Heat and Mass Transfer, 53 (2017) 3319-3325.

[26] F. M. Abbasi, T. Hayat, S. A. Shehzad, F. Alsaadi and N. Altoaibi, Hydromagnetic peristaltic transport of copper-water nanofluid with temperature-dependent effective viscosity. Particuology, 27 (2016) 133-140.

[27] C. Cueva, I. Gil-Sánchez, A. Tamargo, B. Miralles, J. Crespo, B. Bartolomé and M. V. Moreno-Arribas, Gastrointestinal digestion of food-use silver nanoparticles in the dynamic SIMulator of the gastroIntestinal tract (simgi). Impact on human gut microbiota. Food and Chemical Toxicology, 132 (2019) 110657.

[28] M. G. Ibrahim, W. M. Hasona and A. A. ElShekhipy, Concentration-dependent viscosity and thermal radiation effects on MHD peristaltic motion of synovial nanofluid: Applications to rheumatoid arthritis treatment. Computer Methods and Programs in Biomedicine, 170 (2019) 39-52.

[29] M. G. Reddy and O. D. Makinde, Magnetohydrodynamic peristaltic transport of Jeffrey nanofluid in an asymmetric channel. Journal of Molecular Liquids, 223 (2016) 1242-1248.

[30] S. A. Shehzad, F. M. Abbasi, T. Hayat and F. Alsaadi, Model and comparative study for peristaltic transport of water based nanofluids. J. Molecular Liquids, 209 (2015) 723-728.

[31] T. Hayat, N. Aslam, A. Alsaedi and M. Rafiq, Endoscopic effect in MHD peristaltic activity of hyperbolic tangent nanofluid: A numerical study. International Journal of Heat and Mass Transfer, 115 (2017) 1033-1042.

[32] F. M. Abbasi, T. Hayat and A. Alsaedi, Peristaltic transport of magneto-nanoparticles submerged in water: Model for drug delivery system. Physica E, 68 (2015) 123-132.

[33] Z. Mehrez, A. Cafsi, A. Belghith and P. L. Quere, MHD effects on heat transfer and entropy generation of nanofluid flow in an open cavity. Journal of Magnetism and Magnetic Materials, 374 (2015) 214-224.

[34] I. Shahzadi and S. Nadeem, Inclined magnetic field analysis for metallic nanoparticles submerged in blood with convective boundary condition. Journal of Molecular Liquids, 230 (2017) 61-73.

[35] M. G. Reddy and K. V. Reddy, Influence of Joule heating on MHD peristaltic flow of nanofluid with complaint wall. Procedia Engineering, 127 (2015) 1002-1009.

[36] M. Raza, R. Ellahi, S. M. Sait, M. M. Sarafraz, M. S. Shadloo and I. Waheed, Enhancement of heat transfer in peristaltic flow in a permeable channel under induced magnetic field using different CNTs. J Thermal Analysis and Calorimetry, 140 (2019) 1277–1291.

[37] S. Rashidi, J. A. Esfahani and M. Maskaniyan, Application of magnetohydrodynamics in biological systems: A review on the numerical studies. Journal of Magnetism and Magnetic Materials, 439 (2017) 358-372.

[38] F. M. Abbasi, T. Hayat and B. Ahmad, Peristalsis of silver-water nanofluid in the presence of Hall and Ohmic heating effects: Applications in drug delivery. J. Mol. Liq. 207 (2015) 248-255.

[39] O. D. Makinde, T. Iskander, F. Mehbood, W. A. Khan and M. S. Tshehla, MHD Coutte-Poiseuille flow of variable viscosity nanofluid in a rotating permeable channel with Hall effects. Journal of Molecular Liquids, 221 (2016) 778-787.

[40] M. Rafiq, H. Yasmin, T. Hayat and F. Alsaedi, Effect of Hall and ion-slip on the peristaltic transport of nanofluid: A biomedical application. Chinese Journal of Physics, 60 (2019) 208-227.

[41] F. Garoosi, G. Bagheri and M. M. Rashidi, Two phase simulation of natural convection and mixed convection of the nanofluid in a square cavity. Powder Technology, 275 (2015) 239–256.

[42] A. Tanveer, T. Hayat, F. Alsaadi and A. Alsaedi, Mixed convection peristaltic flow of Eyring-Powell nanofluid in a curved channel with compliant walls. Computers in Biology and Medicine, 82 (2017) 71-79.

[43] A. Zeeshan, A. Fatima, F. Khalid and M. M. Bhatti, Interaction between blood and solid particles propagating through acapillary with slip effects. Microvascular Research, 119 (2018) 38-46.

[44] R. U. Haq, S. Nadeem, Z. H. Khan and N. S. Akbar, Thermal radiation and slip effects on MHD stagnation pointflow ofnanofluid over a stretching sheet. Physica E, 65 (2015) 17-23.

[45] M. Mustafa, S. Hina, T. Hayat and A. Alsaedi, Influence of wall properties on the peristaltic flow of a nanofluid: Analytic and numerical solutions. International Journal of Heat and Mass Transfer, 55 (2012) 4871–4877.

[46] N. S. Akbar, S. Nadeem and Z. H. Khan, Numerical simulation of peristaltic flow of a Carreau nanofluid in an asymmetric channel. Alexandria Engineering Journal, 53 (2014) 191–197.

[47] H. Darcy, Les Fontaines Publiques De La Ville De Dijon. Dalmont, Paris (1856) 647.

[48] F. M. Abbasi, T. Hayat and B. Ahmad, Peristaltic transport of copper-water nanofluid saturating porous medium. Physica E. 67 (2015) 47–53.

[49] W. C. Tan and T. Masuoka, Stokes' first problem for an Oldroyd-B fluid in a porous half-space, Phys. Fluids 17 (2005) 3101–3107.

[50] A. Tanveer, T. Hayat, A. Alsaedi and B. Ahmad, On modified Darcy's law utilization in peristalsis of Sisko fluid. J Mol Liq. 236 (2017) 290–297.

[51] A. V. Kuznetsov and D. A. Nield, The Cheng-Minkowycz problem for natural convective boundary layer flow in a porous medium saturated by a nanofluid: A revised model. International Journal of Heat and Mass Transfer, 65 (2013) 682-685.

[52] S. A. Shehzad, F. M. Abbasi, T. Hayat and F. Alsaedi, MHD mixed convective peristaltic motion of nanofluid with Joule heating and thermophoresis effects. Plos One, 9 (2014) e111417.

[53] S. E. Ghasemi, Thermophoresis and Brownian motion effects on peristaltic nanofluid flow for drug delivery applications. Journal of Molecular Liquids, 238 (2017) 115-121.

[54] M. M. Bhatti, A. Zeeshan and R. Ellahi, Simultaneous effects of coagulation and variable magnetic field on peristaltically induced motion of Jeffrey nanofluid containing gyrotactic microorganism. Microvascular Research, 110 (2017) 32-42.

[55] N. S. Akbar, Peristaltically assisted nanofluid transport in an asymmetric channel. Karbala International Journal of Modern Sciences, 4 (2018) 35-49.

[56] H. Sadaf, M. U. Akbar and S. Nadeem, Induced magnetic field analysis for the peristaltic transport of non-Newtonian nanofluid in an annulus. Mathematics and Computers in Simulation, 148 (2018) 36-46.

[57] W. M. Hasona, A. A. Shekhipy and M. G. Ibrahim, Combined effects of magnetohydrodynamic and temperature dependent viscosity on peristaltic flow of Jeffrey nanofluid through a porous medium: Applications to oil refinement. International Journal of Heat and Mass Transfer, 126 (2018) 700-714.

[58] D. Tripathi, A. Sharma and O. A. Bég, Electrothermal transport of nanofluids via peristaltic pumping in a finite micro-channel: Effects of Joule heating and Helmholtz-

Smoluchowski velocity. International Journal of Heat and Mass Transfer, 111 (2017) 138-149.

[59] T. Hayat, S. Farooq and A. Alsaedi, Mixed convection peristaltic motion of copper-water nanomaterial with velocity slip effects in a curved channel. Computer Methods and Programs in Biomedicine, 142 (2017) 117-128.

[60] J. Prakash, D. Tripathi, A. K. Tiwari, S. M. Sait and R. Ellahi, Peristaltic pumping of nanofluids through a tapered channel in a porous environment: Applications in blood flow. Symmetry, 11 (2019) 868.

Turnitin Originality Report

Penstaltic Motion with Nanofluid Characteristics by Bilal Ahmed .

From DRSM (DRSM L)

- Processed on 16-Aug-2021 12:35 PKT
- ID: 1631953131
- Word Count: 31687

Similarity Index
15%
Similarity by Source

Internet Sources:
7%
Publications:
11%
Student Papers:
5%

Focal Person (Turnitin)
Quaid-i-Azam University
Islamabad

sources:

1 1% match (student papers from 03-Sep-2013)
Submitted to Higher Education Commission Pakistan on 2013-09-03

2 1% match (student papers from 22-Mar-2016)
Submitted to Higher Education Commission Pakistan on 2016-03-22

3 < 1% match (student papers from 14-May-2018)
Submitted to Higher Education Commission Pakistan on 2018-05-14

4 < 1% match (student papers from 12-Jan-2018)
Submitted to Higher Education Commission Pakistan on 2018-01-12

5 < 1% match (student papers from 09-Apr-2018)
Submitted to Higher Education Commission Pakistan on 2018-04-09

6 < 1% match (student papers from 08-Jan-2018)
Submitted to Higher Education Commission Pakistan on 2018-01-08

7 < 1% match (student papers from 16-Sep-2009)
Submitted to Higher Education Commission Pakistan on 2009-09-16

8 < 1% match (student papers from 12-Dec-2019)
Submitted to Higher Education Commission Pakistan on 2019-12-12

9 < 1% match (student papers from 17-Jan-2019)
Submitted to Higher Education Commission Pakistan on 2019-01-17

10 < 1% match (student papers from 28-Sep-2017)
Submitted to Higher Education Commission Pakistan on 2017-09-28

11 < 1% match (student papers from 29-Oct-2018)
Submitted to Higher Education Commission Pakistan on 2018-10-29

12 < 1% match (student papers from 29-Dec-2011)
Submitted to Higher Education Commission Pakistan on 2011-12-29

13 < 1% match (student papers from 12-Nov-2013)
Submitted to Higher Education Commission Pakistan on 2013-11-12

14 < 1% match (student papers from 05-Oct-2016)
Submitted to Higher Education Commission Pakistan on 2016-10-05

15 < 1% match (student papers from 31-Jul-2018)
Submitted to Higher Education Commission Pakistan on 2018-07-31

16 < 1% match (student papers from 30-Aug-2014)
Submitted to Higher Education Commission Pakistan on 2014-08-30